UNIVERSITÀ DEGLI STUDI DI PADOVA

FACOLTÀ DI INGEGNERIA

DIPARTIMENTO DI FISICA TECNICA

SCUOLA DI DOTTORATO DI RICERCA IN INGEGNERIA INDUSTRIALE

INDIRIZZO: FISICA TECNICA

CICLO XXII

DEVELOPMENT OF HIGH EFFICIENCY AIR-CONDITIONING AND HEATING SYSTEMS

SVILUPPO DI SISTEMI DI CONDIZIONAMENTO E RISCALDAMENTO AD ALTA EFFICIENZA

DIRETTORE DELLA SCUOLA : CH.MO PROF. PAOLO BARIANI

COORDINATORE D'INDIRIZZO: CH.MO PROF. EZIO FORNASIERI

SUPERVISORE: CH.MO PROF. PIERFRANCESCO BRUNELLO

CORRELATORE: CH.MO PROF. EZIO FORNASIERI

Dottorando: Manuel Chiarello

Alla mia famiglia

Index

Abstract

The energy efficiency is one of the most important topic concerning heating, cooling and refrigerating systems. The objective of researchers and manufacturers is to reduce the energy consumptions of such systems, assuring the same capacity. The interest is related not only to the price of energy, continuously increasing, but also to the need of reduction in the emissions of carbon dioxide, responsible of the global warming. In addition, the optimization of a heating, cooling or refrigerating system must take into consideration economical constrains and restrictions, fixed by national or international organism, concerning the use of refrigerants. The subject has different solutions: in the Introduction of the present work, a review of such options is presented.

In the first part of this work, the theme of the energy efficiency is faced considering the system at rating conditions. Several solutions, to optimize a HVAC&R plant, are investigated, taking into account aspects like the refrigerant, the cycle configuration and the components.

In the second part, the issue of the energy efficiency is studied according to a more recent approach, considering the energy consumptions of a system running at different part load ratios. In this way, the control and management techniques are studied, highlighting the actual seasonal energy consumption of the plant.

The objective of the present work is to provide a wide range of solutions for the energy optimization, taking into consideration the needs and the characteristics of different systems. The fact that there is not an univocal solution of the problem of the energy efficiency, but each plant configuration must be studied, is remarked.

Sommario

Il tema dell'efficienza energetica è uno delle questioni più importanti nell'ambito della ricerca riguardante i sistemi di refrigerazione, condizionamento e riscaldamento. L'obiettivo, infatti, è quello di minimizzare i consumi energetici di tali impianti, garantendo la stessa resa. L'interesse riguardante tale tema è giustificato non solo dal prezzo dell'energia, in costante aumento, ma anche dalla necessità di ridurre le emissioni di anidride carbonica, responsabile del riscaldamento globale. L'ottimizzazione di sistemi di condizionamento e refrigerazione, inoltre, deve sottostare a vincoli di natura economica e ai limiti imposti da normative nazionali ed internazionali riguardo l'uso dei refrigeranti. Il problema presenta molteplici sfaccettature, che saranno brevemente riassunte nell'Introduzione del presente lavoro.

Nella prima parte di questa tesi si affronta il problema dell'efficienza energetica considerando il funzionamento dell'impianto nelle condizioni di progetto. Vengono prese in esame alcune modalità di ottimizzazione di un impianto HVAC&R, considerando aspetti come il refrigerante, il tipo di ciclo e i singoli componenti.

Nella seconda parte il tema dell'efficienza energetica viene affrontato secondo un approccio più moderno, considerando i consumi di un impianto operante a diverse frazioni di carico. In questo caso particolare risalto viene dato alle modalità di controllo e gestione del sistema, evidenziando gli effettivi risparmi energetici annuali.

L'obiettivo finale è offrire un ampio ventaglio di soluzioni per le diverse necessità e le diverse tipologie di impianto, fermo restando che non esiste una soluzione univoca al problema dell'ottimizzazione energetica, ma che ogni singolo caso deve essere studiato nella sua specificità.

Introduction: the energy efficiency

The increasing energy costs and, on other side, the higher interest on environmental issues made the achievement of high efficiency a leading target in HVAC&R system projecting and development.

The energy saving is a topic world-scale challenge, due both to the increasing cost and the scarcity of traditional energy source (fossil fuels). On other hand, the high spread of heating and cooling systems made relevant the global energy consumption for air-conditioning, heating and refrigeration. Thus, the objective of HVAC&R manufacturers is to realize high-efficiency systems, assuring the same performances with lower energy consumptions.

Moreover, current standards in environmental matters are becoming more and more strict, especially concerning the working fluids. The Montreal Protocol (1987) decreed the phase out of the CFC and HCFC fluids, because of their action in the ozone depletion. The Kyoto Protocol (1997) fixed the reduction of "greenhouse gases", responsible to the global warming of anthropic origin. In this way, a large range of halogenated fluids has been banned, and they are now replacing with natural or eco-friendly refrigerants. Unfortunately, their heat transfer properties are often less effective than the ones of the replaced fluid; so, in order to achieve the same performance of current systems, the researchers are considering different solutions to improve the system efficiency; by the way, the replacement of halogenated refrigerants is still an open issue.

At this point, a correct evaluation of the energy efficiency of a system is needed; the traditional way to evaluate the performance of heat pump, air conditioners and liquid chillers is at rated conditions. This condition does not describe completely the actual running of the equipment, because the working conditions can considerably change over a season. Different units, with the same energy efficiency at design conditions, can actually present different energy coefficients at part load conditions. This new perspective led to the introduction

of new coefficients that should take into account the different behaviour of the system at different part load ratios. So, besides the traditional indexes (COP, EER), new energy standards are being developed and adopted all over the world. In the present work, only the European standards will be considered.

Finally, the improvement of the system energy performance can be achieved through the optimization of the different components of the compression vapour inverse cycle. The goal can be achieved in multiple ways, operating on different components. In the present work, some solutions will be studied and described, considering both the performance improvement of the components taken into consideration and the effect on the energy efficiency of the whole unit.

I1   HOW TO EVALUATE THE EFFICIENCY OF A HVAC&R SYSTEM

I1.1   Efficiency at rating conditions

The efficiency of a refrigeration unit is traditionally evaluated using the EER (Energy Efficiency Ratio) index, defined as:

$$EER = \frac{Q_e}{P + \sum P_{aux}} \tag{1}$$

Where Q_e is the evaporator capacity, P is the compressor power and P_{aux} is the consumption power of the auxiliary devices.

The efficiency of a heat pump unit is traditionally evaluated using the COP (Coefficient of performance) index, defined as

$$COP = \frac{Q_c}{P + \sum P_{aux}} \tag{2}$$

Where Q_c is the condenser capacity, P is the compressor power and P_{aux} is the consumption power of the auxiliary devices.

Eurovent introduced an energy classification of the cooling units (see Figure I.1). The classification follows the A to G approach used in the European Energy Label for House hold appliances, but the thresholds between classes have been defined for the existing chillers as listed in the Eurovent directory.

EER Class	Air Cooled	Water cooled	Remote condenser
A	EER ≥ 3.1	EER ≥ 5.05	> = 3,55
B	2,9 ≤ EER< 3,1	4,65 ≤ EER < 5,05	3,4 ≤ EER <3,55
C	2,7 ≤ EER< 2,9	4,25 ≤ EER < 4,65	3,25 ≤ EER <3,4
D	2,5 ≤ EER< 2,7	3,85 ≤ EER < 4,25	3,1 ≤ EER <3,25
E	2,3 ≤ EER< 2,5	3,45 ≤ EER < 3,85	2,95 ≤ EER <3,1
F	2,1 ≤ EER< 2,3	3,05 ≤ EER < 3,45	2,8 ≤ EER <2,95
G	< 2,1	< 3,05	< 2,8

Figure I.1: Chiller energy classification in cooling mode (Saheb et al., 2006)

According to this classification, the distribution of the Eurovent certified chillers is resumed in Figure I.2; it is worth noticing that 7% of certified chillers are in Eurovent class A and only 5% of certified chillers are in Eurovent class G.

Class/kW	0-50	50-100	100-150	150-200	200-500	500-1 000	>1000	Total
A	85	12	4	7	72	85	115	380
B	114	51	46	21	142	179	112	665
C	203	75	76	40	206	229	137	966
D	244	143	106	80	295	213	80	1 161
E	383	131	121	84	432	246	98	1 495
F	287	62	54	52	125	68	29	677
G	152	14	10	8	41	31	19	275
Total	1 468	488	417	292	1 313	1 051	590	5 619

Figure I.2: Distribution of Eurovent certified chillers (Saheb et al., 2006)

These coefficients give an evaluation of the whole system but they can not provide any information on the different components of the cycle. In addition, they are usually calculated at rating conditions, so they can not describe the behaviour of the system under different part load conditions.

There are different ways to evaluate the efficiency of the cycle components; the most common ones are defined in the follow.

I1.1.1 Compressors

Volumetric efficiency

The volumetric efficiency is the ratio (or percentage) of volume of fluid actually entering the cylinder during suction to the actual capacity of the cylinder under static conditions. For non-reciprocating compressors, the volumetric flow rate has to be known. The efficiency is defined as:

$$\eta_{vol} = \frac{\dot{m}}{V_{cyl} \cdot \frac{RPM}{60} \cdot \rho_{suc}} = \frac{\dot{m}}{\dot{V} \cdot \rho_{suc}} \qquad (3)$$

where $\dot{m}$ is the fluid mass flow [kg/s];

V_{cyl} is the cylinder internal volume [m^3];

$\dot{V}$ is the volumetric flow rate [m^3/s];

RPM is the rotation speed [min^{-1}];

ρ_{suc} is the suction vapour density [kg/m^3].

Isentropic efficiency

It considers the entropy losses during the compression process. It is the ratio of the isentropic enthalpy difference to the effective enthalpy difference.

$$\eta_{is} = \frac{\Delta h_{isoentropic}}{\Delta h_{real}} \qquad (4)$$

where $\Delta h_{isentropic} = h_{discharge,isentropic} - h_{suction}$ [J/kg];

$\Delta h_{real} = h_{discharge} - h_{suction}$ [J/kg].

Mechanical efficiency

It considers the mechanical losses of the compressor. It is defined as

$$\eta_{mech} = \frac{\dot{m}\Delta h_{real}}{P_{shaft}} \qquad \text{compressor mechanical efficiency} \qquad (5)$$

where P_{shaft} is the shaft power [W].

The above equation gives the actual mechanical efficiency of the compressor. Nevertheless, often it is not possible or easy to measure the compressor shaft power (for example, in a hermetic compressor). In this case, only the electric power, consumed by the compressor and its motor, is measured. Thus, there can be a different definition of mechanical efficiency, which accounts for mechanical losses in the compressor and in the motor.

$$\eta_{c+m,mech} = \frac{\dot{m}\Delta h_{real}}{P_{electic}} \qquad \text{compressor + motor mechanical efficiency} \qquad (6)$$

where $P_{electic}$ is the electric power [W].

The motor efficiency can be defined as:

$$\eta_{motor} = \frac{P_{shaft}}{P_{electic}} \qquad \text{motor mechanical efficiency} \qquad (7)$$

yielding

$$\eta_{c+m,mech} = \eta_{mech} \cdot \eta_{motor} \qquad (8)$$

Overall isentropic efficiency

It considers both mechanical and entropic losses of the compressor. It is defined as:

$$\eta_{shaft,\ ov\ is} = \frac{\dot{m}\Delta h_{isoentropic}}{P_{shaft}} \qquad \text{compressor overall isentropic efficiency} \qquad (9)$$

The mechanical efficiency can also be accounted for in the definition:

$$\eta_{overall,\ is} = \frac{\dot{m}\Delta h_{isoentropic}}{P_{electric}} \qquad \text{overall isentropic efficiency} \qquad (10)$$

Furthermore

$$\eta_{shaft,\ ov\ is} = \eta_{mech} \cdot \eta_{is} \qquad (11)$$

$$\eta_{overall,\ is} = \eta_{c+m,mech} \cdot \eta_{is} \qquad (12)$$

Because of their ease of measure, the volumetric (3) and overall isentropic (9) efficiencies are the most commonly used parameters to define the performance of a compressor.

II.1.2 Heat exchangers

The evaluation of the performance of the cycle heat exchangers (condenser, evaporator, internal heat exchanger) is more complex than for the compressor; it is possible to point out two different ways, which correspond to the two most common methods to design and to verify a heat exchanger.

Heat transfer coefficient (LMTD method)
The heat exchange can be defined as:

$$Q = K \cdot A \cdot \left(\Delta t_{ml} \right)_{cc} \cdot F_t \tag{13}$$

Where: K: heat transfer coefficient $[Wm^{-2}K^{-1}]$
     A: total heat transfer area $[m^2]$
     $(\Delta t_{ml})_{cc}$:log mean temperature difference (LMTD) for counter-current configuration [K]
     F_t: temperature factor [-]

According to this method, the heat transfer coefficient K can define the performance of a heat exchanger. Nevertheless, some further considerations should be made to properly understand the heat transfer mechanism in the heat exchanger. The global heat transfer coefficient KA describes how the heat is exchanged from one fluid to the other; if the KA value is higher (for the same heat exchanged), the LMTD is lower and the heat transfer is more homogenous. The heat transfer coefficient K evaluates the quality of the heat transfer and it depends on the properties of the fluids and of the materials. Actually, its value is commonly calculated (from equation (13)) using the total heat transfer area of the heat exchanger, not the "actual activated" heat transfer area. This discrepancy can be remarkable if the distribution of the refrigerant is not homogenous inside the heat exchanger, for example in the micro- or minichannel heat exchangers. In this case, K is an "overall" value and it depends also on the way the heat exchanger surface is "exploited" by the refrigerant.

Effectiveness (ε-NTU method)

The effectiveness of a heat exchanger can be defined as:

$$\varepsilon = \frac{Q}{Q_{max}} = \frac{\left|(t_i - t_o)_{max}\right|}{t_i' - t_i''} \qquad (14)$$

Where: Q: heat exchanged [W]

t: temperature [K]

i: inlet

o: outlet

t_i': inlet temperature of the hot fluid

t_i'': inlet temperature of the cold fluid

In this way, a non-dimensional parameter to evaluate the performance of a heat exchanger is provided. It is not affected by the area, so its value takes into account the "actual activated" heat transfer area; thus the shape of its curve, during a test where the conditions may change (for example, in a test on an evaporator in frosting conditions) is the same of the KA value.

I1.2   Efficiency at part load ratios

All the indexes of the previous paragraph represent the performance of the unit at rating conditions and they not describe the behaviour of the equipment over a season. Two different systems, with the same efficiency under design conditions, can provide unequal performances under different conditions. This consideration led the HVAC&R researchers to revise the traditional design rules, taking into account new solutions which may give poor improvements under design conditions, but which can increase the efficiency at part load ratios. Thus the need of new indexes which can describe the behaviour of the unit under the actual running conditions.

For the refrigeration unit, the most common indexes are three:

-   IPLV (Integrated Part Load Value), developed by ARI STANDARD

(North America);

- EMPE (Efficienza Media Ponderata in regime Estivo), presented by Bacigalupo *et al.* (2000) for AICARR; it is an adaptation to the Italian climate of the IPLV;
- ESEER (European Seasonal EER), developed by CEN, (Europe)

The need of a similar index for heat pump units led to an update of these parameters. The CEN (European Committee for Standardization) presented a new standard (prEN 14825:2009). It defines the following indexes:

- SEERon: the ratio of the total amount of heat removed, expressed in Wh, by a unit during the annual cooling operation to the total effective electric energy consumed during the same period, expressed in Wh.
- SCOPon: the ratio of the total amount of heat supplied, expressed in Wh, by a unit during the annual heating operation to the total effective electric energy consumed during the same period, expressed in Wh.

They are calculated by the following formulae:

$$SEERon = \frac{EER_A \cdot A + EER_B \cdot B + EER_C \cdot C + EER_D \cdot D}{100} \tag{15}$$

Where A, B, C, D are the weighting factors affecting the part load EER values and EER_A, EER_B, EER_C and EER_D are the EER values determined for the corresponding part load ratio at the defined temperature conditions.

The weighting factors for SEERon calculation are reported in Table I.1; the temperature conditions are described in the prEN 14825:2009 These values represent the average conditions of use in Europe.

	Part load ratio	Weighting factors
A	100%	4%
B	75%	26%
C	50%	40%
D	25%	30%

Table I.1: Weighting factors for SEERon calculation (prEN 14825, 2009)

$$SCOPon = \frac{100}{\dfrac{A}{COP_A} + \dfrac{B}{COP_B} + \dfrac{C}{COP_C} + \dfrac{D}{COP_D}} \qquad (16)$$

Where A, B, C, D are the weighting factors affecting the part load COP values and COP_A, COP_B, COP_C and COP_D are the COP values determined for the corresponding part load ratio at the defined temperature conditions.

	Part load ratio	Weighting factors
A	100%	50%
B	55%	22%
C	155%	24%
D	20%	4%

Table I.2: Weighting factors for SCOPon calculation (prEN 14825, 2009)

The weighting factors for SCOPon calculation are reported in Table I.2; the temperature conditions are described in the prEN 14825:2009. These values represent the average conditions of use in Europe.

It is worth to notice that, especially for the refrigeration unit, the seasonal efficiency can strongly differ from the full load one, being the weighting factor very low (4%); in this case, the traditional way to compare a refrigerating unit, using the EER, can lead to remarkable errors. For the heat pump, the weighting factor for full load conditions in the highest one, so the error in evaluating a heat pump unit using the traditional COP index is lower than the one for the refrigeration systems.

I2 HOW TO IMPROVE THE EFFICIENCY OF A HVAC&R SYSTEM

The factors which affect the energy efficiency of HVAC&R systems can be resumed in the following points:
- ➢ the refrigerant;
- ➢ the components of the refrigerant units;
- ➢ the cycle configuration;
- ➢ the management of the system;

These factors depend on the design and the development of the unit; actually, in real systems, one more aspect has to be considered:
- ➢ the inertia of the hydraulic circuit

These factors can affect the HVAC&R system energy efficiency at rating conditions or/and at part load ratio. In the present work, the different solutions to improve the energy efficiency will be categorized according to this aspect. On the contrary, in the Introduction the subject is dealt with in a general way and the factors are classified according to the points abovementioned at the beginning of the present paragraph.

I2.1 The refrigerant

The choice of the refrigerant is an important aspect of the unit and it affects the design of the components. Only a small number of fluids presents interesting properties as refrigerant and different applications can require different refrigerants. The most interesting properties for a refrigerant are the thermal conductivity, the specific heat, the volumetric refrigerating effect and the critical pressure. In addition, the current laws are more and more strict concerning the environmental problems. The Montreal Protocol (1987) and the Kyoto Protocol (1997) established that fluids responsible for the depletion of the ozone layer and for the global warming shall be banned. Thus, a large number of traditional halogenated refrigerant is now forbidden, because of their high values of ODP (Ozone Depletion Potential) or/and GWP (Global Warming Potential). Therefore, it implies two major effects; first, the choice of a refrigerant is made not only considering its energy efficiency but, above all, taking into account the

current (and incoming) environmental standards. As pointed out by Fornasieri (2002), this choice is still an open issue because it is difficult to quantify the environmental standard levels. Secondly, the HVAC&R researcher challenge is to find new energy solutions, that is to find new suitable refrigerants or to modify the traditional plants in order to achieve higher performance using allowable (but less efficient) fluids.

At the moment, the most important issue is the phase-out of R22; particularly, the interest is addressed to those fluids which allow a substitution of the refrigerant, without plant modifications ("drop in"). The mixture R407C is a common substitute, but R410A and R134a represent long-term solutions; another alternative can be natural refrigerants: ammonia (R717), propane (R290) and carbon dioxide (R744).

Vio (2006) and Fornasieri (2002) present some methods to compare the energy efficiency of different fluids; this comparison can be carried out considering:

- the basic ideal cycle;
- the exergy losses in a real system;
- aspects related to the compressor.

I2.1.1 The basic ideal cycle

The basic index to compare different refrigerants is the EER (or COP) of the basic ideal cycle.

fluido	massa mol.	t. critica [°C]	p.e.n. (glide) [°C]	p. cond.(*) [bar]	p. evap. (*) [bar]	COP
R22	86,47	96,2	-40,8	15,34	1,64	6,12
R717	17,03	133,0	-33,3	15,55	1,19	6,40
R407C R32/125/134a (23/25/52)	86,20	86,7	-40,2 (6,9)	16,49	1,54	5,93
R410A R32/125 (50/50)	72,58	72,5	-51,4 (<0,1)	24,28	2,73	5,79
R290	44,10	96,8	-42,1	13,69	1,68	5,97
R134a	102,03	101,1	-26,1	10,16	3,26	6,09
R744	44.01	31.06	-87.9	-	37,66	-

Figure I.3: Properties of different refrigerants for a basic ideal cycle -3/-40 °C (Fornasieri, 2002)

According to Fornasieri (2002), this value is mainly affected by the refrigerant

XVIII

critical pressure (fluids with higher critical pressure present higher energy efficiency) and the liquid specific heat (fluids with lower specific heat present higher energy efficiency; this value depends on the molar mass, in the same way). These properties are resumed in Figure I.3, for a basic ideal cycle between the temperatures +3/+40 °C. According to this analysis, the most efficient fluids which can replace R22 are R134a and R717.

I2.1.2 The exergy losses in a real system

The exergy losses in a real system are represent by:
- pressure drops in the pipes;
- compression losses;
- heat transfer losses;

The exergy losses related to the pressure drops in the pipes can be evaluated using the penalty factor introduced in Casson *et al.* (2001)

$$F_P = \frac{1}{\Delta h_{ev}{}^3 \rho_{out,ev}{}^2} \tag{17}$$

where Δh_{ev} is the enthalpy difference at the evaporator and $\rho_{out,ev}$ is the density at the evaporator outlet. The exergy losses related to the compression process depends on several factors; according to Fornasieri (2002), fluids with high operative pressure present a higher exergy efficiency. As regards the exergy losses related to heat transfer, the liquid thermal conductivity λ_l and the vapour density ρ_v are properties which affect the efficiency. The parameters of interest are reported in Figure I.4; they are calculated at the temperature of 3°C. According to these considerations, the mixture R410A presents the most interesting properties, while, for ammonia, the high value of liquid thermal conductivity should overcome the poor properties related to pressure drop.

fluido	F_p [(kg m^6)/J^3]	λ_l [W/(m K)]	ρ_v [kg/m^3]	p_{ev} [bar]
R22	$4{,}91 \ 10^{-19}$	0,0953	23,5	5,48
R717	$0{,}548 \ 10^{-19}$	0,517	3,84	4,80
R407C R32/125/134a (23/25/52)	$4{,}68 \ 10^{-19}$	0,104	23,33	5,52
R410A R32/125 (50/50)	$2{,}16 \ 10^{-19}$	0,114	33,19	8,84
R290	$3{,}98 \ 10^{-19}$	0,105	11,31	5,19
R134a	$13{,}07 \ 10^{-19}$	0,0924	16,00	3,26
R744	-	0.107	107,05	37,66

Figure I.3: Properties which affect the exergy losses in a real cycle, at 3°C (Fornasieri, 2002)

I2.1.3 Aspects related to the compressor

The volumetric cooling effect is the heat flow at the evaporator per unit of refrigerant volume sucked by the compressor; it is defined by the following equation

$$Q_{0v} = \frac{\Delta h_{ev}}{v_{out,ev}} \tag{18}$$

where Δh_{ev} is the enthalpy difference at the evaporator and $v_{out,ev}$ is the specific volume at the evaporator outlet. Other parameters to consider are the discharge temperature and the attitude of a refrigerant to cool the compressor electric engine. In the first case, the discharge temperature is important to highlight the fluids which can have problems with oil (carbonization). The attitude of a refrigerant to cool the compressor engine is defined by the index I_r of equation (19), as suggest by Fornasieri (2002).

$$I_r = \frac{cp}{\Delta h_{comp}} \tag{19}$$

Where cp is the specific heat and Δh_{comp} is the enthalpy difference at the compressor. These parameters are reported in Figure I.5, for a basic ideal cycle between the temperatures +3/+40 °C.

fluido	Q_{0v} [kJ/m³]	t_{fc} [°C]	l_r [°C^{-1}]	p. cond. [bar]
R22	3632	56,0	0,0307	15,34
R717	4124	87,5	0,0162	15,55
R407C R32/125/134a (23/25/52)	3680	53,2	0,0354	16,49
R410A R32/125 (50/50)	5353	56,2	0,0371	24,28
R290	3052	43,8	0,0399	13,69
R134a	2304	44,0	0,0379	10,16
R744	-	-	-	-

Figure I.3: Properties which affect the exergy losses in the compression process, for a basic ideal cycle -3/-40 °C (Fornasieri, 2002)

I2.2   The components of the refrigerant unit

I2.2.1 Compressors

Until some years ago, reciprocating compressors were the most common in HVAC&R applications, with centrifugal compressors (for high power) and rolling piston compressors (for small size applications). At the moment, screw and scroll compressors are replacing the reciprocating ones in several applications. Fornasieri (2002) and Vio (2006) make some consideration on the use of these compressors and reported some isentropic efficiency curves. This analysis is the subject of Chapter 1.1.

The behaviour of the compressors at part load ratio is essential to evaluate the seasonal energy efficiency of an unit. On other hand, the consciousness of this fact by the compressor manufacturers and users is still low and numerical data are scarce.

Reciprocating compressors.

For reciprocating compressors, Fornasieri (2002) suggests three methods for capacity control: by a valve lifter, by an external by-pass and by the suction blocking. In recent years, compressors with inverter, i.e. able to vary the rotational speed, are spreading in the market, as a consequence of lowering of electrical components prices.

Scroll compressors

Scroll compressors are usually used in multi-compressors units (see Chapter 2.1)

and the capacity control is performed switching on/off the single compressor. In recent years, scroll compressors manufacturers introduced different methods to control the capacity; the last one is the control of the rotational speed by inverter.

Screw compressors

Screw compressors are not usually set up on tandem unit, thus the capacity control is performed in the single compressor. A traditional method consists is a movable slide valve that connects the last compression chambers to the suction, creating a by-pass. The penalization at low part loads is remarkable, as shown in Figure 1.1.5. Recently, the capacity control by inverter has been introduced, improving the efficiency at low part load ratios.

I2.2.2 Condensers

In chiller units, the most common condenser is an air-to-refrigerant finned coil; to improve the heat transfer, several modifications of the geometry have been introduced, both air and refrigerant side. On other hand, these solutions can increase the fan power consumption: to have a fair comparison between different geometries, the "Area Goodness Factor Comparison" method should be used, as suggested by Fornasieri (2002). For each geometry, the heat transfer coefficient is plotted against the fan mechanical power per unit of heat exchange area, at different face air velocity.

An important aspect is the optimization of the refrigerant path in the condenser; the counter-current configuration is more efficient, being in the condenser region for desuperheating and subcooling. Particularly, the control of the subcooling is an important issue: the increasing of the refrigeration capacity could compensate the added compression work, due to the higher condensation pressure. Thus a part of the condenser is "flooded" and it is allotted to liquid subcooling. However Fornasieri (2002) suggests the use of an intermediate fluid separator, to share the two-phase and the subcooling regions.

I2.2.3 Evaporators

In chiller units, at the moment the most common evaporator is the plate heat exchanger, while for a long time the most common one was the shell-and-tube. On other hand, in heat pump applications evaporators can be water-to-refrigerant (for geothermal applications) or air-to-refrigerant (in air cooled units). The most

important issues are the distribution of the refrigerant, which enters two-phase the heat exchanger, and the moisture drainage, in air-to-refrigerant evaporators. Solutions to overcome these two points are the most studied and dealt with in the literature.

I2.3   The cycle configuration

The simple vapour compression inverse cycle can be modified, adding other components, in order to achieve a higher efficiency. The most common solution is the use of an internal heat exchanger, between the suction line and the liquid line at the condenser outlet. It can provide a subcooling of the liquid, increasing the evaporator capacity, and a superheating of the vapour at the compressor inlet, increasing the power consumption. An evaluation of the two opposite effects has to be made for each fluid, as suggested by Domanski *et al.* (1994). The cycle can be modified in other several ways, with staged throttling, staged compression, use of flash tank, flash valve, cascade cycle, booster, compressor with economizer, Voorhees cycle, injector and expanders, to quote some examples. Different solutions are chosen considering the application and the size of the unit; in Chapter 1.3, a theoretical study of different solutions for a carbon dioxide unit is reported. Two existing carbon dioxide plants, using both a double stage throttling and a single and double stage compression, are described in Chiarello *et al.* (2007).
A key option to reduce the energy consumption is the Free Cooling: as reported by Adnot and Waide (2003), with a very limited over cost of 2% of overall system costs, it can provide a reduction of chiller electric consumption of 20%.

I2.4   The management of the system

The management of the system is fundamental to improve the energy efficiency at part load ratio. As explained in paragraph I2.2.2, the fan power consumption can sensibly affect the EER (or the COP) of the whole unit. This influence is higher at low part loads, as pointed out by Vio (2006). Recently, the control of

the fan power consumption is gaining more interest among the HVAC&R system manufactures and users. It can be performed according to an on/off controller or using an inverter to regulate the air velocity.

In general, the management of an air conditioning or heating unit depends on the characteristics of the plant and of the controlled environment. However, a basic principle is the reduction of the difference between condensation and evaporation temperature.

Considering the condensation in chiller units, the operators usually keep the saturation temperature above a certain value, to assure a safe running of compressors and throttling valves. This operation makes sense only in case of scroll compressors and traditional thermostatic throttling valves, but it represents an absurdity from the thermodynamic point of view. A correct management of the throttling valve and a rational choice of the compressor can overcome this point. In heat pump applications, the reduction of the condensation temperature can be achieved choosing an efficient way to heat the environment, for example using a floor radiant system.

As regards evaporators, in air conditioning units the water supply temperature is usually set at 7°C, and the plant is designed to provide a water temperature difference of 5°C. The system is developed in order to supply both the sensible and the latent heat, assuring the correct temperature and humidity. At low part loads, the needed cooling capacity is considerably reduced and the water supply temperature can be increased, thus increasing the evaporation temperature. Finally, an efficient way to cool the environment should be desirable, but a radiant system can not supply the latent heat. A system with two different cooling devices (for example, radiant system and fan coils) can achieve a higher efficiency that can justify the additional expense.

I2.5   The inertia of the hydraulic circuit

The inertia of the hydraulic circuit is an external factor of the unit, but it can sensibly affect the energy efficiency, especially at part load ratios. As explained in Vio (2006), the quantity of water in the circuit determines the number of start-ups of the compressor(s). If the water quantity is too low, the number of start-

ups is high and it can imply an energy penalization of the system.

I3 REFERENCES

1. Adnot J., Waide P., (2003), Energy Efficiency and Certification of Central Air Conditioners (EECCAC), *Final Report*, Vol. 3.
2. Bacigalupo E., Vecchio C., Vio M., Vizzotto M., (2000), L'efficienza media ponderata dei gruppi frigoriferi a compressione: la proposta AICARR per un metodo di calcolo, *Convegno AICARR "Condizionamento, ventilazione e contaminazione ambientale, riscaldamento, refrigerazione: innovazioni e tendenze"*.
3. Casson V., Cecchinato L., Fornasieri E. (2001), Quale fluido per quale impianto: un esame ragionato dei requisiti e delle caratterizzazioni dei fluidi frigorigeni, *Il Freddo*, 5/01: 37-45.
4. CEN TC113/WG7, prEN 14825, (2009), Air conditioners, liquid chilling packages and heat pumps, with electrically driven compressors, for space heating and cooling – Testing and rating at part load conditions, European Committee for Standardization CEN.
5. Chiarello M., Del Col D., (2007), Design rules for optimisation of heat exchangers to be used with natural working fluids, *Deliverable D12, COLL-CT-2004-500229* SHERHPA.
6. Chiarello M., Fornasieri E., Minetto S., Zilio C., (2007), Recent developments in commercial refrigeration systems using CO_2 as the refrigerant, *IIR Int. Conf.*,
7. Domanski P. A., Didion D. A., Doyle J. P., (1994), Evaluation of suction-line/liquid-line heat exchange in the refrigeration cycle, *Int. J. Refrigeration,* 17(7): 487-493.
8. Fornasieri E. (2002), Refrigeratori d'acqua con compressore volumetrico: come promuovere l'efficienza energetica, *43° Convegno annuale AICARR*, 3: 17-46.
9. Kyoto protocol to the United Nations framework convention on climate change, (1997), *United Nations*.
10. Montreal Protocol on Substances that Deplete the Ozone Layer, (1987),

United Nations.

11. Saheb Y., Becirspahic S., Simon J., (2006), Effect of the certification on chiller energy efficiency, *5th Int. Conf. IEECB*.

12. Vio M., (2006), Air-water chillers energetic performances at full and partial load, *Proc. of AICARR Conf.*, First session, 113-159.

PART 1   EFFICIENCY AT RATING CONDITIONS

In this part, the subject of the energy efficiency is faced considering the system at rating conditions. This approach can not give any information on the seasonal energy consumption of a system, but it is useful in the optimization of the cycle configuration or of the single component.

The effect of the compressor is studied in Chapter 1.1, just considering compressors for natural fluids. In Chapter 1.2, the effect of the refrigerant is highlighted: a comparison between different fluids, under different rating conditions, is performed. The cycle configuration importance is pointed out in Chapter 1.3, theoretically analyzing the energy performance of different carbon dioxide kinds of cycle. In Chapter 1.4, the effect of the heat transfer area is investigated; the objective is to find the limit for energy increase, increasing the heat transfer area of condensers and evaporators. The use of minichannel heat exchangers is analyzed in Chapter 1.5, 1.6 and 1.7. Chapter 1.5 is a review concerning technological constrains in use of minichannel heat exchangers. In Chapter 1.6, performances of minichannel condensers are studied. In Chapter 1.7, some preliminary studies on the use of minichannel evaporators are presented.

**Chapter 1.1   Review on natural fluid compressor efficiency:
SHERHPA project**

This work had been prepared in the framework of the European project SHERHPA, which had the objective of increasing the knowledge in the use of natural fluids, mainly on heat pump applications. The present work is the subject of a paper (Cavallini A., Chiarello M., Del Col D., Zilio C., (2007), Compressors for natural refrigerants: state-of-the-art review, *22nd IIR Int. Conf. of Refrig,* ICR07-B1-1065, 1-8), translated by S. Bobbo for the Italian magazine "Il freddo", n. 5, October 2009.

1.1.1   Introduction

After the Montreal protocol in 1987 sanctioned the phase out of CFCs and HCFCs, the group of suitable refrigerants was reduced to hydrofluorocarbons (HFCs) and natural refrigerants. Although HFCs were adopted as a good alternative because of their null Ozone Depletion Potential, their Global Warming Potential can be high and thus some HFCs are included in the list of fluids whose production has to be reduced in the next years. As a sound alternative, natural refrigerants are more and more looked at as the most feasible long term solution, because their effects on the environment are perfectly known since they have been in the atmosphere for a long time so far.

Among the alternatives, carbon dioxide, ammonia and hydrocarbons are the most considered. Regarding CO_2, it has the disadvantage of working at very high pressure and this requires a complete redesign of the existing system. Nevertheless, the interest for the use of carbon dioxide as refrigerant is confirmed by the high number of papers presented or published in the last years on carbon dioxide systems and components. In the present work, the most updated advancements on CO_2 compressors are reviewed, as reported in more than 50 references on this subject. Reciprocating compressors, axial piston compressors and rotary compressors are considered and their efficiencies are compared.

In the case of ammonia, since ammonia compressors are easily available on the market, the work focuses on the two most common types, open reciprocating and screw ones.

Although recent results show that scroll compressors are more efficient, only reciprocating compressors are available at the moment for propane. Among hydrocarbons, propane is the most suitable refrigerant for heat pump and refrigerating applications.

1.1.2   Refrigerant properties

By knowing the main properties of each fluid, it is possible to evaluate the energy efficiency of a theoretical cycle; on the other hand, for the selection of the right compressor, the main drawbacks and risks, implied by the choice of a certain fluid, should take into account. Particularly, the attention is focussed on the problems of oil and safety (toxicity and flammability).

To evaluate the energy efficiency of the cycle, these properties must be considered:

- Energy Efficiency Ratio of an ideal cycle (EERid).
- Pressure losses along the fluid path. The pressure drops in the heat exchangers are counted as "saturation temperature losses". They are quantified by the Penalty Factor, proposed by Cavallini (2002).
- Heat exchange attitude; it defines the heat exchange performance, but it is not quantified by a single parameter. Several variables are needed; the most important are:
    a) Liquid thermal conductivity λ_L .
    b) Suction vapour density ρ_V.
    c) Working pressure (evaporation pressure is considered).

In addition, to evaluate the efficiency of the compression process, other parameters are important:

- Volumetric refrigerating effect; it is defined as:

$$Q_V = \frac{\Delta h_{ev}}{v} \qquad (1)$$

where: Δh_{ev}: enthalpy difference between the evaporator inlet and outlet [J/kg];

v: suction specific volume [m^3kg^{-1}].

A high volumetric refrigerating effect is usually a favourable feature. However, in the case of centrifugal compressors, a high value of Q_V may be a problem due to the compactness of the impeller.

- Discharge temperature; it must not be too high, to prevent oil carbonisation and damage of compressor components.

Some of these properties are reported in Tables 1.1.2, 1.1.4 and 1.1.6, with those of two of the most common refrigerants, R22 and R134a; they are calculated using REFPROP 8.0 by NIST (2007). The cycle temperatures were chosen according to the EN 12900 (1999) for mean evaporation temperature applications, except for carbon dioxide.

Besides these properties, it is important to consider the behaviour of these fluids with oil, in order to assure a reliable lubrication of compressors; the most important property which identifies the optimal lubricant for a given refrigerant is solubility. For heat pump and refrigeration systems, good solubility is usually desirable to obtain efficient oil return rate and to avoid heat transfer degradation. If a refrigerant has good solubility with a lubricant, there are not problems of oil circulation and the accumulation of oil in the lowest points of the rig is avoided. Thus, to assure adequate compressor lubrication, piping must be designed to promote an uniform oil movement through the system and back to the compressor. On the other hand, under certain conditions (low oil temperatures and high pressures) high solubility can lead to a decrease of viscosity. In this case, it may be necessary to choose a lubricant with lower solubility or to increase viscosity. In addition, high miscibility may affect heat transfer properties of a refrigerant, penalizing the efficiency of evaporators and condensers (or gas-coolers).

On the contrary, if lubricants are not soluble in the refrigerant, oil circulation must be considered in a different way; an oil separator, after the compressor, is needed, to keep oil and to send it to the crankcase. Nevertheless, a certain amount of oil is drawn by the refrigerant and it collects in the lowest points of the rig. It must be removed periodically, and this implies high running costs and a dedicated staff.

1.1.2.1 Ammonia (R717) properties

Ammonia presents interesting thermodynamic properties: the theoretical EERid and the volumetric refrigerating effect values are higher than those of the two halogenated refrigerants. On other hand, the condensation pressure and the discharge temperature are higher, especially compared to those of R134a. The normal boiling point is -33.3°C: it is recommended not to use R717 in low temperature applications, to prevent air introduction. The most important drawbacks of its use are the incompatibility with copper and its alloys, so the refrigerant cannot directly cool the compressor electrical motor and the compressors are usually open. Moreover, being ammonia toxic and flammable (ASHRAE safety group: B2), this refrigerant cannot be used in places where there are people, animals, food, etc.

Condensation temperature	45	°C
Evaporation temperature	-10	°C
Superheat	5	K
Subcooling	0	K

Table 1.1.1: Cycle temperatures for R717, for mean evaporation temperature, according to EN 12900 (1999).

	R717	R22	R134a	
EERid	3.716	3.427	3.339	-
Q_V	2.417	2.112	1.232	MPa
Evaporation pressure	0.291	0.355	0.201	MPa
Condensation pressure	1.783	1.729	1.160	MPa
Discharge temperature	131.9	80.8	61.1	°C

Table 1.1.2: Some parameters of interest for R717, R22 and R134a, at the conditions of Table 1

In conventional R717 systems, predominately mineral oils (MO) are used, partly also poly-alpha olefin (PAO) and alkyl benzene (AB). These lubricants have no solubility with R717; it is not a heavy problem since flooded evaporators are normally used. For the compressor lubrication, insolubility is an advantage, because oil dilution is avoided; oil recovery is easy, by gravity: it collects at the lowest points of the system, for example at the bottom of flooded evaporators. Recently,

automatic systems of recycling and oil return are available, allowing savings on running costs. With the new generation of compact liquid chillers and cooling units, different types of evaporators are used; thus, miscible lubricants are now necessary. A few years ago, soluble Poly alkylene glycol oils (PAG)) were developed, to use in direct expansion systems or semi-flooded evaporators; however, the practical management of PAG oils requires particular care. These oils are extraordinarily hygroscopic, a characteristic that implies corrosion problems; even with the use of special dryers, the operating experiences are not always satisfactory.

1.1.2.2 Propane (R290) properties

Propane EERid is slightly lower than the two halogenated fluids and its volumetric refrigerating effect is lower than that of R22. The operative pressures are close to those of R22, while the theoretical discharge temperature is very close to that of R134a.

It is not toxic (only light narcotic effect), but it is extremely flammable (ASHRAE safety group: A3). There is no incompatibility with any metal.

Condensation temperature	45	°C
Evaporation temperature	-10	°C
Superheat	10	K
Subcooling	0	K

Table 1.1.3: Cycle temperatures for R290, for mean evaporation temperature, according to EN 12900 (1999).

	R717	R22	R134a	
EERid	3.264	3.427	3.339	-
Q_V	1.751	2.112	1.232	MPa
Evaporation pressure	0.345	0.355	0.201	MPa
Condensation pressure	1.534	1.729	1.160	MPa
Discharge temperature	60.5	80.8	61.1	°C

Table 1.1.4: Some parameters of interest for R290, R22 and R134a, at the conditions of Table 3.

Propane has full chemical compatibility with nearly all existing lubricants that are commonly used in refrigeration systems. Good miscibility is maintained with most

lubricants under all operating conditions. Mineral oils (MO) are the most commonly used, due to their low cost and easy handling. Due to the good solubility, a high viscosity grade oil will be chosen, to avoid possible thinning at high temperatures. Also alkyl benzene (AB) and semi-synthetic (AB/M blend) oils are fully soluble and their viscosity grades are suitable for all applications. Polyolester (POE) oils have excessive solubility with hydrocarbons and it is usually necessary to higher their viscosity grade; Poly-alpha-olefins (PAO) oils are soluble with hydrocarbons, but they are commonly used only for low temperature applications. Poly alkylene glycol (PAG) oils have limited applications and poly vinyl-ether (PVE) and hydro-treated mineral oils are not suitable. Lubricants containing silicone or silicate (anti-foaming agents) are not compatible with hydrocarbons.

1.1.2.3 Carbon dioxide (R744) properties

Being the carbon dioxide critical temperature 31.06°C, a comparison considering the condensation temperature 45°C is not possible. The EN 12900 (1999) does not give any instructions regarding carbon dioxide refrigeration systems, so these comparisons are at 25°C of condensation temperature.

Condensation temperature	25	°C
Evaporation temperature	-10	°C
Superheat	10	K
Subcooling	0	K

Table 1.1.5: Cycle temperatures for R744.

	R717	R22	R134a	
EERid	4.031	6.093	6.061	-
Q_V	10.430	2.492	1.513	MPa
Evaporation pressure	2.649	0.355	0.201	MPa
Condensation pressure	6.434	1.044	0.665	MPa
Discharge temperature	67.2	53.0	39.8	°C

Table 1.1.6: Some parameters of interest for R744, R22 and R134a, at the conditions of Table 5.

These comparisons highlight the problem in the use of carbon dioxide as refrigerant: the critical temperature is very low and the operative pressures are very high. On other hand, R744 shows interesting heat transfer properties (for example, the refrigerating volumetric effect), which justify the researcher interest for these fluid, especially in specific applications. In addition, carbon dioxide is completely natural, neither toxic nor flammable (ASHRAE safety group: A1) and there is no compatibility problems with metals.

Special oils are required: PAG, PAO and POE. They are very expensive and can only be managed with difficulty, because their hygroscopicity. The behaviour of these oils with CO_2 is described by Fornasieri and Zilio (2004). A problem which is pointed out by these authors is the so-called "phase inversion". Pure oil density varies slightly with temperature, while R744 density is about 1076 kg/m^3 at -30°C and about 468 kg/m^3 at critical point. R744 floats on PAG oils at temperatures higher than -20°C. For POA oils, instead, density can be a problem; in fact POA density is lower than 850 kg/m^3, so at temperatures lower than 10°C the oil floats on R744. It means that it is impossible to recover it because oil traps are usually at the lowest point of the circuit. PAG and POE oils are more used in trans-critical cycles, even if it is important to consider high POE solubility in R744. Severe viscosity reduction possibly limits its use to low temperature cascade systems and there could be the problem of starting foaming. PAG solubility is lower, so these problems are less important; also hygroscopicity is lower.

1.1.3 Ammonia compressors

1.1.3.1 Displacement and refrigeration capacity

R717 has been used for long time as a refrigerant and ammonia compressor technology has to be regarded as a traditional one. Ammonia compressors are usually open (the semi-hermetic ones have aluminum electrical windings), not used in applications that need compact sizes and mainly used in industrial processes. On the market, there is a wide range of ammonia compressors, for different refrigerating capacities and displacements. Swept volume [m^{3}h^{-1}] and nominal refrigeration capacity data sets, taken from company web sites or from researcher

papers, have been compared in Figures 1.1.1 to 1.1.4. The difference between screw and reciprocating compressor displacement is remarkable. The reciprocating compressor swept volume can reach, at most, 3000 m^3h^{-1}, even for two-stage machines (Figure 1.1.1). Screw compressors, instead, can display a far larger swept volume, which can reach 10000 m^3h^{-1} (Figure 1.1.2). Also single-screw compressors are available on the market: they have compact dimensions and low displacement. Ammonia screw compressors can reach very high refrigeration power and there is a wide selection of models (Figure 1.1.3). Except for single-screw ones, all the models have a nominal cooling capacity higher than 100 kW; some of them go over 1000 kW. On the contrary, nominal refrigeration powers of reciprocating compressors are far lower and only few of them have a cooling capacity higher than 300 kW (Figure 1.1.4).
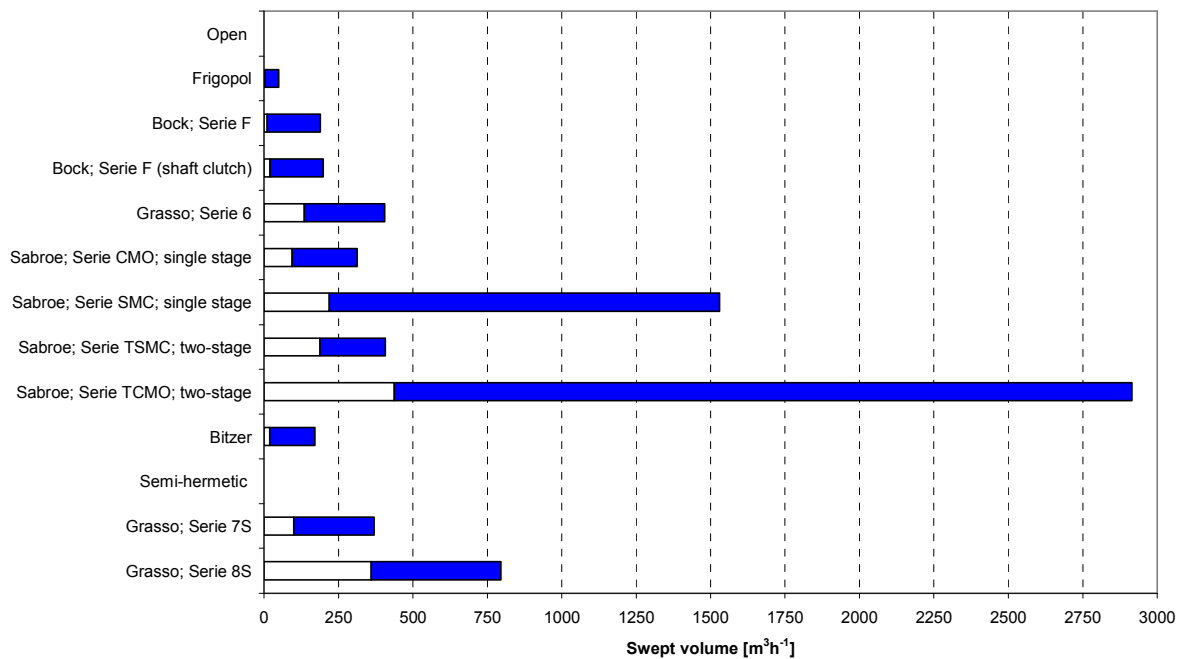
Figure 1.1.1: Ammonia reciprocating compressor swept volume
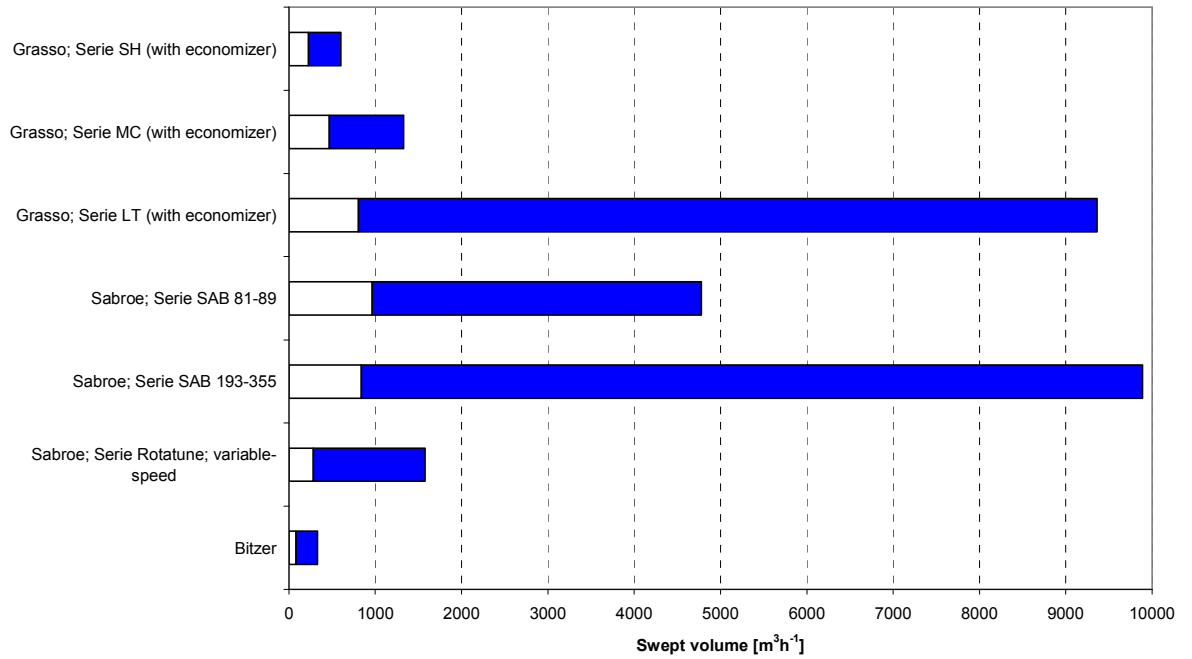
Figure 1.1.2: Ammonia screw compressor swept volume
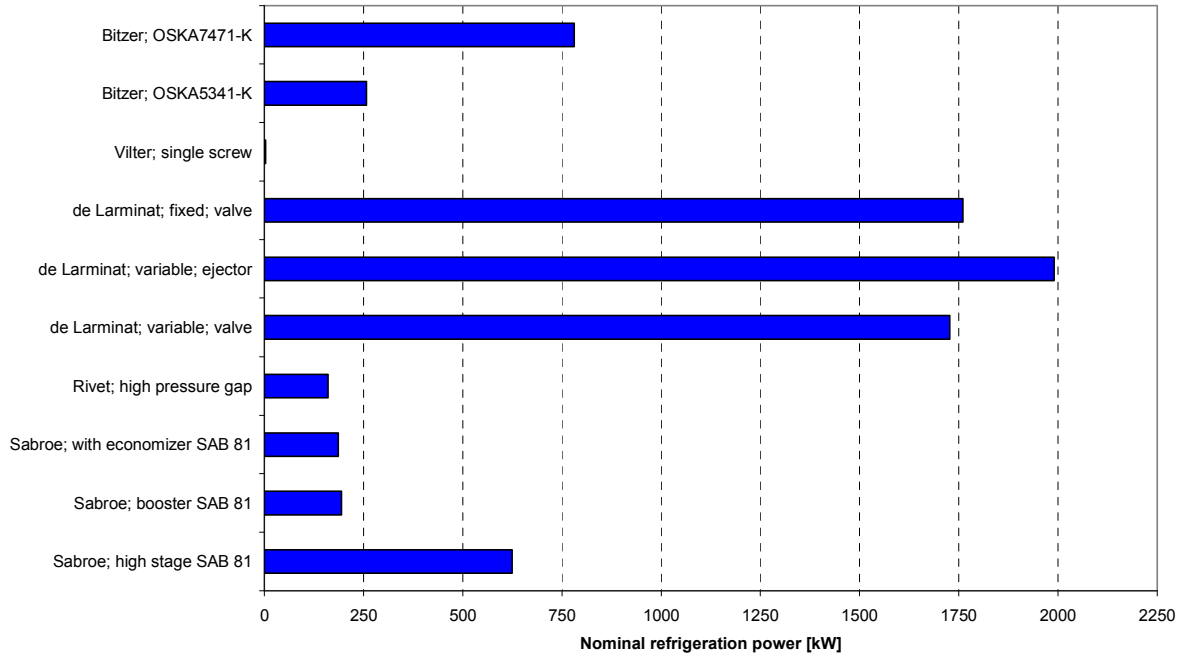
Figure 1.1.3: Ammonia screw compressor nominal refrigeration power
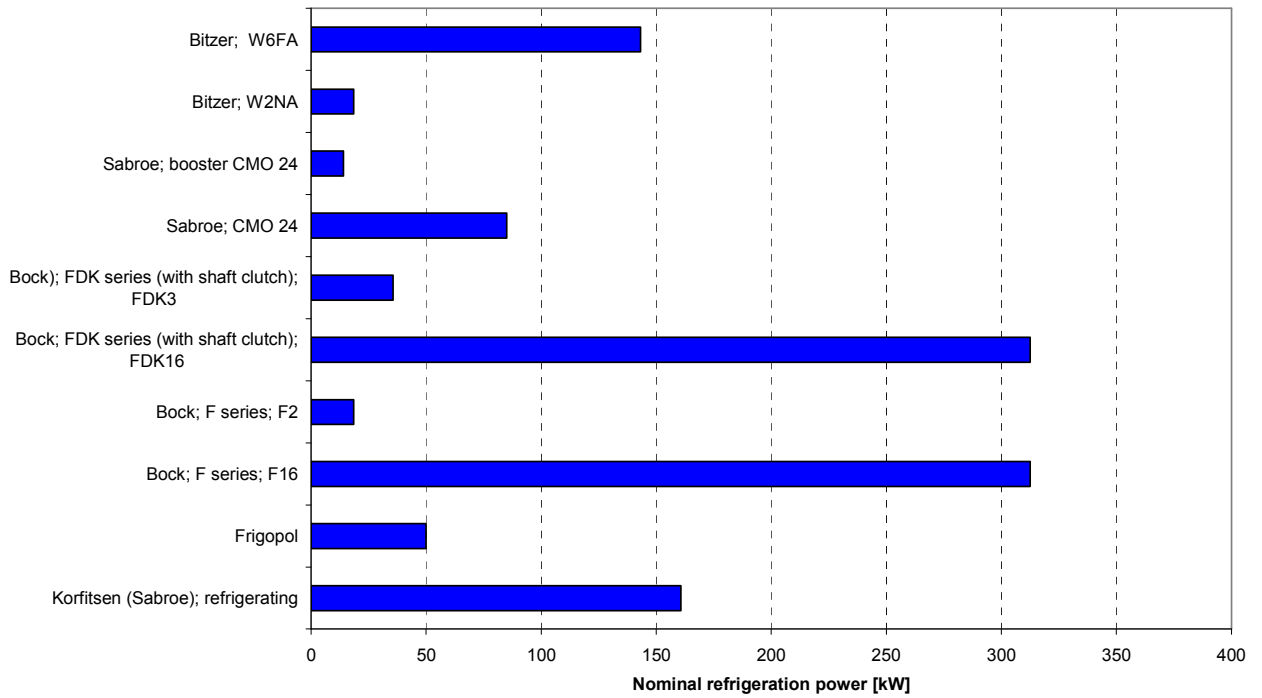
Figure 1.1.4: Ammonia reciprocating compressor nominal refrigeration power

An other important aspect to consider is the application where the compressor will be used; in fact, screw compressors efficiency fades sharply, decreasing the load ratio (Figure 1.1.5). This fact is penalizing especially in heat pump systems, where the operative conditions can widely vary.
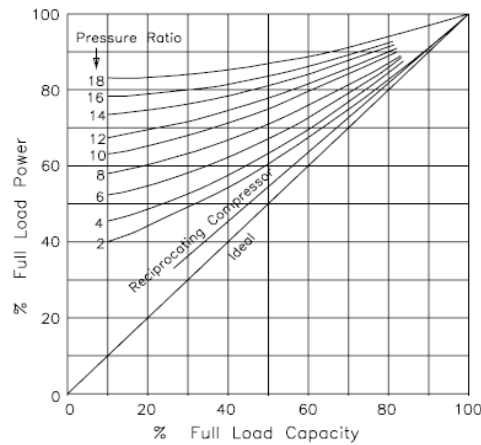
Figure 1.1.5: Ammonia compressors regulation power (Bowater, 2004)

1.1.3.2   Efficiency analysis

In the literature it is hard to find papers which report the efficiency of a single compressor; more often the EER of the whole cycle is provided.

The first data set by Bowater (2004) refers to experimental tests on a reciprocating, two-stage compressor. It is compared to data for some different screw compressors: single-stage with super-feeding, two-stage with super-feeding and single-stage without super-feeding. There are not significant differences between reciprocating and screw compressors and between systems with or without super-feeding; considerable improvements can be observed if a two-stage compressor is used instead of a single-stage one. Rivet's data points (2004) refer to screw compressors used in ammonia cascade systems. Data of Korfitsen and Kristensen (2005) are taken from experimental tests on a reciprocating compressor; it is used both in a refrigerant cycle and as a heat pump. All this data shows that the EER decreases when pressure ratio increases.
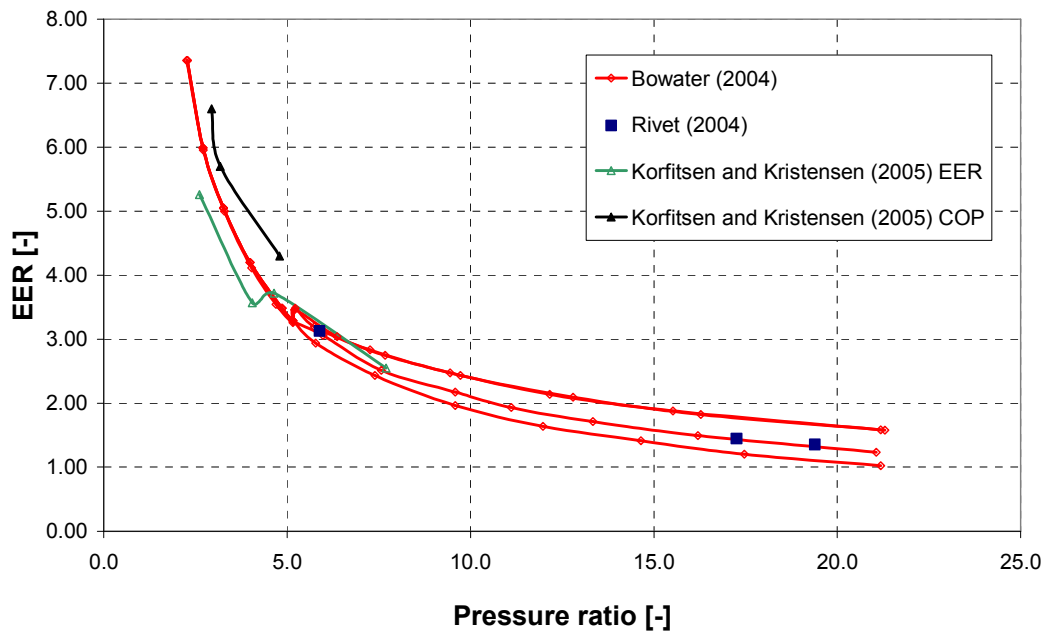
Figure 1.1.6: Ammonia compressor EER

In the market there are commercial programs that allow calculating the overall isentropic efficiency; in this analysis, Bitzer compressors, reciprocating and screw, have been chosen. The efficiency of the reciprocating compressors is higher than that of the screw ones; they are approaching at around a pressure ratio value of 5 (Figure 1.1.7). Thus some compressor models have been considered. First, reciprocating compressors have taken into consideration: it is possible to single 4 different overall isentropic efficiency curves, which are plotted in Figure 1.1.8. Curve 1 represents the overall isentropic efficiency of compressor with the following stroke x bore dimensions: 60 x 40; 60 x 57; 55 x 57 [mm]. Curve 2 is the efficiency of the compressors with dimensions 70 x 55 [mm]; Curve 3 for 75 x 55 [mm]; Curve 4 for 82 x 55 [mm]. The number of cylinder does not influence the overall isentropic efficiency, which, on the contrary, is affected by the shape of the cylinder.
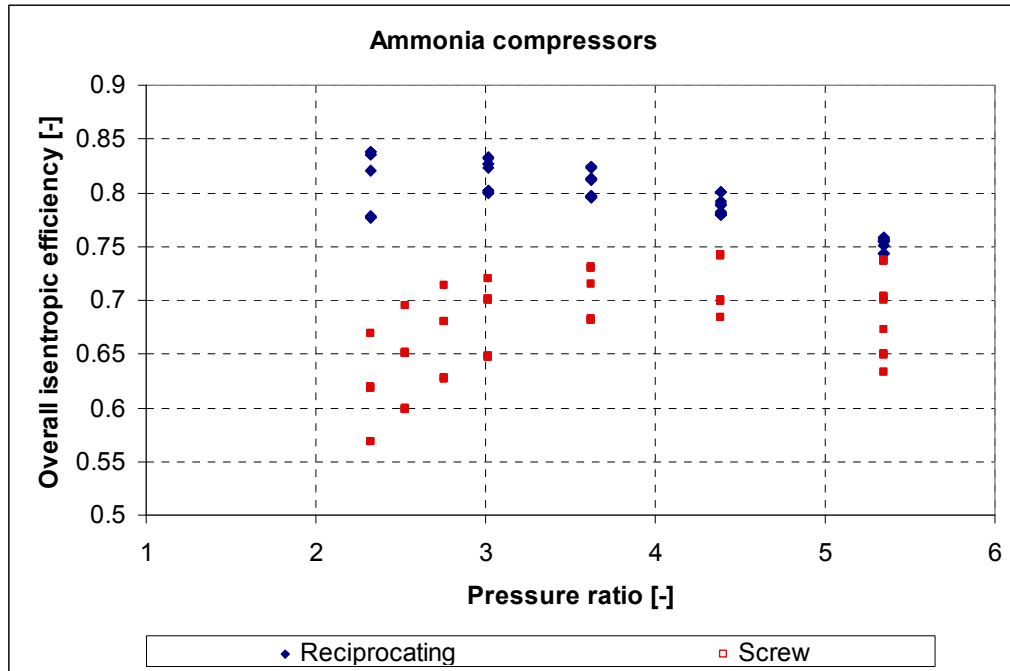
Figure 1.1.7: Bitzer ammonia compressor overall isentropic efficiency.
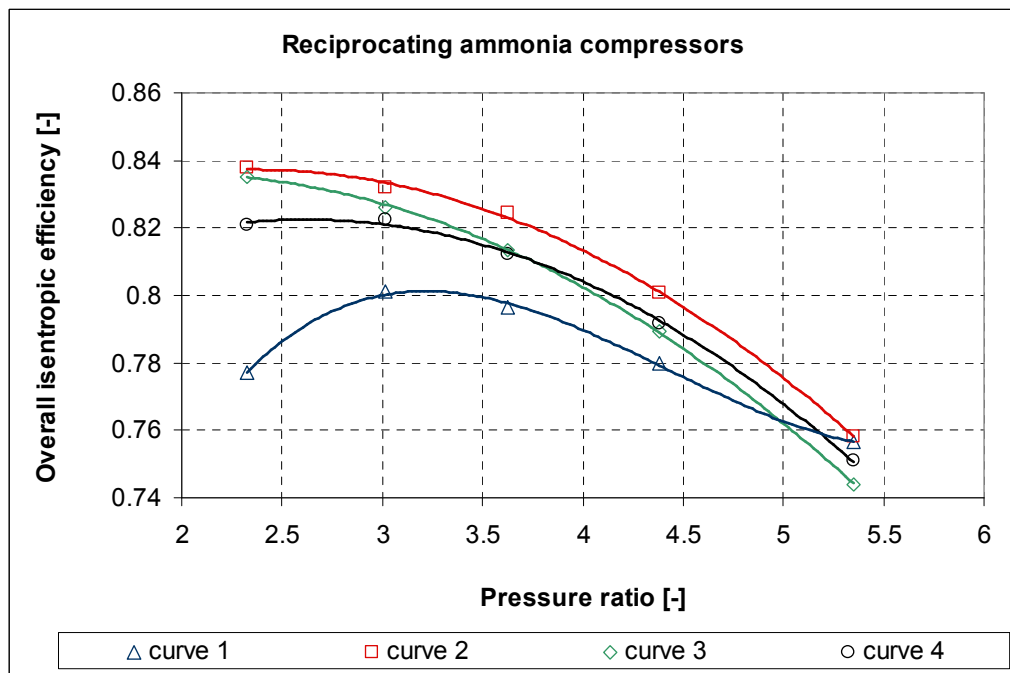
Figure 1.1.8: Bitzer ammonia reciprocating compressor overall isentropic efficiency curves

As regards the screw compressor, the overall isentropic efficiency curves of two

different compressors, at different condensation temperatures, are plotted in Figure 1.1.9. The solid lines represent a compressor with a swept volume of 84 m³/h at 2900 rpm, while the dashed lines represent a compressor with a swept volume of 192 m³/h at 2900 rpm. The bigger compressor has a higher efficiency, while the condensation pressure does not affect noticeably the efficiency. The curves are flat in this pressure range, but the efficiency decreases sharply at higher compression ratios.
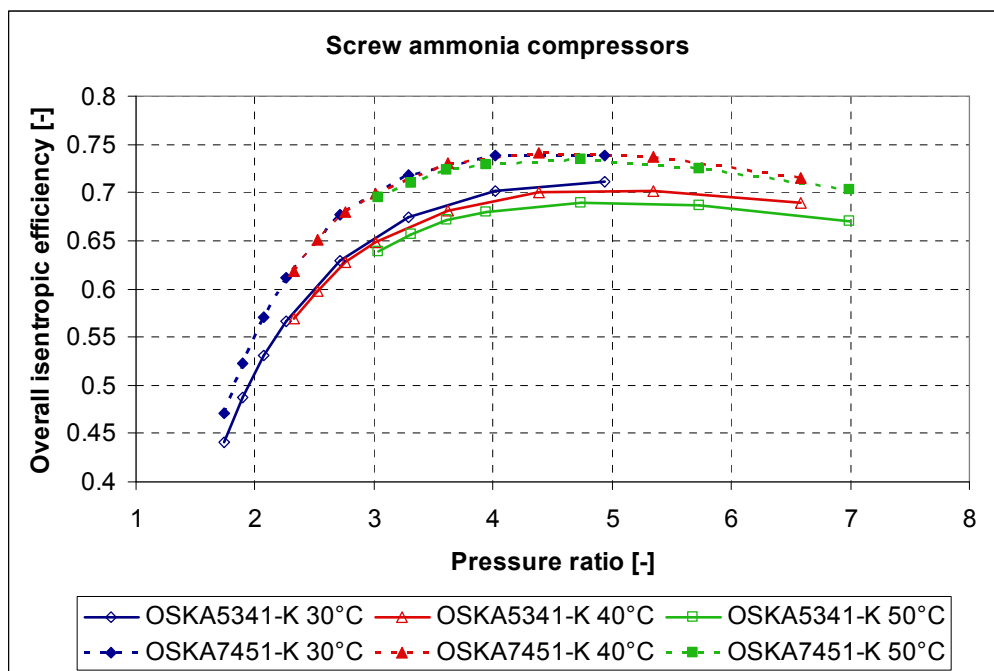
Figure 1.1.9: Overall isentropic efficiency of two Bitzer ammonia screw compressors, at different condensation temperatures

1.1.4 Propane compressors

1.1.4.1 Displacement and refrigeration capacity

There are a few companies which have developed compressors for propane, and they are not as widespread as for other natural refrigerants. The only type of compressor that is easily available on the market is the hermetic or semi-hermetic

16

reciprocating one.

As for ammonia, several manufacturer and researcher data have been considered. Displacement of propane compressors available on the market ranges from 5 to 25 cm^3, both for high back pressure (HBP) and low back pressure (LBP) applications. With regard to cooling capacity, low back pressure compressors have a narrow operating field: available nominal power is less than 1 kW. High back pressure compressors, instead, can reach 2.5÷2.8 kW, with a wider regulation range.

1.1.4.2   Efficiency analysis

In the literature there is not so much data about propane compressor efficiency; most of it comes from Corberan's research group, of the Universidad Politècnica de Valencia (UPV). Other research teams have studied and tested propane compressors, but they reported only the whole cycle EER, instead of compressor efficiency. Some other authors did investigate a hydrocarbon mixture.
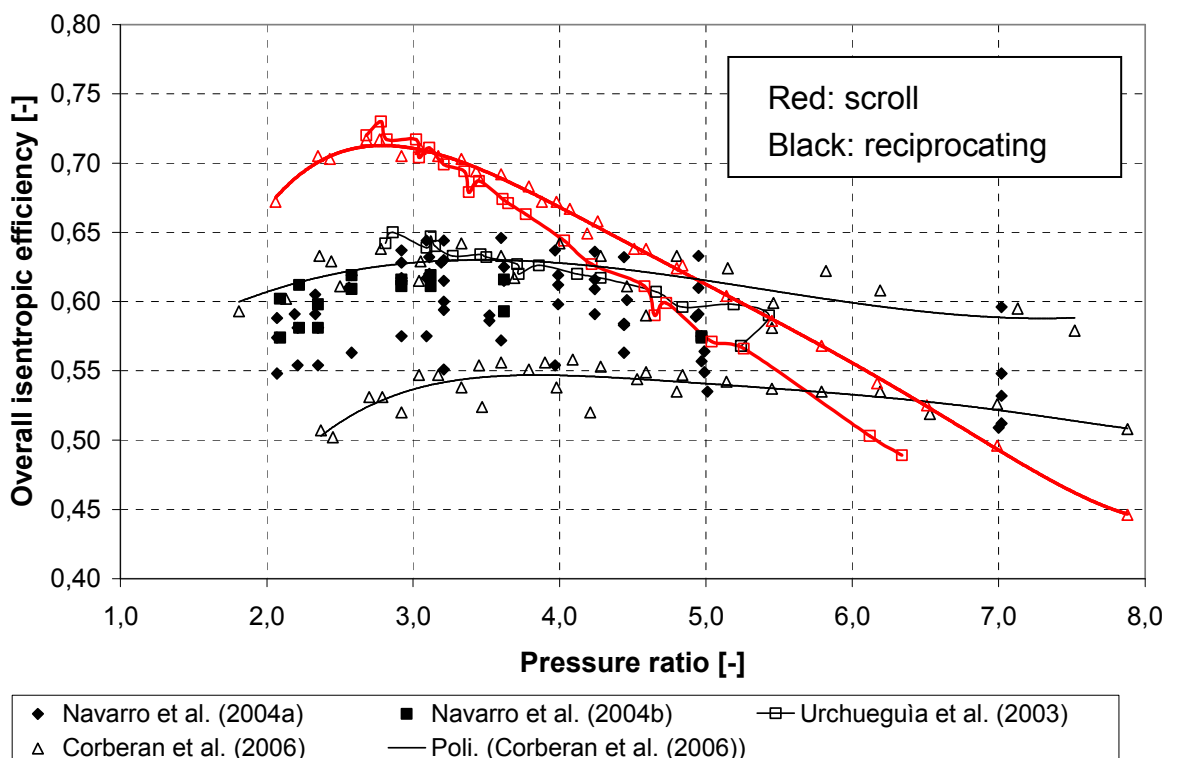
Figure 1.1.10: Propane compressors overall isentropic efficiency
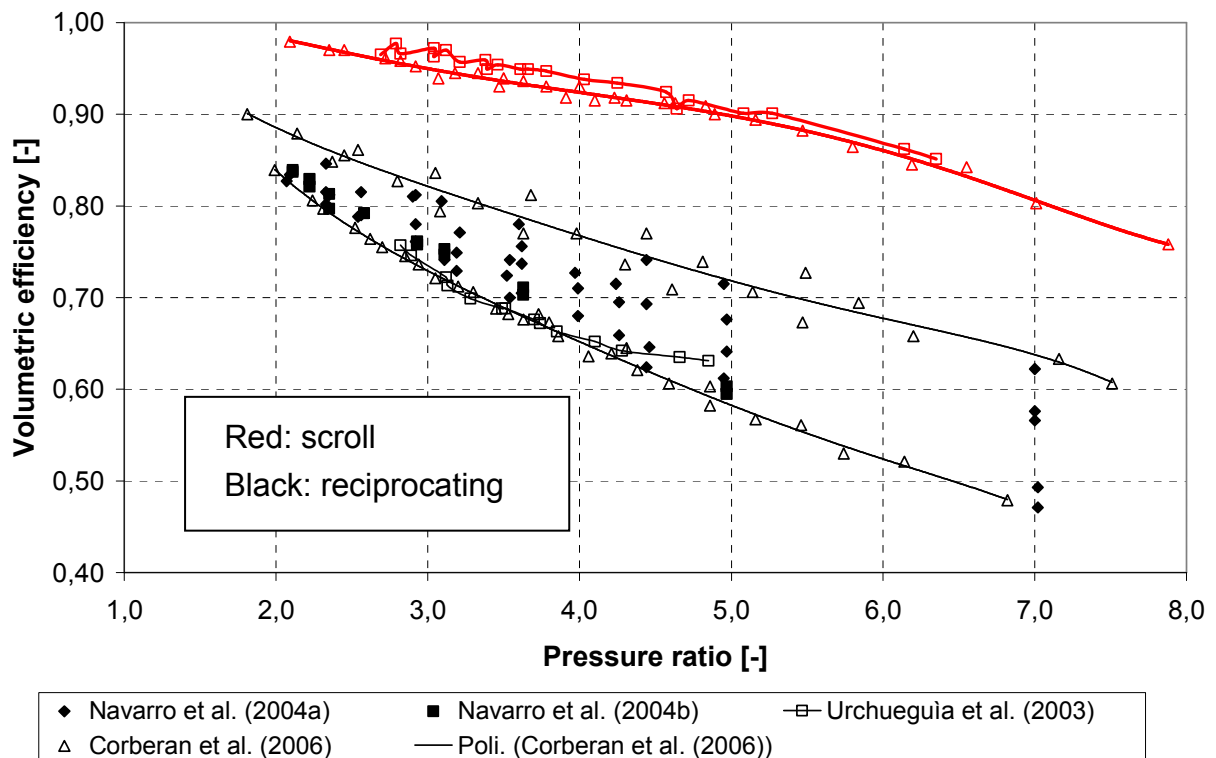
Figure 1.1.11: Propane compressors volumetric efficiency

The first data set by Navarro *et al.* (2004a) refers to experimental tests on five different hermetic reciprocating compressors under two different operating conditions. The overall isentropic efficiency increases with the number of cylinders, if the dead space ratio remains the same. The efficiency decreases if the dead space ratio increases, so compressors with a longer stroke are more efficient. The second data set by Navarro *et al.* (2004b) refers to experimental tests on a hermetic reciprocating compressor, using two different types of oil: traditional mineral oil (MO) and polyolester oil (POE). The use of more expensive oils like POE does not improve the efficiency of a propane compressor; on the contrary, at same pressure ratio, it could penalize the machine. The data set by Urchueguìa *et al.* (2003) and a more recent data set provided by Corberan *et al.* (2006) show a comparison between different types of compressors: hermetic reciprocating, semi-hermetic reciprocating and hermetic scroll compressors. These tests are carried out at the same refrigeration capacity and they show that semi-hermetic and, specially, scroll compressors are more efficient than traditional hermetic reciprocating ones, below

a certain value of pressure ratio (about 4.5). Scroll compressor efficiency decreases sharply when pressure ratio increases. The volumetric efficiency, as the overall isentropic efficiency, increases as displacement increases. The use of POE oils instead of traditional mineral oils does not modify the behaviour of the compressor. It can be seen that the efficiency of a scroll compressor is far higher as compared to that of a reciprocating one (about 20%). As usual, volumetric efficiency decreases sharply when pressure ratio increases, for any type of compressor and under any working condition.

1.1.5   Carbon dioxide compressors

1.1.5.1   Displacement and refrigeration capacity

Reciprocating compressors have the largest operative range. Axial piston compressors have a very tight operative range, as regard to refrigerating capacity. Rotary compressors have a larger operational range, but their efficiency strongly varies with pressure ratio. Scroll, screw or centrifugal compressors are not used for carbon dioxide. Centrifugal compressors are not suitable for carbon dioxide: CO_2 has a very high volumetric refrigerating effect and this leads to some problems in the impeller design, due to the small flow sections required. Screw compressors are not considered in the literature: there are high costs connected to the geometry of the screws and there are problems with the use of oil, even if there are some models in the market. Scroll and swing compressors are of common use in sanitary hot water heat pump applications, especially in the Japanese market. Furthermore, scroll compressors are proposed by some manufacturers for automotive conditioning. They are not considered in this report because of lack of efficiency data.

In the open literature there are several data of carbon dioxide compressors; they are here divided according the refrigerating capacity; the evaporation temperature of these data is -10°÷0°C.

1.1.5.2   Refrigerating capacity: 0-3 kW; efficiency analysis

Data of this analysis are reported in Figure 1.1.12 (overall isentropic efficiency) and 1.1.13 (volumetric efficiency).

Available compressors are reciprocating and rotary ones. The overall isentropic efficiencies of the two compressor types are not so different, even if rotary compressor performances are slightly better. Moreover, their volumetric efficiencies are higher and almost constant when pressure ratio varies. On the other hand, their construction is more complex as compared to a simple reciprocating compressor. The experimental data sets by Suess and Veje (2004) refer to a semi-hermetic reciprocating compressor with a single cylinder and with none, one and two piston rings respectively; it is noticeable that the presence of piston rings improves the overall isentropic efficiency by more than 10%. The solid black lines are linear regressions deduced by Suess and Veje (2004) from experiences at different suction pressures with the same compressor. It can be pointed out that the efficiency improves as pressure ratio rises.

Figure 1.1.12: Overall isentropic efficiency of CO_2 reciprocating (black lines) and rotary (red lines) compressors; refrigeration power: 0-3 kW

The data sets by Ibrahim and Fleming (2003) refer to a mathematical model of a hermetic, single-cylinder reciprocating compressor. They are obtained by simulations at different suction pressures, compression rotational speeds and discharge pressures. The estimated values show that the efficiency improves as pressure ratio increases, although they are appreciably higher than those by Suess and Veje. Klein's (2006) data is implemented in a program that simulates the runs of three small hermetic reciprocating compressor prototypes. Results are close to the linear regression from Suess data. Christen *et al.* (2006) investigated several compressor types: small semi-hermetic reciprocating compressor efficiency data sets are here reported.

Figure 1.1.13: Volumetric efficiency of CO$_2$ reciprocating (black lines) and rotary (red lines) compressors; refrigeration power: 0-3 kW

Tests by Hubacher and Groll (2002) are carried out on a hermetic double-stage rotary compressor available on the market; they point out the strong influence of the oil on efficiency. These tests are carried out at different suction pressures and different degrees of superheat. Tests by Tadano *et al.* (2000) are carried out on a

21

hermetic double-stage rotary compressor, both at high and low operating pressures. With regard to volumetric efficiency, the data sets by Suess and Veje (2004) confirm what was found for the overall isentropic efficiency: the compressor performance improves using piston rings. It is noticeable that the efficiency significantly decreases as the pressure ratio increases. This is pointed out also by Ibrahim and Fleming (2003): for these simulations, the volumetric efficiency changes slightly at different working conditions. Results of Christen *et al.* (2006) are in between, while the Yanagisawa *et al.* (2000) data, which refers to experimental tests on a single-cylinder compressor, agrees with Suess' data.

1.1.5.3 *Refrigerating capacity: 3-6 kW; efficiency analysis*

Data of this analysis are reported in Figure 1.1.14 (overall isentropic efficiency) and 1.1.15 (volumetric efficiency).

The available compressors are reciprocating, axial pistons and rotary ones. With regard to overall isentropic efficiency, it can be noticed that best performances are reached by axial piston compressors. In this case, the efficiency is about 70% and it remains quite constant in the whole pressure ratio range. Concerning reciprocating compressors, they seldom reach these values, when using particular technological solutions. Within this power range, the overall isentropic efficiency of rotary compressors is significantly lower as compared to the others. As regard to volumetric efficiency, the performances of the different families of compressors are similar, with a decreasing trend as pressure ratio increases. Axial piston compressors are characterized by compactness, low weight and easy setting; these features make them very suitable for automotive conditioning systems. Reciprocating compressors are used in other applications because of their larger sizes and weight. The best efficiency is reached at pressure ratios lower than 5. Beyond this value, the overall isentropic efficiency decreases below 0.5. This trend is clear from the experimental tests by Dorin and Neksa (2002) on a semi-hermetic single-stage compressor and by Forsterling *et al.* (2002) on an open single-stage one. From Dorin and Neksa's tests on a double- stage semi-hermetic compressor, it is noticeable that the efficiency reduction (as pressure ratio rises) is less evident and, of course, it is possible to reach higher discharge pressures. Experimental tests by Casson (2001) show a lower efficiency; they were carried out using a semi-

hermetic reciprocating compressor, at two different working conditions: with the compressor motor cooled by the same refrigerating fluid or by an auxiliary fluid. In the second case, the efficiency is higher by around 15%. A characteristic of almost all these curves is the sharp reduction of the efficiency for pressure ratios lower than 2, both in single-stage and in double-stage compressors. With regard to axial piston compressors, the numerical simulation by Koehler et al. (2003) shows a slope pretty constant for the overall isentropic efficiency, at pressure ratios higher than 1.5. Experimental tests carried out by Kuhn et al. (2001) and Forsterling et al. (2002) confirm the results of the numerical simulation. They were conducted by testing different practical solutions.
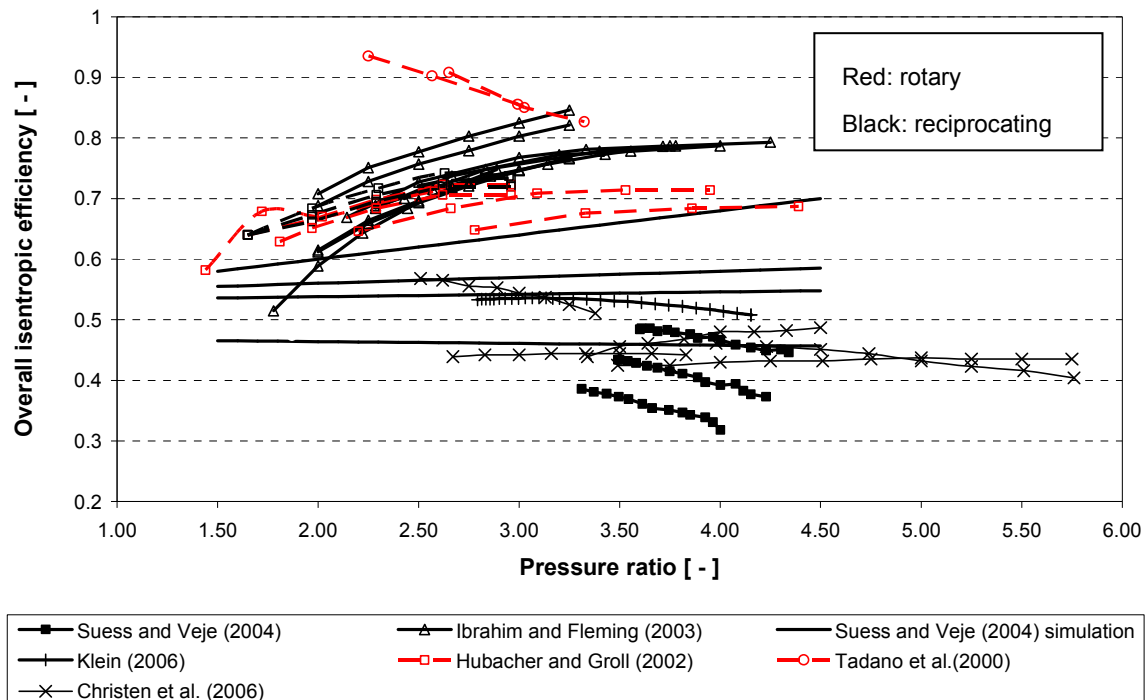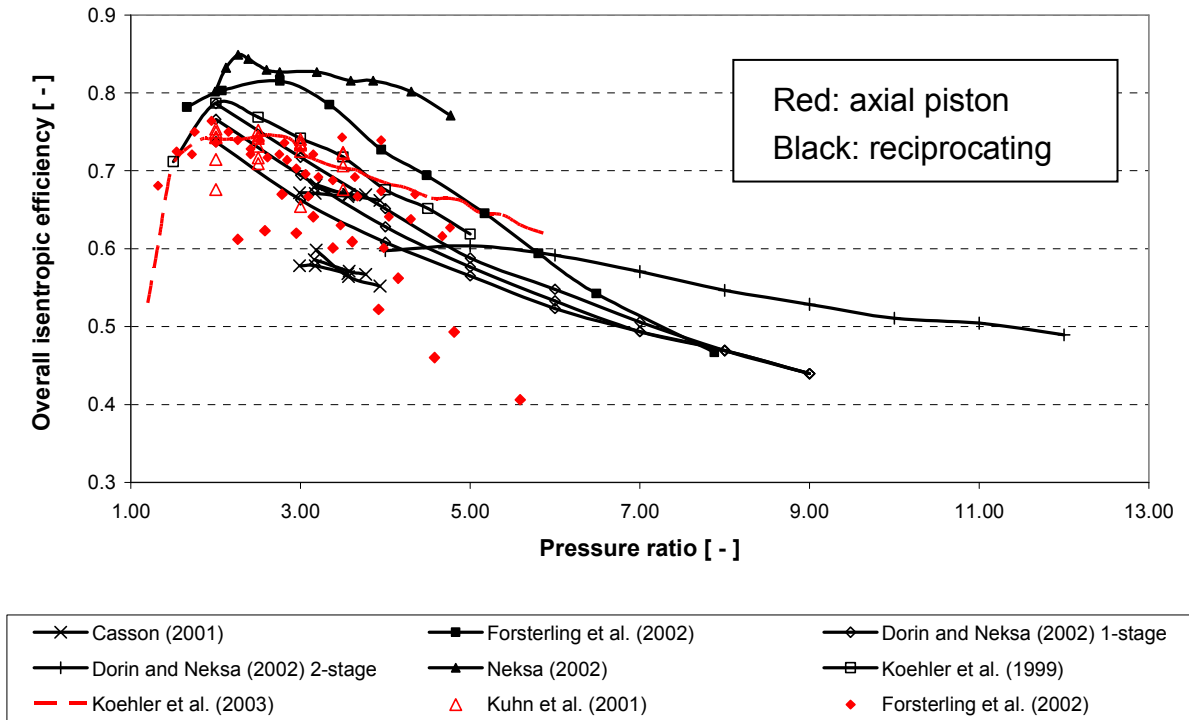

Figure 1.1.14: Overall isentropic efficiency of CO_2 reciprocating (black lines) and axial piston (red lines) compressors; refrigeration power: 3-6 kW

The experimental tests by different authors give very similar values for the volumetric efficiency. Concerning single-stage compressors, the efficiency curve starts from very high values (0.8÷0.9) at low pressure ratios, but it decreases sharply. However, to get a fairly good volumetric efficiency, higher than 50%, the

compression ratio should be lower than 5. It is remarkable the great positive effect of double-stage compression (Dorin and Neksa, 2002): efficiency remains at high levels, more than 70%, even for high pressure ratios. With regard to axial piston compressor, the numerical simulation by Koehler *et al.* (2003) shows poor agreement with experimental tests, especially for pressure ratio lower than 2. Experimental tests show a behaviour, which is similar to that of reciprocating compressors: the volumetric efficiency decreases sharply as pressure ratio increases.
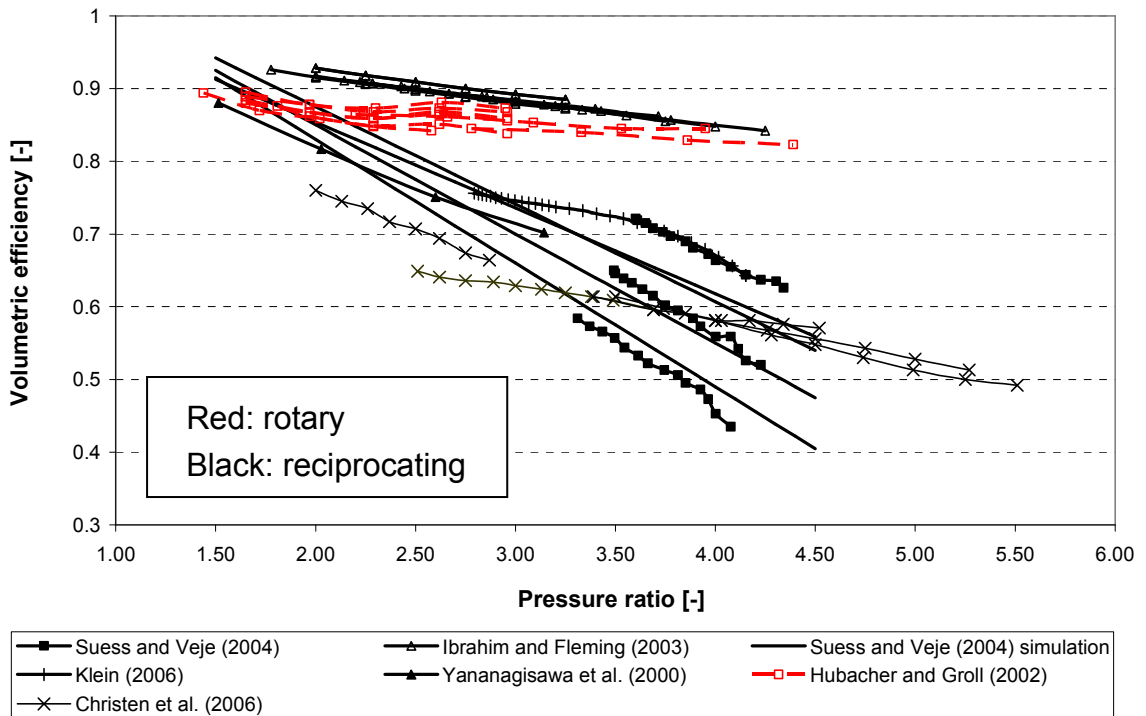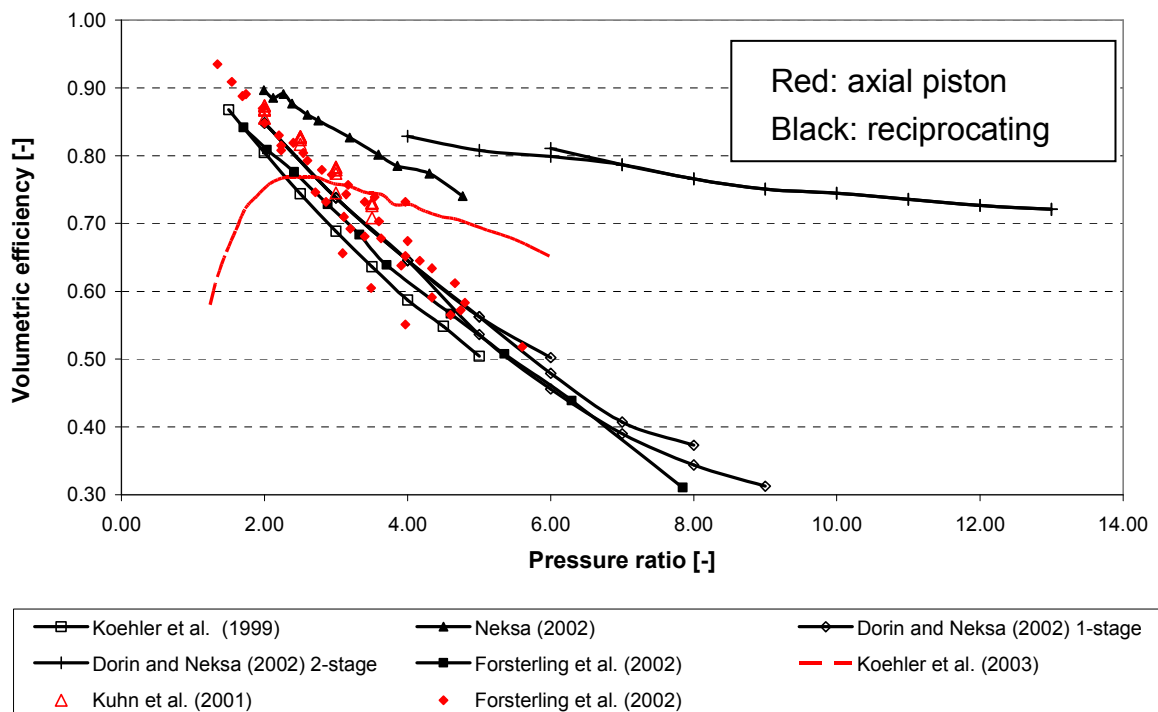

Figure 1.1.15: Volumetric efficiency of CO_2 reciprocating (black lines) and axial piston (red lines) compressors; refrigeration power: 3-6 kW

1.1.5.4 Refrigerating capacity: > 6 kW; efficiency analysis

Data of this analysis are reported in Figure 1.1.16 (overall isentropic efficiency) and 1.1.17 (volumetric efficiency).

On the market only reciprocating compressors are available; in fact, at high refrigeration capacities, rotary compressors have low efficiency and scroll or axial piston compressors cannot cover this working range. Thus, the above observations

about reciprocating compressors are still valid. Cutler *et al.* (2000) report an efficiency higher than 0.65: they refer to semi-hermetic, single-stage reciprocating compressors. Data sets by Hubacher and Groll (2002) and by Christen *et al.* (2006) refer to experimental tests at different suction pressures and different degrees of superheat, on semi-hermetic reciprocating compressors. They show a lower efficiency (from 0.40 to 0.60) and no big variation among the different operating conditions. Data by Pisano (2007) shows an efficiency higher by 10%: they regard a single-stage semi-hermetic reciprocating transcritical compressor. The overall isentropic efficiency by Dreimar *et al.* (2004) is measured on a prototype of a hermetic double-stage rotary compressor; the authors reported an efficiency lower than 60%. The experimental tests by Cutler *et al.* (2000), by Pisano (2007), by Hubacher and Groll (2002) and by Christen *et al.* (2006) present similar values of volumetric efficiency, even if the first two are higher, as for the overall isentropic efficiency.
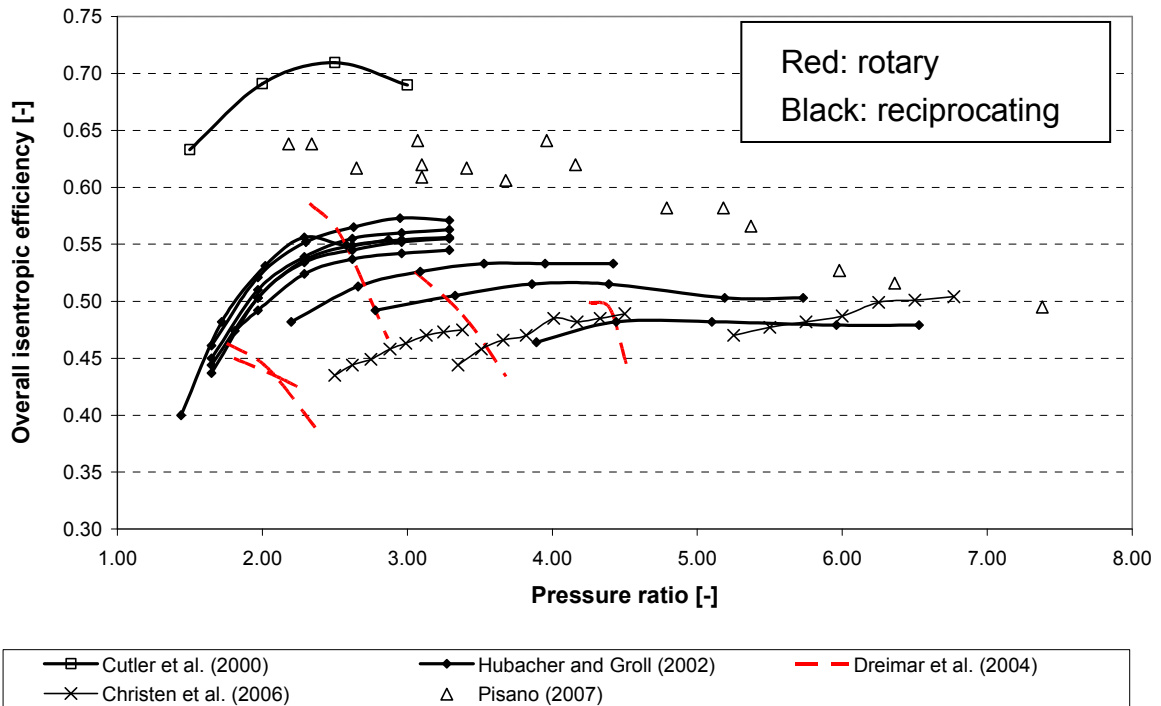
Figure 1.1.16: Overall isentropic efficiency of CO_2 reciprocating (black lines) and rotary (red lines) compressors; refrigeration power: > 6 kW

25
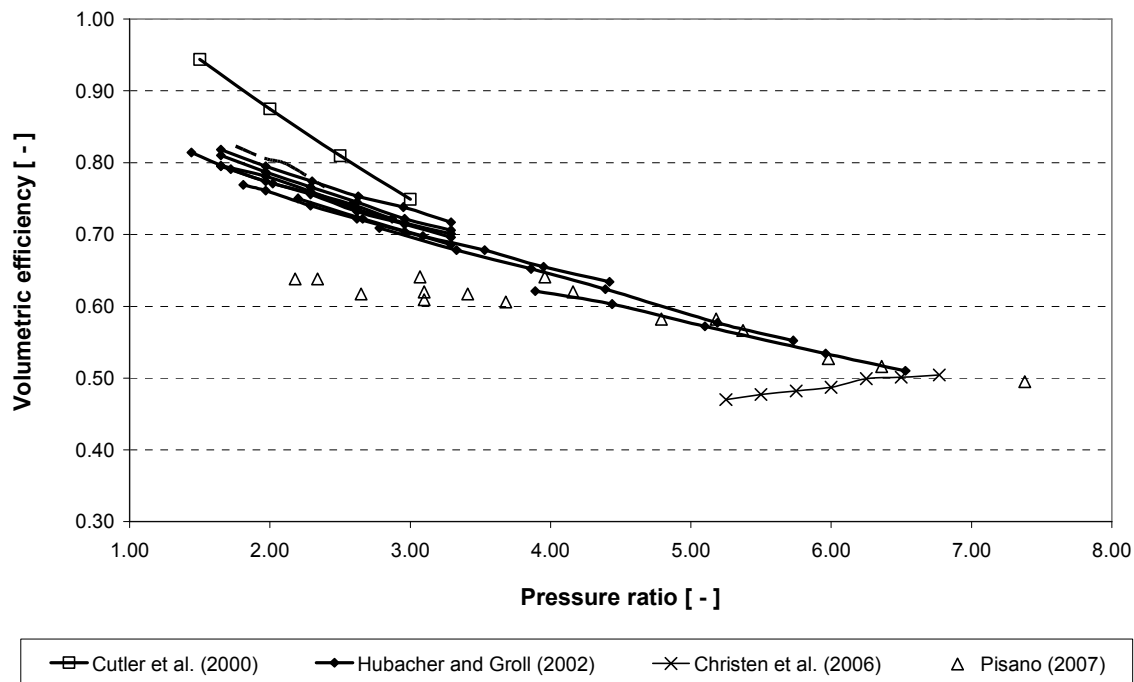
Figure 1.1.17: Volumetric efficiency of CO_2 reciprocating compressors;
refrigeration power: > 6 kW

1.1.6 Conclusions

Performance data of compressors for natural refrigerants have been presented. Ammonia compressors EER has been shown, pointing out the improvement that different technological solutions could give. Analysis of propane compressors has underlined the higher overall isentropic and volumetric efficiencies of scroll compressors, compared to reciprocating ones. CO_2 compressors have been divided according to refrigeration capacity: at low cooling capacity, rotary compressors proved to be the most efficient, while reciprocating ones result the most flexible and widespread. Axial piston compressors are commonly used in automotive air conditioning and hot water heat pump, as swing and scroll ones; in this case performance data are not easily available.

1.1.7 References

1. Bobbo S., Scattolini M., Camporese R., Fedele L., Stryjek R., (2006), Solubility of carbon dioxide in some commercial POE oils, 7th *IIR G. Lorentzen Conf.,* Preprints 409-411.

2. Bowater F. J., (2004), Selection of compressors for low temperature ammonia refrigeration systems, 6th *IIR G. Lorentzen Conf.,* 4c: 1-12.

3. Casson V., (2001), Theoretical and experimental analysis on the use of carbon dioxide in commercial refrigeration (in Italian), *Doctoral thesis at Padua University*, DFT, Italy.

4. Cavallini A., (2002), Heat transfer and energy efficiency of working fluids in mechanical refrigeration, *Bulletin IIR*, 5-21.

5. Cavallini A., Chiarello M., Del Col D., Zilio C., (2007), Compressors for natural refrigerants: state-of-the-art review, 22nd *IIR Int. Conf. of Refrig,* ICR07-B1-1065, 1-8.

6. Chiarello M., Del Col D., (2006), Guidelines for selecting optimal compressors for natural fluids, *SHERHPA Project,* Deliverable D11.

7. Christen T., Hubacher B., Bertsch S. S., Groll E. A., (2006), Experimental performance of prototype carbon dioxide compressors, 11th *Int. Refr. Air-Conditioning Conf.*, C131: 1-10

8. Corberan *et al*., (2006), Private communication, Universidad Politècnica de Valencia (UPV).

9. Cutler B., Hwang Y., Bogdanic L., Radermacher R., (2000), Development of a transcritical carbon dioxide environmental control unit, 4th *IIR – G. Lorentzen Conf.,* 91-98.

10. de Larminat P., (2000), Expanding the use of ammonia, *ASHRAE Journal*, 35-39.

11. Dorin F. M., Neksa P., (2002), CO_2 compressors and equipment, use and availability, 9th *Annual Conference of the Institute of Refrigeration; Beating the Ban - is CO_2 a viable alternative?*

12. Dreimar N., Bunch R., Hwang Y., Radermacher R., (2004), Two-stage rolling piston carbon dioxide compressor, *Int. Compressor Engineering Conf.,* C010: 1-8.

13. EN 12900, (1999), Refrigerant compressors – Rating conditions, tolerances and

presentation of manufacturer's performance data.

14. Fagerli B., (1996), Development and experiences with a hermetic CO_2 compressor, *Int. Compressor Engineering Conf.*, 229-234.

15. Fornasieri E., Zilio C., (2004), Componenti per impianti a CO_2, *European Seminar. Carbon dioxide as a refrigerant.*

16. Forsterling S., Tegethoff W., Kohler J., (2002), Theoretical and experimental investigations on Carbon Dioxide compressors for mobile air conditioning system and transport refrigeration, *Compressor Engineering & Refrigeration Air Conditioning Conf.*, 193-200.

17. Halozan H., Rieberer R., (2006), Heat pump systems with ammonia as refrigerant, *7th IIR – G. Lorentzen Conf.*, Preprints, 80-83.

18. Hammad M. A., Alsaad M. A., (1999), The use of hydrocarbon mixtures as refrigerants in domestic refrigerators, *Applied Thermal Engineering*, 19: 1181-1189.

19. Hubacher B., Groll E. A., (2002), Measurement of performance of carbon dioxide compressors, *Final report, Air-conditioning and refrigeration technology institute*, 21CR (611-10070): 1-89.

20. Hwang Y., Radermacher R., (1998), Development of hermetic carbon dioxide compressor, *Int. Refrigeration Conf.*, 171-176.

21. Ibrahim A. G., Fleming J. S., (2003), Performance assessment of a trans-critical CO_2 heat pump using a reciprocating compressor, *21st IIR Int. Congress of Refrigeration*, 644: 1-10.

22. Klein S. A., (2006), Engineering Equation Solver. Danfoss TN-compressors for CO_2 (prototypes), *F-Chart Software 1.26*, Distributable version, Compressor Performance Calc.

23. Köhler J., Lemke N., Sonnenkalb M., (1999), Second year of city busses with transcritical CO_2 air-conditioning units, *SAE Meeting*.

24. Köhler J., Tegethoff W., Lemke N., Correia C., Cavalcante P., (2003), CO_2-Total cycle and components, *VDA Alternate Refrigerant Winter Meeting*.

25. Korfitsen E., Kristensen A. P. R., (2005), Ammonia high pressure heat pumps in food refrigeration applications, *Int. J. Refrigeration,* 21(3): 212-218.

26. Kuhn, Graz, Obrist, Parsch, Rinne, (2001), Carbon Dioxide R744 as a Refrigerant in Automotive Air-Conditioning System, *ATZ worldwide 12/2001*, 103: 11-14.

27. Lemmon E. W., McLinden M. O., Huber M. L., (2007), "REFPROP 8.0", *NIST*, Standard Reference Database 23.

28. Liao S. M., Zhao T. S., Jakobsen A., (2000), A correlation of optimal heat rejection pressures in transcritical carbon dioxide cycles, *Applied Thermal Engineering*, 20: 831-841.

29. Navarro E., Urchueguìa J. F., Gonzàlvez J., Corberàn J. M., (2004), Comparative experimental investigation of performance in reciprocating compressors of different sizes using propane (R290) and R407C as refrigerants, *6th IIR G. Lorentzen Conf.,* 2c-1, 1550: 1-9.

30. Navarro E., Urchueguìa J. F., Gonzàlvez J., Corberàn J. M., (2004), Comparative experimental investigation of oil behaviour in a hermetic piston compressor using propane (R290) as refrigerant, *6th IIR G. Lorentzen Conf.,* 2c-2, 1610: 1-9.

31. Navarro E., Urchueguìa J. F., Gonzàlvez J., Corberàn J. M., (2005), Test results of performance and oil circulation rate of commercial reciprocating compressors of different capacities working with propane (R290) as refrigerant, *Int. J. of Refrigeration*, 28: 881-888.

32. Neksa P., (2002),, CO$_2$ heat pumps systems, *Int. J. Refrigeration*, 25: 421-427.

33. Pisano G., (2007), Private communication, Officine Mario Dorin S.p.A.

34. Palm B., (2005), Ammonia in small capacity heat pump and refrigeration systems, *Ammonia refrigerating systems IIF_IIR,* 1-6.

35. Rivet P., (2004), Green solutions for freezing applications, *6th IIR G. Lorentzen Conf.,* 4b: 1-8.

36. Suess J., Veje C., (2004), Development and performance measurement of a small compressor for transcritical CO$_2$ application, *Int. Compressor Engineering Conf.,* C112: 1-6.

37. Tadano M., Ebara T., Oda A., Susai T., Takizawa K., Izaki H., Komatsubara T., (2000), Development of the CO$_2$ hermetic compressor, *4th IIR – G. Lorentzen Conf.,* 323-330.

38. Urchueguìa J. F., Corberàn J. M., Gonzàlvez J., Dìaz J. M., (2003), Experimental characterization of a commercial-size scroll and reciprocating compressor working with R22 and propane (R290) as refrigerant, *21st IIR Int. Congress of Refrigeration*, 320: 1-8.

39. Yanagisawa T., Fukuta M., Sakai T., Kato H., (2000), Basic operating

characteristics of reciprocating compressor for CO_2 cycle, *4th IIR – G. Lorentzen Conf.,* 331-338.

Web sites

ACC compressors, www.the-acc-group.com
Bitzer, www.bitzer.de
Bock, www.bock.de
Copeland, www.copeland-corp.com
Danfoss, www.danfoss.com
Denso, www.denso-europe.com
Dorin, www.dorin.com
Embraco, www.embraco.com
Frigopol, www.frigopol.com
Grasso, www.grasso-global.com
LuK, www.luk.de
Mitsubishi, www.mitsubishielectric.com
Mycom, www.mycomcpc.com
Obrist, www.obrist.at
Sabroe, www.sabroe.com
Sanyo, www.sanyo.com
Shecco, www.shecco.com
Tecumseh, www.tecumseh.com
Vilter, www.vilter.com
Visteon, www.visteon.com

Chapter 1.2 THE EFFECT OF THE REFRIGERANT: FEASIBILITY ASSESSMENT OF

AN AIR-CONDITIONING SYSTEM USING NATURAL FLUIDS

The aim of this feasibility study was to investigate the energy performance of different air-conditioning plant configurations, using different refrigerants. The considered fluids are ammonia (R717) and carbon dioxide (R744); their performances were compared to those of R410A, one of the most commonly used refrigerant in HVAC systems.

This study was conducted for SCM Frigo; the company purpose was to evaluate the possibility of manufacturing an air-conditioning system using natural fluids: the choice is between ammonia and carbon dioxide.

1.2.1   Introduction

In this Chapter, the importance of the refrigerant will be highlighted; as pointed out in the Introduction, the choice of the appropriate fluid is an important aspect in the design of the whole system and it can strongly affect the energy performance. Only a limited number of fluids presents interesting properties for an HVAC&R system. Moreover, the environmental problem is becoming more and more pressing and the governments of the major countries all over the world are sensitive to this subject. The Montreal Protocol (1987) and the Kyoto Protocol (1997) established the phase-out of halogenated refrigerants, the most commonly used in the market. Thus the strong interest of the company to find some allowed fluids that can replace the banned ones. One of the possible solutions is to use natural refrigerants: they are already present in the atmosphere, their environmental properties are well known and they are cheap and widely available. On other hand, as pointed out in Chapter 1.1, they presents various constrains: they are toxic (for example, ammonia), or flammable (for example, hydrocarbons) or their cycle performance is poor (for example, carbon dioxide). In addition, in same cases the current technology is not ready for these fluids; two examples are meaningful. The

operative pressures of a carbon dioxide cycle are usually very high and the components (heat exchangers, compressors, valves, filters) are not easily findable in the market. Ammonia corrodes copper and its alloys: since lots of components contains copper (compressors in the electrical windings, heat exchangers in brazed parts), R717 needs dedicated (and more expensive) components, like open compressors.

For these reasons, the interest of the HVAC&R companies for these fluids is high, but their use needs a heavy investment, of money and know-how. Thus, before taking the decision of manufacturing a plant with natural fluid, a feasibility study is mandatory. For this purpose, a simulation code was developed; this program must be reliable but also quick and easy to use: it is described in paragraph 1.2.3. This code simulates the running of a chiller and/or heat pump unit, under different operative conditions; in each condition, the compressor is working full load, being not considered the option of a capacity control. Different conditions are simulated, especially for carbon dioxide: besides the traditional subcritical cycle, a transcritical one is simulated. In addition, some solutions to improve the energy efficiency are investigated: the more promising and easy to realize are the modification of the simple cycle, using an auxiliary compressor, and the utilization of the latent heat of the water, using an adiabatic saturator in the gas cooler air inlet.

1.2.2 Nomenclature

To describe the mathematical model of the code, these symbols are necessary

A heat transfer surface [m^2]

COP heat pump energy efficiency [-]

c_p specific heat at constant pressure [$J\ kg^{-1}\ K^{-1}$]

$\dot{C}$ heat capacity rate [$W\ K^{-1}$]

EER chiller energy efficiency [-]

h enthalpy [$J\ kg^{-1}$]

hd   heat dissipation factor [-]

k   transmittance correction coefficient [-]

$\dot{m}$ mass flow rate [kg s^{-1}]

N   compressors number

P   power absorption [W]

p   pressure [Pa]

Q   thermal power [W]

Re Reynolds number: $\mathrm{Re} = \dfrac{\dot{m} \cdot d}{S \cdot \mu}$ [-]

T   temperature [°C]

UA thermal transmittance [W K^{-1}]

$\dot{V}$ volumetric flow rate [m^3 s^{-1}]

Greek letters

α heat transfer coefficient [W m^{-2} K^{-1}]

ε effectiveness [-]

η_{is} overall isentropic efficiency [-]

η_v volumetric efficiency [-]

θ temperature mean logarithmic difference [K]

ρ density [kg m^{-3}]

Subscripts

aux auxiliary

c   condenser/condensation

D   design

e   evaporator/evaporation

gc   gas cooler/gas cooling

i   inlet

int   intermediate

k   compressor

opt optimal

out outlet

r   refrigerant

SC   subcooling

SH   superheat

sf   secondary fluid

1.2.3   Mathematical model

1.2.3.1   Subcritical conditions

The efficiency of vapour compression chillers and heat pumps depends strongly on the temperature levels of the external sources and on the unit capacity control system. Therefore, to calculate a unit energy consumption with a reasonable accuracy, it is necessary to compute its energy efficiency and thermal capacity in actual working conditions. On other hand, a simplified model is needed to avoid difficult and long calculations. For the calculation of the parameters at full load condition but with external fluid temperatures different from the design values, Binotto *et al.* (2006) suggested a constant heat exchangers transmittance approach. The adopted procedure corrects the design transmittance taking into account heat transfer coefficient variations associated to refrigerant and secondary fluid mass flow rate variations.

The following data are required for the model application to a given refrigeration unit:

- the refrigerant fluid and the evaporator and condenser kind of secondary fluids;

- design evaporation and condensation temperatures, $T_{c,D}$ and $T_{e,D}$, together with refrigerant evaporator outlet superheat and condenser outlet subcooling values, $\Delta T_{SH,D}$ e $\Delta T_{SC,D.}$
- compressor coefficients with reference to the EN 12900 (2005) polynomial equations;
- secondary fluids design inlet temperature, temperature glides and pressure drops, $T_{sf,D}$, $\Delta T_{sf,D.}$
- heat exchanger pumps or fans power absorptions, $P_{aux,D}$;
- for a chiller, the rated cooling capacity, $Q_{e,D}$, and compressor power absorption, $P_{k,D}$ (or design efficiency, *EER*) in design conditions;
- for a chiller, the rated thermal capacity, $Q_{c,D}$, and compressor power absorption, $P_{k,D}$ (or efficiency, *COP*) in design conditions;
- heat exchangers design ratios between refrigerant and secondary fluid heat transfer surfaces;
- heat exchangers design ratios between refrigerant and secondary fluid heat transfer coefficients;
- refrigerant and secondary fluid circuits architecture description;
- compressor management information with relation to capacity control;
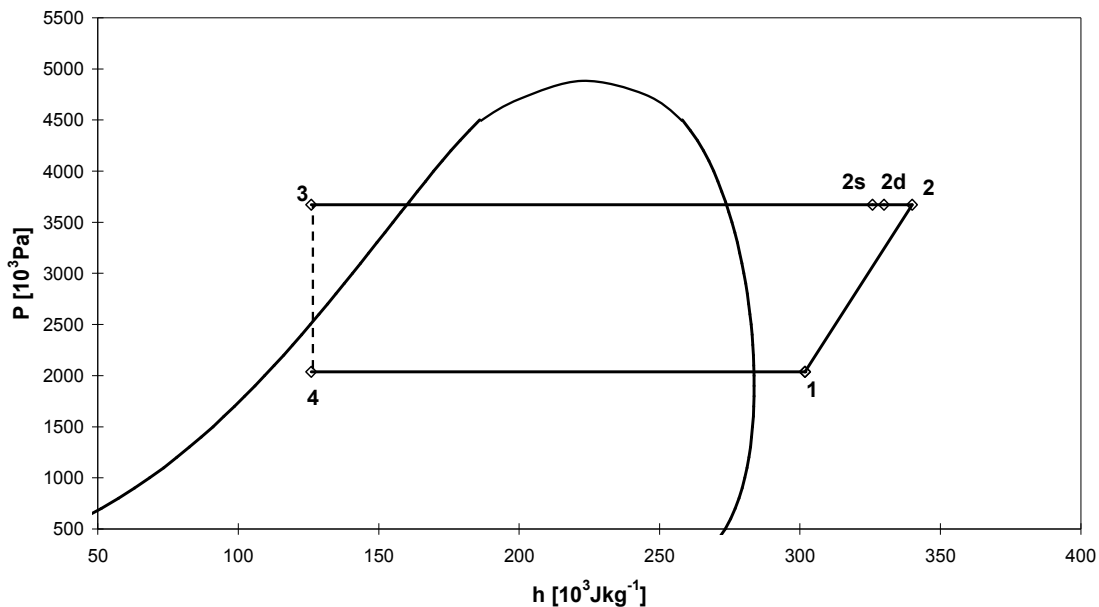
Figure 1.2.1: R410A p-h diagram (subcritical cycle)

Refrigerant pressure drops in the heat exchangers data are not required since they are not easily available in manufacturers' data sheets. Considering the single stage vapour compression cycle shown in Figure 1.2.1, the thermodynamic properties of points 1, 2s, 3 and 4 can now be determined in design conditions. The thermodynamic properties associated to points 2 and 2d depend on the compressor characteristics. With reference to EN 12900 (1999) superheat and subcooling standard values, it is possible to express the cooling capacity, the power absorption and the refrigerant mass flow rate with the following polynomial equations. The volumetric η_v and the overall isentropic efficiency η_{is} are calculated as defined in the Introduction.

$$\hat{Q}_e = a_1 + a_2 \cdot T_e + a_3 \cdot T_c + a_4 \cdot T_e^2 + a_5 \cdot T_e \cdot T_c + a_6 \cdot T_c^2 + ...$$
$$... + a_7 \cdot T_e^3 + a_8 \cdot T_e^2 \cdot T_c + a_9 \cdot T_e \cdot T_c^2 + a_{10} \cdot T_c^3 \tag{1}$$

$$\hat{P}_k = b_1 + b_2 \cdot T_e + b_3 \cdot T_c + b_4 \cdot T_e^2 + b_5 \cdot T_e \cdot T_c + b_6 \cdot T_c^2 + ...$$
$$... + b_7 \cdot T_e^3 + b_8 \cdot T_e^2 \cdot T_c + b_9 \cdot T_e \cdot T_c^2 + b_{10} \cdot T_c^3 \tag{2}$$

$$\hat{\dot{m}} = \frac{\hat{Q}_e}{\hat{h}_1 - \hat{h}_4}, \tag{3}$$

In the hypothesis of independency of the efficiencies values from the refrigerant superheat at the compressor suction, the cooling capacity, the power absorption and the refrigerant mass flow rate can be calculated with reference to the superheat and subcooling values of Figure 1.2.1 cycle:

$$\dot{m} = \eta_v \cdot \dot{V} \cdot \rho_1, \tag{4}$$

$$Q_e = \dot{m}(h_1 - h_4), \tag{5}$$

$$P_k = \dot{m}(h_2 - h_1), \tag{6}$$

being the refrigerant enthalpy at the end of the compression, h_2, defined by the following equation:

$$h_2 = h_1 + \frac{h_{2s} - h_1}{\eta_{is}}$$

(7)

The compressor discharge enthalpy, h_{2d}, can be defined as a function of the compressor heat dissipation factor, hd:

$$h_{2d} = h_2 - \frac{P_k \cdot hd}{\dot{m}}$$

(8)

Through equations (7) and (8), the thermal power to be dissipated in the condenser can be calculated as:

$$Q_c = \dot{m}(h_{2d} - h_4) = \dot{m}\left[\left(h_1 + \frac{h_{2s} - h_1}{\eta_{is}} - \frac{P_k \cdot hd}{\dot{m}}\right) - h_4\right]$$

(9)

The vapour compression system energy efficiency is obtained with the following two expressions, for a refrigeration and a heat pump unit respectively:

$$EER = \frac{Q_e}{P_k + \sum P_{aux,D}}$$

(10)

$$COP = \frac{Q_c}{P_k + \sum P_{aux,D}}$$

(11)

Combining equations (1-11), the vapour compression cycle design operating temperatures, $T_{c,D}$ and $T_{e,D}$, can be determined solving the following equations system:

$$\begin{cases} Q(T_{e,D}, T_{c,D}) - Q_D = 0 \\ P_k(T_{e,D}, T_{c,D}) - P_{k,D} = 0 \end{cases}$$

(12)

where Q represent the cooling or the heating capacity for a chiller and a heat

pump unit respectively.

The evaporator and condenser transmittances in design conditions can be subsequently determined with a temperature mean logarithmic difference approach. If the heat exchanger heat transfer surface is divided into M partitions of equal refrigerant enthalpy difference, its transmittance can be calculated with the following expression in the co-current hypothesis:

$$UA = \sum_{j=1,M} \frac{\dot{m} \cdot (h_j - h_{j-1})}{\vartheta_j},$$

(13)

where ϑ_j is defined as the temperature mean logarithmic difference between the refrigerant and the secondary fluid with reference to the j-th subdivision of the refrigerant enthalpy difference. It can be calculated solving the following algebraic system:

$$\begin{cases} \begin{cases} h_j = h_{j+1} - \dfrac{h_{out} - h_{in}}{N} \\ T_{sf,j} = T_{sf,j+1} - \dfrac{\dot{m} \cdot (h_{out} - h_{in})}{N \cdot \dot{m}_{sf} \cdot c_{p,sf}} \end{cases} , j = 0, N-1 \\ \begin{cases} h_j = h_{out} \\ T_{sf,j} = T_{sf,in} \end{cases} , j = N \end{cases} .$$

(14)

Through these equations, it is possible to calculate the design energy performance together with the heat exchangers transmittance, $UA_{e,D}$ and $UA_{c,D}$, for a given refrigeration unit. For each heat exchanger secondary fluid, the volumetric flow rate is calculated on the basis of the following equation, neglecting mass transfer phenomena:

$$\dot{V}_{sf} = \frac{Q}{\rho_{sf} \cdot c_{p,sf} \cdot \Delta T_{sf}},$$

(15)

where Q is the heat exchanger thermal power.

For secondary fluids temperature values different from design conditions, it is

possible to determine the refrigeration machine working conditions and energy efficiency basing on design data in the following hypotheses:

- constant design evaporator outlet superheat and condenser outlet subcooling values;
- refrigerant pressure drops variations influence is neglected;
- constant design heat exchangers secondary fluids volumetric flow rates and pressure drops;
- refrigerant and secondary fluids heat transfer coefficient, α, proportional to the *m*-th power of Reynolds number: $\alpha \propto \text{Re}^m$.

The vapour compression cycle operating temperatures, T_c and T_e, determination problem can be reduced to the solution of the following non-linear equations system:

$$\begin{cases} f_e\left(T_e, T_c\right) = UA_e - UA_{e,D} \cdot k_e = 0 \\ f_c\left(T_e, T_c\right) = UA_c - UA_{c,D} \cdot k_c = 0 \end{cases}, \tag{16}$$

where the heat exchanger transmittances, UA, are obtained from equations (1-7, 9) and (13-14) that represent the basic equations system of a refrigerating unit for given values of evaporation and condensation temperatures The condenser and evaporator transmittance correction coefficients, k, are calculated with the following expression:

$$k = \frac{1 + \left(\dfrac{\alpha_{sf}}{\alpha_r}\right)_D \cdot \left(\dfrac{A_{sf}}{A_r}\right)_D}{\left(\dfrac{\dot{m}}{\dot{m}_D}\right)_{sf}^{-m_{fs}} + \left(\dfrac{\alpha_{sf}}{\alpha_r}\right)_D \cdot \left(\dfrac{A_{sf}}{A_r}\right)_D \cdot \left(\dfrac{\dot{m}}{\dot{m}_D}\right)_r^{-m_r}} \cdot \tag{17}$$

where A_r and A_{sf} are the heat transfer surface on the refrigerant and secondary fluid side respectively and α_r and α_{sf} are the corresponding heat transfer coefficients.

Usually air condensed units for civil and commercial refrigeration are equipped with condensation temperature control systems to assure safe working conditions for the compressor and the expansion valve. These systems regulate the condenser

air volumetric flow rate in order to keep or the condensation temperature above a minimum value, $T_{c,min}$, or the pressure difference at the two ends of the throttling valve, above a minimum value, $Dp_{c,min}$. In this case, the system (16) must be replaced with the following constrained equations system:

$$
\begin{cases}
f_e\left(T_e,\dot{V}_{sf,c}\right) = UA_e - UA_{e,D} \cdot k_e = 0 \\
f_c\left(T_e,\dot{V}_{sf,c}\right) = UA_c - UA_{c,D} \cdot k_c = 0 \, . \\
T_c = T_{c,min} \text{ or } T_c = T\left(p_e + \Delta p_{min}\right)
\end{cases}
\tag{18}
$$

Neglecting condenser air density and viscosity variations and being constant the volumetric flow rate, fans power absorption is considered constant.

1.2.3.2 Transcritical conditions

Being its critical temperature rather low (31.06°C), a CO_2 system often operates according to a simple transcritical cycle when the temperature of the secondary fluid exceeds a specific value (for example, 15-20 °C for atmospheric air). In this case the upper pressure is higher than the critical one and heat transfer does not involve two phase transformation (condensation) but only gas cooling (consequently the heat exchanger is named gas cooler). Being a single phase process, the temperature is not constant and the system has a further degree of freedom, which is the upper pressure. For this reason, the compressor manufacturers can not provide any polynomial equations in the form of (1) and (2); in this case, volumetric and overall isentropic efficiencies are calculated using the following equations:

$$
\eta_v = a_1 + a_2 \cdot \left(\frac{p_{gc}}{p_e}\right),
\tag{19}
$$

$$
\eta_{is} = a_1 + a_2 \cdot \left(\frac{p_{gc}}{p_e}\right) + a_3 \cdot \left(\frac{p_{gc}}{p_e}\right)^2 + a_4 \cdot \left(\frac{p_{gc}}{p_e}\right)^3,
\tag{20}
$$

As for subcritical conditions, the thermodynamic properties of points 1, 2s, 3 and

4 of Figure 1.2.2 can be determined in design conditions. In this case, the upper pressure and the refrigerant temperature at the gas cooler outlet have to be determined. Being this parameter a degree of freedom, it is chosen in order to achieve the highest efficiency (Kim *et al.*, 2004); its optimal value is named $p_{gc,opt}$.
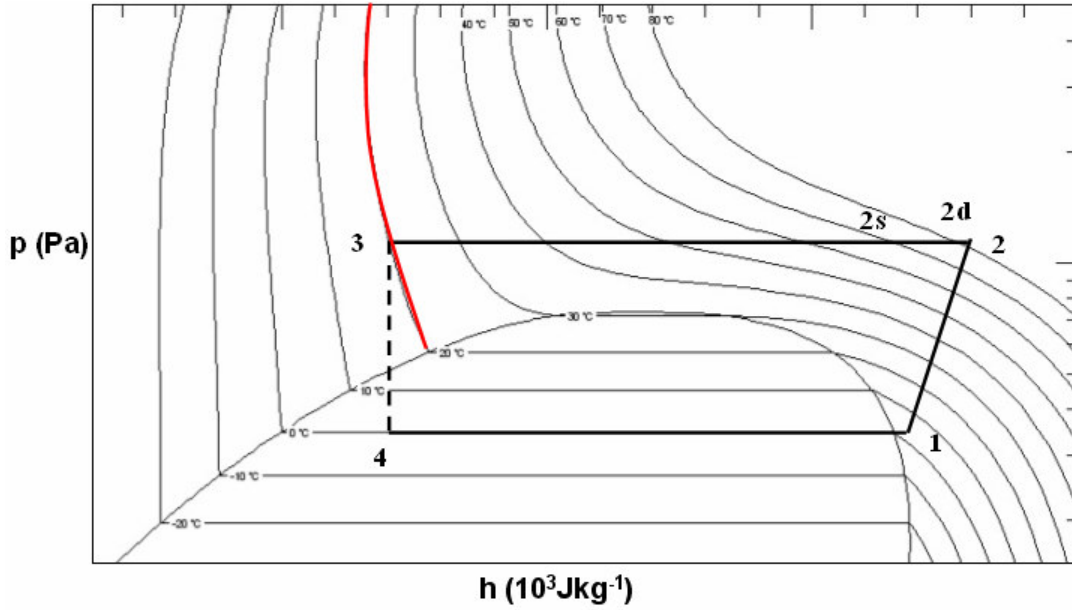
Figure 1.2.2: R744 p-h diagram (transcritical cycle)

In the open literature there are several correlations to find the optimal gas cooler pressure. In this model, the chosen correlation is that of Liao *et al.* (2000): it allows to find $p_{gc,opt}$ as a function of the evaporation temperature and the refrigerant gas cooler outlet temperature $T_{gc,out}$ (red line in the ph diagram of Figure 1.2.2). In this case, a fixed approach (temperature difference between the refrigerant gas cooler outlet and the secondary fluid) is assumed. For secondary fluids temperature values different from design conditions, maintaining the same hypothesis of the subcritical conditions, the system of equation (16) becomes:

$$
\begin{cases}
f_e\left(T_e, T_{gc,out}, p_{gc,opt}\right) = UA_e - UA_{e,D} \cdot k_e = 0 \\
f_{gc}\left(T_e, T_{gc,out}, p_{gc,opt}\right) = h_{2d} - h_{gc,in} = 0 \\
p_{gc,opt} = p_{gc,opt}\left(T_e, T_{gc,out}\right)
\end{cases}
\tag{21}
$$

where the temperature of the refrigerant at the gas inlet $T_{gc,in}$ is calculating as a function of the effectiveness ε of the gas cooler, solving the following system of equations, dividing the gas cooler in a finite number of elements N:

$$\begin{cases} \begin{cases} h_j = h_{j+1} + \dfrac{\dot{C}_{sf}}{\dot{m}}\left(T_{sf,j} - T_{sf,j+1}\right) \\ T_{sf,j+1} = T_{sf,j} + \dfrac{1}{\dot{C}_{sf}} \dfrac{\varepsilon_j \cdot \dot{C}_{min,j}}{1 + \dfrac{\varepsilon_j \cdot \dot{C}_{min,j}}{\dot{c}_{r,j}}} \cdot \left(T_{j+1} - T_{sf,j}\right) \end{cases} \, , j = 0, N-1 \\ \\ \begin{cases} h_j = h_{gc,out} \\ T_{sf,j} = T_{sf,in} \end{cases} \, , j = N \end{cases} \tag{22}$$

calculating, in each j-th volume, the refrigerant temperature, the effectiveness and the minimum heat capacity rate through the following equation

$$T_j = T\left(h_j, p_{gc,opt}\right), \tag{23}$$

$$\varepsilon = 1 - e^{-\frac{UA_{gc,D} \cdot k_{gc}}{N \cdot \dot{C}_{min}}}, \tag{24}$$

$$\dot{C}_{min,j} = \min\left(\dot{C}_{r,j}, \dot{C}_{sf}\right). \tag{25}$$

1.2.3.3 Cycle with auxiliary compressor

In order to achieve a higher efficiency, especially for those refrigerants whose simple cycle is thermodynamically penalized, some solutions are investigated. Particularly, for carbon dioxide, different cycles are presented and described in Chapter 1.3. The adoption of a different (and more complex) cycle can improve the thermodynamic efficiency of an unit, with the drawbacks of a higher unit cost. In addition, the choice of using the evaporative cooling at the gas cooler can improve the energy efficiency, allowing a lower temperature at the gas cooler outlet; this solution is presented in the following paragraph.

The studied cycle is shown in Figures 1.2.3 and 1.2.4: it is a double throttling, single compression cycle with an auxiliary compressor. In the Figures there are two

optional internal heat exchangers, which are not simulated in the code. The simulation of the cycle can follow the same rules of the simple cycle, but there is a further degree of freedom: the intermediate pressure p_{int}. With this variable, all the points of the cycle are known and it is possible to find the value of χ, ratio of the flow rate of the main stream from the gas cooler on the flow rate of the stream to the evaporator. As for the gas cooler optimal pressure, the intermediate optimal pressure $p_{int,opt}$ is calculated. The chiller EER is defined as:

$$EER = \frac{\left(h_5 - h_4\right)}{\left(h_6 - h_5\right) + \left(\dfrac{1}{\chi} - 1\right)\left(h_8 - h_7\right)} \, , \tag{26}$$

while, for heat pump, the COP is defined as

$$COP = \frac{\left(h_8 - h_1\right)}{\chi\left(h_6 - h_5\right) + \left(1 - \chi\right)\left(h_8 - h_7\right)} \, . \tag{27}$$

With the considered assumptions and being fixed the values of evaporation and external cooling agent temperatures, from equation (26) and (27) the dependence of the EER and the COP from the independent variables can be easily written:

$$EER = f\left(p_{gc}, p_{int}, \chi\right) \tag{28}$$

$$COP = f\left(p_{gc}, p_{int}, \chi\right) \tag{29}$$

thus reducing the problem of finding the optimum values of the independent variables to the solution of a multi-variable root-finding problem of a nonlinear equation.
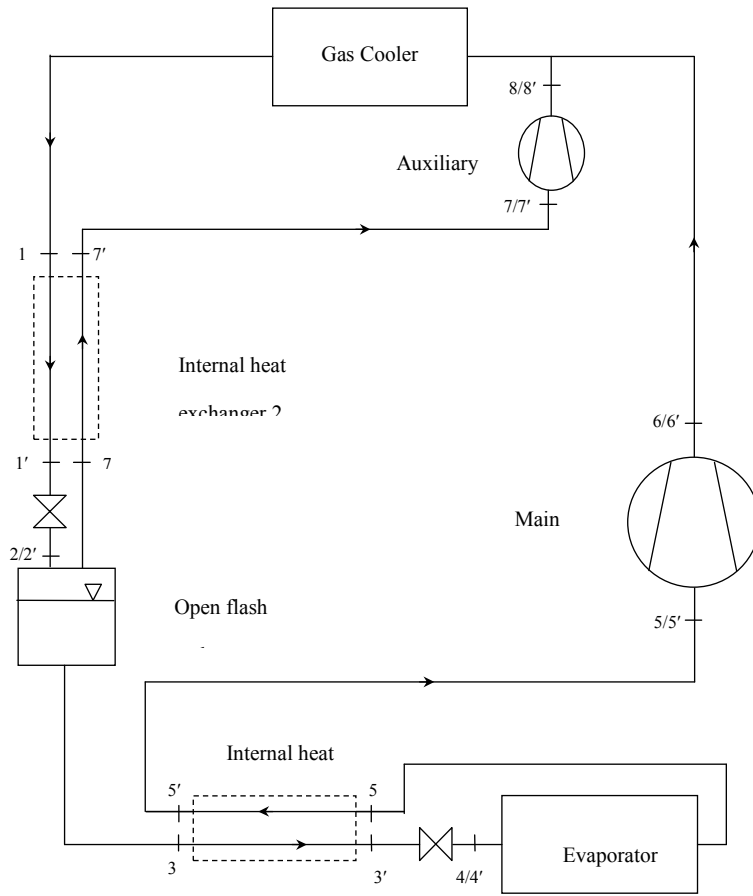
Figure 1.2.3: R744 cycle with auxiliary compressor
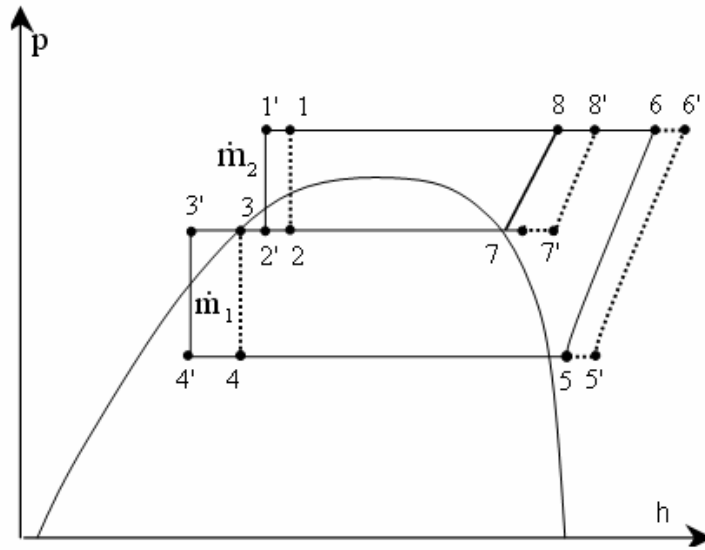
Figure 1.2.4: R744ph diagram of the cycle with auxiliary compressor

1.2.3.4 Evaporative cooling

The utilization of the evaporative cooling can lower the temperatu   at the gas cooler outlet condensation temperature, or the temperature at the gas cooler outlet, improving the cycle efficiency. It provides an adiabatic saturation of the air at the finned coil air inlet, thus taking advantage of the latent heat of the wet air. In this case, a commercial adiabatic saturator is chosen: its features are resumed in the following diagrams (the parametric lines represent the thickness of the package, in mm).
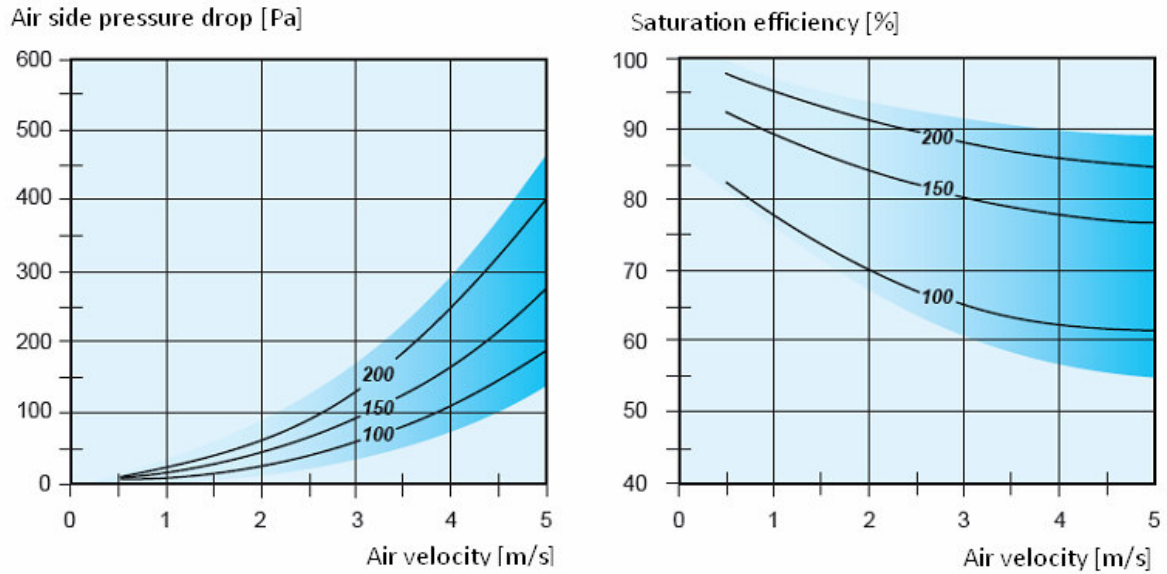
Figure 1.2.5: Features of the adiabatic saturator

Being the air velocity 2 m/s, the relative humidity 50% and the thickness of the package, 150 mm, the air side supplementary pressure drop is 50 Pa and the saturation efficiency is 85%; in this way, it is possible to calculate the air temperature at the gas cooler inlet, though the following equations:

$$\eta = \frac{x_{out} - x_{in}}{x_w - x_{in}},$$ (30)

where

η: saturation efficiency [-]

x_{in}:   specific humidity at the package inlet [g/g$_{dry\ air}$]

x_{out}:   specific humidity at the package outlet [g/g$_{dry\ air}$]

x_w: wet temperature specific humidity [g/g$_{dry\ air}$]

46

1.2.4 Air conditioning systems simulated

1.2.4.1 Design and operative conditions

The following air conditioning systems are simulated:
- single stage throttling and single stage compression (baseline), operating with R410A
- single stage throttling and single stage compression (baseline), operating with R134a
- single stage throttling and single stage compression (baseline), operating with R744
- single stage throttling and single stage compression (baseline), operating with R717
- single stage throttling and single stage compression, operating with R744, with adiabatic saturator
- single stage throttling and single stage compression, operating with R717, with adiabatic saturator
- double stage throttling, with auxiliary compressor, operating with R744
- double stage throttling, with auxiliary compressor, operating with R744, with adiabatic saturator

The system is a reversible machine: it acts as chiller, for summer air-conditioning, and as heat pump, for winter heating. The system is traditional air-to-water, with a finned coil heat exchanger, that acts as condenser (gas cooler) in cooling mode and as evaporator in heating mode, and a plate heat exchanger.

The air-conditioning system is simulated using the following design conditions:
- Air-conditioning running mode
- Evaporation temperature: 3°C
- Superheat: 5K
- Approach at the plate heat exchanger (temperature difference between the secondary fluid at the heat exchanger inlet and the refrigerant at the heat exchanger outlet): 5K
- Dry-bulb air temperature at the finned coil inlet: 35°C
- Air relative humidity at the finned coil inlet: 50%

For subcritical cycle:

- Condensation temperature: 50°C
- Subcooling: 8K
- Approach at the finned coil (temperature difference between the refrigerant at the heat exchanger outlet and the secondary fluid at the heat exchanger inlet): 5K

For transcritical cycle:
- Approach at the finned coil (temperature difference between the refrigerant at the heat exchanger outlet and the secondary fluid at the heat exchanger inlet): 2K
- Gas cooler pressure (it is a function of the air temperature): 9.33 MPa

Under these design conditions, the heat exchangers transmittance, $UA_{e,D}$ and $UA_{c,D}$, are calculated. Then, the behaviour of the reversible unit (chiller and heat pump) is simulated under different conditions. For summer air-conditioning:
- Secondary fluid temperature at the evaporator inlet: 12°C.
- External air temperature range: 24÷40°C (step 2K)

For winter heating:
- Secondary fluid temperature at the condenser/gas cooler inlet: 30°C.
- External air temperature range: -10÷14°C (step 2K).

1.2.4.2 Compressors

The chosen compressors are model available in the market; they are simulated using the polynomial curves provided by the manufacturers.

They are:
- R410A: scroll compressor Copeland ZP385KCE-TWD; the swept volume is 60.79 m³/h at 50Hz of power supply. The polynomial curves are in the form of equation (1) and (2); they are available in the web site http://www.ecopeland.com/.
- R134a: screw compressor Refcomp 134-S-140; the swept volume is 560 m³/h at 50Hz of power supply. The polynomial curves are in the form of equation (1) and (2); they are available in the web site http://www.refcomp.it/.
- R717: open screw compressor Bitzer OSKA5361-K; the swept volume is 118 m³/h at 50Hz of power supply. The polynomial curves are in the form

of equation (1) and (2); they are available in the web site http://www.bitzer.de/.

- R744: reciprocating compressor Bitzer. The polynomial curves are in the form of equation (19) and (20); they are given from the compressor manufacturer through a private communication and they are not available in the market. The values of the polynomial coefficients are resumed in Table 1.2.1.

	η_v	η_{is}
a1	1.0249	0.3722
a2	-0.0877	0.3236
a3	-	-0.1022
a4	-	0.0096

Table 1.2.1: R744 compressor polynomial curves

The design conditions are resumed in Table 1.2.2; power consumptions and refrigerating capacities are very different, but the comparison is on the performance, that is EER value in cooling mode and COP in heating mode. In the power consumption, the auxiliary power is computed

	R410A	R134a	R744	R717
T_E [°C]	3	3	5	3
T_C ($T_{gc,out}$) [°C]	50	50	37	50
p_{GC} [MPa]	-	-	9.33	-
SC [K]	0	5	-	0
SH [K]	10	10	10	5
P [10^3W]	25.5	92.0	12.9	33.4
Q_e [10^3W]	76.5	312.4	31.5	109.2
EER [-]	3.00	3.40	2.44	3.27

Table 1.2.2: Design conditions of the different chillers

1.2.5   Simulation results

1.2.5.1   Baseline air conditioning chiller

The first comparison is among air conditioning chiller operating according to a single stage throttling and single stage compression cycle. The results under different temperatures of external air, with the same temperature of secondary fluid at the evaporator inlet (12°C), are shown in the diagram of Figure 1.2.6 and resumed in Table 1.2.3.
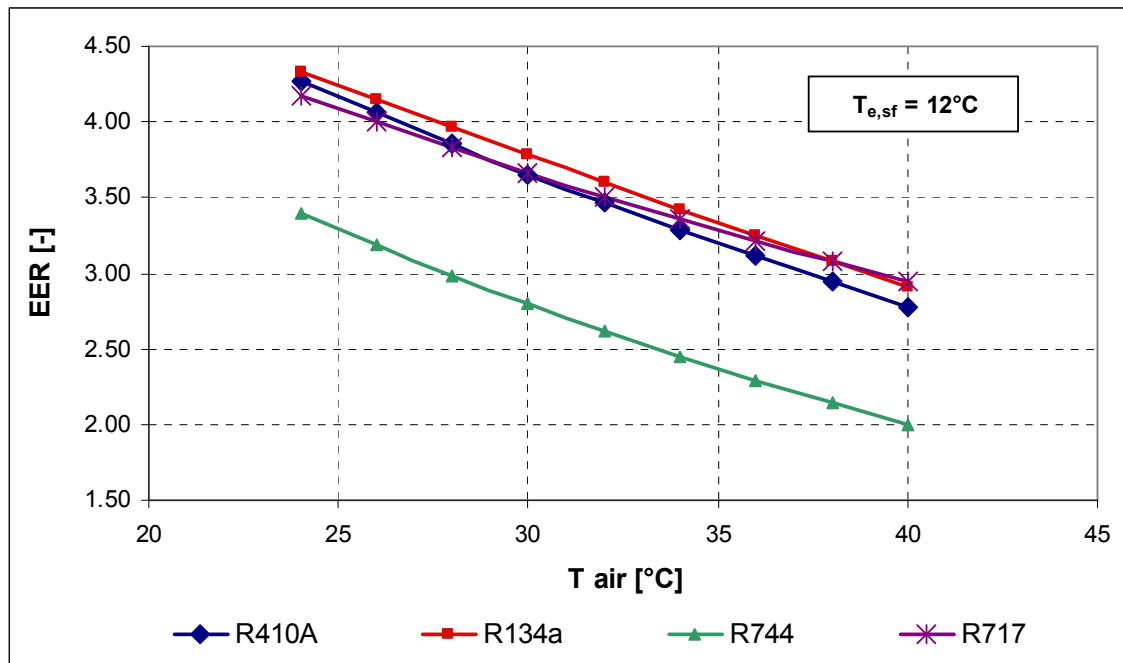
Figure 1.2.6: Baseline chiller, simulation results at $T_{e,sf}$=12°C and external air temperature=24÷40°C

The performance of the carbon dioxide chiller is clearly lower than those of the other refrigerants; the performances of R410A, R134a and R717 are close, even if R134a results the most efficient and R717 presents interesting results at high temperatures of external air. Considering the R134a EER as reference, the percentage differences are resumed in Table 1.2.4.

		EER			
$T_{e,sf}$	T air	R410A	R134a	R744	R717
°C	°C	-	-	-	-
12	24	4.27	4.32	3.39	4.17
12	26	4.06	4.14	3.19	4.00
12	28	3.85	3.96	2.99	3.83
12	30	3.65	3.78	2.80	3.67
12	32	3.47	3.60	2.62	3.51
12	34	3.29	3.42	2.45	3.36
12	36	3.11	3.25	2.29	3.22
12	38	2.94	3.08	2.14	3.08
12	40	2.78	2.91	2.00	2.95

Table 1.2.3: Baseline chiller, simulation results at $T_{e,sf}$=12°C and external air temperature=24÷40°C

$T_{e,sf}$	T air	R410A	R134a	R744	R717
°C	°C	%		%	%
12	24	-1.2	-	-21.6	-3.5
12	26	-2.0	-	-23.0	-3.5
12	28	-2.7	-	-24.6	-3.4
12	30	-3.3	-	-26.0	-3.0
12	32	-3.8	-	-27.3	-2.5
12	34	-4.0	-	-28.6	-1.8
12	36	-4.2	-	-29.6	-1.0
12	38	-4.4	-	-30.5	0.0
12	40	-4.6	-	-31.3	1.1
Average	%	-3.4	-	-26.9	-2.0

Table 1.2.4: Baseline chiller, simulation at $T_{e,sf}$=12°C and external air temperature=24÷40°: percentage difference with reference to R134a

1.2.5.2   Baseline heat pump

The comparison is repeated on the same machines, operating as heat pumps; the simulations are carried out at 30°C of temperature of secondary fluid at the condenser inlet. It is a common temperature for low-temperature heating system,

for example floor heating. The results are shown in Figure 1.2.7 and resumed in Table 1.2.5.
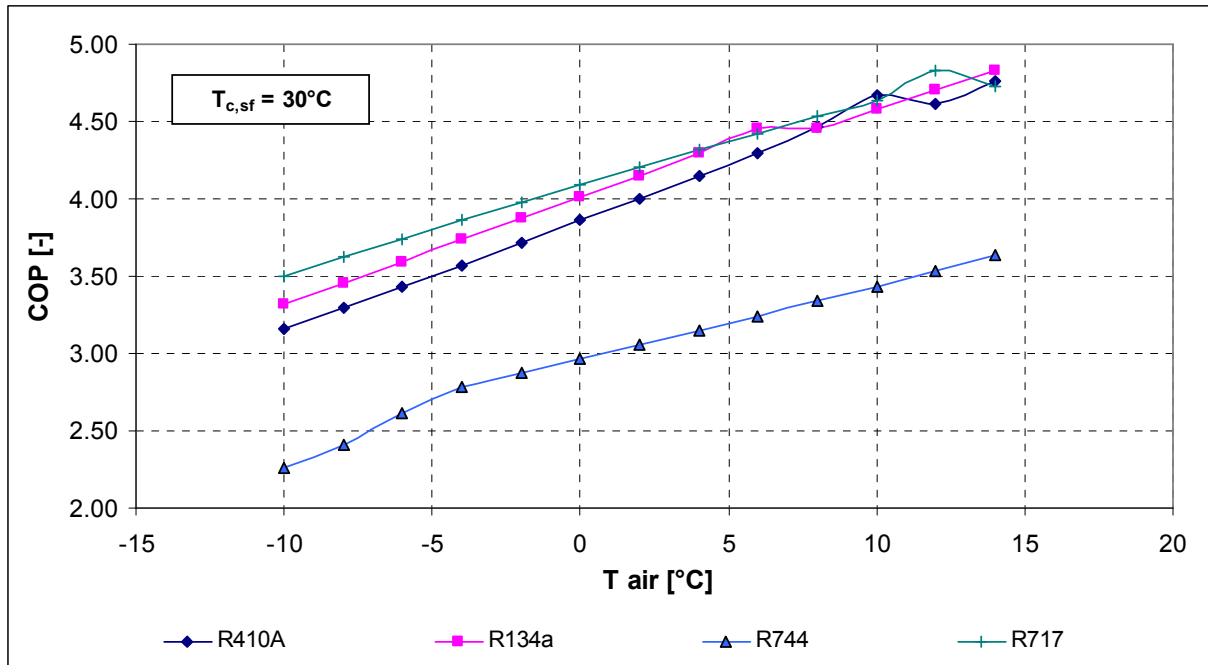
Figure 1.2.7: Baseline heat pump, simulation results at $T_{c,sf}$=30°C and external air temperature=-10÷14°C

Even in this case, CO_2 is strongly penalized, while ammonia presents the highest efficiency; even in this case, the EER percentage differences to the EER of R134a are reported in Table 1.2.6.

Considering these two first set of simulations, it is clear that a carbon dioxide simple cycle is less efficient in comparison with the other refrigerants. Both in an air-conditioning system and in a heat pump, the energy penalization is from 20% to 30% and it is higher at high temperature of external air. In the following simulations, some solutions are considered to improve the R744 energy performance.

$T_{c,sf}$	T air	COP			
		R410A	R134a	R744	R717
°C	°C	-	-	-	-
30	-10	3.16	3.32	2.26	3.50
30	-8	3.29	3.46	2.41	3.62
30	-6	3.43	3.59	2.61	3.74
30	-4	3.57	3.73	2.78	3.86
30	-2	3.71	3.87	2.87	3.98
30	0	3.86	4.01	2.96	4.09
30	2	4.00	4.15	3.05	4.21
30	4	4.15	4.29	3.15	4.32
30	6	4.30	4.45	3.24	4.42
30	8	4.46	4.46	3.34	4.53
30	10	4.67	4.58	3.43	4.63
30	12	4.62	4.71	3.54	4.83
30	14	4.76	4.83	3.64	4.73

Table 1.2.5: Baseline heat pump, simulation results at $T_{c,sf}$=30°C and external air temperature=-10÷14°C

$T_{c,sf}$	T air	R410A	R134a	R744	R717
°C	°C	%		%	%
30	-10	-5.0	-	-31.9	5.2
30	-8	-4.7	-	-30.3	4.8
30	-6	-4.7	-	-27.3	4.0
30	-4	-4.5	-	-25.6	3.4
30	-2	-4.1	-	-25.9	2.7
30	0	-3.8	-	-26.1	2.0
30	2	-3.4	-	-26.4	1.4
30	4	-3.3	-	-26.7	0.6
30	6	-3.4	-	-27.2	-0.7
30	8	0.1	-	-25.2	1.6
30	10	1.8	-	-25.1	1.0
30	12	-1.9	-	-24.9	2.5
30	14	-1.4	-	-24.7	-2.0
Average	%	-2.9	-	-26.7	2.0

Table 1.2.6: Baseline heat pump, simulation at $T_{c,sf}$=30°C and external air temperature=-10÷14°C; percentage difference with reference to R134a

1.2.5.3 *Air conditioning chiller with adiabatic saturator*

The first considered option to improve the energy efficiency of an air conditioning system is the use of an adiabatic saturator upstream the air finned coil. This heat exchanger is a condenser/gas cooler when the unit is running as chiller and an evaporator in heating mode. In the first case, the use of the adiabatic saturator is positive: the air at the heat exchanger inlet is cooled down, taking advantage of the evaporative cooling, even if there is an air side pressure drop due to the presence of the package. On the contrary, in heating mode the adiabatic saturator represents an adding thermal load for the unit, so its effect is penalizing. In this case, the package of the adiabatic saturator is considered not fed by water: in this way the temperature of the air is the same and it implies just an adding air side pressure drop. In this paragraph, the effect of the adiabatic saturator in an air conditioning chiller is analyzed. It is used only in the natural refrigerant units (R744 and R717).

In the first comparison, the only effect of the adiabatic saturator is highlighted; the energy improvement is clear, especially for carbon dioxide. The averaged EER increasing is around 22% and it increases with the external air temperature, reaching the 28.1% at 40°C. Nevertheless, the performance of the ammonia chiller are still higher, even those of the chiller without the adiabatic saturator. For R717, the EER improvement is less relevant: it is from 2.1% at 24°C to 9.9% at 40°C. These data are plotted in Figure 1.2.8 and resumed in Table 1.2.7.
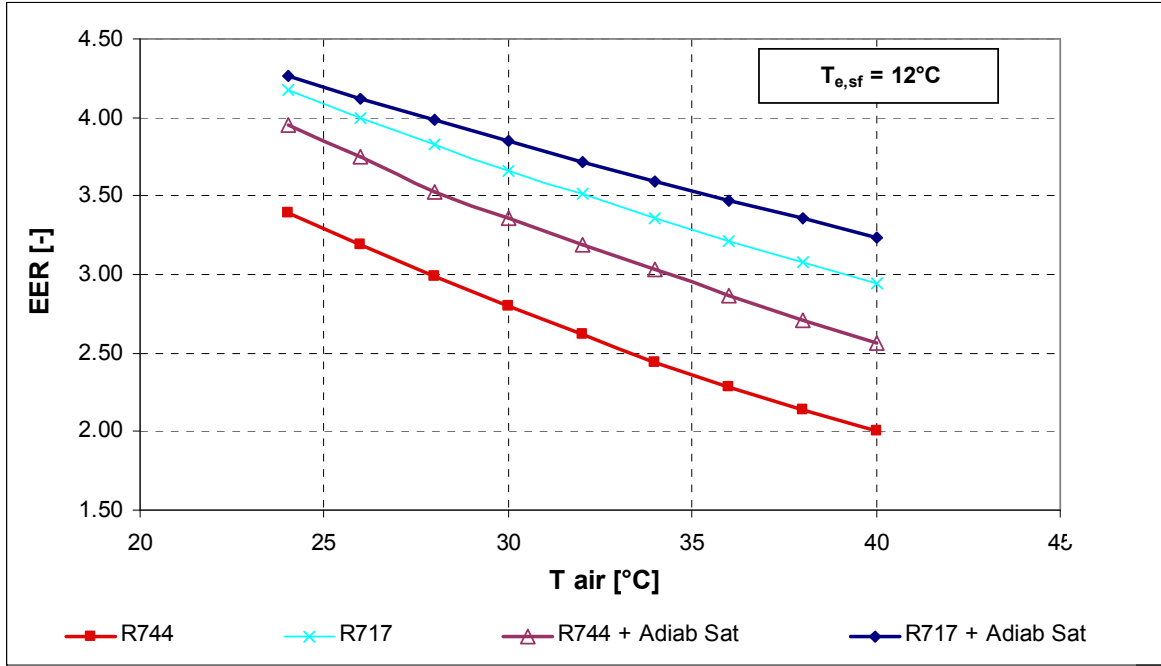
Figure 1.2.8: Chiller with adiabatic saturator, simulation results at $T_{e,sf}$=12°C and external air temperature=24÷40°C

$T_{e,sf}$	T air	EER				
		R134a	R744	R744 + Adiab Sat	R717	R717 + Adiab Sat
°C	°C	-	-	-	-	-
12	24	4.32	3.39	3.95	4.17	4.26
12	26	4.14	3.19	3.75	4.00	4.12
12	28	3.96	2.99	3.53	3.83	3.98
12	30	3.78	2.80	3.35	3.67	3.85
12	32	3.60	2.62	3.19	3.51	3.72
12	34	3.42	2.45	3.03	3.36	3.60
12	36	3.25	2.29	2.86	3.22	3.47
12	38	3.08	2.14	2.71	3.08	3.35
12	40	2.91	2.00	2.56	2.95	3.24

Table 1.2.7: Chiller with adiabatic saturator, simulation results at $T_{e,sf}$=12°C and external air temperature=24÷40°C

In Figure 1.2.9, the two chillers with adiabatic saturator are compared with the R134a chiller: the energy performance of the ammonia chiller is higher, while the CO_2 is still penalized. In addition, the daily water consumption is plotted; in this

case it is around $1 \div 1.5$ m^3/day.
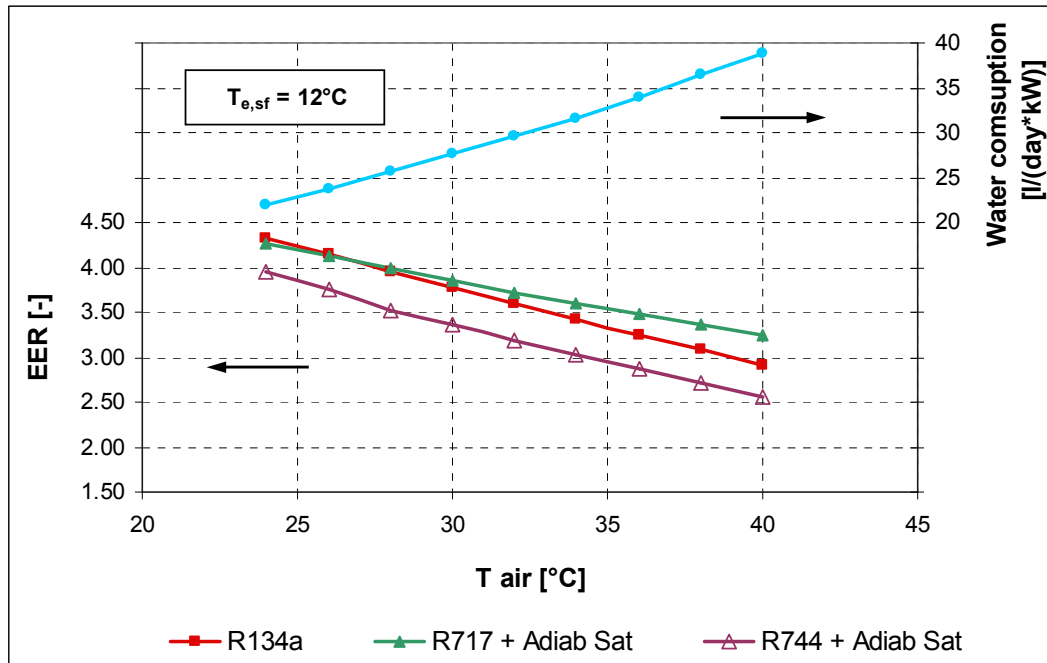
Figure 1.2.9: Chiller with adiabatic saturator, simulation results and daily water consumption at T$_{e,sf}$=12°C and external air temperature=24÷40°

1.2.5.4 Heat pump with adiabatic saturator

The drawbacks of the use of an adiabatic saturator are explained in the previous paragraph; in this case the adiabatic saturator implies an adding pressure drop and the cycle efficiency is penalized. The aim of this simulation is to quantify the energy losses in the case of a reversible machine that use a non-removable adiabatic saturator in cooling mode. In heating mode, the package is considered not fed with water.

In the case of CO_2, the energy penalization is around $7 \div 9$ % under different running conditions, while for NH_3 it is $9 \div 14$ %. Thus the adoption of an adiabatic saturator should be evaluated by a year-long energy consumption simulation. The values are reported in Tables 1.2.8 and plotted in Figure 1.2.10.
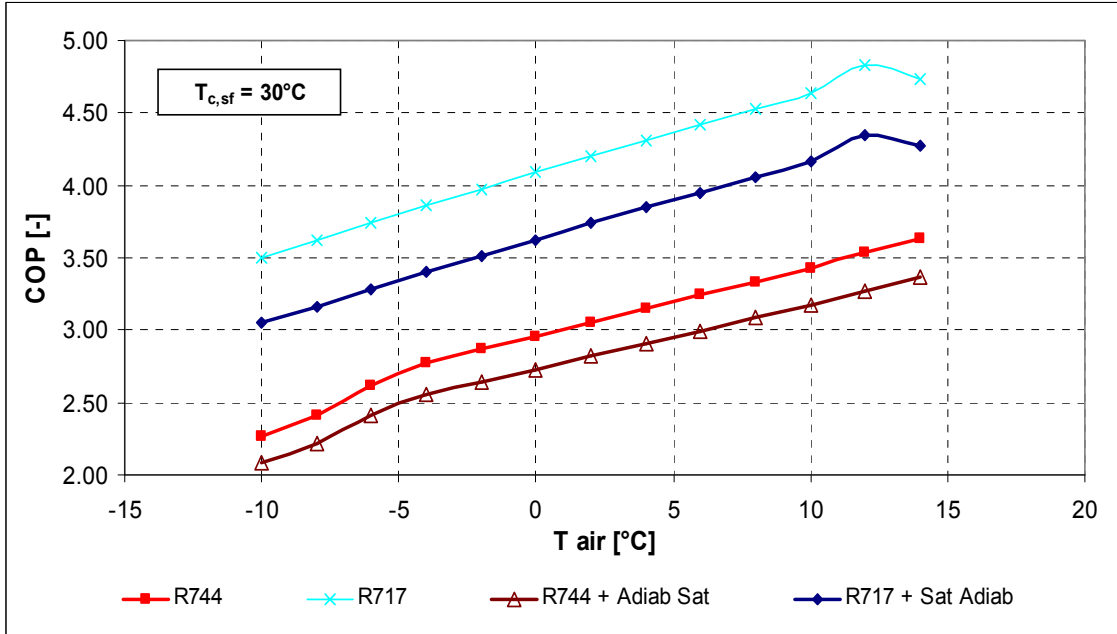
Figure 1.2.10: Heat pump with adiabatic saturator, simulation results at T$_{c,sf}$=30°C and external air temperature=-10÷14°C

| T$_{c,sf}$ | T air | COP | | | | |
		R134a	R744	R744 + Adiab Sat	R717	R717 + Adiab Sat
°C	°C	-	-	-	-	-
30	-10	3.32	2.26	2.08	3.50	3.05
30	-8	3.46	2.41	2.22	3.62	3.17
30	-6	3.59	2.61	2.41	3.74	3.28
30	-4	3.73	2.78	2.56	3.86	3.40
30	-2	3.87	2.87	2.64	3.98	3.51
30	0	4.01	2.96	2.73	4.09	3.63
30	2	4.15	3.05	2.82	4.21	3.74
30	4	4.29	3.15	2.91	4.32	3.85
30	6	4.45	3.24	3.00	4.42	3.95
30	8	4.46	3.34	3.09	4.53	4.06
30	10	4.58	3.43	3.18	4.63	4.16
30	12	4.71	3.54	3.28	4.83	4.35
30	14	4.83	3.64	3.37	4.73	4.28

Table 1.2.8: Heat pump with adiabatic saturator, simulation results at T$_{c,sf}$=30°C and external air temperature=-10÷14°C.

1.2.5.5 *R744 air conditioning chiller operating according to a cycle with auxiliary compressor*

The second solution involves a whole cycle configuration modification; the traditional vapour compression inverse cycle is changed as shown in Figure 1.2.3 and 1.2.4. In this cycle configuration, the liquid throttling is made in two stages and an auxiliary compressor compresses the flash vapour after the first throttling stage. This configuration is studied only for the most penalized fluid, the carbon dioxide. An interesting option should be the use of part of the main compressor to carry out the auxiliary compression; for example, if the chosen compressor is a 4-cylinder reciprocating one, one cylinder can act as auxiliary compressor. In this case, the hypothesizes is that there are 3 or 4 compressor, with 4 cylinders each. All the possible swept volume ratios (i.e. the number of cylinders which act as auxiliary compressor on the total number of cylinders) have been investigated. The most energy favorable ratio is 1/4 (that is 1 cylinder on 4 for the single compressor, or 3 cylinders on 12 for a 3-compressor chiller, or 4 cylinders on 16 for a 4-compressor chiller).

This configuration provides a considerable energy improvement: the average EER increase, with respect to the baseline cycle, is 11.8% and it ranges from 9.4% to 13.6%, increasing with external air temperature. Nevertheless, the R744 EER is still lower than those of the R134a and R717 baseline cycles: on average, it is, respectively, 18.4% and 16.7% lower. These results are plotted in the diagram of Figure 1.2.11 and reported in Table 1.2.9.
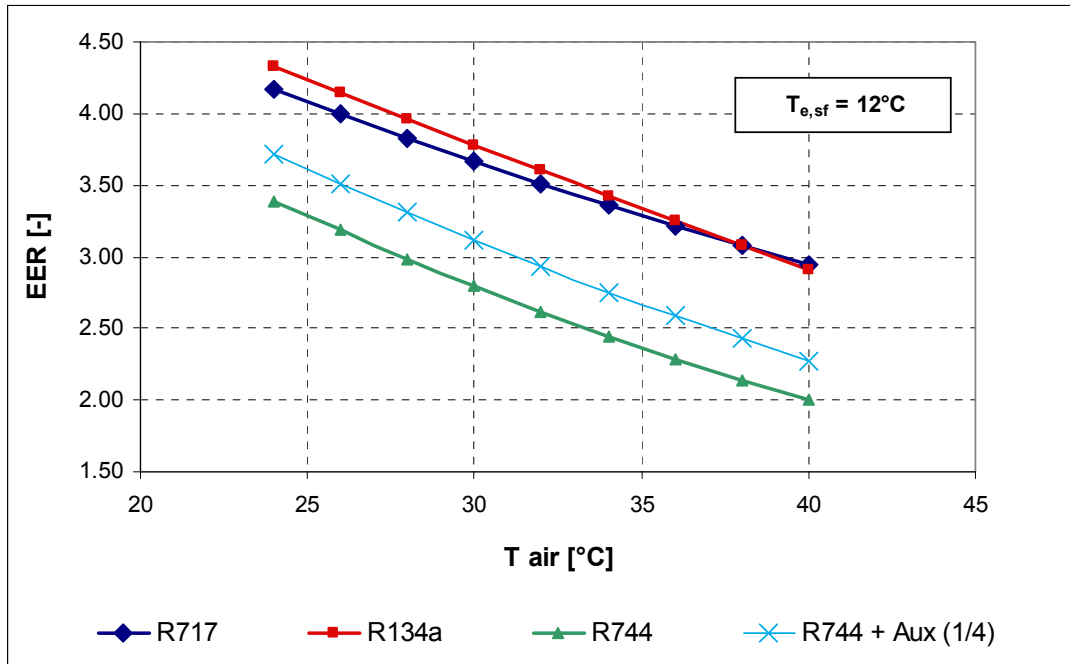
Figure 1.2.11: Chiller with auxiliary compressor, simulation results at $T_{e,sf}$=12°C and external air temperature=24÷40°C.

$T_{e,sf}$	T air	EER			
		R134a	R744	R744 + Aux (1/4)	R717
°C	°C	-	-	-	-
12	24	4.32	3.39	3.71	4.17
12	26	4.14	3.19	3.51	4.00
12	28	3.96	2.99	3.31	3.83
12	30	3.78	2.80	3.11	3.67
12	32	3.60	2.62	2.93	3.51
12	34	3.42	2.45	2.75	3.36
12	36	3.25	2.29	2.59	3.22
12	38	3.08	2.14	2.43	3.08
12	40	2.91	2.00	2.27	2.95

Table 1.2.9: Chiller with auxiliary compressor, simulation results at $T_{e,sf}$=12°C and external air temperature=24÷40°C

1.2.5.6 R744 heat pump operating according to a cycle with auxiliary compressor

The same modifications are made for the heating system, even in this case only for carbon dioxide. This solution provides an energy improvement ranging from 8% to 14% with respect to the baseline, but it is not enough to reach the COP of R134a and R717 heat pump. In fact, the COP is 14÷19% and 16÷21% lower, respectively compared to R134a and R717 baseline heat pumps, as shown in Figure 1.2.12 and Table 1.2.10.
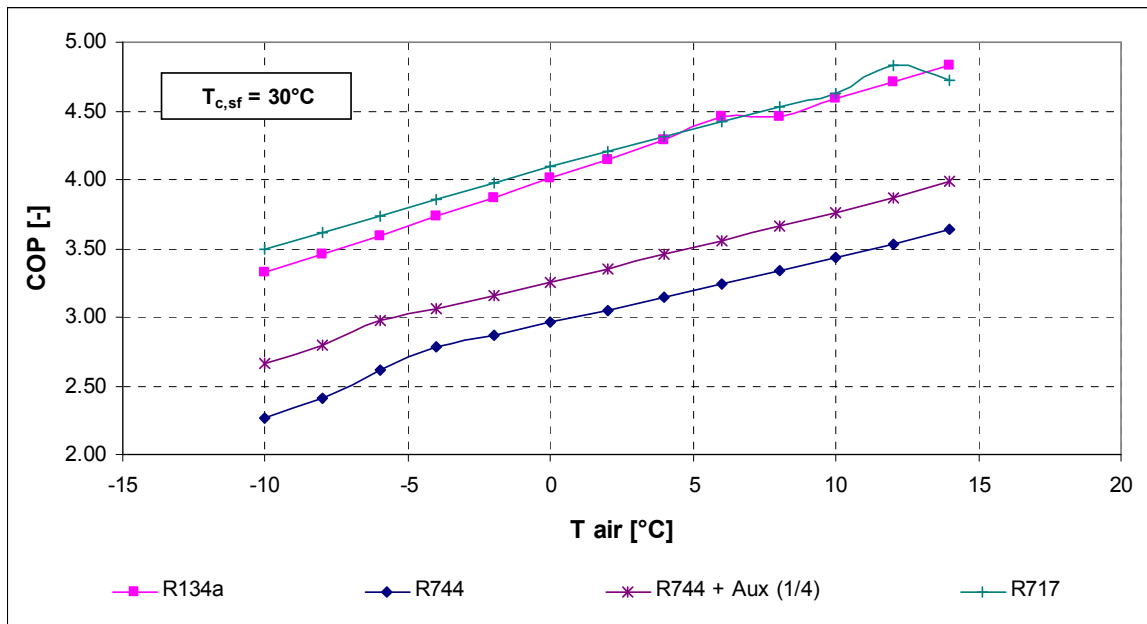
Figure 1.2.12: Heat pump with auxiliary compressor, simulation results at $T_{c,sf}=30°C$ and external air temperature=-10÷14°C

$T_{c,sf}$	T air	COP			
		R134a	R744	R744 + Aux (1/4)	R717
°C	°C	-	-	-	-
30	-10	3.32	2.26	2.67	3.50
30	-8	3.46	2.41	2.79	3.62
30	-6	3.59	2.61	2.97	3.74
30	-4	3.73	2.78	3.07	3.86
30	-2	3.87	2.87	3.16	3.98
30	0	4.01	2.96	3.26	4.09
30	2	4.15	3.05	3.35	4.21
30	4	4.29	3.15	3.45	4.32
30	6	4.45	3.24	3.56	4.42
30	8	4.46	3.34	3.66	4.53
30	10	4.58	3.43	3.76	4.63
30	12	4.71	3.54	3.87	4.83
30	14	4.83	3.64	3.98	4.73

Table 1.2.10: Heat pump with auxiliary compressor, simulation results at $T_{c,sf}$=30°C and external air temperature=-10÷14°C.

1.2.5.7 R744 air conditioning chiller operating according to a cycle with auxiliary compressor, with adiabatic saturator

The last solution considers both the use of the adiabatic saturator and the cycle with auxiliary compressor. The objective is to investigate how close to the efficiency of an air conditioning system operating with traditional refrigerants a CO_2 chiller can go. This solution is compared to the baseline R134a and R717 chillers and to the R717 chiller with adiabatic saturator.

In this case the efficiency of the system is comparable to that of the baseline R134a and R717 chillers, with a penalization of 2.8% and 0.8%, respectively. In the case of a R717 chiller with adiabatic saturator, the energy penalization is 6.8%. These results are plotted in Figure 1.2.13 and reported in Table 1.2.11
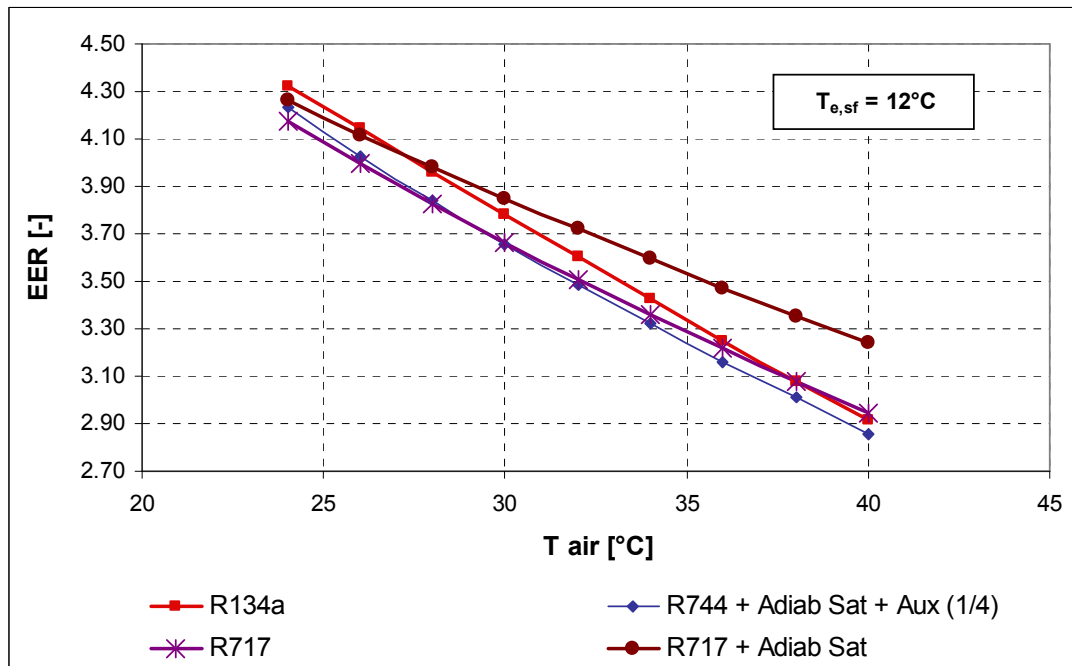
Figure 1.2.13: Chiller with auxiliary compressor and adiabatic saturator, simulation results at
$T_{e,sf}$=12°C and external air temperature=24÷40°C

$T_{e,sf}$	T air	EER			
		R134a	R744 + Adiab Sat + Aux (1/4)	R717	R717 + Adiab Sat
°C	°C	-	-	-	-
12	24	4.32	4.23	4.17	4.26
12	26	4.14	4.03	4.00	4.12
12	28	3.96	3.84	3.83	3.98
12	30	3.78	3.65	3.67	3.85
12	32	3.60	3.48	3.51	3.72
12	34	3.42	3.33	3.36	3.60
12	36	3.25	3.16	3.22	3.47
12	38	3.08	3.01	3.08	3.35
12	40	2.91	2.86	2.95	3.24

Table 1.2.11: Chiller with auxiliary compressor and adiabatic saturator, simulation results at
$T_{e,sf}$=12°C and external air temperature=24÷40°C

1.2.5.8 R744 heat pump operating according to a cycle with auxiliary compressor, with adiabatic saturator

In heating mode, the adiabatic saturator undoes the energy advantages of the cycle with auxiliary compressor. The reversible machine is considered equipped with a non-removable adiabatic saturator; it is not fed with water, in heating mode. The energy penalization is remarkable, it is 27÷34% and 30÷36% in comparison with the baseline cycle operating with R134a and R717, respectively. It is noticeable that the baseline R744 cycle and the present solution provide the same energy efficiency, as shown in Figure 1.2.14.
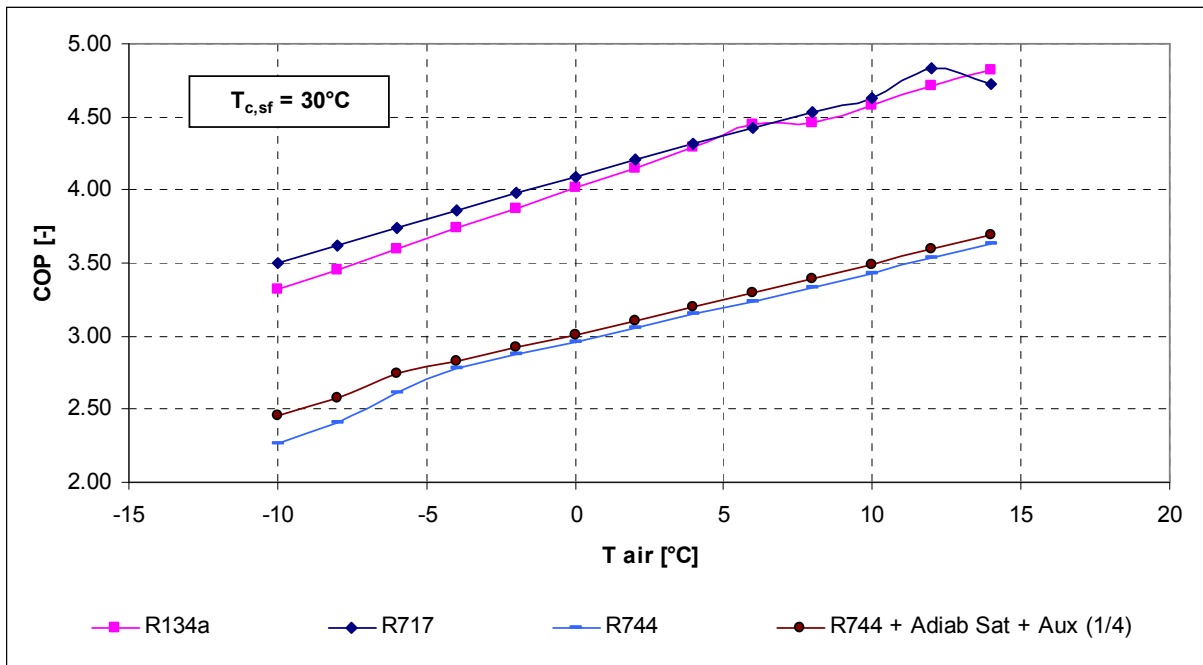
Figure 1.2.14: Heat pump with auxiliary compressor and adiabatic saturator, simulation results at $T_{c,sf}$=30°C and external air temperature=-10÷14°C

$T_{c,sf}$	T air	COP			
		R134a	R744 + Sat Adiab + Aux (1/4)	R717	R744
°C	°C	-	-	-	
30	-10	3.32	2.46	3.50	2.26
30	-8	3.46	2.58	3.62	2.41
30	-6	3.59	2.74	3.74	2.61
30	-4	3.73	2.83	3.86	2.78
30	-2	3.87	2.92	3.98	2.87
30	0	4.01	3.01	4.09	2.96
30	2	4.15	3.10	4.21	3.05
30	4	4.29	3.20	4.32	3.15
30	6	4.45	3.29	4.42	3.24
30	8	4.46	3.39	4.53	3.34
30	10	4.58	3.49	4.63	3.43
30	12	4.71	3.59	4.83	3.54
30	14	4.83	3.69	4.73	3.64

Table 1.2.12: Heat pump with auxiliary compressor and adiabatic saturator, simulation results at $T_{c,sf}$=30°C and external air temperature=-10÷14°C

1.2.6 Conclusions

The objective of this feasibility assessment was to investigate the possibility of use of natural refrigerant in air conditioning application. A simulation code, based on the assumption of correcting the design transmittance according to refrigerant and secondary fluid mass flow rate variations, was developed. The considered system was a reversible machine, which can acts both as air conditioner in cooling mode and as heat pump in heating mode. The studied natural fluids were R717 (NH_3) and R744 (CO_2). Due to its interesting environmental properties, carbon dioxide is widely studied, even if its cycle efficiency is lower than the other refrigerant. Ammonia provides a higher efficiency, comparable to that of halogenated fluids, but its toxicity and flammability limits its use, especially in places with people.

As a first step, the efficiencies of a single throttling, single compression cycle, for different refrigerant (R134a, R410A, R717, and R744) were compared, in cooling and heating mode. The penalization of the carbon dioxide system is clear, so different solutions were taken into account. The use of an adiabatic saturator

provides a good energy improvement in cooling mode, but it implies a relevant water consumption and an energy penalization, in heating mode, if it is not removable. Thus its use can be interesting in some applications; by the way, the R744 energy efficiency is still lower than those of the other fluid baseline cycles. The modification of the cycle, with a two stage throttling and an auxiliary compressor, increases the efficiency in both cooling and heating mode. The disadvantage is the extra cost for the components and for the modification of the cycle; even in this case, the R744 efficiency is still lower of than those of the other fluid baseline cycles. A comparable efficiency can be achieved, in cooling mode, using both the adiabatic saturator and the cycle with auxiliary compressor, while in heating mode carbon dioxide can not reach a good efficiency. As regards R717, the results are more interesting and the performances are comparable or even higher than halogenated refrigerants.

For these reasons, at the moment, carbon dioxide is not competitive in air conditioning applications with other refrigerants: the additional cost can not provide attractive results for the market. As regards ammonia, the performances are interesting and, if the constrains related to its toxicity and flammability can be overcome, it will be a possible alternative of halogenated fluids in HVAC systems.

1.2.7 References

1. Binotto C., Cecchinato L., De Carli M., Mantovan M., Scarpa M., Zecchin R., (2006), Numerical model for the estimation of performances, *5th Int. Conf. on Sustainable Energy Technologies*.
2. Cecchinato L., Chiarello M., Corradi M., Fornasieri E., Minetto S., Stringari P., Zilio C., (2009), Thermodynamic analysis of different two-stage transcritical carbon dioxide cycles, *Int. J. Refrigeration,* 32:1058-1067.
3. EN 12900 (1999), Refrigerant compressors. Rating conditions, tolerances and presentation of manufacturer's performance data.
4. Kim M. H., Pettersen J., Bullard C. W., (2004), Fundamental process and system design issues in CO_2 vapour compression systems. *Energy and Combustion Science*, 30(2): 1119-1174.

5. Kyoto protocol to the United Nations framework convention on climate change, (1997), *United Nations*.

6. Liao S. M., Zhao T. S., Jakobsen A., (2000), A correlation of optimal heat rejection pressures in transcritical carbon dioxide cycles. *Appl. Therm. Eng.*, 20: 831–841.

7. Montreal Protocol on Substances that Deplete the Ozone Layer, (1987), *United Nations*.

Chapter 1.3   EFFICIENCY IMPROVEMENT RELATED TO THE TYPE OF CYCLE: A THEORETICAL STUDY OF DIFFERENT TWO-STAGE TRANSCRITICAL CARBON DIOXIDE CYCLES

1.3.1   Introduction

In this chapter the influence of the type of cycle on the global efficiency is investigated; as pointed out in Chapter 1.2, a carbon dioxide vapour compression inverse cycle, for air conditioning applications, is strongly penalized with respect to other refrigerants, for example R717 or R134a. On other hand, some modifications of the baseline cycle allow a considerable energy improving, increasing the exergy efficiency. Traditional methods to reduce the exergy losses imply staged compression and throttling, that is two-stage throttling and inter-refrigeration of the vapour at the intermediate pressure of two-stage compression. Five different two-stage transcritical carbon dioxide cycles are studied: baseline single stage cycle, single-throttling with two-stage compression cycle, split cycle, phase separation cycle and single-stage cycle coupled with a gas cooling circuit. Each cycle is analysed for the effect of internal heat transfer between different streams of refrigerants and an analysis on the Plank cycle for intermediate pressure higher than critical one is performed. Each cycle is optimized calculating the optimal values of both the upper and the intermediate pressures; in the case of split cycle, the ratio of the mass flow rate in the main stream to the one in the auxiliary stream is also optimized.

The results of the present work were published in Cecchinato *et al.* (2009); they were performed using a FORTRAN code, developed in the Department of Fisica Tecnica of the Università of Padova.

1.3.2 Nomenclature

h enthalpy [Jkg^{-1}]

L specific mechanical energy [Jkg^{-1}]

$\dot{m}$ mass flow rate [kgs^{-1}]

p pressure [Pa]

Q specific refrigeration capacity [Jkg^{-1}]

Rp pressure ratio [-]

s entropy [Jkg^{-1}K^{-1}]

T temperature [°C]

Greek letters

η efficiency [-]

χ mass flow ratio [-]

Subscripts

$1s$ first stage compressor

$2s$ second stage compressor

A auxiliary cycle compressor (in DTAC)

E evaporator

e external cooling agent

G gas cooler

I intermediate

i inlet

is isentropic

M main cycle compressor (in DTAC)

o outlet

1.3.3 Theoretical simulation: cycle types and assumptions

Two-stage compression and two-stage throttling are widely employed with traditional inverse cycles as means for improving energy efficiency; the improvement results mainly from a reduction of the exergy losses during throttling often combined with an increase in compression isentropic efficiency, as a consequence of reduced pressure ratio; another significant advantage is present in transcritical cycles, related to inter-stage cooling with external heat rejection. This practice in traditional cycles is seldom used, since the temperature of the compressed vapour at the intermediate pressure is rather low and therefore does not allow significant heat rejection to the outside environment. In transcritical CO_2 cycles, the superheat of the compressed vapour is far higher and for that reason external heat rejection is often effective in reducing compression work.

The simulated cycles are:

1) Single-Throttling, Single-Compression (STSC): the basic cycle with a single-throttling valve and a single compressor. This cycle is performed by a refrigerating circuit similar to the one shown in Figure 1.3.1, except for substituting a single-stage compression for the two-stage compression here represented.

2) Single-Throttling, Double-Compression (STDC): the cycle with a single-throttling valve and two-stage compression with intercooling of the vapour at the intermediate pressure, as in Figure 1.3.1.

3) Double-Throttling, Double-Compression, Split Cycle (DTDC_SC): the cycle represented in Figures 1.3.2 and 1.3.3. The high pressure fluid after the gas cooler is split into two streams; one of them is throttled down to the intermediate pressure and is used to cool the residual stream of high pressure gas, before the throttling valve that feeds the evaporator.

4) Double-Throttling, Double-Compression, Open Flash Tank (DTDC_OFT): the cycle represented in Figures 1.3.4 and 1.3.5. The high pressure gas after the gas cooler is throttled down to the intermediate pressure and enters a vessel (OFT) from which the vapour is sucked by the high pressure compressor; the stream of the vapour produced by flashing is used to cool the high pressure gas exiting from the gas cooler. The liquid collected inside the open flash tank is throttled down to the evaporation pressure.

5) Double-Throttling, Auxiliary Compressor Cycle (DTAC): the cycle is represented in Figure 1.3.6. After the gas cooler, the gas undergoes a further cooling process, provided by an auxiliary circuit, using an Internal Secondary Heat exchanger (ISHX). The gas is then throttled down to the evaporation pressure.
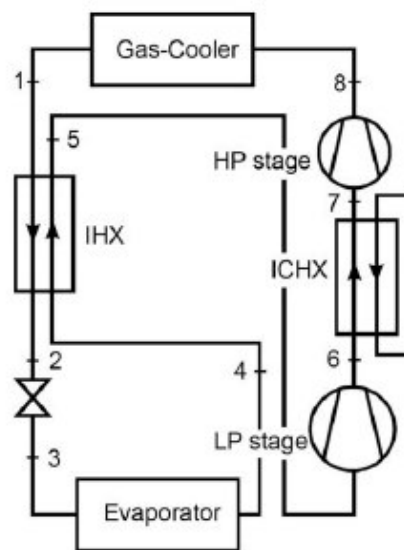
Figure 1.3.1: Single-Throttling, Double-Compression Cycle (STDC); Cecchinato et al. (2009).

All the investigated cycles, except the Double-Throttling, Auxiliary Compressor Cycle (DTAC) include an internal heat exchanger (IHX) between the line of high pressure fluid (gas or liquid) going to main throttling valve (the one before the evaporator) and the vapour line before the compressor.
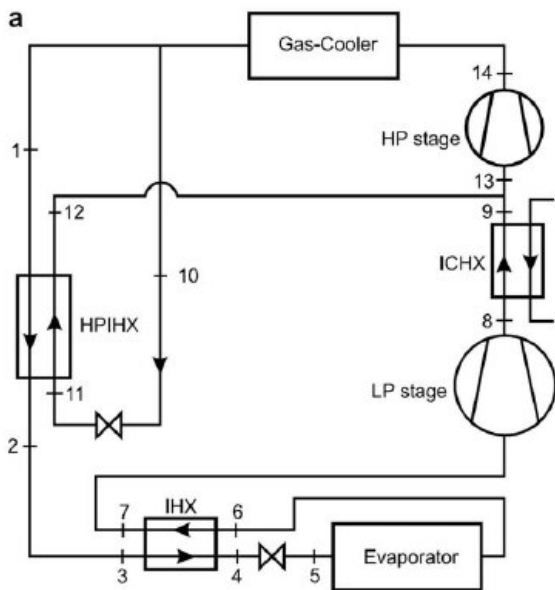
Figure 1.3.2: Double-Throttling, Double-Compression, Split Cycle (DTDC_SC); Cecchinato et al. (2009)
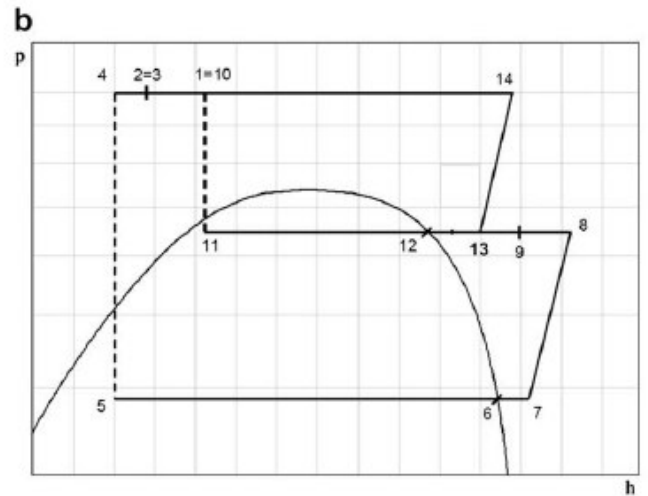
Figure 1.3.3: Double-Throttling, Double-Compression, Split Cycle (DTDC_SC), p-h diagram; Cecchinato et al. (2009)
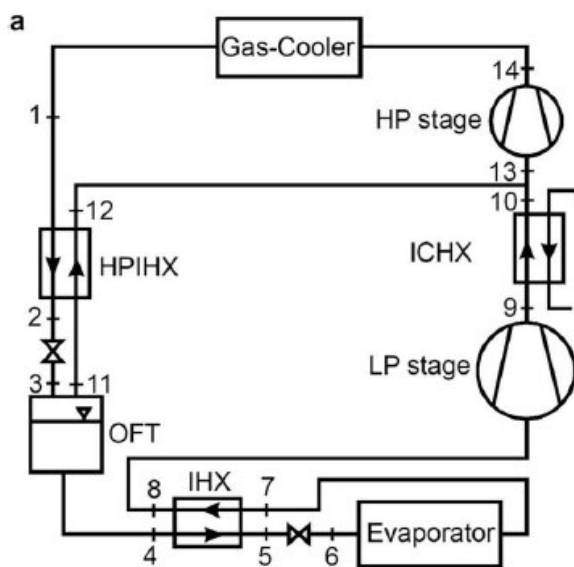
Figure 1.3.4: Double-Throttling, Double-Compression, open Flash tank Cycle (DTDC_OFT); Cecchinato et al. (2009)
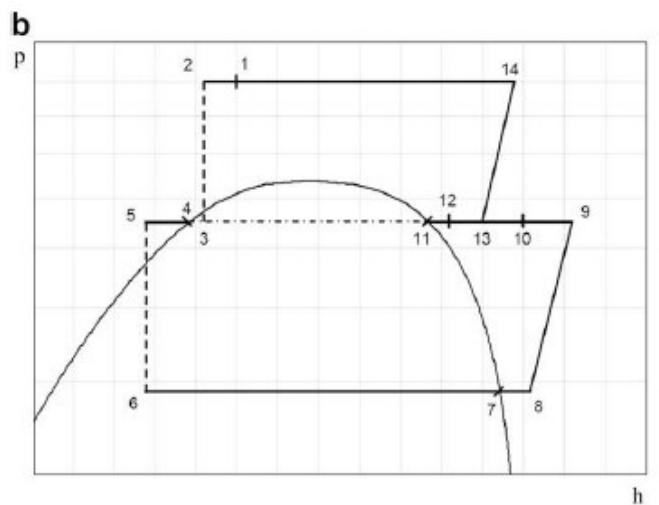
Figure 1.3.5: Double-Throttling, Double-Compression, open Flash tank Cycle (DTDC_OFT), p-h diagram; Cecchinato et al. (2009)
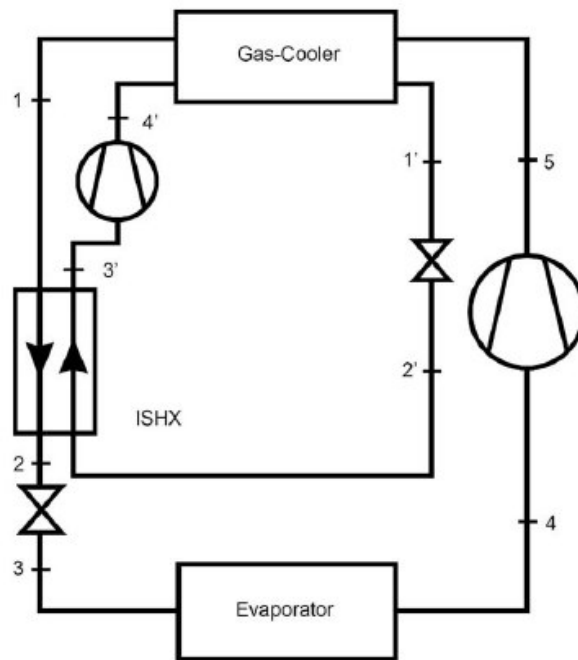
Figure 1.3.6: Double-Throttling, Auxiliary Compressor Vapour Cycle (DTAC); Cecchinato et al.

(2009)

The running conditions are those of air-conditioning systems (T_E=4°C), medium temperature refrigeration applications (T_E=-10°C) and low temperature refrigeration applications (T_E=-30°C); the assumptions for the simulations are:

- evaporation temperature: 4°C;
- saturated vapour at the evaporator outlet (no superheat);
- no superheat at ISHX of the DTAC cycle, at the evaporation side;
- temperature approach at gas cooler, at ICHX, IHX and ISHX heat exchangers = 3°C. For gas cooler and ICHX the same external cooling agent was considered; its flow rate was supposed large enough to realize the closest approach between the fluids flowing inside heat exchangers at the cold end;
- the overall isentropic compressor efficiency η_{is} depends on the compression ratio, according to the diagram in Figure 1.3.7. Two different curves are assumed, depending on the compressor suction pressure. The coefficient of these curves (equation (1) and (2)) are reported in Table 1.3.1. Curve (a), in Figure 1.3.7, is applied whenever suction pressure is higher than 2 MPa,

while curve (b) is used if suction pressure is lower than 2 MPa. Curve (a) is derived from a combination of experimental data on a Bitzer single-stage semi-hermetic reciprocating compressor (Bernabei *et al.*, 2008) and catalogue data of a Dorin two-stage semi-hermetic reciprocating compressor (Dorin, 2007) for transcritical applications. Curve (b) is interpolated from catalogue data of Bitzer reciprocating semi-hermetic compressors for subcritical applications (Bitzer, 2004). Overall isentropic compressor efficiency includes the electric losses of the motor, as explained in paragraph I.1.1.1.

Coefficient	Curve a	Curve b
C1	0.83865566	-0.891405609
C2	-0.953945484	17.47700343
C3	0.122611176	-101.9321882
C4	-0.007305908	339.5261331
C5	-0.0000147827	-598.6927616
C6	-1.275287329	199.2676481
C7	0.158331665	1486.93172
C8	-0.008846742	-3474.094151
C9	-0.0000985139	3644.734427
C10	-	-1927.009223
C11	-	414.6827975

Table 1.3.1: Coefficients of the compressor polynomials

$$\eta_{is} = \frac{C1 + C2*Rp^2 + C3*Rp^4 + C4*Rp^6 + C5*Rp^8}{1 - C6*Rp^2 + C7*Rp^4 + C8*Rp^6 + C9*Rp^8}, \qquad (1)$$

$$\eta_{is} = C1 + C2*Rp^{-1} + C3*Rp^{-2} + C4*Rp^{-3} + C5*Rp^{-4} +$$
$$+C6*Rp^{-5} + C7*Rp^{-6} + C8*Rp^{-7} + C9*Rp^{-8} + \qquad , \qquad (2)$$
$$+C10*Rp^{-9} + C11*Rp^{-10}$$

The variables subjected to optimisation depend on the considered cycle. It is well known that in transcritical inverse cycles the upper pressure is not any more linked

to the temperature of the heat rejection, but it is an independent variable to be optimised: as a matter of fact, if the refrigerant temperature at the gas cooler outlet is constant, the increase in the discharge pressure implies an increase in the compression work and, at the same time, a higher value for the refrigerating effect so as to give rise to the maximum EER for a definite value of the upper pressure. Beyond this variable, two-stage compression entails an optimal value of the intermediate pressure with respect to EER. Moreover, in the split cycle (DTDC_SC) there is one more degree of freedom, the ratio χ of the flow rate of the main stream exiting from the gas cooler to the remaining part. In fact the condition of a definite approach temperature inside the High Pressure Internal Heat exchanger (HPIHX) is not sufficient to determine this flow rate ratio. It follows that the optimal subdivision of the main stream has to be determined. This optimization has to be carried out considering that the specific heat of the fluid can vary in an unpredictable way as a function of temperature.

In the case of the auxiliary compressor cycle (DTAC), the optimisation process involves the evaporation pressure of the secondary cycle instead of the intermediate pressure, as well as the high pressure of the same cycle. The evaporation pressure of the secondary cycle determines the mass flow ratio χ, defined as the ratio of the auxiliary cycle mass flow rate on the main cycle mass flow rate, required to match the specified approach at ISHX.
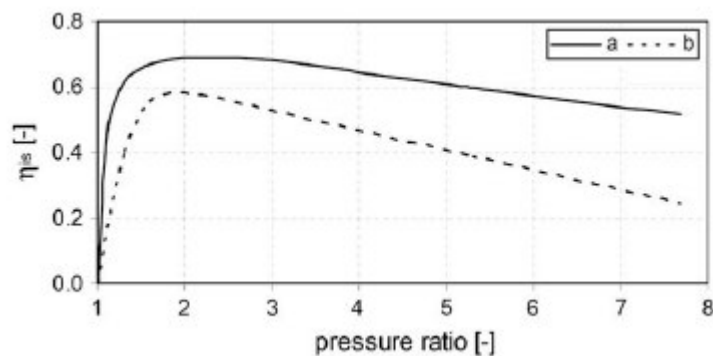
Figure 1.3.7: Overall isentropic efficiency as a function of pressure ratio for evaporation pressure higher (a) and lower (b) than 2 MPa; Cecchinato et al. (2009)

For all the considered cycles, except DTAC, a generalized form of the system energy efficiency ratio can be written as:

$$EER = \frac{\left(h_{o,E} - h_{i,E}\right)}{\left(h_{o,1s} - h_{i,1s}\right) + \left(1 + \chi\right)\left(h_{o,2s} - h_{i,2s}\right)} \tag{3}$$

For the DTAC, it can be written as:

$$EER = \frac{\left(h_{o,E} - h_{i,E}\right)}{\left(h_{o,M} - h_{i,M}\right) + \chi\left(h_{o,A} - h_{i,A}\right)} \tag{4}$$

With the considered assumptions and being fixed the values of evaporation and external cooling agent temperatures, from equation (4) the dependence of the EER from the independent variables can be easily written:

$$EER = f\left(p_G, p_I, \chi\right) \tag{5}$$

thus reducing the problem of finding the optimum values of the independent variables to the solution of a multi-variable root-finding problem of a nonlinear equation.

1.3.4 Analysis of the simulation results

1.3.4.1 Optimization of the cycles

The considered cycles have been simulated at different evaporation temperatures (+4°C, -10°C and -30 °C), corresponding to the different applications, air-conditioning, medium temperature refrigeration and low temperature refrigeration. The temperature of the external cooling agent ranges from 25°C to 35°C.
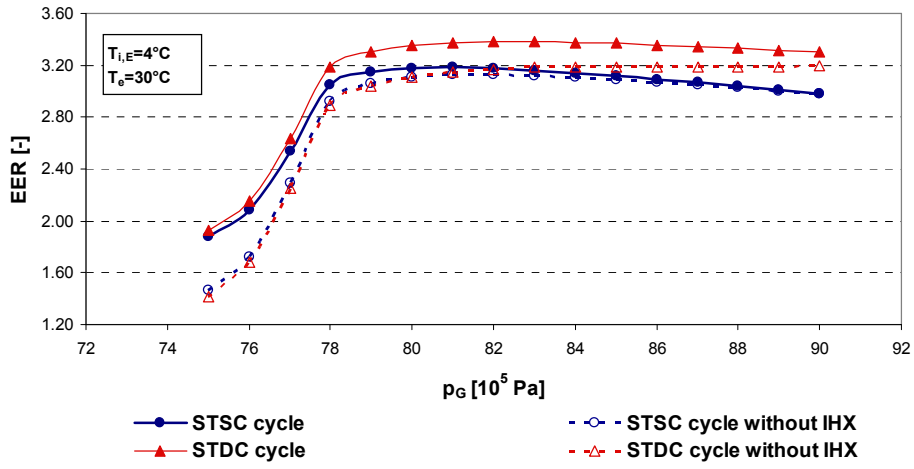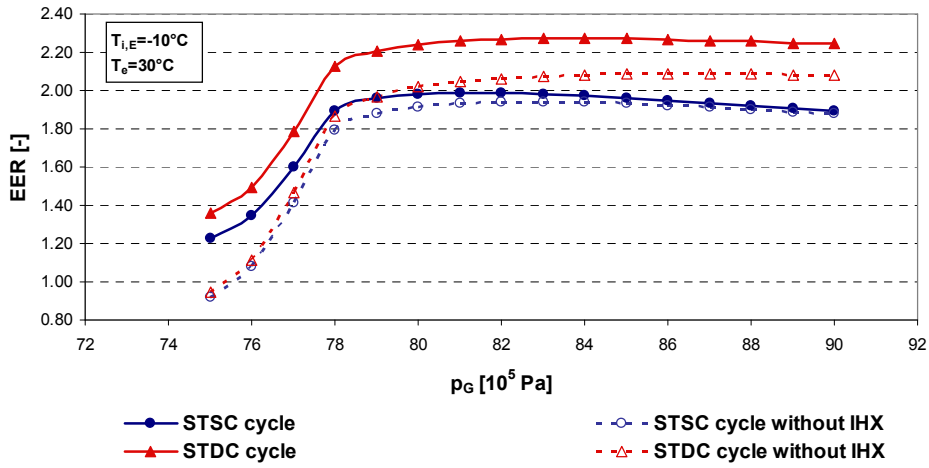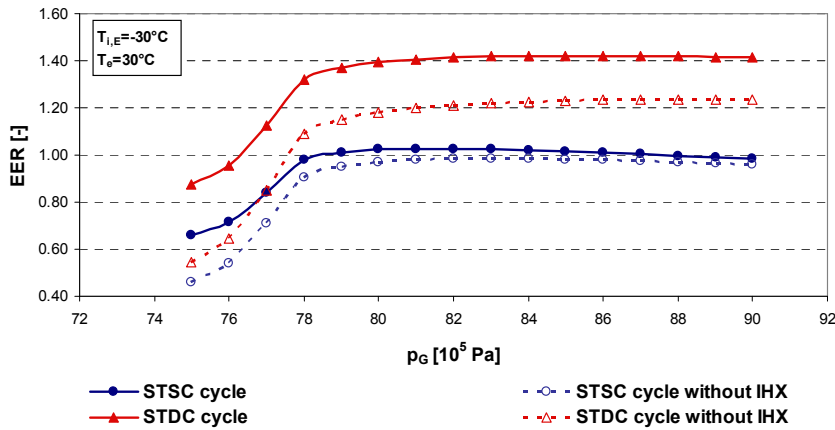
Figure 1.3.8 (a): EER of a STSC and a STDC cycle, with and without IHX, at $T_{i,E}$=4°C.

Figure 1.3.8 (b): EER of a STSC and a STDC cycle, with and without IHX, at $T_{i,E}$=-10°C.

Figure 1.3.8(c): EER of a STSC and a STDC cycle, with and without IHX, at $T_{i,E}$=-30°C

In Figures 1.3.8 (a), (b) and (c), the effects of the staged compression and of the internal heat exchanger (IHX) are shown. STSC and STDC cycles are simulated (blue and red lines in Figures 1.3.8, respectively), with and without the internal heat exchanger (solid and dashed lines in Figures 1.3.8, respectively), at 30 °C external cooling agent temperature. Different gas cooler pressures, ranging from 75 to 90 bar, have been simulated.

In air conditioning applications (Figure 1.3.8(a)) the inter-cooled compression and the use of an IHX provide an energy improvement at every gas cooler pressure. In all solutions, a sharp EER increasing is noticeable, at around 79 bar of gas cooler pressure; at higher values, the EER curve is flat. At lower gas cooler pressures, the performance of a STSC cycle is higher than that of a STDC cycle without IHX, vice versa at higher gas cooler pressures. Thus the benefits of IHX are clear at upper pressures ranging from 75 to 78 bar, while the advantages of the inter-cooled compression are remarkable at gas cooler pressures higher than 85 bar. This effect is even more evident in medium temperature refrigeration applications (Figure 1.3.8(b)); the shapes of the curves are the same of the air conditioning system and even in this case the best efficiency is achieved with the STDC solutions, with IHX. The benefits of the staged compression are higher than those provided by the IHX; in a STSC cycle, the use of an IHX gives poor energy improvement. In low temperature refrigeration applications (Figure 1.3.8(c)), the EER values of a STSC cycle, with or without IHX, are very low, around 1. A staged compression is recommended: the increase provided by a STDC cycle with IHX is about 40%. From these data, an optimal value of upper pressure can not be fixed: the higher efficiency is achieved at values ranging from 80 to 85 bar. For STDC cycle, the EER values are found optimizing the intermediate pressure.

The role played by upper and intermediate pressure in energy efficiency is illustrated in Figures 1.3.9(a), (b) and (c) at +4°C, -10°C and -30°C evaporation temperature and 30°C external cooling agent temperature. In this case, STDC, DTDC_SC, DTDC_OFT and DTAC cycles, with IHX, are simulated. Under all conditions, the efficiency decreases when the upper pressure rises. In air conditioning applications, the effect of the upper pressure is clear: the curves of the four different cycles can be grouped together according to the gas cooler pressure. For low intermediate pressures, no significant improvement appears from using more sophisticated cycles than STDC, except DTAC cycle. In this specific situation

DTAC performs better than the other cycles because the pressure ratios of both compressors allow higher values of isentropic efficiency At lower upper pressures (8 MPa), it is easy to point out an intermediate pressure value corresponding to the maximum EER; this value can vary according to the type of cycle. At higher gas cooler pressures (11.5 MPa), only for the DTAC it is possible to find a maximum, while the other curves are monotonically increasing. If the intermediate pressure is higher than the critical one (7.377 MPa), a peculiar effect can be highlighted: the curves present a sharp increase for values of intermediate pressure close to the critical one. This is the "Plank cycle" and it will be fully described in paragraph 1.3.5. For retail refrigeration of fresh foodstuffs (Figure 1.3.9(b)), the difference due to the upper pressure is less clear: for example, the EER of the DTDC_SC cycle at 10MPa gas cooler pressure is close to that of the DTAC at 8MPa gas cooler pressure. The DTAC cycle is the most energy penalized, while the highest efficiencies are performed by DTDC_SC and DTDC_OFT. For retail refrigeration of frozen foodstuffs (Figure 1.3.9(c)), the importance of the staged throttling is highlighted; the DTAC and STDC cycles are the least efficient, while the performances of cycles with double stage throttling are far better, at every upper pressures. In addition, the intermediate pressure value corresponding to the highest energy efficiency can clearly be found and the EER sharply decreases moving away from that point.
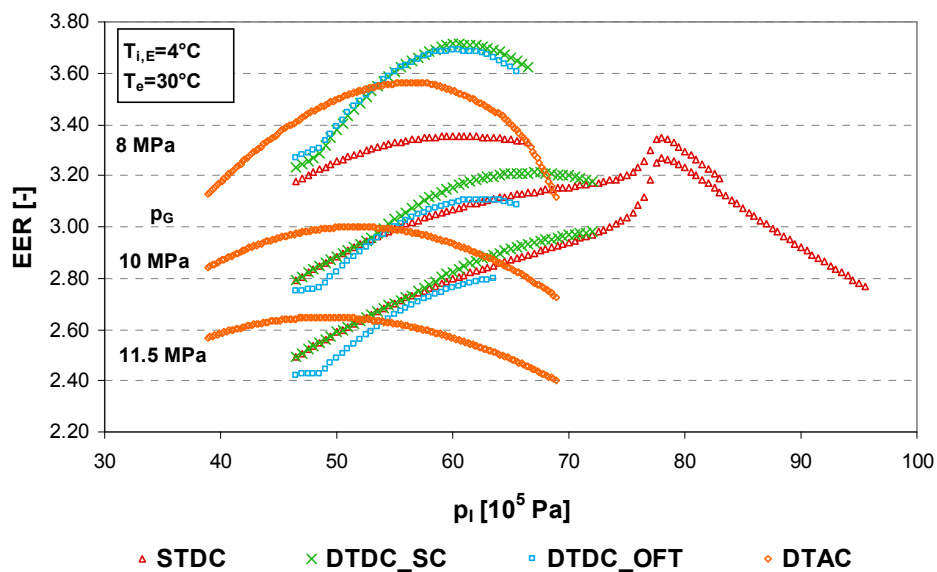
Figure 1.3.9(a): EER of different cycles with IHX and ICHX, at different upper pressures, at $T_{i,E}=4°C$.
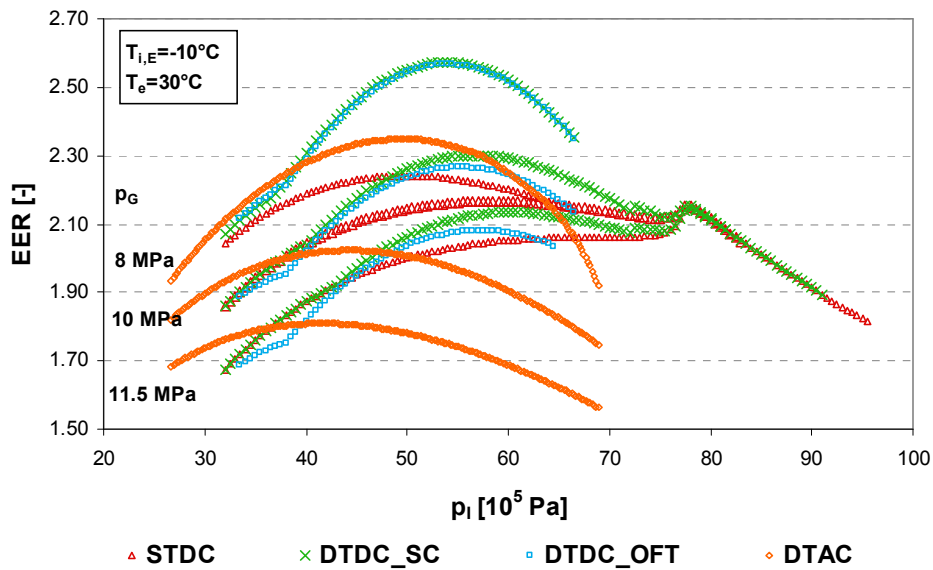
Figure 1.3.9(b): EER of different cycles with IHX and ICHX, at different upper pressures at $T_{i,E}=-10°C$.
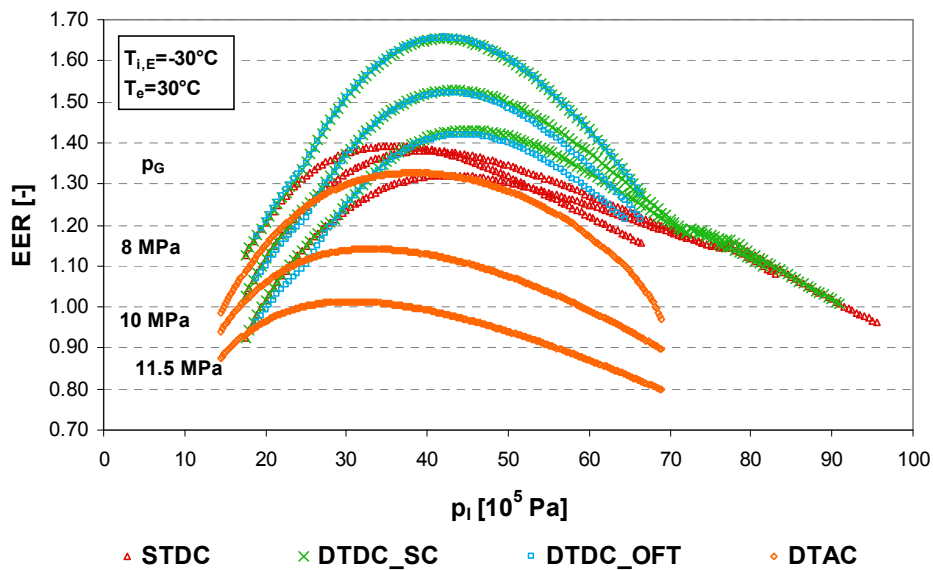
Figure 1.3.9(c): EER of different cycles with IHX and ICHX, at different upper pressures, at $T_{i,E}=-30°C$.

In Figure 1.3.10 the curves of STDC and DTDC_OFT cycles with or without IHX and ICHX are plotted with the purpose of separating the effects of heat exchange from those resulting from double throttling. For STDC cycle, the effect of the IHX is strong, especially at 8 MPa upper pressure, while for DTDC_OFT its benefits are smaller, even null at low intermediate pressure. The conclusion is that for transcritical CO_2 cycles, unlike for the traditional application of two-stage inverse cycles, energy saving resulting from inter-stage cooling during compression is even

more important than the one resulting from staged throttling.
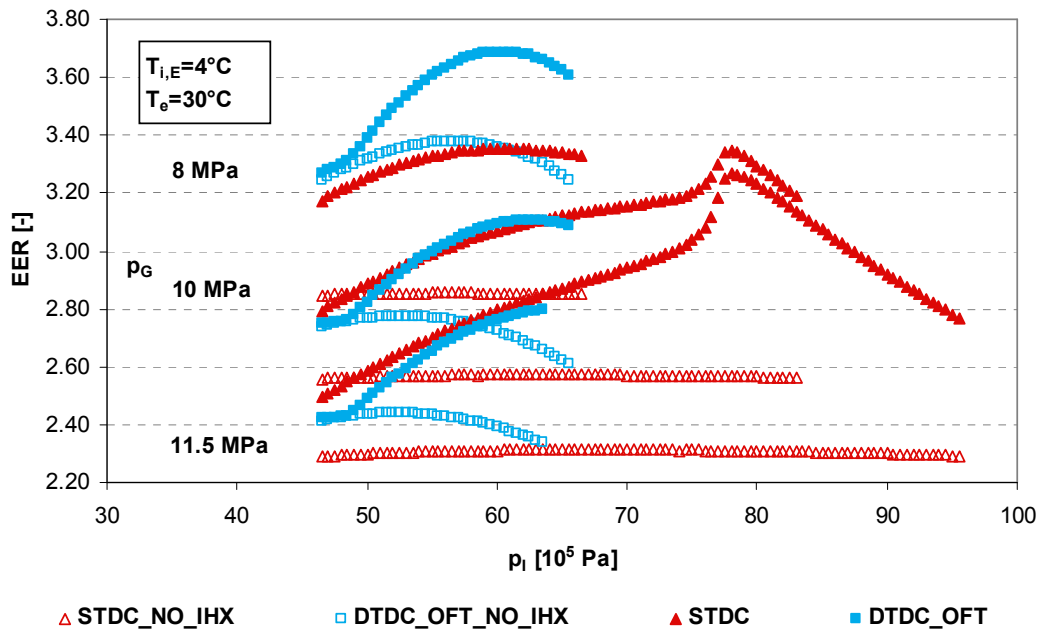
Figure 1.3.10: EER of STDC and DTDC_OFT cycles with and without IHX, at different intermediate pressures, at $T_{i,E}=4°C$

1.3.5   Consideration on the Plank cycle

As it can be easily noticed in Figures 1.3.9 and 1.3.10 for STDC and DTDC_SC systems, when the intermediate pressure just exceeds the transcritical one, a sharp maximum in the COP curve can be observed; this phenomenon is known as Plank cycle (Plank, 1912) and was already outlined by Inokuty (1924). The high efficiency is due to the fact that the second stage compressor is fed by high density gas, thus reducing its volumetric capacity and the mechanical energy needed for this compression.

In order to investigate the Plank cycle efficiency and the peculiar shape of its efficiency curve a simple theoretical STDC cycle was simulated. It is worth noting that when the intermediate pressure level is higher than the critical one, STDC and DTDC_SC systems show very similar performances, because no evaporation can

occur in the HPIHX of the DTDC_SC system and the heat exchanged between the two streams is almost negligible (see Figure 1.3.9). To better point out the phenomenon the following assumptions were made:

1) evaporation temperature is set at 4°C in order to reduce the fraction of first stage compression work on the overall compression work;

2) internal heat exchanger (IHX) is not included in the cycle to simplify the investigation of the problem;

3) overall isentropic compressor efficiency is considered unitary (η_{is}=1) to avoid masking effect due to compressor variable efficiency.
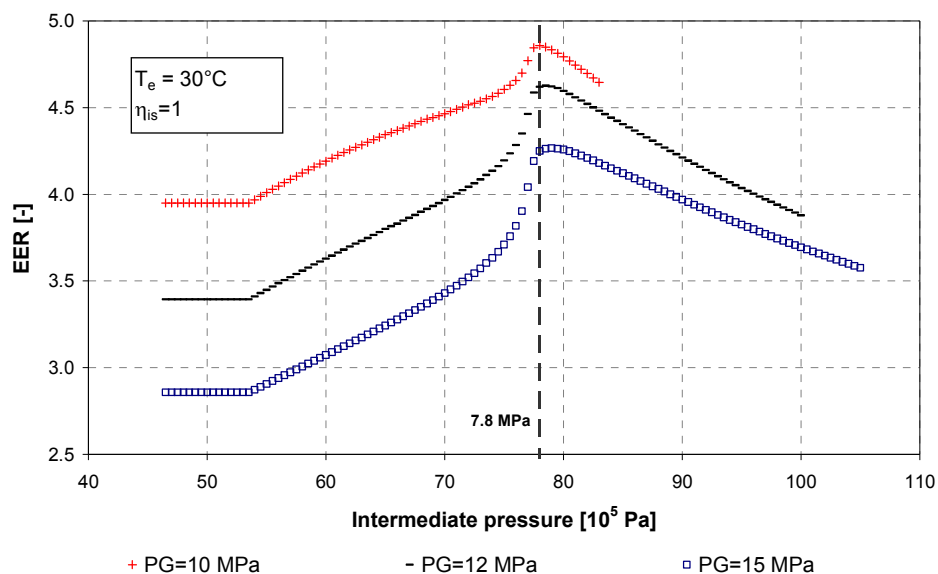
Figure 1.3.11: Theoretical EER of STDC cycle, at different upper pressures, at T_E=4°C

In Figure 1.3.11 EER is plotted against intermediate pressure for four different upper pressure levels (p_G = 10, 12, 15 MPa) at the same external cooling agent temperature of 30°C while, in Figure 1.3.12, three temperatures were considered (T_e = 30, 33, 36°C) at the same upper pressure of 12 MPa. It appears that at the same external cooling agent temperature, the intermediate pressure level corresponding to the maximum efficiency is not strongly sensitive to upper pressure variations (it is constant at 7.8 MPa), whereas the effect of the cooling agent temperature is remarkable, being constant the upper pressure. In this case the value increases as the temperature of the cooling agent increases.
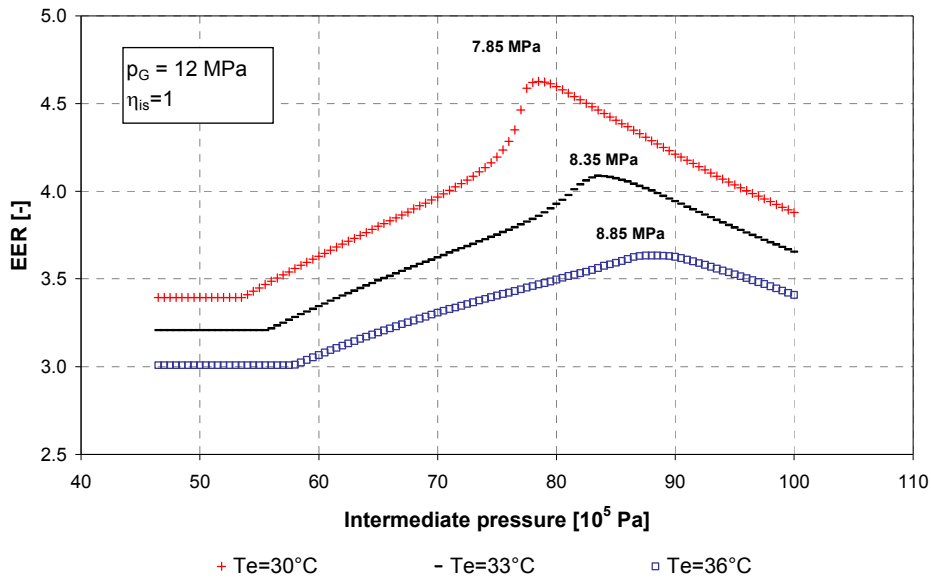
Figure 1.3.12: Theoretical EER of STDC cycle, at different outlet intercooler temperatures, at $T_E=4°C$
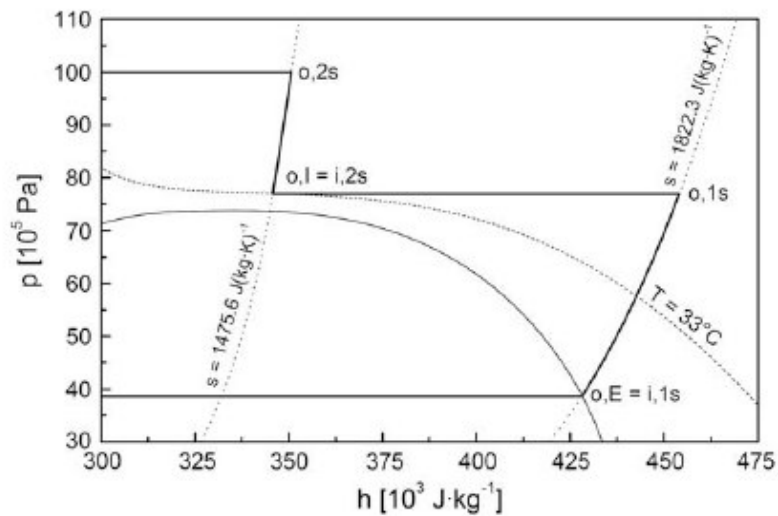
Figure 1.3.13: p-h diagram of a two-stage compression for a transcritical intermediate pressure; Cecchinato et al. (2009)

Keeping constant the upper pressure value, and thus the refrigerating capacity for a set external cooling agent temperature, the EER maximization problem for the STDC cycle reduces to the minimization of the mechanical compression specific work that can be expressed as:

$$L = (h_{o,1s} - h_{i,1s}) + (h_{o,2s} - h_{i,2s})$$ (6)

where the subscripts refer to the points in Figure 1.3.13.

Considering h as function of p and s, in the pressure range of interest the partial derivative of enthalpy with respect to pressure at constant entropy $\left(\dfrac{\partial h}{\partial p}\right)_s$ is nearly constant along an isentropic line, therefore equation (4) can be written as:

$$L = \left(\frac{\partial h}{\partial p}\right)_s\bigg|_{o,E} (p_I - p_E) + \left(\frac{\partial h}{\partial p}\right)_s\bigg|_{o,I} (p_G - p_I)$$ (7)

The minimum of the compression specific work can be now calculated, finding the zero of the partial derivative of equation (6) with respect to the intermediate pressure p_I :

$$\frac{dL}{dp_I} = \frac{d}{dp_I}\left[\left(\frac{\partial h}{\partial p}\right)_s\bigg|_{o,E}\right](p_I - p_E) + \left(\frac{\partial h}{\partial p}\right)_s\bigg|_{o,E} +$$
$$+ \frac{d}{dp_I}\left[\left(\frac{\partial h}{\partial p}\right)_s\bigg|_{o,I}\right](p_G - p_I) - \left(\frac{\partial h}{\partial p}\right)_s\bigg|_{o,I} = 0$$ (8)

Keeping in mind that the term $\left(\dfrac{\partial h}{\partial p}\right)_s\bigg|_{o,E}$ in (7) is not dependent on p_I, the first term of equation (8) is null, while the second term is constant, not depending on upper or intermediate pressure values; equation (8) therefore can be rewritten as follows, being the constant equal to $\left(\dfrac{\partial h}{\partial p}\right)_s\bigg|_{o,E}$:

$$\frac{d}{dp_I}\left[\left(\frac{\partial h}{\partial p}\right)_s\bigg|_{o,I}\right](p_G - p_I) - \left(\frac{\partial h}{\partial p}\right)_s\bigg|_{o,I} + const. = 0$$ (9)

83

To understand the trends of the curves in Figure 1.3.9, it is useful to observe how the derivative $\dfrac{dL}{dp_I}$ depends on p_I. This derivative is composed of 3 terms, according to (9); in Figure 1.3.14 the curves representing the first term and the sum of the last terms are plotted. While the sum of the last terms is subjected to rather small variations as the intermediate pressure p_I changes, the first term is a strong function of p_I. In particular this curve presents always a negative value and shows in general a rising profile, interrupt by a sharp and deep depression. The derivative of the total work with respect to p_I follows the shape of the first term, that is only slightly lifted by the sum of the last terms. Keeping in mind that the trends of work and EER are opposite, it follows that a sharp fall of the derivative means a sharp increase in EER; this happens at a value of p_I close to 7.70 MPa for $T_e = 30°C$, irrespective of the value of the upper pressure of the cycle and the maximum value of EER is just after the sharp increase, since immediately the derivative of the total work cross the axis of abscissas. The reason why the first term of (9) behaves in such a way can be traced to the shape of the isotherms in the p-h diagram of CO_2 in the near-critical region (see Figure 1.3.13) ; it is clear that, when the slope of the isothermal line corresponding to $T_{o,I}$ flattens and is close to an horizontal line, the derivative in the first term of (9), which has always a negative value, increases much in modulus; for the critical isotherm the slope becomes horizontal and the modulus of the derivative is infinite. For the isothermal lines above the critical one, the peak of the derivative occurs close to the flex of each line.

It is now interesting to weight the influence of the upper pressure value in the determination of the intermediate pressure that minimizes the mechanical compression specific work; an analysis of each term and of the whole equation was carried out. Keeping constant the cooling agent temperature at 30°C, different levels of upper pressure (10, 12, 15 MPa) were considered. The equation values have been evaluated with a 0.01 MPa step, approximating the derivative to a Newton quotient with a 10 Pa pressure step. The results are shown in Figures 1.3.14(a), (b) and (c), where the minimum compression work associated to the Plank cycle corresponds to the zero of the bold solid line. The optimal intermediate pressure values for the Plank cycle corresponds to 7.77, 7.82, 7.86 MPa for upper pressure of 10, 12, 15 MPa respectively. As it was also observed in Figure 1.3.9, the optimal intermediate pressure is not strongly affected by upper pressure

variations, this is due to the shape of the first term of equation (9), represented by a thin solid line in Figures 1.3.14. This term has a sharp minimum value corresponding to 7.71 MPa that depends only on T_I, and it is therefore independent from the upper pressure level. In fact, the pressure difference (p_G-p_I) only affects the magnitude of the first term in equation (9), but not the p_I value of the minimum. Therefore, due to the very narrow p_I range, where the sharp variation occurs, the pressure value that optimizes the COP, remains nearly constant (less than 2.0% of variation for a p_G ranging from 10 to 15 MPa) varying p_G.
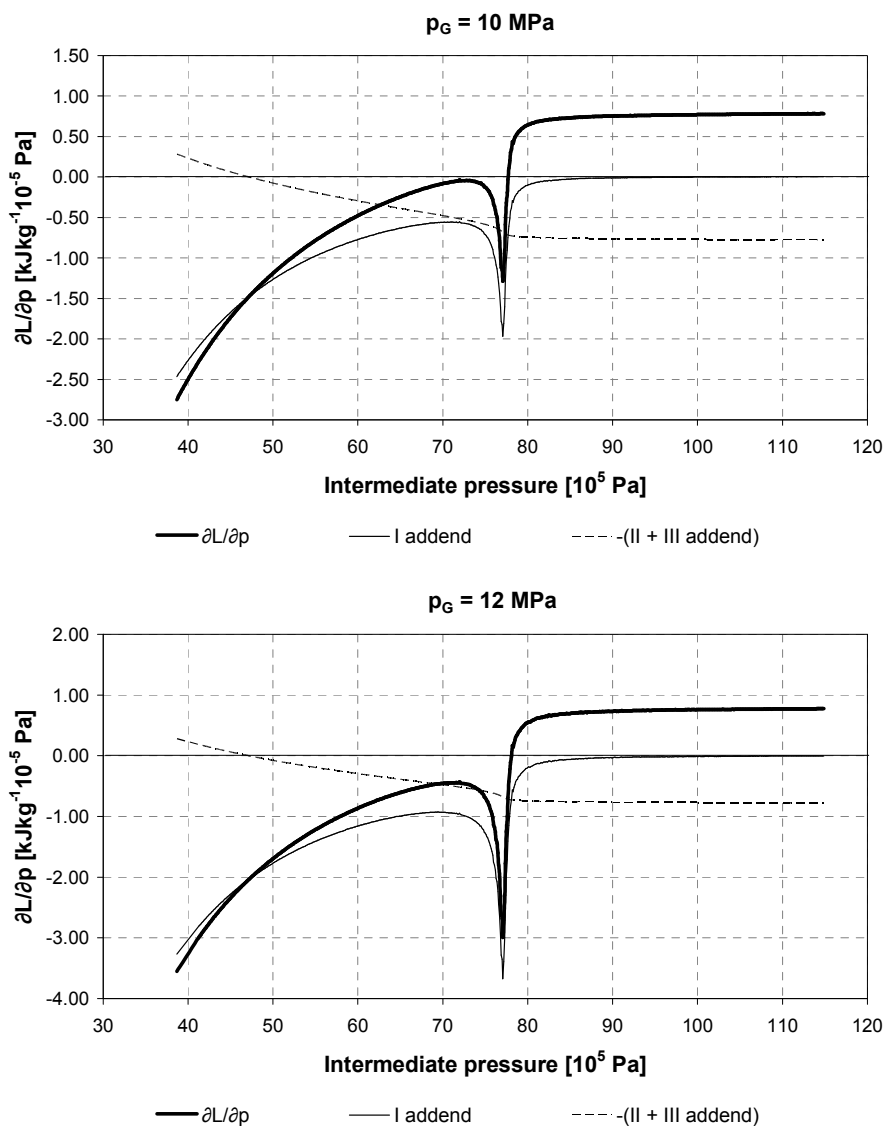
Figure 1.3.14(a): Derivative of the mechanical specific work (equation (9)), at p_G=10 MPa.

Figure 1.3.14 (b): Derivative of the mechanical specific work (equation (9)), at p_G=12 MPa.
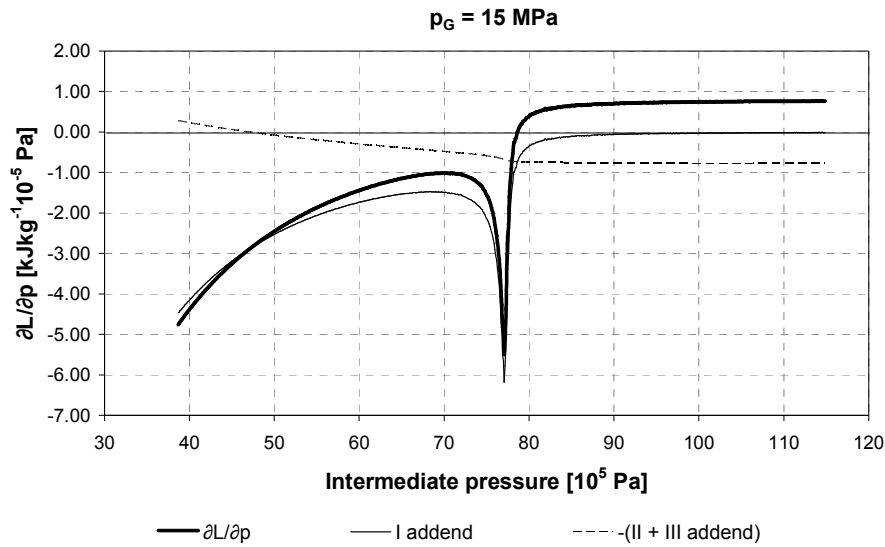
Figure 1.3.14 (c): Derivative of the mechanical specific work (equation (9)), at p_G=15 MPa.

1.3.6   Energy efficiency at different external cooling agent temperatures

The five cycles depicted in paragraph 1.3.3 are analysed with reference to the typical working conditions of air conditioning ($T_E = 4°C$), retail refrigeration of fresh foodstuffs ($T_E =-10°C$) and retail refrigeration of frozen foodstuffs ($T_E =-30°C$).

The temperature of the external cooling agent was varied in the range from 25°C to 35°C, and for air conditioning the range was extended up to 50°C, with reference to automotive applications; the fluid temperature at the gas cooler outlet is assumed 3°C higher than the temperature of the external cooling agent. It is worth reminding that the same assumptions made in paragraph 1.3.3 about evaporator superheat, internal heat exchanger approach and overall isentropic compression efficiency are kept.

The EER values of the investigated cycles are shown in Figure 1.3.15 and 1.3.16, respectively for retail refrigeration and air conditioning, as functions of the temperature of the external cooling agent (T_e). The energy improvement provided by the stages expansion is remarkable, especially for low temperature refrigeration applications, while at medium temperature refrigeration the advantages of the staged throttling are close to those provided by the mechanical subcooling. As

86

regards the air conditioning system, the DTAC cycle achieves an higher efficiency than the STDC and its penalization, compared to DTDC_SC and DTDC_OFT, is less heavy. In fact, the pressure drop in the expansion device is less large and the benefits of a staged throttling are smaller compared to medium or low temperature applications.
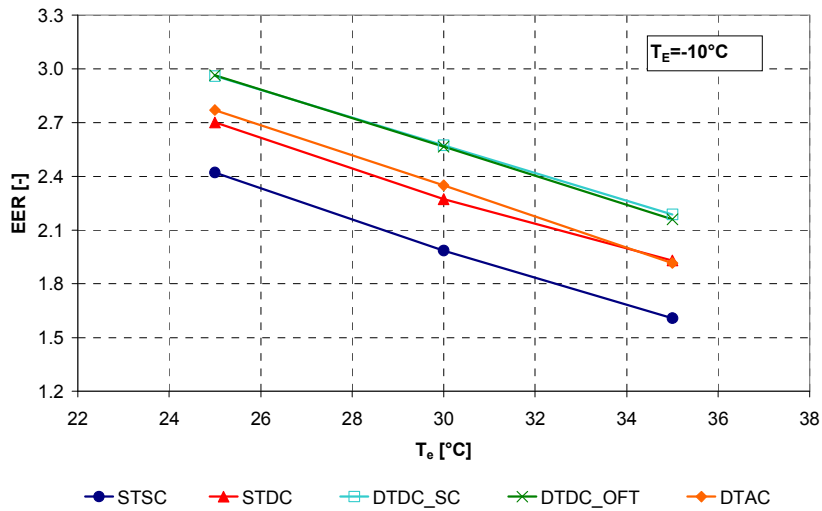
Figure 1.3.15(a): EER of different cycles, as a function of different external cooling agent temperature, at T_E=-10°C
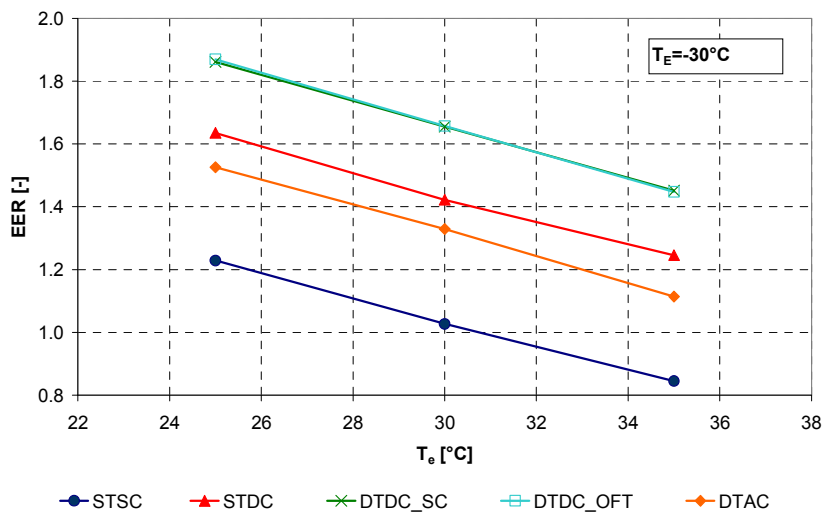
Figure 1.3.15 (b): EER of different cycles, as a function of different external cooling agent temperature, at T_E=-30°C.
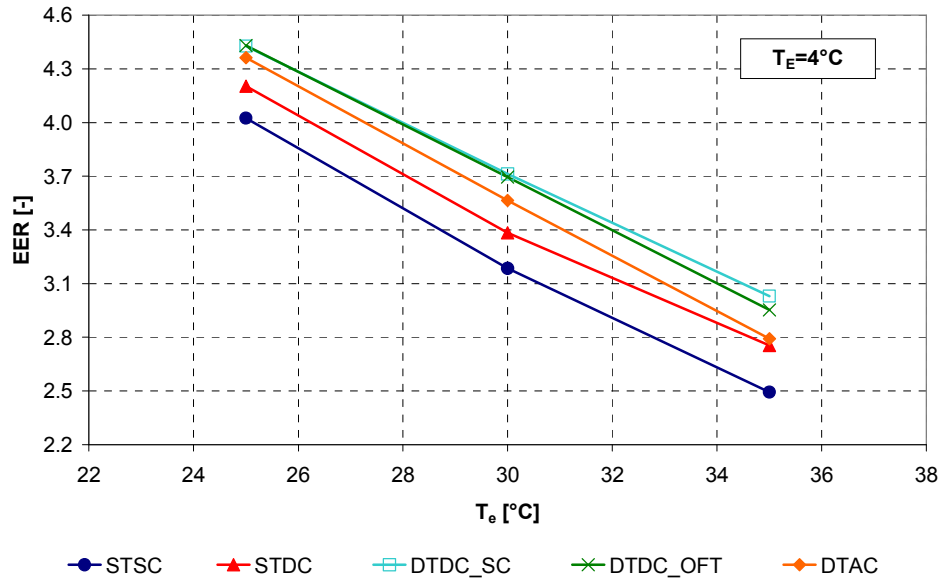
Figure 1.3.16: EER of different cycles, as a function of different external cooling agent temperature, at $T_E=4°C$

The optimised values of the upper cycle pressure (p_G, solid line) and of the intermediate pressure (p_I, dashed line) for DTDC_SC, DTDC_OFT and DTAC cycles are shown in Figures 1.3.17 and 1.3.18. The optimised ratio χ is also displayed (thin solid line); for DTDC_SC it is a further degree of freedom, while for DTDC_OFT and DTAC it depends on the intermediate pressure. However, the difference of χ values between DTDC_SC and DTDC_OFT is very small. For air conditioning system, the optimal intermediate pressure and pressure ratio χ of DTDC_SC and DTDC_OFT are different, while the optimal upper pressure values are close for every cycle type.
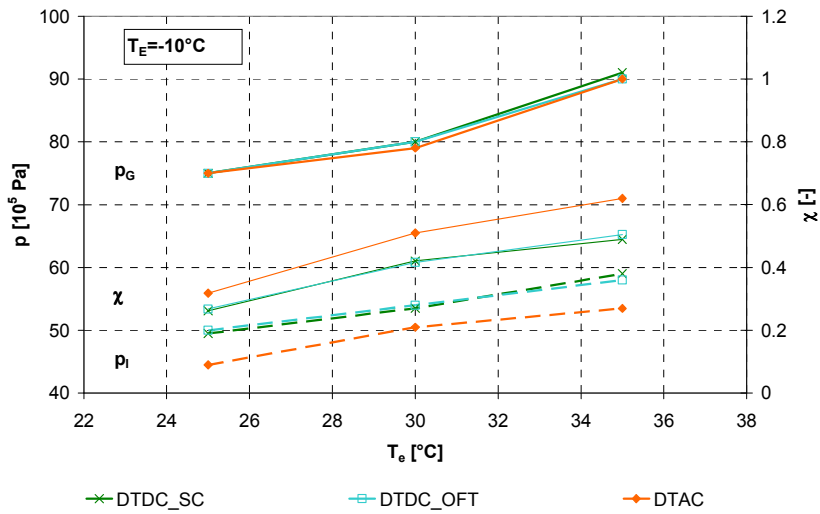
Figure 1.3.17(a): Upper pressure, intermediate pressure and mass flow ratio of different cycles, as functions of different external cooling agent temperature, at T_E= -10 °C
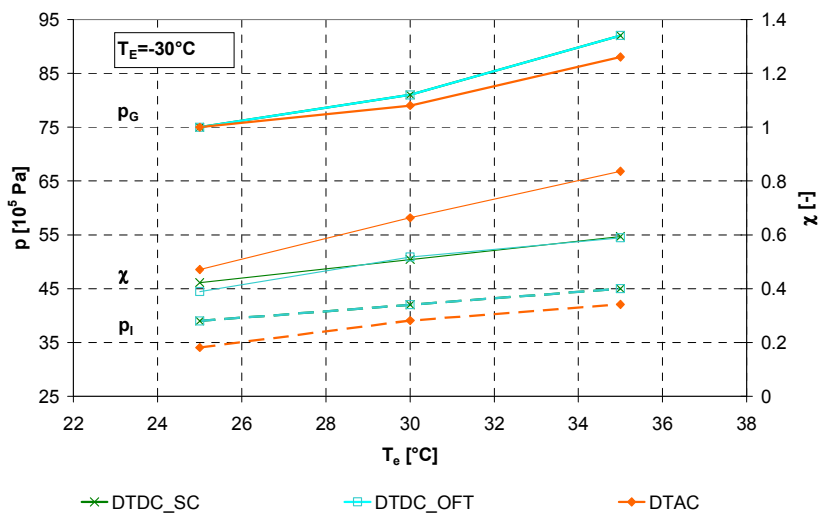
Figure 1.3.17 (b): Upper pressure, intermediate pressure and mass flow ratio of different cycles, as functions of different external cooling agent temperature, at T_E= -30 °C
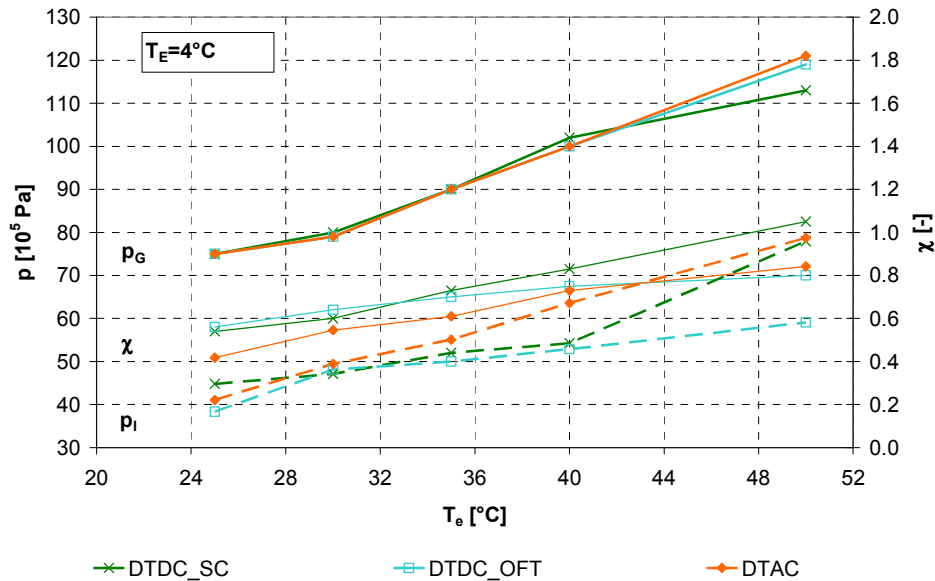
Figure 1.3.18: Upper pressure, intermediate pressure and mass flow ratio of different cycles, as functions of different external cooling agent temperature, at T_E= -4 °C

For every working condition, it results that the split (DTDC_SC) and the phase separation (DTDC_OFT) cycles outperform all other options, showing 20.6 and 16.8% average increase respectively in energy efficiency over the STSC cycle at 4°C evaporation temperature, 29.3 and 28.7% increase respectively at -10°C. At -30°C, where STSC cycle is hardly advisable, the increase over the STDC cycle is of 15.6 and 15.7% respectively.

The single-stage cycle coupled with a gas cooling circuit (DTAC) shows a 17.3% increase in energy efficiency in comparison with the basic single-stage (STSC) cycle at −10°C evaporation temperature, outperforming also the single-throttling, double-compression (STDC) cycle. As it can be seen in Figure 1.3.16, at 4°C evaporation temperature, its performance fades when external cooling agent temperature rises.

1.3.7   Conclusions

It is well known that the theoretical transcritical inverse cycle operated on carbon dioxide involves a penalisation in energy efficiency in comparison with the

90

traditional vapour compression cycles. However the favourable characteristics of this fluid concerning heat transfer, pressure drop and probably the compression process in a real system can partially compensate for this intrinsic thermodynamic penalisation. On the other hand, energy efficiency is an essential requirement for complying with the regulations dictated by the environmental emergency concerning global warming; thus the need of more sophisticated cycles to overcome the thermodynamic disadvantage.

As the traditional compression vapour inverse cycle, exergy losses during throttling and gas cooling process are responsible for low energy efficiency; the remedies are the same, namely, staged throttling, or strong cooling of the fluid before the expansion, and staged compression with intercooling.

The analysis performed in this study have shown that, unlike traditional cycle, staged compression with intercooling carried out with an external fluid for the heat rejection plays a major role in improving energy efficiency. Since this heat rejection depends heavily on the value of the intermediate pressure, the optimal value of this parameter is a crucial choice; for the same reason, an effective heat exchanger between the suction line and the line before the throttling valve often allows a significant benefit in energy efficiency.

Different cycles are analysed and optimised in this Chapter. As expected, the most elaborate cycles (Double-Throttling, Double-Compression in both versions Open Flash Tank and Split Cycle) present the greatest improvement, especially for the heaviest operating conditions (the lowest evaporation temperature and the highest external temperature); for $-30/+35°C$ (evaporation temperature/external temperature) both cycles behave similarly and give rise to 70% increase in energy efficiency against the simplest solution (Single-Throttling, Single-Compression). Being the double compression mandatory for limiting the temperature at the compressor outlet in such conditions, the only alternative is Single-Throttling, Double-Compression (roughly 50% increase in energy efficiency). The final choice therefore results from the best trade-off between increased installation costs and decreased operating costs, taking into account also the reliability and the safety characteristics of the system.

For less severe operating conditions, probably a cheaper system design can be preferable; for example at $+4/+30°C$ operations, the best cycles (again DTDC_OFT and DTDC_SC) improve energy efficiency by 16% against the cheapest solution

(STSC), while the system with an auxiliary compressor (DTAC) is quoted for 12% improvement. Since the last system is rather simple, reliable and cost effective, this solution is worth considering.

The Plank cycle (staged compression with intermediate pressure above the critical one) could be the optimal choice only for very high value of the external cooling agent temperature and, thus, of the optimal upper pressure. A thermodynamic analysis of this cycle has been proposed to fill a gap in the knowledge of the possibility of transcritical cycles.

As follows from the results of the present analysis, it is not always easy to choose the best system for a definite application and this problem is often complicated by the need of finding the optimal values for one or two independent operating variables: a reliable simulation model to be used as an optimisation tool is mandatory.

In this work a merely thermodynamic optimisation of different cycle was performed. In order to turn into reality the suggestions arising from the present analysis, technological solutions are needed for controlling the cycle parameters and for keeping them at the optimal values; this is not a simple task, especially when searching for a good cost/benefit ratio. This further analysis is beyond the scope of this work; however it is worth noting that, while the control of the upper cycle pressure is rather easily accomplished by a proper action of a back-pressure throttling valve, the value of the intermediate pressure for staged compression depends on the swept volume ratio between the compressors and needs to be controlled by variable-frequency drive or other means; moreover the thermodynamic optimisation of DTDC_SC cycle entails a suitable control on the auxiliary throttling valve and the optimisation of DTAC cycle requires to control the swept volumes of the two compressors.

1.3.8   References

1. Bernabei M., Cecchinato L., Chiarello M., Corradi M., Fornasieri E., (2008), Design and experimental analysis of a carbon dioxide transcritical chiller, *8th IIR G. Lorentzen Conf.,* M3-04.
2. Cecchinato L., Chiarello M., Corradi M., Fornasieri E., Minetto S., Stringari P.,

Zilio C., (2009), Thermodynamic analysis of different two-stage transcritical carbon dioxide cycles, *Int. J. Refrigeration,* 32:1058-1067.

3. Inokuty H., (1924), Theory and experiments on vapour compression refrigerating machine with some modified cycles, *Journal of the Society of Mechanical Engineers*, 27(90):876-911.

4. Lemmon E. W., McLinden M. O., Huber M. L., (2002), NIST Reference Fluid Thermodynamic and Transport Properties Refprop 7.0, *NIST Std. Database*.

5. Plank R., (1912), Arbeitsverfahren an Kompressionskältemaschinen, insbesondere für Kälteträger mit tiefer kritischer Temperatur, *German Patent No. DE278095*.

Chapter 1.4   ENERGY EFFICIENCY RELATED TO HEAT TRANSFER AREA: EVALUATION OF POTENTIAL FOR EFFICIENCY INCREASE

1.4.1   Introduction

One solution to improve the cycle efficiency is to increase the size of the heat exchangers (condenser and evaporator). If the heat exchange area is larger, the temperature difference of the two fluids is smaller and the efficiency of these components is higher. In addition, being the difference between condensation and evaporation temperature smaller, the compression work is lower. It is useful to refer to the ideal Rankine (Evans-Perkins) cycle: it is a theoretical Rankine cycle, with the condenser and the evaporator of infinite heat exchange area and ideal compressor; in this cycle, the saturation temperatures (condensation and evaporation ones) are the temperatures of the secondary fluids.

The purpose of this part is to make the heat exchanger bigger, relative to the refrigeration capacity, in order to approach the ideal Rankine (Evans-Perkins) EER while keeping isentropic efficiency fairly constant. In this way, the temperature differences between secondary fluids and refrigerant and the compressor power shall decrease and the EER shall increase. By the way, the EER improvement is not proportional with the increase of the heat exchanger sizes; the aim is to investigate how far it is possible to go, how close to ideal Rankine (Evans-Perkins) EER is possible to get. Beyond a certain point, further increase of heat exchangers size provides negligible effects; in addition, the energy consumptions of the auxiliary devices (for example, the fans) become relevant compared to the total one.

Instead of physically change the size of the heat exchangers, the refrigerating capacity is experimentally decreased by changing speed compressor, while tracking the isentropic efficiency and keeping fixed indoor (27°C, dry conditions) and outdoor (35°C, dry conditions) air conditions. The refrigerant is R410A.

In Figure 1.4.1, an example of the theoretical improvements of a real cycle is shown; the results of an experimental test are reported in Table 1.4.1. The first

passage is to avoid considering the pressure drops inside the heat exchangers.

Qevap	3.45kW
Tevap	14.0°C
Tcond	42.5°C
Cond. subcooling	2°C
Evap superheat	1°C
DP cond.	18kPa
DP evap	133 kPa
Isent efficiency	0.72
EER	4.94

Table 1.4.1: Results of the experimental test
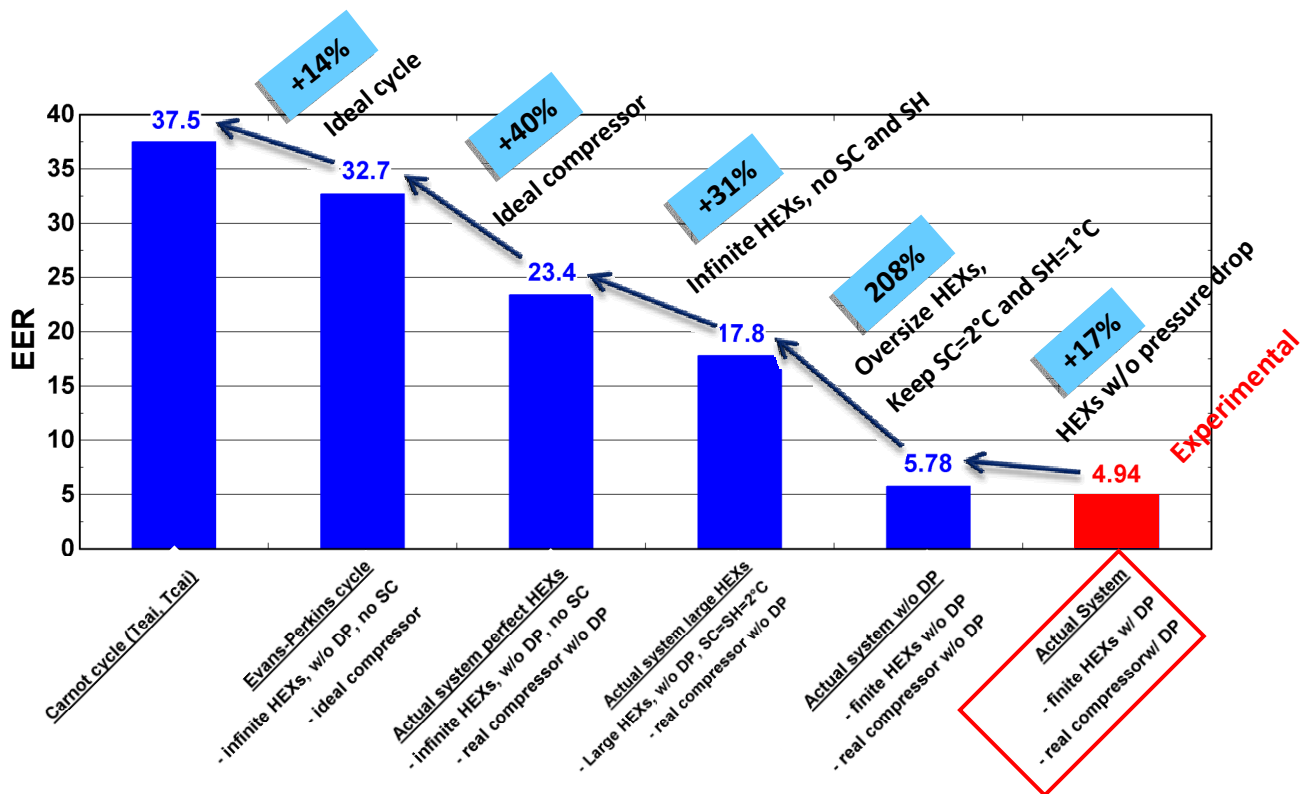
Figure 1.4.1: Theoretical improvements of a Rankine cycle

The oversizing of the heat exchangers, with optimized subcooling and

superheat, provides a remarkable improvement of the system EER. The use of ideal heat exchangers and of ideal compressor gives similar improvements, 31% and 40% respectively. The EER of the Evans-Perkins cycle is only 14% lower than that of the ideal Carnot cycle

1.4.2   Nomenclature

These experimental tests were carried out during an experience, as visiting scholar, at the Air Conditioning and Refrigeration Center of the University of Illinois at Urbana-Champaign. The recorded system was different from the ones used in laboratories in Italy and the variables were called by different names, so the reader is recommended to refer to the following nomenclature, regarding the present Chapter.

comp	Compressor
cond	Condenser
DP	Pressure drop [Pa]
EER	chiller energy efficiency ratio, Q_{evap}/W_{comp} [-]
evap	Evaporator
h	Enthalpy [Jkg^{-1}]
x in	Absolute humidity at the evaporator inlet [kg/kg dry air]
x out	Absolute humidity at the evaporator outlet [kg/kg dry air]
$\dot{m}$	mass flow rate [kg s^{-1}]
P	Pressure [Pa]
Pcpri	Refrigerant pressure at the compressor inlet [Pa]
Pcpro	Refrigerant pressure at the compressor outlet [Pa]
Qcond	Condenser capacity [W]
Qevap	Evaporator capacity [W]

Sc   Subcooling [K]

Sh   Superheat [K]

T   Temperature [°C]

Tcai   Air temperature at the condenser inlet [°C]

Tcao   Air temperature at the condenser outlet [°C]

Tcpri   Refrigerant temperature at the compressor inlet [°C]

Tcpro   Refrigerant temperature at the compressor outlet [°C]

Tcri   Refrigerant temperature at the condenser inlet [°C]

Tcri_sat Refrigerant saturation temperature at the condenser inlet [°C]

Tcro   Refrigerant temperature at the condenser outlet [°C]

Tcro_sat Refrigerant saturation temperature at the condenser outlet [°C]

Teai   Air temperature at the evaporator inlet [°C]

Teao   Air temperature at the evaporator outlet [°C]

Teri   Refrigerant temperature at the evaporator inlet [°C]

Teri_sat Refrigerant saturation temperature at the evaporator inlet [°C]

Tero   Refrigerant temperature at the evaporator outlet [°C]

Tero_sat Refrigerant saturation temperature at the evaporator outlet [°C]

Tevro   Refrigerant temperature at the expansion valve outlet [°C]

Wcomp Compressor power [W]

Wfan   Fan power [W]

Greek letters

η efficiency [-]

ρ density [kg m^{-3}]

1.4.3   Plant description and the types of heat exchangers tested

The experiment setup consists of two separate environmental chambers, used to attain operation conditions. Each chamber contains a wind tunnel, with either the indoor heat exchanger or outdoor heat exchanger installed, along with the required instrumentation to obtain pressure, temperature, and mass flow measurements. All the heat exchangers were installed flat and perpendicular to the air flow, so it is assumed that the air velocity distribution is uniform over the entire heat exchanger. The compressor is located in the condenser chamber, and is heavily insulated. It is a Daikin 2YC32GXD swing compressor; its image is in Figure 1.7.8. Being a hermetic compressor, the measurement of the shaft torque is not allowed. Chamber details and layout are shown in Figure 1.4.2. For heat pump testing, the heat exchangers were switched between chambers instead of changing the refrigerant flow direction with the four-way valve, as the condenser chamber did not have a cooling unit capable of generating the required temperature. In the evaporator chamber, an R404A chiller was installed and was used to achieve lower temperatures.

Each chamber allows three independent energy balances, and serves as a check for how accurately the capacities can be measured. The air inside the chambers is conditioned using several heaters and a water chiller in the condenser chamber, and the combination of resistance heater and glycol chiller in the evaporator chamber. The energy inputs and outputs for each chamber are used in an energy balance (the "chamber balance") to calculate the capacity of each heat exchanger. A mass flow meter is located at the inlet of the expansion valve to measure the mass flow rate of the refrigerant, and the pressure and temperature instrumentation installed with the refrigerant piping in each chamber is used to calculate refrigerant enthalpies, which are used to calculate the refrigerant balance. A six inch nozzle in each wind tunnel, coupled with an air-side pressure drop measurement, air temperature and dew point measurements, was used to find the mass flow rate of air through the tunnel, in accordance with the ANSI/ASHRAE Standard 41.2-1987 (RA92). Using the flow rate, temperature grids and dew point sensors located upstream and downstream of the test heat exchanger, the air-side balance is calculated.
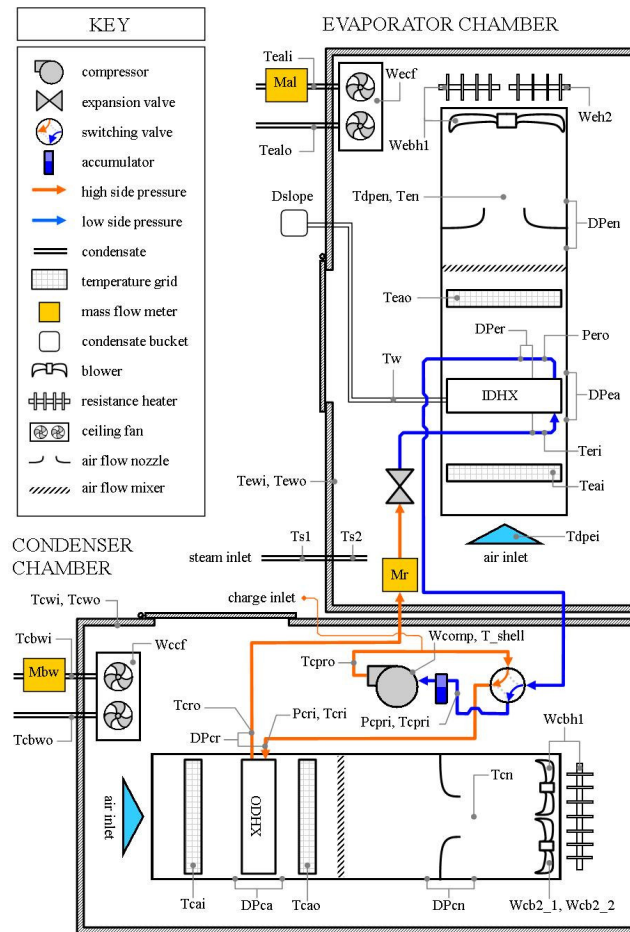
Figure 1.4.2: Schematic of the environmental chambers

The inlet temperature grid for each chamber is comprised of four thermocouples connected together to give an average value. The outlet temperature grid is made up of 45 thermocouples laid out 10 cm apart. The thermocouples used for the measurement are divided into six sections, each composed by a set of welded wire thermocouples grouped together to give an average value for that section. The sections can be seen in Figure 1.4.3, with different section sizes to accommodate the different sizes of the indoor and outdoor heat exchangers. The acronyms present in Figure 1.4.3 are: TL: top left; TM: top middle; TR: top right; BL: bottom left; BM: bottom middle; BR: bottom right. A single welded wire thermocouple is used to measure the temperature at the center of the nozzle. Condensate is calculated using the difference in dew points measured before and after the evaporator, though

100

it is considered zero when conditions are "dry," in which no steam is added to regulate humidity.

thermocouple grids for the outdoor heat exchangers   thermocouple grids for the indoor heat exchanger
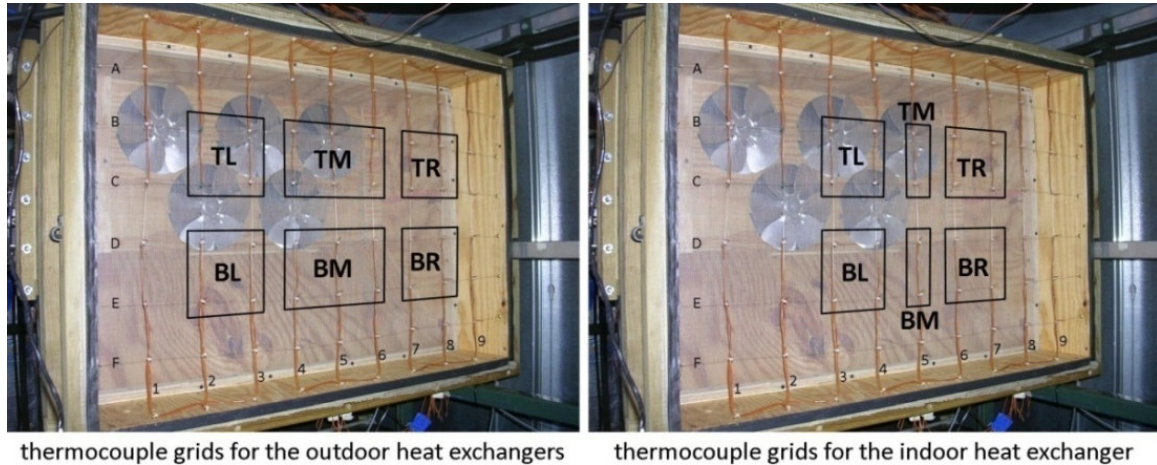
Figure 1.4.3: Outlet temperature grids

Data acquisition was done using a Hewlett Packard HP 75000 series B data logger and Agilent Technologies Agilent VEE software. The software used to control the system was a maintenance program used for the residential unit, modified for this application. The instrumentation, as well as its accuracy, is listed in Tables 1.4.2. Values recorded using the Agilent VEE program were used in the Engineering Equation Solver (EES) software to further analyze the data. The EER of the system is calculated from the measured capacity and the compressor work.

variable	unit	instrument	brand	model	accuracy	range
charge	[g]	scale	Acculab	model VA 16000	± 0.5g	0-16 kg
DPca	[Pa]	differential air pressure transducer	Setra	model 239	± 0.14% FS	0-2.5" WC
DPcn	[Pa]	differential air pressure transducer	Setra	model 264	± 1.0% FS	0-2.5" WC
DPcr	[kPa]	differential pressure transducer	Sensotec	model Z/6930-01	± 0.25% FS	0-50 psid
DPea	[Pa]	differential air pressure transducer	Setra	model 239	± 0.14% FS	0-1" WC
DPen	[Pa]	differential air pressure transducer	Setra	model 239	± 0.14% FS	0-5" WC
DPer	[kPa]	differential pressure transducer	Sensotec	model Z/6930-01	± 0.25% FS	0-50 psid
Dslope	[kg/s]	load cell	Sensotec	750214	± 0.03%	0-25 lb
Mal	[g/s]	mass flow meter	Micro Motion	Elite CMF025	± 0.05%	0-80 lb/min
Mbw	[g/s]	mass flow meter	Micro Motion	Elite CMF025	± 0.05%	0-80 lb/min
Mr	[g/s]	mass flow meter	Micro Motion	model D	± 0.15%	0-25 lb/min
Pcpri	[kPa]	pressure transducer	Bell & Howell	type no. 4-395-0101	± 0.25%	0-1000 psia
Pcri	[kPa]	pressure transducer	Setra	model 280E	± 0.11% FS	0-500 psia
Pero	[kPa]	pressure transducer	Setra	model 280E	± 0.11% FS	0-500 psia
T_shell	[C]	welded thermocouple	Omega	T-type	± 0.5 ºC	0-350 ºC
Tcai_avg	[C]	welded thermocouple	Omega	T-type	± 0.5 ºC	0-350 ºC
Tcao_BL	[C]	welded thermocouple	Omega	T-type	± 0.5 ºC	0-350 ºC
Tcao_BM	[C]	welded thermocouple	Omega	T-type	± 0.5 ºC	0-350 ºC
Tcao_BR	[C]	welded thermocouple	Omega	T-type	± 0.5 ºC	0-350 ºC
Tcao_TL	[C]	welded thermocouple	Omega	T-type	± 0.5 ºC	0-350 ºC
Tcao_TM	[C]	welded thermocouple	Omega	T-type	± 0.5 ºC	0-350 ºC

Table 1.4.2(a): Instrumentation for all measured values (1/3)

variable	unit	instrument	brand	model	accuracy	range
Tcao_TR	[C]	welded thermocouple	Omega	T-type	± 0.5 ºC	0-350 ºC
Tcbwi	[C]	thermocouple probe	Omega	T-type	± 0.5 ºC	0-350 ºC
Tcbwo	[C]	thermocouple probe	Omega	T-type	± 0.5 ºC	0-350 ºC
Tcn	[C]	welded thermocouple	Omega	T-type	± 0.5 ºC	0-350 ºC
Tcpri	[C]	thermocouple probe	Omega	T-type	± 0.5 ºC	0-350 ºC
Tcpro	[C]	thermocouple probe	Omega	T-type	± 0.5 ºC	0-350 ºC
Tcri	[C]	thermocouple probe	Omega	T-type	± 0.5 ºC	0-350 ºC
Tcro	[C]	thermocouple probe	Omega	T-type	± 0.5 ºC	0-350 ºC
Tcwi	[C]	welded thermocouple	Omega	T-type	± 0.5 ºC	0-350 ºC
Tcwo	[C]	welded thermocouple	Omega	T-type	± 0.5 ºC	0-350 ºC
Tdpci	[C]	dew-point sensor	General Eastern	model D2	± 0.2 ºC	1.5-100% RH
Tdpei	[C]	dew-point sensor	General Eastern	model D2	± 0.2 ºC	1.5-100% RH
Tdpen	[C]	dew-point sensor	General Eastern	model D2	± 0.2 ºC	1.5-100% RH
Teai_avg	[C]	welded thermocouple	Omega	T-type	± 0.5 ºC	0-350 ºC
Teali	[C]	thermocouple probe	Omega	T-type	± 0.5 ºC	0-350 ºC
Tealo	[C]	thermocouple probe	Omega	T-type	± 0.5 ºC	0-350 ºC
Teao_BL	[C]	welded thermocouple	Omega	T-type	± 0.5 ºC	0-350 ºC
Teao_BM	[C]	welded thermocouple	Omega	T-type	± 0.5 ºC	0-350 ºC
Teao_BR	[C]	welded thermocouple	Omega	T-type	± 0.5 ºC	0-350 ºC
Teao_TL	[C]	welded thermocouple	Omega	T-type	± 0.5 ºC	0-350 ºC
Teao_TM	[C]	welded thermocouple	Omega	T-type	± 0.5 ºC	0-350 ºC

Table 1.4.2(b): Instrumentation for all measured values (2/3)

variable	unit	instrument	brand	model	accuracy	range
Teao_TR	[C]	welded thermocouple	Omega	T-type	± 0.5 ºC	0-350 ºC
Ten	[C]	welded thermocouple	Omega	T-type	± 0.5 ºC	0-350 ºC
Teri	[C]	thermocouple probe	Omega	T-type	± 0.5 ºC	0-350 ºC
Tero	[C]	thermocouple probe	Omega	T-type	± 0.5 ºC	0-350 ºC
Tewi	[C]	welded thermocouple	Omega	T-type	± 0.5 ºC	0-350 ºC
Tewo	[C]	welded thermocouple	Omega	T-type	± 0.5 ºC	0-350 ºC
Ts1	[C]	thermocouple probe	Omega	T-type	± 0.5 ºC	0-350 ºC
Ts2	[C]	thermocouple probe	Omega	T-type	± 0.5 ºC	0-350 ºC
Tw	[C]	thermocouple probe	Omega	T-type	± 0.5 ºC	0-350 ºC
Wcb2_1	[kW]	single-phase watt transducer	Ohio Semitronics	GW5-011CX5	0.20%	0-2 kW
Wcb2_2	[kW]	single-phase watt transducer	Ohio Semitronics	GW5-021X5	0.20%	0-8 kW
Wcbh1	[kW]	three-phase watt transducer	Ohio Semitronics	PC5-113X5	± 0.5% FS	0-8 kW
Wccf	[kW]	single-phase watt transducer	Ohio Semitronics	GW5-011X5	0.20%	0-2 kW
Wcomp	[kW]	single-phase watt transducer	Ohio Semitronics	GW5-020X5	0.20%	0-4 kW
Webh1	[kW]	three-phase watt transducer	Ohio Semitronics	GW5-023CX5	0.20%	0-8 kW
Wecf	[kW]	single-phase watt transducer	Ohio Semitronics	GW5-020CX5	0.20%	0-4 kW
Weh2	[kW]	single-phase watt transducer	Ohio Semitronics	GW5-020CX5	0.20%	0-4 kW

FS - full scale, the uncertainty is the maximum rate multiplied by the percent FS	RH - relative humidity
psid - pounds per square inch differential	WC - water column

Table 1.4.2(c): Instrumentation for all measured values (3/3).

The experimental tests were carried out on round-tube air-to-refrigerant evaporator and condenser; the pictures and the geometrical characteristics are reported in Table 1.4.3. The refrigerant paths are shown in Figure 1.4.4(a) and (b).
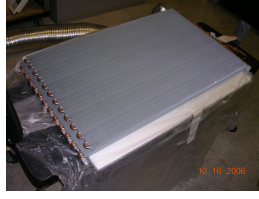
		Evaporator	condenser
Designation		Daikin IDHX	Daikin ODHX
Picture			
tube material	-	Cu	Cu
tube type	-	Round tube	Round tube
# of passes (tubes/pass)	#	40	48
# of tube rows	#	2	2
# of tubes	#	40	48
tube OD	mm	6.35	7.00
tube ID	mm	4.83	5.48
tube wall thickness	mm	0.76	0.76
fin material	-	Al	Al
fin type	-	louvered plate	flat plate
fin pitch	#/in	21.17	20.00
Height	m	0.360	0.504
Width	m	0.610	0.829
core depth	mm	23.0	36.0
face area	m²	0.220	0.418
air-side HT area	m²	7.617	21.750
ref. HT area	m²	0.370	0.672
core volume	cm³	5051	15032
ref volume (w/o header)	cm³	446.3	920.2

Table 1.4.3: Condenser and evaporator characteristics
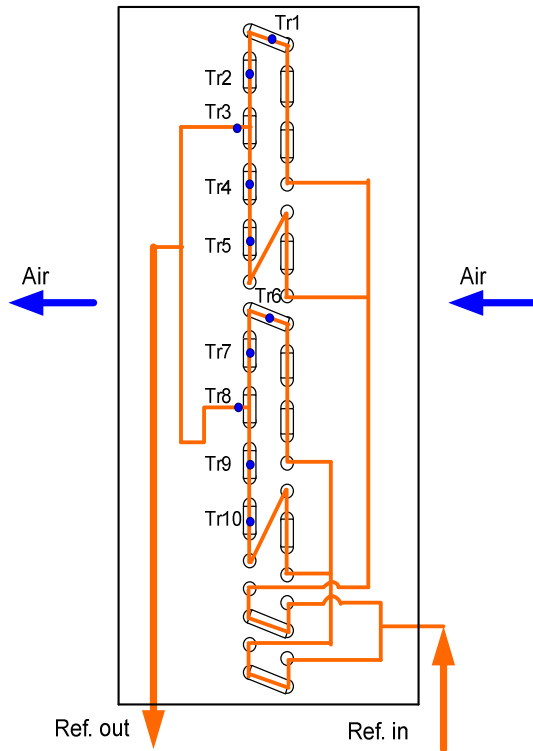
Figure 1.4.4(a):The refrigerant path of the round tube evaporator tested
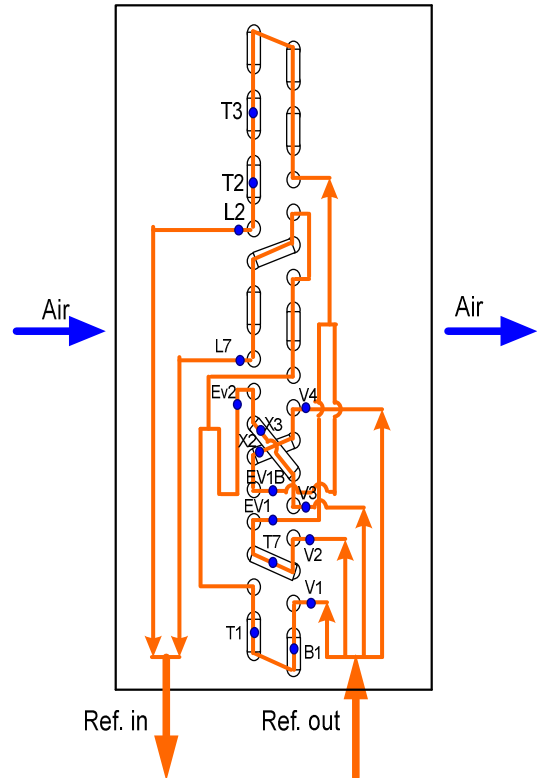
Figure 1.4.4(b): The refrigerant path of the round tube condenser tested

1.4.4 Experimental data

In the experimental tests, the temperatures of the air at the condenser inlet and at the evaporator inlet are kept constant, respectively 35°C and 27°C, in dry conditions; both air flow rates are constant, respectively around 2400 kg/h and 1100 kg/h. The subcooling is set at 2.3 K and the superheat is set at 1.3 K, by controlling the opening of the throttling valve and the refrigerant charge. Different tests are carried out at decreasing compressor speed, from 4200 RPM (70 Hz) to 360 RPM (6 Hz). The experimental results are reported in Table 1.4.4.

The refrigerant inventory and the compressor running are described in Table 1.4.4; decreasing the compressor speed, the charge is increased in order to keep the same subcooling and superheat. The evaporation pressure increases and the

condensation pressure decreases, approaching the theoretical Evans-Perkins cycle. The compressor overall isentropic efficiency (as defined in paragraph I.1.1) presents a maximum at 1680 RPM and 1260 RPM, then it decreases sharply, as shown in the graph of Figure 1.4.5.
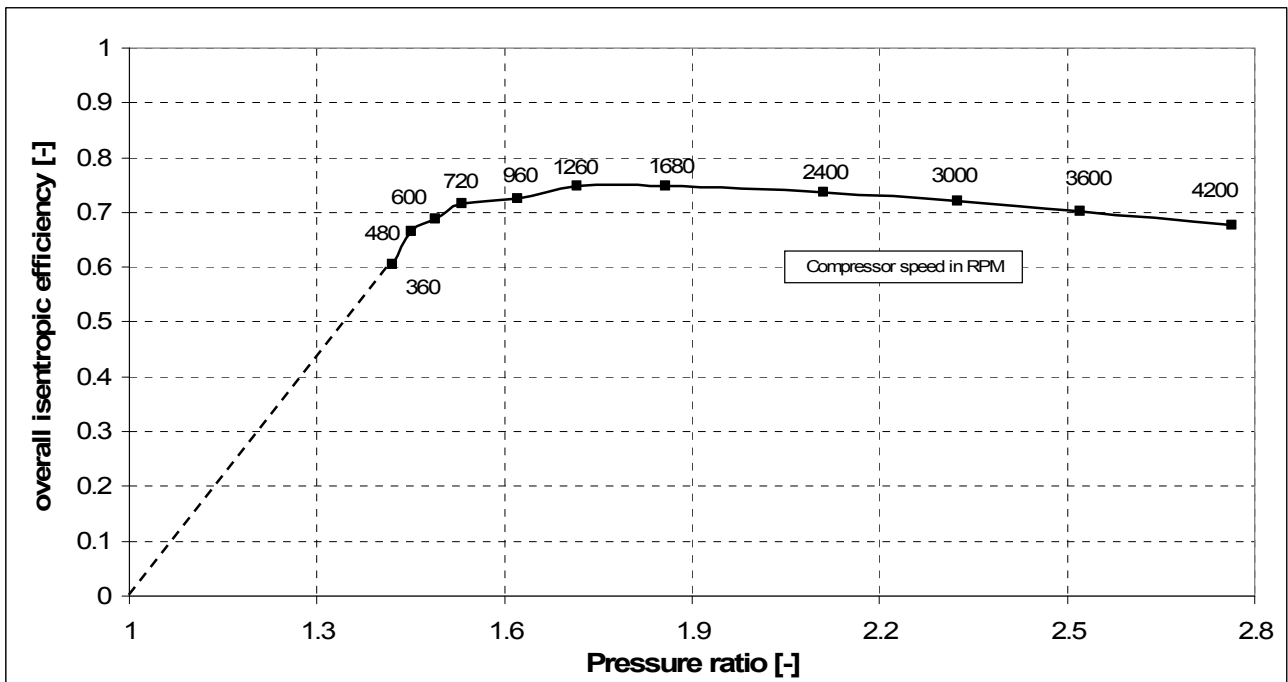
Figure 1.4.5: Overall isentropic efficiency vs. pressure ratio; the compressor speed is reported in the labels

	R410A		Compressor						
Test	mass flow	charge	Pcpri	Tcpri	Pcpro	Tcpro	speed	pressure ratio	η overall is
	kg/h	g	bar	°C	Bar	°C	RPM	-	-
1	95.1	1064	9.67	11.2	26.71	69.8	4200	2.76	0.676
2	86.7	1090	10.38	13.1	26.17	65.8	3600	2.52	0.703
3	77.9	1152	11.07	15.1	25.73	62.6	3000	2.32	0.720
4	67.6	1200	11.89	17.2	25.08	58.9	2400	2.11	0.737
5	53.2	1233	13.10	20.1	24.32	54.0	1680	1.86	0.749
6	42.8	1258	13.88	22.6	23.83	51.5	1260	1.72	0.749
7	34.7	1361	14.49	24.0	23.48	49.5	960	1.62	0.725
8	27.4	1466	15.02	25.7	23.01	47.2	720	1.53	0.717
9	23.4	1578	15.40	26.4	22.93	46.2	600	1.49	0.689
10	19.5	1772	15.74	27.7	22.84	44.9	480	1.45	0.666
11	14.9	2106	16.09	28.4	22.85	44.0	360	1.42	0.606

Table 1.4.4: Experimental results (refrigerant charge and compressor running)

Chapter 1.4: Energy efficiency related to heat transfer area: evaluation of potential for efficiency increase

The approaching to the theoretical Evans-Perkins cycle is shown in Figure 1.4.6(a), (b), (c) and (d). In these p-h diagrams the actual cycle of different tests and the Evans-Perkins cycle are plotted. The difference of the first test from the ideal cycle is clear, while in the test n. 11 the two cycles are very close.
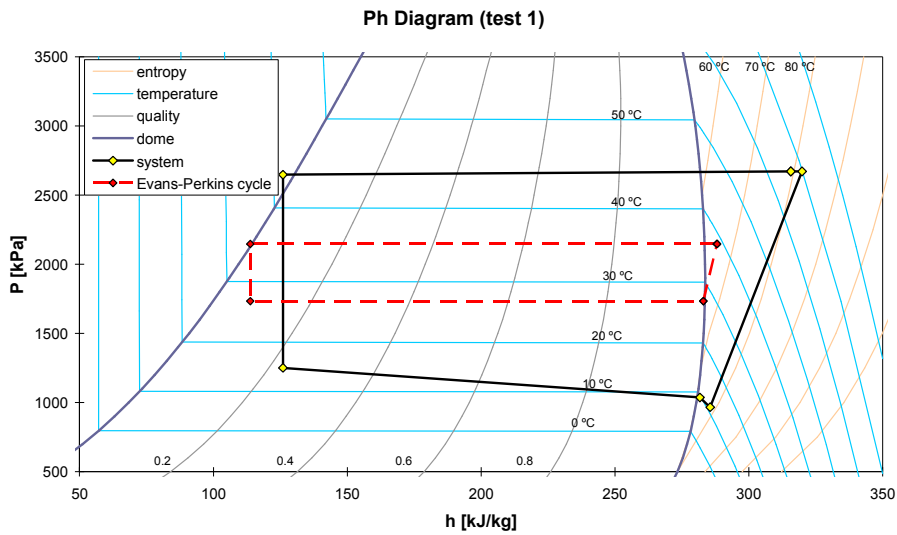
Figure 1.4.6(a): Actual cycle and Evans-Perkins cycle in a ph diagram of test n. 1
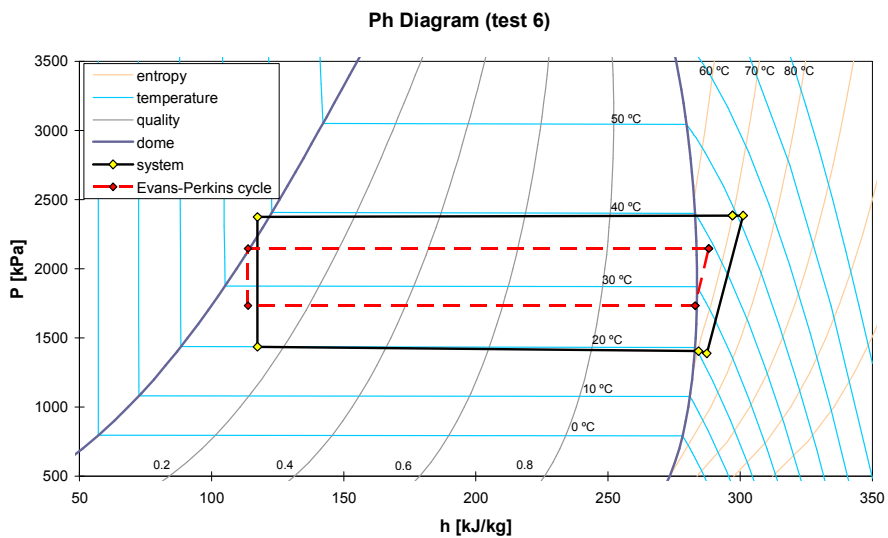
Figure 1.4.6(b): Actual cycle and Evans-Perkins cycle in a ph diagram of test n. 6
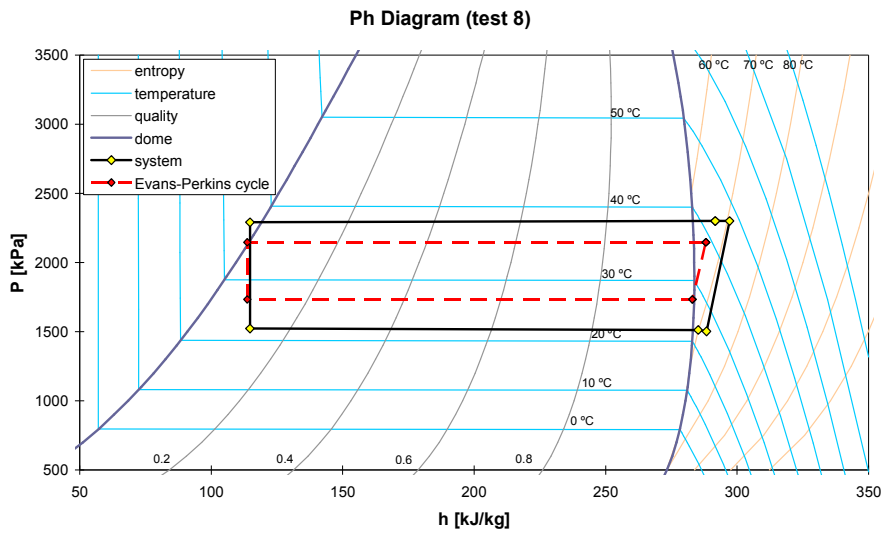
Ph Diagram (test 8)

1.4.6(c):

Actual cycle and Evans-Perkins cycle in a ph diagram of test n. 8

Ph Diagram (test 11)
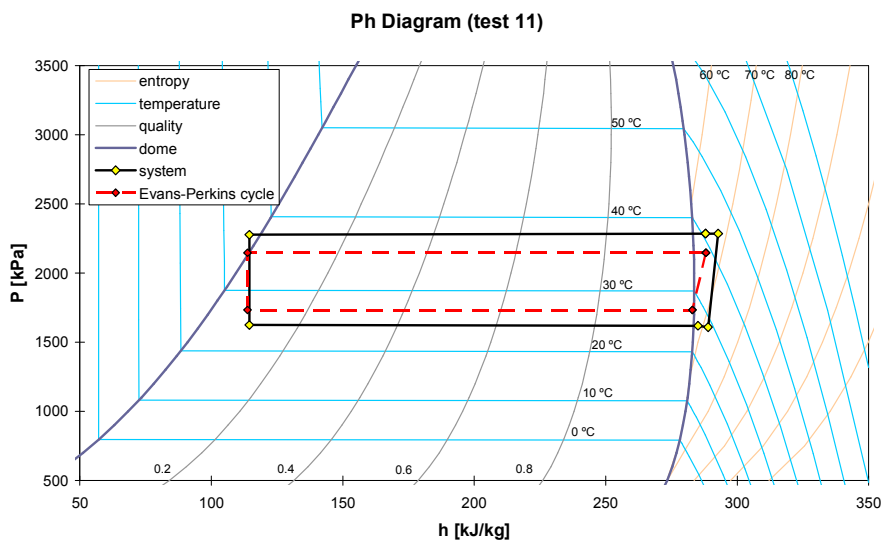
1.4.6(d):

Actual cycle and Evans-Perkins cycle in a ph diagram of test n. 11

The experimental conditions at the condenser and at the evaporator are reported in Tables 1.4.5 and 1.4.6(a) and (b). In the former refrigerant parameters are reported, in the latter air-side conditions are listed. The refrigerant pressure drops in both heat exchangers decrease sharply, especially in the evaporator, where it passes from 215 Pa to 5 Pa. The air temperature differences decrease sharply, both at the condenser and at the evaporator; in the former, the air temperature difference passes from 8.2 K to 1.3 K, while in the latter the air cooling decreases from 13.7 K to 1.9 K. The refrigerant desuperheat at the condenser is strongly reduced, from 22.6 K to 3.3 K.

Chapter 1.4: Energy efficiency related to heat transfer area: evaluation of potential for efficiency increase

Test	Condenser					Evaporator					
	Tcri	Tcro	DP cond	Tcro_sat	Sc	Teri	Tevro	Tero	DP evap	Tero_sat	Sh
	°C	°C	Pa	°C	K	°C	°C	°C	Pa	°C	K
1	66.6	41.8	23	44.0	2.2	15.1	41.5	9.6	215	8.5	1.1
2	63.0	40.8	21	43.2	2.4	15.3	40.4	11.3	171	10.2	1.0
3	58.5	40.1	19	42.5	2.3	15.8	39.8	13.2	133	12.0	1.2
4	56.0	39.0	15	41.4	2.4	16.7	38.6	15.2	92	14.0	1.1
5	51.2	37.6	13	40.1	2.5	18.5	37.2	18.0	52	17.1	1.0
6	48.4	37.0	11	39.3	2.3	19.8	36.5	20.4	31	19.0	1.4
7	44.8	36.1	10	38.7	2.5	20.9	35.6	21.8	19	20.5	1.3
8	43.3	35.6	9	37.8	2.2	22.0	35.0	23.5	11	21.7	1.8
9	43.2	35.6	9	37.7	2.1	22.8	34.9	24.0	8	22.6	1.4
10	41.9	35.5	7	37.5	2.1	23.7	34.0	25.0	7	23.4	1.6
11	40.9	35.5	7	37.6	2.1	24.4	30.5	25.7	5	24.2	1.5

Table 1.4.5: Experimental results at condenser and evaporator, refrigerant side

Test	Condenser			
	air mass flow cond	Tcai	Tcao	DP cond
	kg/h	°C	°C	Pa
1	2411.6	35.1	43.3	19
2	2415.8	35.0	42.3	18
3	2403.7	35.1	41.4	18
4	2413.6	34.9	40.3	18
5	2424.0	35.0	38.6	18
6	2390.2	35.1	38.8	18
7	2401.1	35.1	38.2	18
8	2398.9	35.0	37.8	18
9	2405.7	35.1	37.2	18
10	2401.5	35.0	37.0	18
11	2399.6	35.0	36.3	18

Table 1.4.6(a): Experimental results at condenser, air side

| Test | air mass flow evap | Evaporator | | | | |
| | | Teai | Teao | x in | x out | DP evap |
	kg/h	°C	°C	g/kg	g/kg	Pa
1	1120.8	26.8	13.1	5.9	5.9	17
2	1113.8	26.9	14.2	6.0	6.0	17
3	1106.1	27.0	15.4	5.8	5.8	17
4	1103.6	26.9	16.8	6.2	6.2	17
5	1094.7	27.0	19.0	6.5	6.5	17
6	1091.7	27.0	20.7	6.7	6.7	17
7	1087.0	27.0	22.0	6.7	6.7	17
8	1082.8	26.9	23.2	6.7	6.7	17
9	1084.2	27.0	23.9	6.0	6.0	17
10	1067.9	27.0	24.5	6.3	6.3	17
11	1070.9	27.0	25.1	6.6	6.6	17

Table 1.4.6(b): Experimental results at evaporator, air side

The performances of the different components are reported in Table 1.4.7; compressor power, condenser and evaporator capacity decrease in the same way

| Test | W comp | Q cond | Q evap |
	kW	kW	kW
1	1.113	5.011	4.125
2	0.878	4.521	3.813
3	0.698	3.975	3.467
4	0.518	3.447	3.053
5	0.328	2.676	2.446
6	0.230	2.131	1.994
7	0.171	1.700	1.634
8	0.120	1.340	1.293
9	0.099	1.149	1.106
10	0.080	0.945	0.921
11	0.063	0.719	0.707

Table 1.4.7: Component performances

1.4.5 Efficiency analysis

The unit efficiency is analyzed calculating the EER; in this facility, the power consumption of the auxiliary devices (i.e., the fans in both chambers) is not measured, so the EER value does not take it into account. Nevertheless, this consumption is important to our purposes: at low compressor speed (or at high heat

110

exchanger sizes), the fan power becomes relevant, compared to the compressor power. To have an idea of the auxiliary energy consumption, it was estimated considering fixed fan efficiency, using the following equation.

$$\eta_{fan} = \frac{\dfrac{\dot{m}_{air}Dp}{\rho}}{W_{fan}}, \tag{1}$$

The ERR values, with or without the fan power, are affected by the compressor overall isentropic efficiency, that depends on both the pressure ratio and the compressor speed (see Figure 1.4.5). In this way, the comparison of the EER values is not fair: in the real system the compressor speed is supposed to be the same, in a limited pressure ratio range, while the heat exchanger sizes change. Thus, the EER with an ideal compressor (with unitary overall isentropic efficiency) is calculated; even in this case, the EER value with and without the fan power are calculated.

Finally, the EER of an ideal Rankine cycle (Evans-Perkins cycle) is calculated: in this case the condensation temperature is the air temperature at the condenser inlet and the evaporation temperature is the air temperature at the evaporator inlet. In the actual cycle, there are subcooling and superheat: the Evans-Perkins EER is also calculated considering a higher condensation temperature (condenser air inlet temperature + subcooling) and a lower evaporation temperature (evaporator air inlet temperature − superheat).

Test	EER no fans	EER fans	EER id comp No fans	EER id comp Fans	EER E-P	EER E-P sh sc
	-	-	-	-	-	-
1	3.707	3.529	5.487	5.114	31.953	22.152
2	4.343	4.086	6.179	5.681	32.764	22.467
3	4.969	4.613	6.901	6.242	32.617	21.964
4	5.891	5.338	7.994	7.019	32.879	22.230
5	7.461	6.421	9.960	8.203	32.943	22.444
6	8.682	7.074	11.588	8.907	32.428	21.633
7	9.571	7.329	13.201	9.306	32.384	21.357
8	10.759	7.543	15.008	9.438	32.768	21.264
9	11.120	7.297	16.132	9.198	32.760	22.166
10	11.500	6.969	17.274	8.776	33.144	22.135
11	11.138	6.138	18.376	7.886	32.869	22.028

Table 1.4.8: Cycle EER values

The results are reported in Table 1.4.8 and plotted in Figure 1.4.7; the fan efficiency was set at 0.3. In Table 1.4.9, the EER values are related to that of the Evans-Perkins cycle; these ratios are also shown in Figure 1.4.8.

The EER without fan power (EER no fans; blue line in the graph of Figure 1.4.7) remarkably increases in the first tests: passing from 4.125 kW to 1.994 kW of refrigerating capacity, i.e. doubling the sizes of the heat exchangers, the EER passes from 3.707 to 8.682 (134% higher). Further doubling the size, the increase is lower: at 0.921 kW of refrigerating capacity, the EER is 11.500, with an increase of 32%. These values are affected by the fading compressor overall isentropic efficiency. Considering the fan power (EER fans; red line), the EER increase is even lower: passing from 4.125 kW to 1.994 kW of refrigerating capacity, the EER doubles, from 3.529 to 7.074, but it early starts to decrease, at 1.293 kW of refrigerating capacity. This value is penalized by both the compressor efficiency and the increasing weight of fan power. The EER of an ideal compressor without the fan power (EER id comp No fans; orange line) is not affected by these two penalizations and its improvement is more homogeneous: it passes from 5.487 to 11.588 (111% higher) first doubling the heat exchanger sizes, and to 17.274 (49% higher) at the second double. The most meaningful value is that of EER of an ideal compressor with the fan power (EER id comp Fans; green line): it is not altered by the compressor efficiency but it takes into account the weight of the auxiliary devices. It presents a remarkable increase passing from 4.125 kW to 1.994 kW of refrigerating capacity, from 5.114 to 8.907 (74%), but it reaches the maximum at 1.293 kW. The turning point, where the heat exchanger oversizing becomes useless, can be set at 1.5 kW. Being the shape of the curve of EER with fans and of EER of ideal compressor with fans (red and green lines) very similar, it is possible to conclude that the effect of the auxiliary devices is higher than the effect of the compressor efficiency.
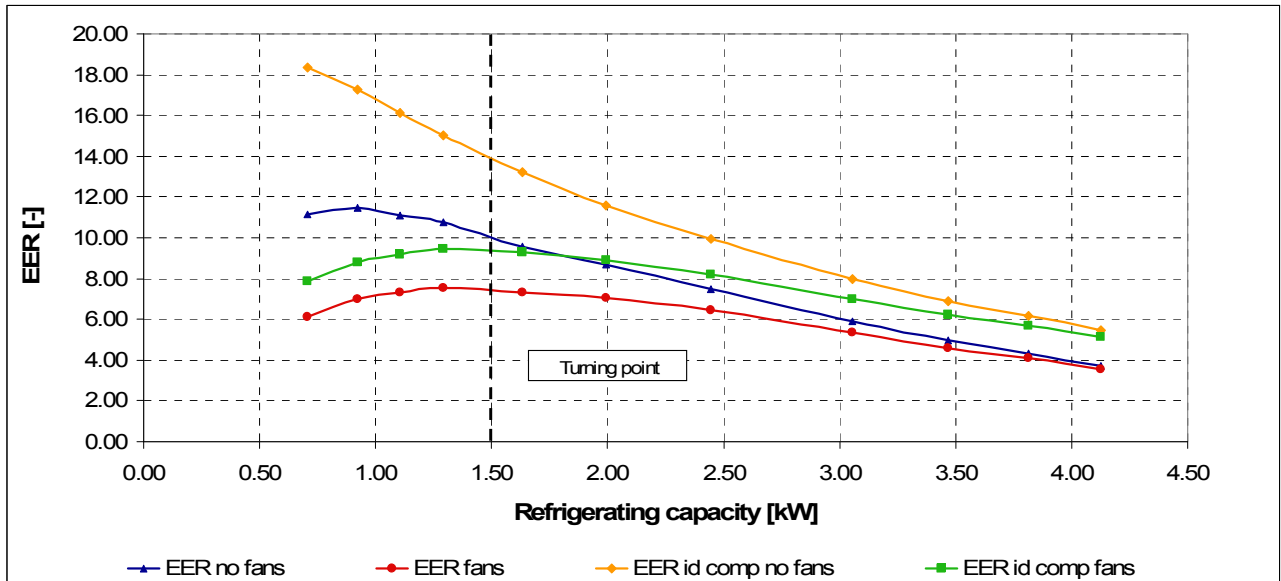
Figure 1.4.7: Cycle EER values

Test	EER E-P sh sc / EER E-P	EER no fans / EER E-P	EER id comp no fans / EER E-P	EER id comp fans / EER E-P
	-	-	-	-
1	0.693	0.116	0.172	0.160
2	0.686	0.133	0.189	0.173
3	0.673	0.152	0.212	0.191
4	0.676	0.179	0.243	0.213
5	0.681	0.226	0.302	0.249
6	0.667	0.268	0.357	0.275
7	0.659	0.296	0.408	0.287
8	0.649	0.328	0.458	0.288
9	0.677	0.339	0.492	0.281
10	0.668	0.347	0.521	0.265
11	0.670	0.339	0.559	0.240

Table 1.4.9: Cycle EER values related to Evans-Perkins cycle EER

The ratio between the Evans-Perkins cycle EER (EER E-P) and the Evans-Perking cycle with subcooling and superheat (EER E-P sh sc), marked with red line in the graph of Figure 1.4.8, highlights the penalization due to the temperature differences from the saturation. This ratio is fairly constant (small variations are due to the temperature control of the system) and the average is 0.673. As expected, the ratio of the EER of ideal compressor without fan power to the Evans-Perkins

EER tends to this value at null refrigeration capacity (red and green dashed lines).
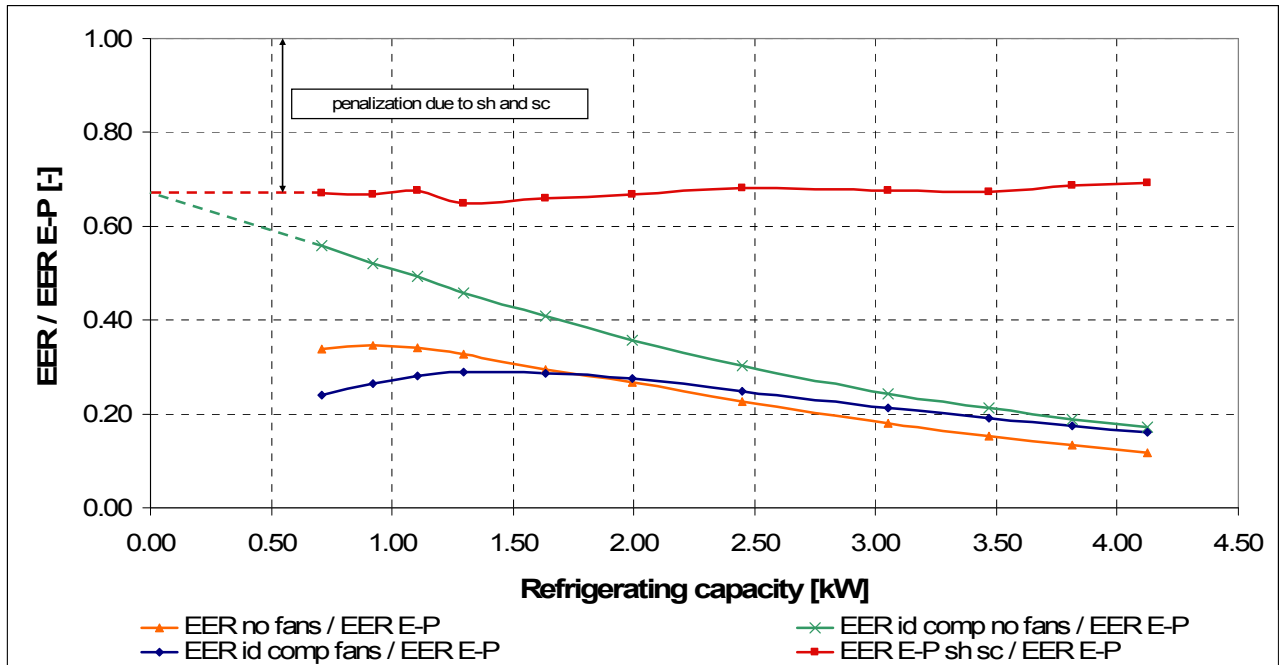
Figure 1.4.8: Cycle EER values related to Evans-Perkins cycle EER

1.4.6   Temperature analysis

The efficiency analysis shows that the increase of the heat exchanger size is useful until a certain point; beyond it, the energy improvement provided by the larger dimension is poor and it is penalized by the auxiliary consumption. To understand the reason of this turning point, at around 1.5 kW of refrigeration capacity, the temperature differences between air and refrigerant, at the condenser and at the evaporator, are analyzed; they are reported in Tables 1.4.9(a) and (b).

Condenser				
Test	Sc	Tcri – Tcri_sat	Tcro_sat - Tcai	Tcri_sat - Tcao
	K	K	K	K
1	2.2	22.6	9.1	0.8
2	2.4	19.8	8.3	0.8
3	2.3	16.0	7.5	1.0
4	2.4	14.6	6.6	1.1
5	2.5	11.1	5.2	1.5
6	2.3	9.1	4.3	0.5
7	2.5	6.1	3.6	0.4
8	2.2	5.5	3.0	0.1
9	2.1	5.5	2.8	0.5
10	2.1	4.4	2.6	0.6
11	2.1	3.3	2.7	1.2

Table 1.4.9(a): Temperature difference between air and refrigerant at the condenser

Evaporator			
Test	Sh	Teai - Teri_sat	Teao - Tero_sat
	K	K	K
1	1.1	18.4	4.7
2	1.0	16.7	4.0
3	1.2	15.1	3.4
4	1.1	13.0	2.7
5	1.0	10.0	1.9
6	1.4	8.1	1.6
7	1.3	6.6	1.5
8	1.8	5.3	1.5
9	1.4	4.5	1.2
10	1.6	3.7	1.1
11	1.5	2.8	0.9

Table 1.4.9(b): Temperature difference between air and refrigerant at the evaporator

The difference between the refrigerant temperature at the condenser inlet and in saturation conditions (green line in the graph of Figure 1.4.9) decreases sharply, from 22.6 K to 3.3 K, reducing desuperheat losses. The temperature difference between the saturated refrigerant at the outlet and the air linearly decreases until it reaches values close to the subcooling. At Qevap=1.634 kW, the difference between the subcooling and the temperature difference between the saturated refrigerant and the air (blue dashed and orange lines) is 1.1 K; beyond the turning point, at Qevap=1.293 kW, it is 0.8 K and it tends to zero at low refrigerating

capacity. Thus, a first conclusion can be that the heat exchanger oversizing is useful until the temperature difference between the refrigerant at the condenser outlet and the air is higher than 1 K.

Figure 1.4.9: Temperature difference between air and refrigerant at the condenser
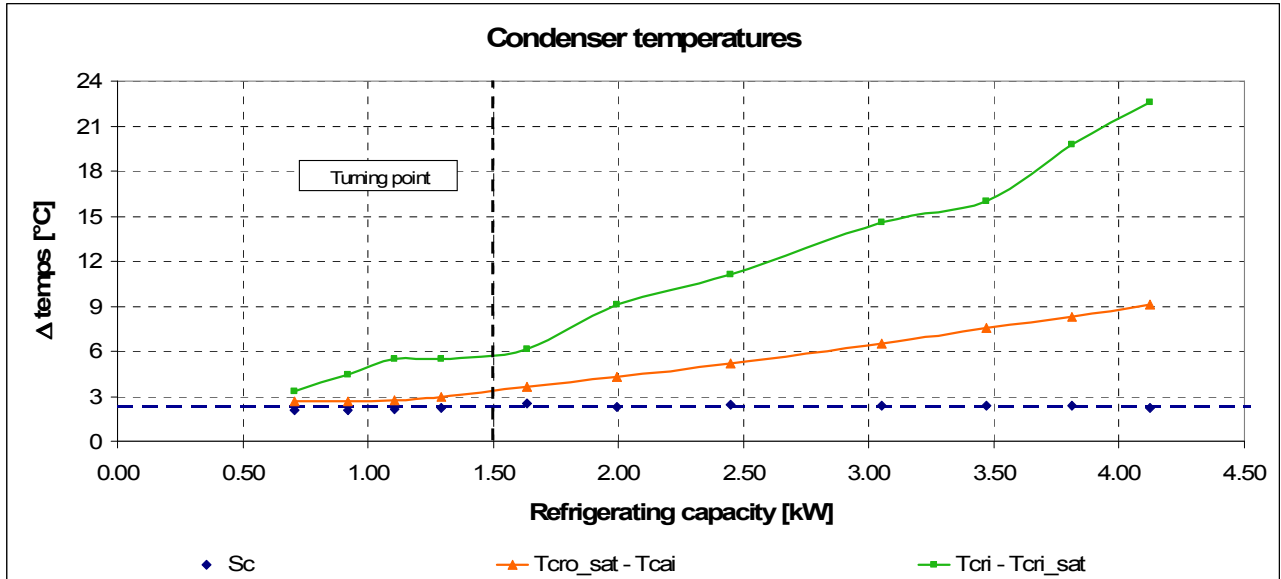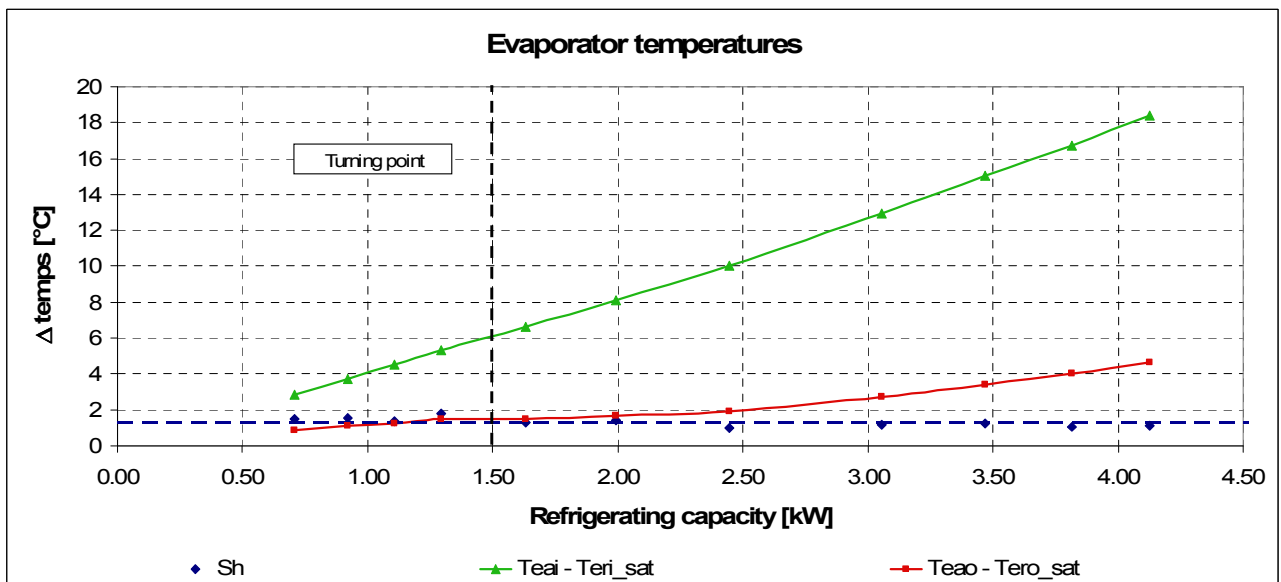

Figure 1.4.10: Temperature difference between air and refrigerant at the evaporator

The temperature difference between the air at the evaporator inlet and the

saturated refrigerant at the inlet (green line in the Figure 1.4.10) decreases linearly, increasing the heat exchanger size. The temperature difference between the air at the outlet and the saturated vapour (red line) gets close, or even lower, to the superheat at low refrigerating capacity. At Qevap=1.634 kW, it is 0.2 K higher than the superheat, at Qevap=1.293 kW it is 0.3 K lower. Being this temperature difference at Qevap=1.994 kW just 0.2 K higher than the superheat, a second conclusion can be that the temperature difference between the supplied air and the refrigerant at the evaporator outlet can be very low, close to 0 K. Nevertheless, good improvements are recorded where the temperature differences between air and saturated refrigerant, of both condenser and evaporator, decrease linearly; in this case, the optimal oversizing is 1.69 times, at Qevap=2.446 kW.

1.4.7   Conclusions

The purpose of this part was to investigate how much the heat exchanger oversizing is useful in an air-to-air conditioning system. The evaporator and condenser oversizing was simulated decreasing the refrigerating capacity by reducing the compressor speed. Two major constrains affected this analysis: the fan power consumption was not measured in the facility and the compressor overall isentropic efficiency fades at low rotational speed. In the first case, fan efficiency was assumed and the auxiliary consumption was calculated; in this way, the EER with and without fan power were evaluated. The second problem was heavier: the overall isentropic efficiency is penalized by both the decreasing compressor speed (i.e. affecting also the electrical efficiency of the motor) and by the lowering pressure ratio, but it is not possible to share these two effects. A fairly constant efficiency was assumed in the considered pressure ratio range and the experimental data were compared considering an ideal compressor. Finally, the Evans-Perkins (ideal Rankine) cycle EER was calculated, with and without the effect of subcooling and superheat.

The performance analysis points out that subcooling and superheat strongly penalized the Evans-Perkins cycle efficiency, decreasing the theoretical efficiency of around 30%. The EER curves show the penalization given by the auxiliary

power consumption and by the low compressor overall isentropic efficiency. Nevertheless, even neglecting these effects, the efficiency does not increase linearly. A turning point can be found, beyond which the heat exchanger oversizing is useless: for this system, the sizes of evaporator and condenser can be increase of 2.75 times, even if the higher effect is reached just increasing the size of 1.69 times.

To better understand the reason of this turning point, the temperature differences between refrigerant and secondary fluid in the two heat exchangers were studied. The condenser oversizing is useful until the temperature difference between the air at the inlet and the refrigerant at the outlet is at least 1 K. For the evaporator, the temperature difference between the air and the refrigerant at the outlet can be close to 0 K.

These statements are valid only for this plant, with this configuration of heat exchangers and these peculiar refrigerant paths. By the way, the conclusions concerning the temperature differences can be extended to air-to-refrigerant condenser, with overall counter-flow configuration, and air-to-refrigerant evaporator, with overall parallel-flow configuration. Another important drawback is that it is not possible to study the effect of oversizing in the two heat exchangers separately. Probably, the optimal oversizing is different for condenser and evaporator, but this method can not share the effects. Looking at the temperature profiles, the oversizing is clearly useful until the temperature differences between air and saturated refrigerant, of both condenser and evaporator, decrease linearly. Thus, it is worth to assume that the optimal condenser oversizing, for this configuration, may be 2.75 times, while for this configuration of evaporator, the optimal oversizing may be 1.69.

Chapter 1.5 **E**FFICIENCY IMPROVEMENT RELATED TO HEAT EXCHANGER TYPE: THE MINICHANNEL HEAT EXCHANGERS

1.5.1 Introduction

A review on the microchannel air-to-refrigerant heat exchanger is presented. This kind of heat exchanger is gaining more and more interest in the latest years, but, at the same time, its use implies some technological constrains, which are not completely overcome.

1.5.2 Definition of micro- and minichannel heat exchangers

1.5.2.1 Definition

Being this technology relatively young, even the definition of micro- and minichannel is not univocal in the scientific literature. Thome and Ribatski (2005) present two definitions, by Kandlikar and Grande (2003) and by Kew and Cornwell (1997). In the first case, the distinction is the following:

D_h>3 mm: conventional channel;

3 mm>D_h>200 μm: minichannel;

200 μm>D_h>10 μm: microchannel;

where D_h is the hydraulic diameter. In the present work the distinction between mini- and microchannel is not considered.

Kew and Cornwell (1997) provide a distinction between micro- and macro-channels, fixing a threshold hydraulic diameter, defined as:

$$D_{th} = \left(\frac{4\sigma}{g(\rho_L - \rho_V)} \right)^{1/2},$$

(1)

where:

σ: surface tension [N/m];

g: gravity acceleration [9.801 m/s^2];

ρ_L: liquid density [kg/m^3];

ρ_V: vapour density [kg/m^3].

For example, for R410A, at three saturation temperatures (-10°C, 0°C and 10°C), the values are:

$D_{th,\ -10°C}$: 2.120 mm;

$D_{th,\ 0°C}$: 2.037 mm;

$D_{th,\ 10°C}$: 1.951 mm.

1.5.2.2 *Advantages in the use of microchannels*

The heat transfer mechanisms have been deeply investigated and described by several authors, for both single and two phase fluid flow. Particularly, the interest of the researchers is addressed to the heat exchangers used in HVAC&R applications, i.e. condensers and evaporators. In this chapter, only the air-to-refrigerant heat exchanger will be analyzed and described.

The main advantages of the microchannel heat exchangers, with respect to the traditional finned coil, are:

- charge reduction
- smaller size
- high heat transfer area on core volume ratio
- high pressure resistance
- low costs.
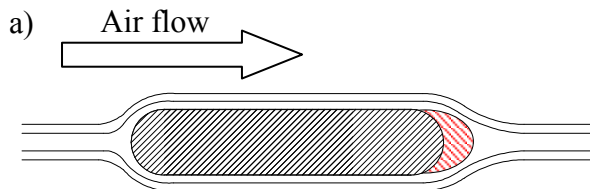
a)   Air flow

b)
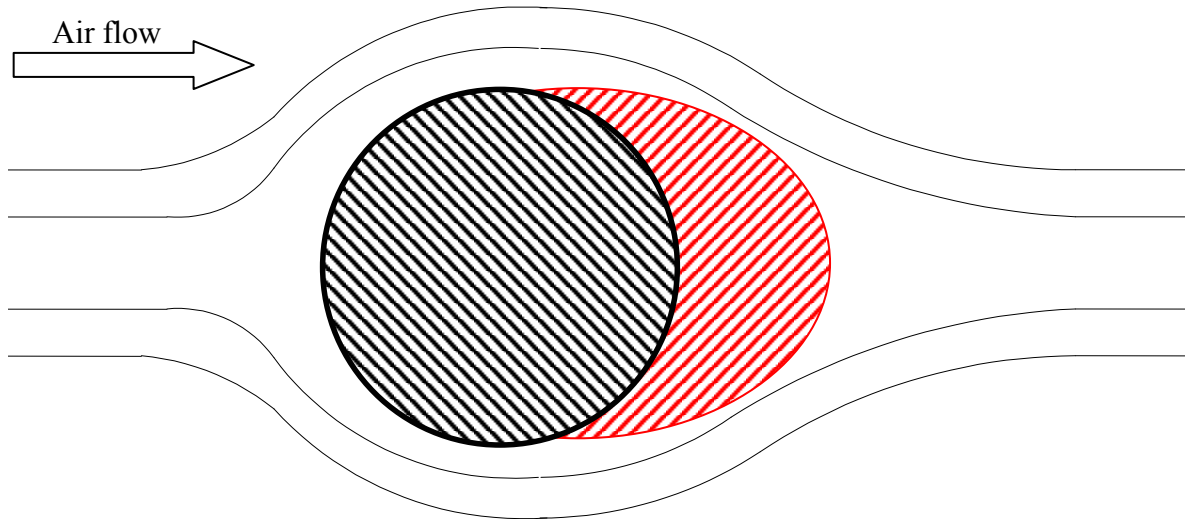
Figure 1.5.1: Tube section, wake and streamlines of a microchannel (a) and a round tube (b)

The advantages provided by a high heat transfer area and by a charge reduction were dealt with in Chapter 1.4; in addition, the heat transfer is favored by the shape of the channel. This is shown in Figure 1.5.1: the black-hatched shape is the tube section, the red-hatched shape is the wake and the lines are the streamlines, for a microchannel (a) and for a round tube (b). The percentage of the microchannel heat exchange area which is "not activated", because of the wake, is significantly smaller than for the round tube (the microchannels are also called "flat tubes"), so the heat transfer is improved. Due to these features, they are widely used in applications which need narrow dimensions (for example, electrical circuit cooling or automotive air conditioning) and they are characterized by high thermal fluxes. The main drawbacks are the high pressure drops, both air-side and refrigerant side, and some technological constrains, such as the moisture drainage, the defrosting management and the maldistribution.

In Figure 1.5.2, some examples of microchannel are shown.
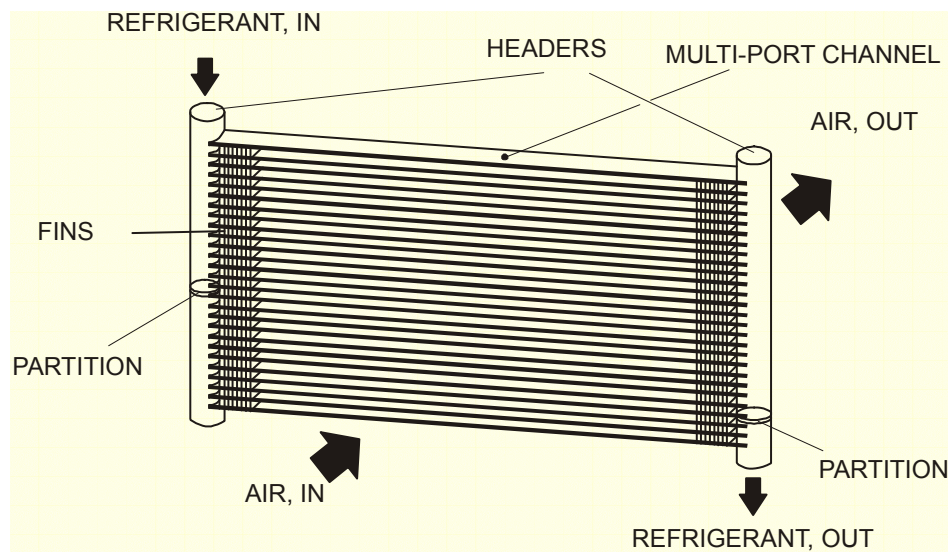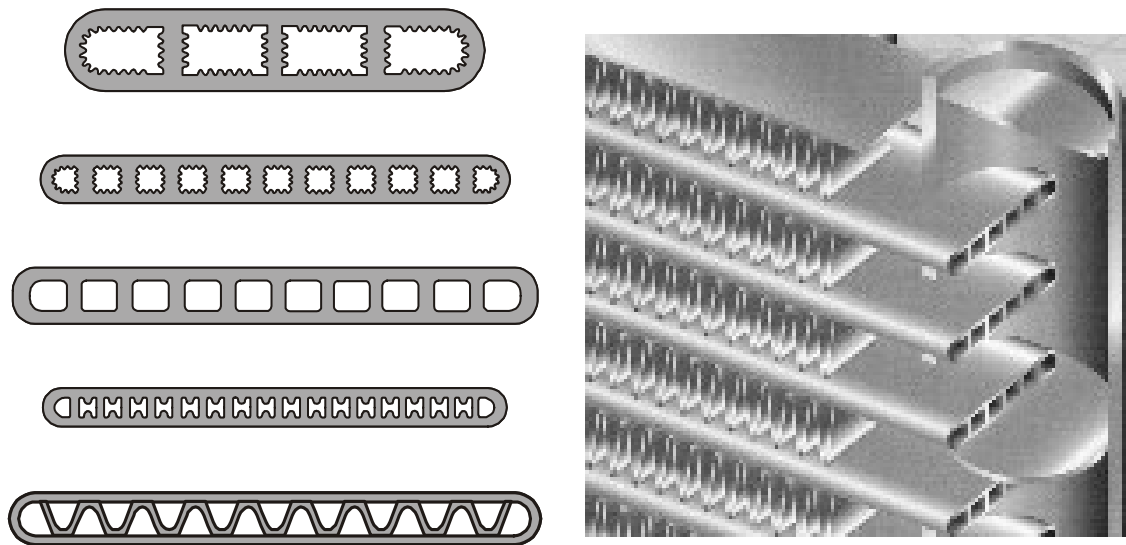
Figure 1.5.2: Some examples of geometries of microchannel heat exchangers

1.5.3   Heat transfer coefficient predictive models

The microchannel and minichannel heat exchangers were firstly studied by Tuckerman and Pease (1982), for single phase fluid flow. Until the middle 90's, the use of this technology in two phase heat exchangers was rather remote; the research

122

on micro- and minichannels received great push in the first years of the new millennium. In this period, the first correlations of heat transfer and pressure drop for two-phase conditions were presented in the open literature.

As regards evaporation, Kandlikar *et al.* (2005) highlight some advantages of the evaporation inside micro- or minichannels with respect to single phase heat exchange. Particularly, the heat transfer coefficients and the cooling capacity per refrigerant mass unit are higher. For example, the heat flux of water inside a minichannel of hydraulic diameter of 200 μm, in laminar flow, is 10 times higher during evaporation in comparison with single phase. In the open literature, several correlations have been proposed for evaporation in minichannels; their reliability and effectiveness are investigated in different reviews. The reports by Del Col *et al.* (2005), Kandlikar (2005) and Thome (2006) deserve to be considered. In these papers several correlations are presented; they regard mainly evaporation of pure fluids. So far, only Pamitran *et al.* (2007) present a model for R410A; they compare the experimental data with the simulation results calculated using the flow pattern map of Wojtan *et al.* (2005) and the model of Wang *et al.* (1997). The former correlations were developed on experimental tests on R410A evaporating inside a 13.6 mm channel, the latter ones on experimental tests on R407C evaporating inside a 6.5 mm channel. The results of these models are not satisfactory, so the authors developed a new correlation that predicts the heat transfer coefficient with a mean deviation of 11.20%.

In her Ph.D. thesis, Fantini (2005) took into consideration some predictive models, of CO_2 evaporation, and compared their results with the experimental data by Yun *et al.* (2005) and Pettersen (2004). She studied the models by Zhang *et al.* (2004), Kandlikar *et al.* (2005), Cheng *et al.* (2006) and Tran *et al.* (1996): as shown in Figure 1.5.3, the precision of these models is poor.
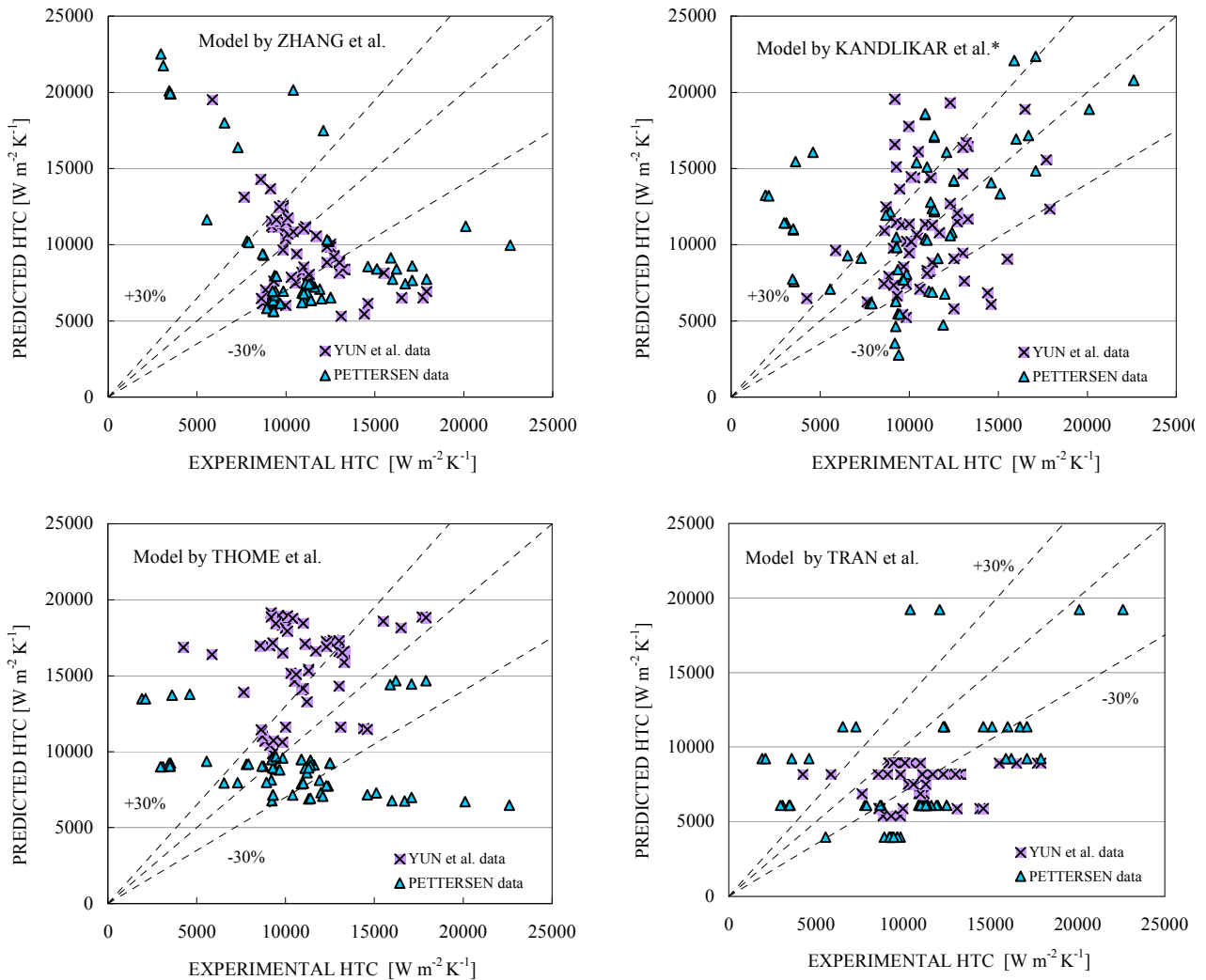
Figure 1.5.3: Experimental data vs. simulation results of 4 predictive models; Fantini (2005)

As regards condensation, Cavallini *et al.* (2005, 2006) presented two complete review on the state-of-the-art; they considerer a wide database of experimental data. They took into exam the models by Moser *et al.* (1998) modified by Zhang *et al.* (2001), Cavallini *et al.* (2002), Akers *et al.* (1959), Koyama *et al.* (2003) and Wang *et al.* (2002). The authors point out that the most accurate models are the first two, even if their reliability is restricted to non-dimensional gas velocities lower than 10, as shown in Figure 1.5.4. This velocity is defined as:

$$J_V = \frac{Gx}{\left[\rho_V\left(\rho_L - \rho_V\right)g\, D_h\right]^{0.5}} \; ,$$

(2)

where:

G: mass velocity [kg/m^{2}s];

x: quality;

g: gravity acceleration [9.801 m/s^2];

ρ_L: liquid density [kg/m^3];

ρ_V: vapour density [kg/m^3];

D_h: hydraulic diameter [m].

For J_V higher than 10, the models underestimate the heat transfer coefficient, probably because the fluid flow is not annular at high non-dimensional gas velocity. Garimella, in Kandlikar *et al.* (2005), lists all the available correlations, highlighting the applicability range and the suitable refrigerants. He also describes some of these correlations and provides some calculation examples.
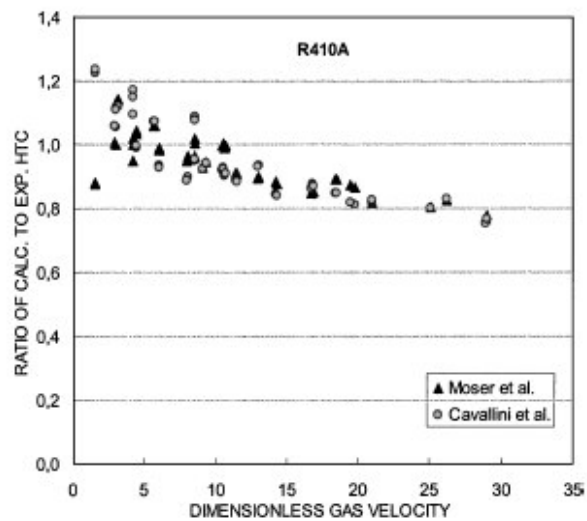
Figure 1.5.4: Ratio of calculated heat transfer coefficients on experimental ones vs. non-dimensional gas velocity; Cavallini et al. (2005)

1.5.4   **Pressure drop predictive models**

With the heat transfer mechanism, the air side and refrigerant side pressure drops in a microchannel heat exchanger have been investigated since the middle 90's. As regards evaporation, a comparison between different predictive models is presented by Ribatski *et al.* (2006). The authors consider a wide database of experimental data, from 9 different research groups, on different refrigerants, and they compare these data with the simulation results using 12 different pressure drop correlations. The most accurate model is that by Müller-Steinhagen and Heck (1986), even if it was made for macro-channels. Good results can be achieved by using a homogeneous model, with the viscosity correlation by Cicchitti *et al.*, (1960), or the model proposed by Mishima and Hibiki (1996). However, the precision of the results can not be considered satisfactory: only in few cases the simulation errors are within a band of $\pm$ 30%, and the precision fades down at quality higher than 0.6. These results should be improved through further investigations on the evaporation mechanisms.

As regards condensation, Cavallini's research group presented different review on the state-of-the-art. In Cavallini *et al.* (2005), the authors consider 5 different predictive models and compare the simulation results with the experimental data of tests on R134a and R410A. For R134a the average error is rather low (lower than 10%, except for the model of Yan and Lin, 1999). For R410A, the available correlations overestimate the actual pressure drops: the most fitting model is that of Zhang and Webb (2001), which provides an average error of 32.4%. In a following review (Cavallini *et al.*, 2006), the authors considered 10 different correlations, but even in this case the pressure drops of R410A can be predicted with sufficient reliability and even in this case the most fitting correlation is that of Zhang and Webb (2001). Garimella, in Kandlikar *et al.* (2005), presents a wider list of correlations and describes some of them, but he does not provide any comparison with experimental data.

1.5.5   Technological constrains: the refrigerant maldistribution

One of the most important technological drawbacks in the use of microchannel heat exchangers, for two phase fluids, is the maldistribution of the refrigerant. As regards the condensers, this problem is heavier at the outlet header: the vapour in the inlet header is superheated (thus single phase), while in the outlet header the fluid is saturated or subcooled liquid. The presence of two phase fluid at the expansion valve inlet can imply malfunction of the throttling process. As regards the evaporators, constrains are even heavier; the refrigerant enters the header in two phase conditions, downstream the throttling device, and this implies a separation of the phases. The higher the quality at the header inlet, the stronger the separation of the phases, and the lower the evaporator effectiveness. In fact, only a part of the heat exchange surface of the evaporator is wet by refrigerant, while the remaining part is completely dry, with low heat transfer efficiency. The energy loss due to this malfunction is evaluated higher than 20% by Hrnjak (2004). The maldistribution implies malfunction also at the evaporator outlet: in some channels the fluid can be not completely evaporated and a liquid fraction can be merged in the superheated vapour. This fact increases the liquid suction possibility at the compressor inlet. It is remarkable that the orientation of the headers does not affect significantly the distribution of the two phases. Cho *et al.* (2002) and Tompkins *et al.* (2002) pointed out that, even placing the header horizontally and the channels vertically, this problem is not overcome. In case of low mass flow rates, the fluid flow in the header can be considered as a stratified flow inside tubes and the liquid can feed only the channels close to the header inlet port. Otherwise, for high mass flow rates, the fluid flow can be considered annular: the farther channels are flooded while the channels closer to the header inlet port are scarcely fed with liquid.

1.5.5.1   Non-intrusive techniques for maldistribution detecting

The fist step is to find a non-intrusive method to highlight the maldistribution; the most common methods are described by Hrnjak (2004), they are the infrared visualization, the frost presence and the exit air temperature profile. Using an infrared camera, one could get information about the surface temperature of the heat exchanger. This method is non-intrusive, except for the presence of the

infrared camera upstream the heat exchanger, which can affect the air flow. The costs of a thermal camera can be considerable, but the method is the most precise, since it is possible to highlight the region fed by liquid (coldest tubes) or fed by vapour (hottest tubes). In Figure 1.5.5, an example of infrared image of a two-passage microchannel condenser is shown. The inlet and outlet points and the two passages are marked.
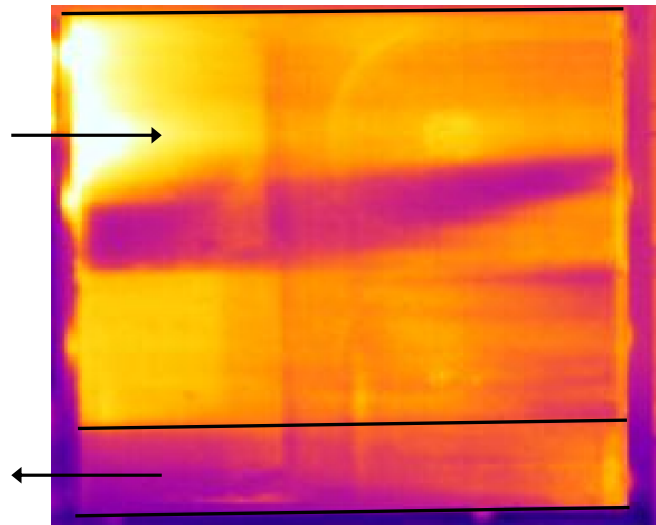
Figure 1.5.5: Infrared image of a microchannel condenser.

The presence of frost on the heat exchanger surface is a clear sign of the temperature of the surface; in fact, if the temperature of the tube surface is below 0°C, the air humidity condenses and, later, freezes on the heat exchanger. The parts covered by frost are the coldest, where the channels are fed by liquid. This method is less expensive and easier than the previous one (Song *et al.*, 2002), but it can be applied only for evaporators. In the following, some images of frosting, by different authors, are shown.

Figure 1.5.6: Frosting of a 2-passage microchannel evaporator

Figure 1.5.7: Frosting of a 3-passage microchannel evaporator (Macrì, 2006)
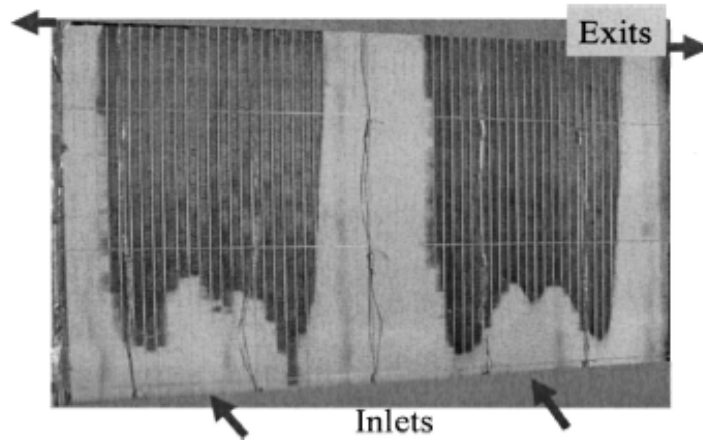
Figure 1.5.8: Frosting of a R744 microchannel evaporator (Hrnjak 2004)

The measure of the exit air temperature profile is the least precise method: the turbulence of air at the heat exchanger exit, with the turbulence produced by the measurement system, can significantly affect the temperature profile. In the following, some images of outlet air temperature profiles, by different authors, are shown.
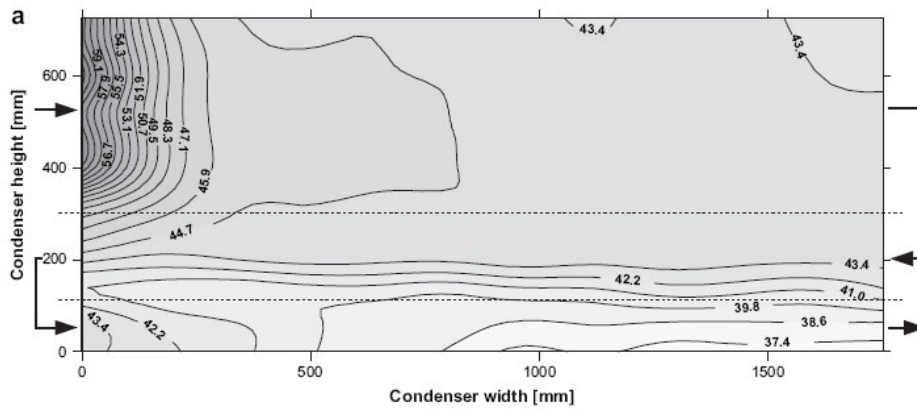
Figure 1.5.9: Air exit temperature profile of a minichannel condenser (Park and Hrnjak, 2008)
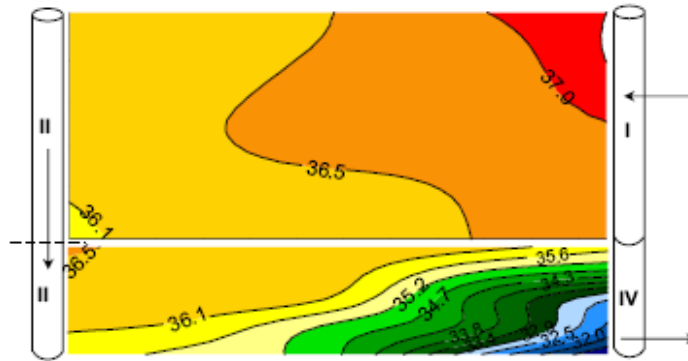
Figure 1.5.10: Air exit temperature profile of a microchannel ammonia condenser (Hrnjak and Litch, 2008)

1.5.5.2   *Factors which affect the flow distribution*

A fundamental issue is to identify the factors which affect the distribution of the refrigerant in a microchannel heat exchanger. These factors are:

- geometrical factors related to the headers;
- two-phase flow regime;
- maldistribution due to the heat transfer itself;
- fouling and/or corrosion.

The last two factors regard the heat transfer and the heat exchanger maintenance, so they are not faced in the present work.

A complete review on the factors which affect the refrigerant distribution was presented by Webb and Chung (2005); the authors studied in particular the effect of the header design. They pointed out that the flow distribution is strongly influenced by the header orientation (horizontal or vertical) and by the number of tubes. Other factors are the flow direction in the header (upflow or downflow), the header shape and tube end projection into the header, and the location and orientation of the inlet and exit ports. Different orientations of the header are shown in Figure 1.5.11: each of these is affected, in different ways, by maldistribution due to the stratification of the two-phase flow. The header functions are depicted in Figure 1.5.12: in this case the source of two-phase flow distribution problems is the positioning of the dividing headers, while the outlet headers have no influence on the refrigerant maldistribution. Another factor is the position of the inlet port in the header: three possible positions are shown in Figure 1.5.13, even if the side inlet (c) is not commonly used. Webb and Chung (2005) also classified the headers according to

the flow direction: it can be parallel, reverse or normal flow, as shown in Figure 1.5.14. The authors found that the reverse flow header has less flow maldistribution than the parallel flow header, while the normal flow is actually two reverse flow manifolds connected in parallel and the flow is affected by the position of the inlet port. Even the tube end projection (Figure 1.5.15) can influence the flow maldistribution, except if a D-shaped header is used. Finally, the header cross-section area has been considered; they defined the ratio A_R as the ratio of the header cross-sectional area to total cross-sectional area of all branch tubes. Bajura and Jones (1976) recommend $A_R > 1.0$ for single-phase headers. The authors simulated the flow distribution according to Bajura and Jones (1976) model, for different A_R values (0.5, 1.0, 2.0) and different header Reynolds numbers (250, 2500, 25000). The results are plotted in the diagram of Figure 1.5.16: Reynolds number has little effect and A_R=0.5 strongly penalizes the flow distribution.

Webb and Chung (2005) also investigated the effect of the mass velocity of the two-phase fluid in the header. The phase separation may cause significant flow maldistribution, as shown in Figure 1.5.17. This problem can occur along the refrigerant path in the header, in a multipass design heat exchanger (Figure 1.5.17(a)), or in the inlet header. If the header is a bottom-dividing one (Figure 1.5.17(b)), the farther tubes are fed with liquid, while the closer tubes are fed with vapour. Vice versa if the header is a top-dividing one (Figure 1.5.17(c)).

Chapter 1.5: Efficiency improvement related to heat exchanger type: the minichannel heat exchangers
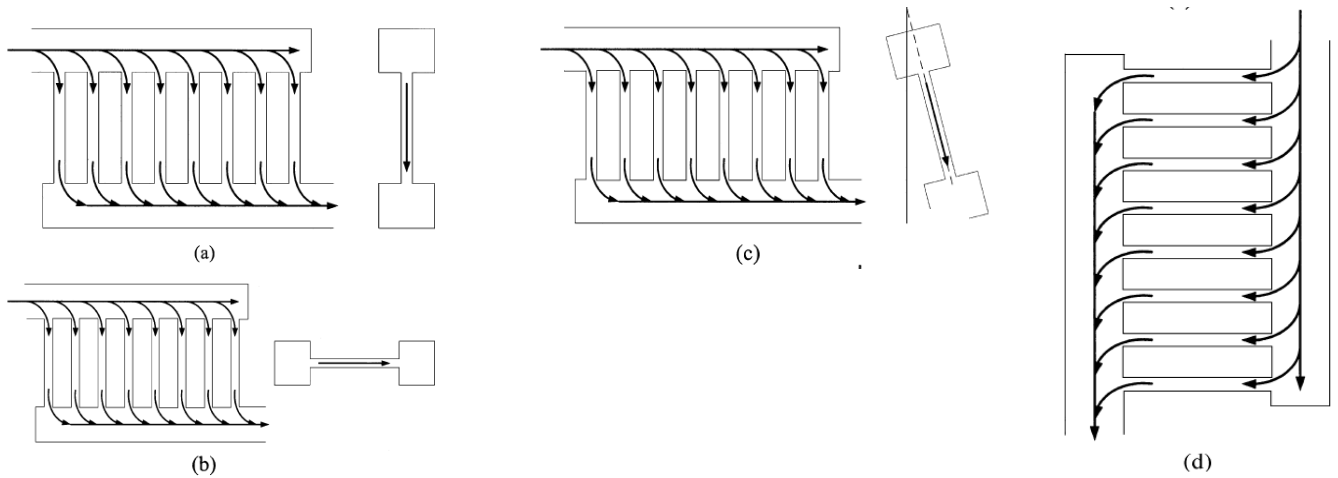
Figure 1.5.11: Classification of header-tube junctions: (a) Horizontal Header—Vertical Tube junction (HH—VT), (b) Horizontal Header—Horizontal Tube junction (HH—HT), (c) Horizontal Header—Inclined Tube junction (HH—IT),(d) Vertical Header-Horizontal Tube junction (VH—HT) (Webb and Chung, 2005)
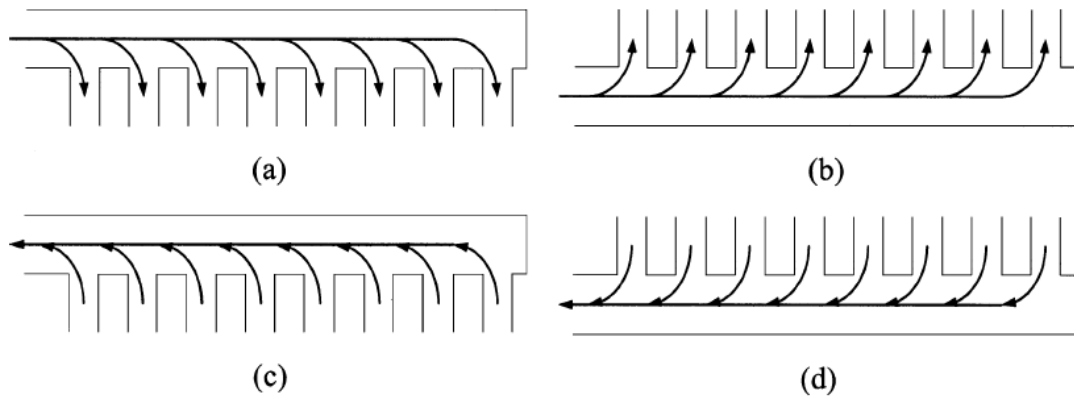
Figure 1.5.12: Classification of header function and location: (a) top-dividing header (downflow), (b) bottom-dividing header (upflow), (c) top combining header (upflow), (d) bottom-combining header (downflow); (Webb and Chung, 2005)
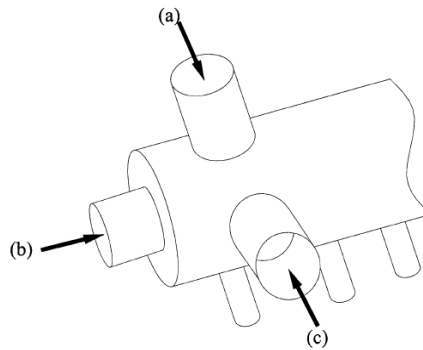
Figure 1.5.13: Classification of header connecting pipes: (a) normal inlet (parallel to tubes), (b) normal inlet (perpendicular to tube), (c) side inlet (normal to tubes); (Webb and Chung, 2005)
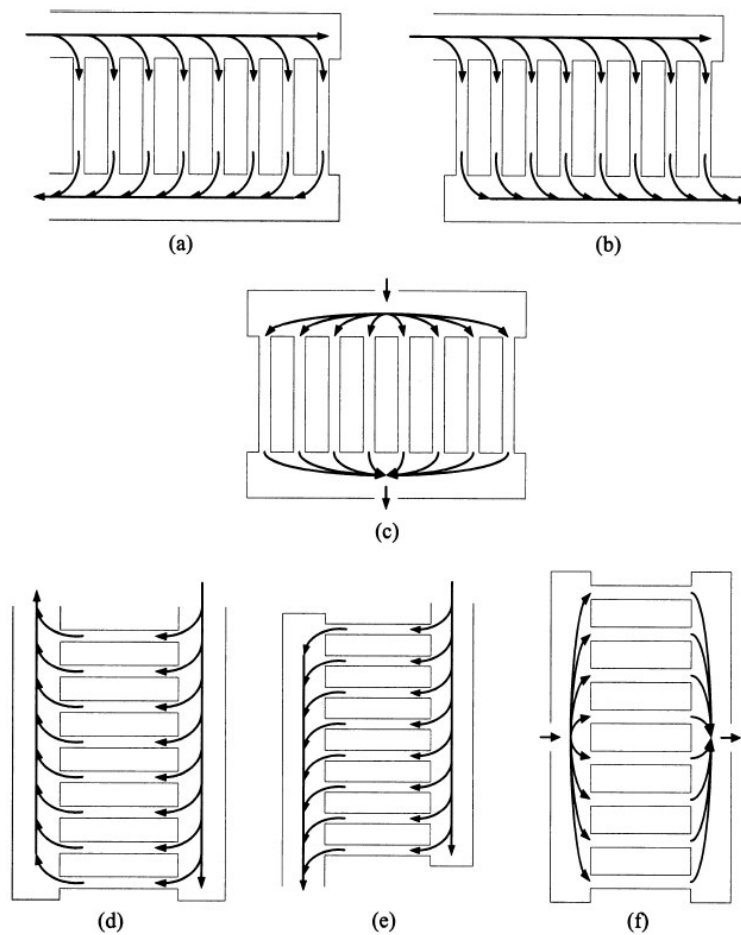
Figure 1.5.14: Classification of header flow direction: (a) horizontal reverse flow, (b) horizontal parallel flow, (c) horizontal normal flow, (d) vertical reverse flow,(e) vertical parallel flow, (f) vertical normal flow; (Webb and Chung, 2005)

134
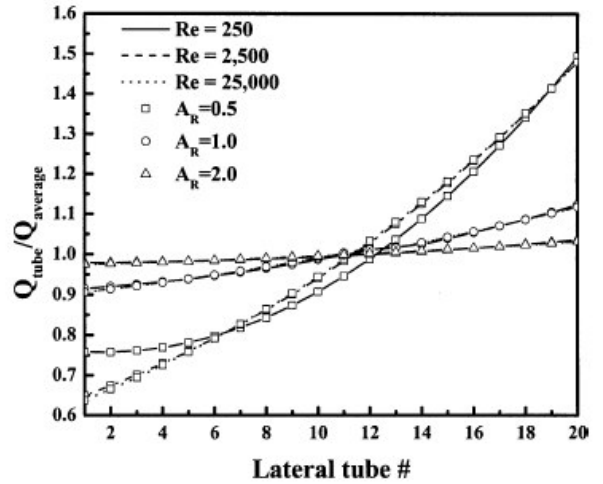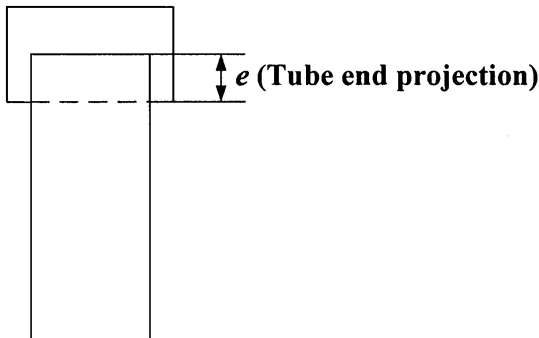
*Figure 1.5.15: Tube end projection;
(Webb and Chung, 2005)*

*Figure 1.5.16: Analytic prediction of single-phase parallel
flow distribution in lateral tubes for different area ratios;
(Webb and Chung, 2005)*
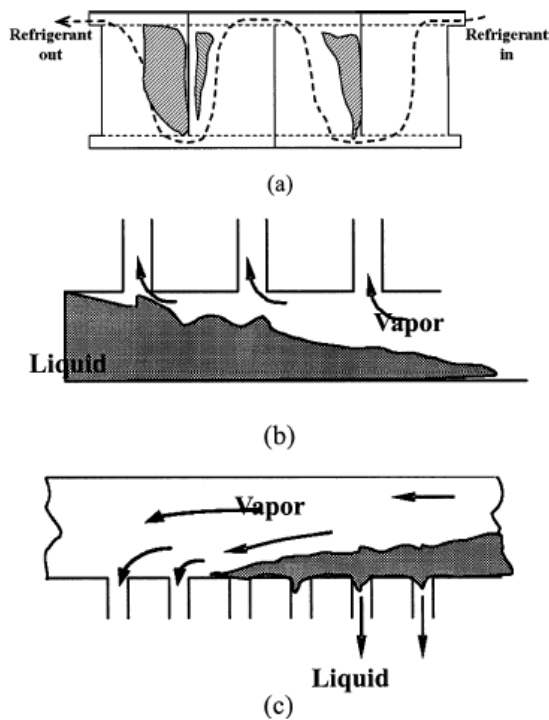
*Figure 1.5.17: Horizontal Header—Vertical Tube junction (HH–VT): (a) illustration of multi-pass
design, (b) bottom-dividing header, (c) top-dividing header; (Webb and Chung, 2005)*

The effect of the phase separation in the header on the flow maldistribution was

also investigated by Song *et al.* (2002). They studied a multipass R744 evaporator, with horizontal tubes and vertical headers, and used the frost deposition to highlight the maldistribution. Photographs suggest that the refrigerant flow in the low-quality sections is gravity dominated (more liquid in bottom tubes), while the inertial and shear forces are less important. Along the refrigerant path, in the following passages, the frost deposition suggests the presence of more liquid in the farther tubes: being the refrigerant velocity high, the inertial forces are playing a more significant role than the gravity. Another important conclusion is that the refrigerant flow distribution is more uniform when the inlet quality is low. Hrnjak (2004) studied the two-phase flow in vertical and horizontal headers, providing some images of the flow regimes. He identified different flow regimes (stratified, liquid jet, jet with front pooling, mist and jet with rear pooling) and built a flow pattern map, shown in Figure 1.5.18.
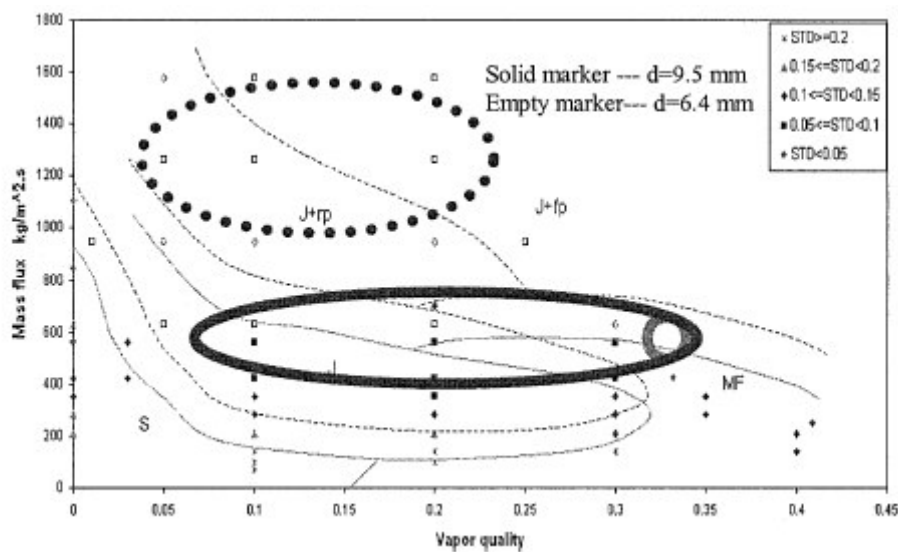
Figure 1.5.18: Flow regimes in a horizontal header with an indication of areas with reasonable well distribution; (Hrnjak, 2004)

Hwang *et al.* (2007) investigated the effects of geometry and of operating conditions on the distribution of the refrigerant in the horizontal evaporator manifold. Experimental results showed that for all test conditions, non-uniform distribution of the liquid and vapor phase mass flow rate and of the inlet and outlet vapor quality was found. The refrigerant distribution was strongly affected by the

136

inlet location, the inlet mass flux, and the inlet vapor quality of the manifold inlet.

Finally, Mukherjee and Kandlikar (2005) studied the effect of the bubble growth during flow boiling in microchannels and developed a numerical model to predict the bubble behaviour. As observed by Balasubramanian and Kandlikar (2004), in some of the parallel microchannels, the upstream interface of the vapor plug moves towards the inlet, in a reverse flow, until the header (Figure 1.5.19). To prevent flow instabilities and pressure rise, they proposed to increase the area ratio in the direction of desired flow, but this solution is not easy to realize.
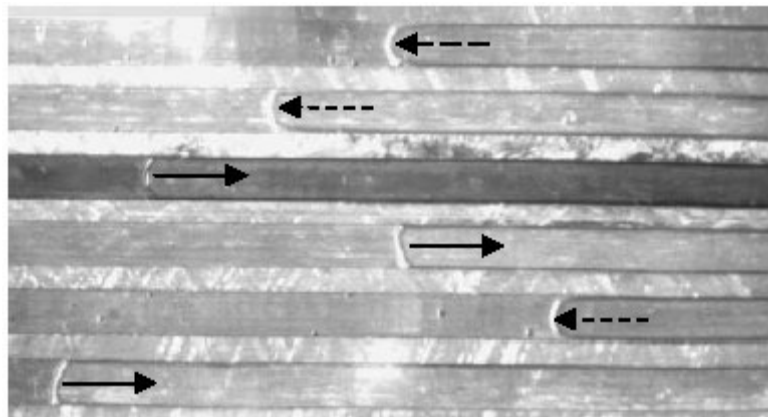
Figure 1.5.19: Reversed flow in parallel microchannels (Balasubramanian and Kandlikar, 2004)

1.5.5.3 Solutions to improve the flow distribution

In the open literature, there are many suggested solutions to improve the flow distribution; in 2005, Webb and Chung (2005) found 79 patents on technology intended to improve two-phase flow distribution. The most common solutions to improve the flow distribution are:

1) modifying the headers
2) feeding the heat exchanger with low quality refrigerant (only for evaporators)
3) improving the local thermal transmittance in certain regions of the heat exchanger surface.

Webb and Chung (2005) focused their attention on the first method; they found that there are two basic approaches to improved flow distribution, acting on the headers:

- installing obstacles (weir, inserts, or throttle plates) at the inlet end of the header or adjust the tube projection in the header
- installing special distributor devices in the header, which locally feeds the fluid to the branch tubes

Chiba and Toshihara (1999) proposed to divide the bottom inlet header in three chambers and to feed them by small distributors, as shown in Figure 1.5.20.
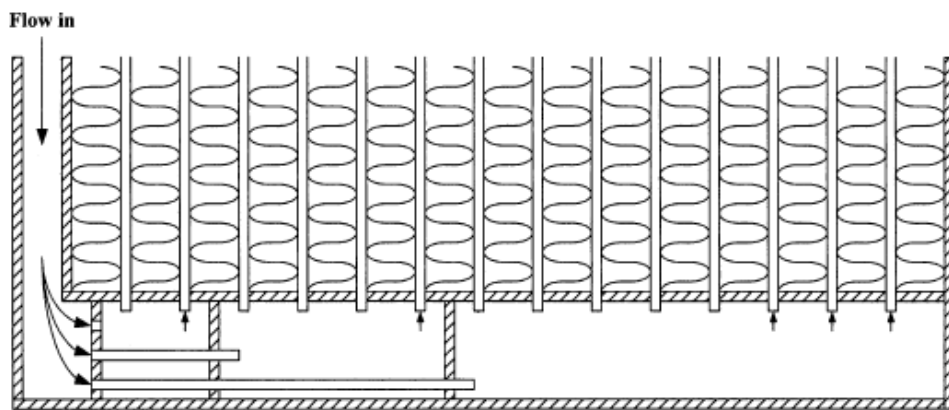
Figure 1.5.20: Inlet header divided in three chambers, solution proposed by Chiba and Toshihara (1999); (Webb and Chung, 2005)

Haussmann (2001) suggested to divide the header in four chambers and to feed them by a long, small-diameter distributor with holes on its bottom side; to increase the refrigerant velocity, a screen-wire sieve is placed at the header inlet. Osthues *et al.* (1998) presented an easier solution, without the sieve and the chamber division, with a porous element inside the distributor; both of them are shown in Figure 1.5.21 and 1.5.22. Nagasawa *et al.* (2002) presented a similar solution for a 4-passes 2-raws automotive evaporator: the bottom-dividing headers are divided into three chambers by separating plates, as shown in Figure 1.5.23(a) and (b).
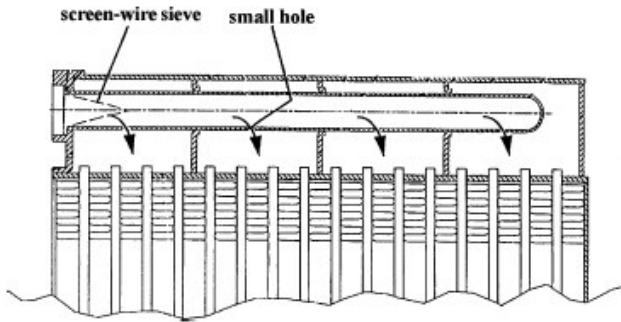
Figure 1.5.21: Inlet header divided in four chambers, with a distributor equipped with sieve; solution proposed by Haussmann (2001); (Webb and Chung, 2005)
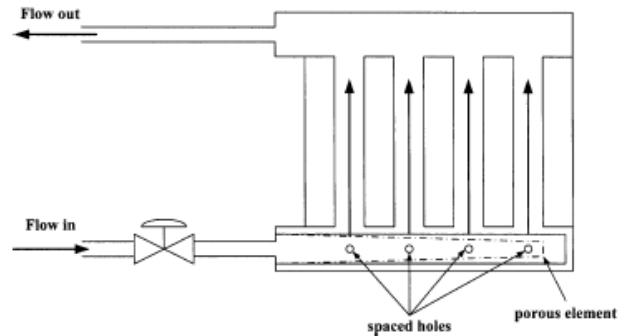
Figure 1.5.22: Inlet header with a distributor with porous element; solution proposed by Osthues et al. (1998); (Webb and Chung, 2005)
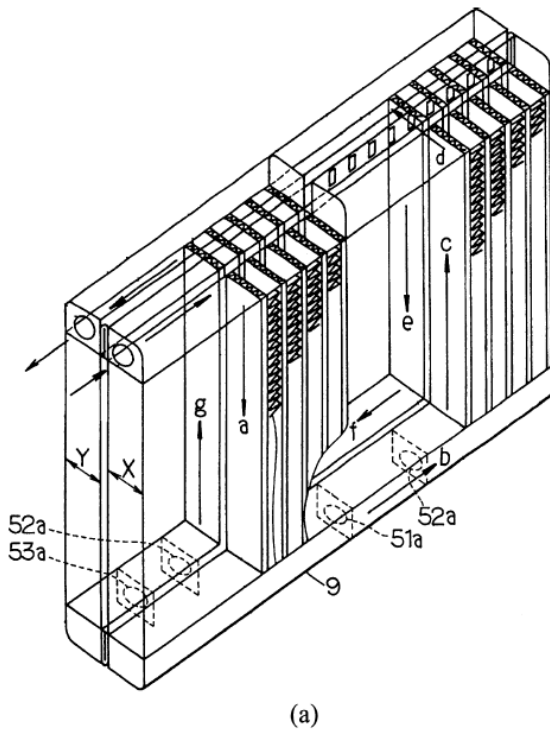
Figure 1.5.23 (a): Automotive evaporator proposed by Nagasawa et al. (2002); (Webb and Chung, 2005)
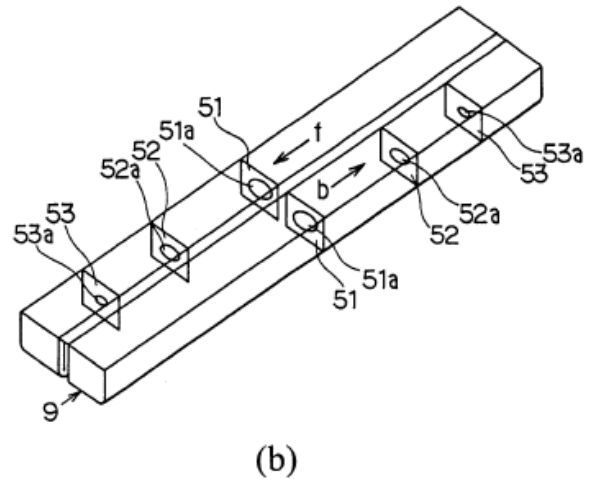
Figure 1.5.23 (b): Automotive evaporator proposed by Nagasawa et al. (2002): the bottom-dividing headers; (Webb and Chung, 2005)

The conclusions by Webb and Chung (2005) are that in the open literature there are several solutions to improve the flow distribution, but they required design modifications. If the operating conditions are altered, the design of such devices must be modified. The design of such devices is highly empirical and requires a

significant amount of data on geometry alterations to get good flow distribution. For these reason, these solutions presents some drawbacks as higher costs and poor operating flexibility.

Other patents have been considered: some of them are presented in the following. Some of them take into exam modifications of the headers. Taras *et al.* (2006) proposed to modified the tube end projections, decreasing along the inlet header, as shown in Figure 1.5.24(a); in this way, the local pressure drops for the farther tubes are lower than for the tubes close to the inlet port. This solution has the same effect of installing obstacles inside the header: in this case the obstacle is the tube end projection. Another solution presented in the same paper is to modify the header shape, changing the flow section in order to realize some obstacles, as shown in Figure 1.5.24(b). Even in this case, the main drawbacks are high costs and low flexibility.
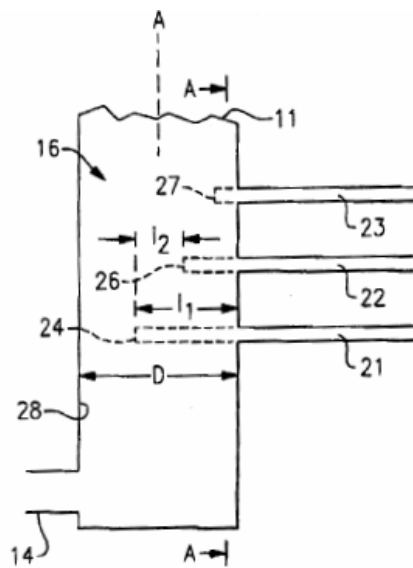
Figure 1.5.24 (a): Inlet header with different tube end projections; (Taras et al., 2006).
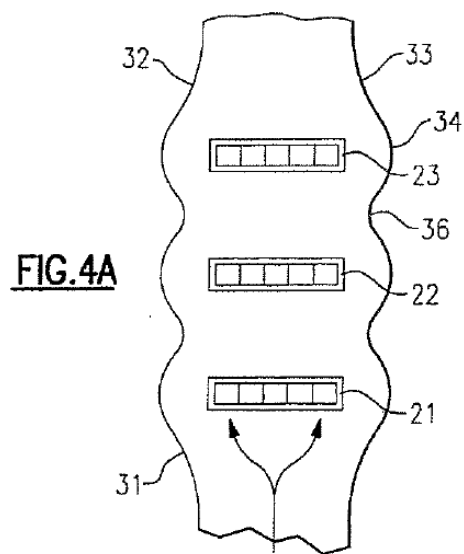
Figure 1.5.24 (b): Inlet header with different flow sections; (Taras et al., 2006).

The effect of the tube end projection on the fluid flow inside the header was studied by Lee *et al.* (2004), but they considered the same tube end projection along the header. In Figure 1.5.25, some images of the fluid flow in the headers with different tube end projections are reported
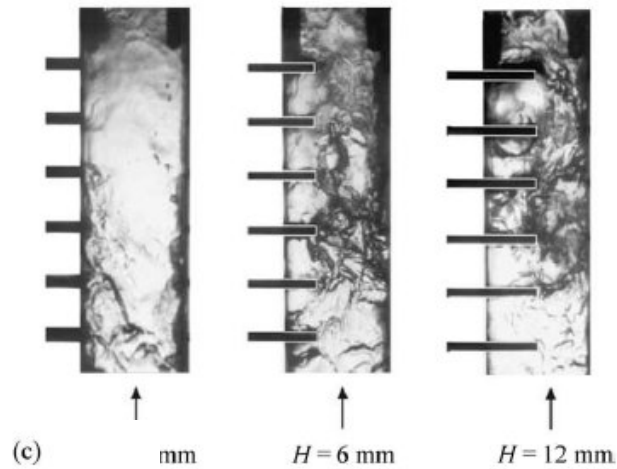
Figure 1.5.25: Headers with different tube end projections; (Lee et al., 2004).

Another type of header was theoretically studied by Kulkarni *et al.* (2004); they considered a horizontal inlet header, for automotive application, and defined the behaviour of the refrigerant solving the equations of heat transfer and pressure drop. To describe the fluid flow in the header, they used the correlations for fluid flow in macro-channels. They determined the ideal dimension of an inlet header and proposed the system depicted in Figure 1.526, with a radial feeding of the tubes.
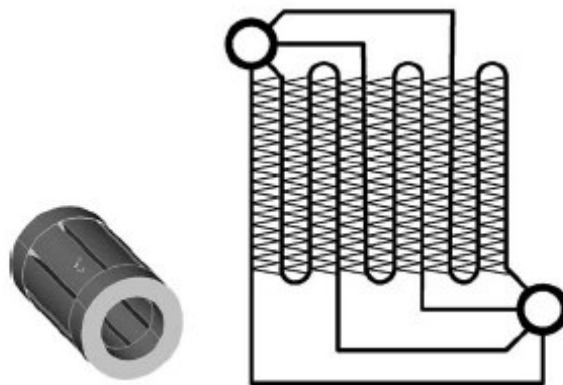
Figure 1.526: System with radial feeding of the tubes; (Kulkarni et al., 2004).

The second solution to improve the refrigerant distribution is to feed the heat exchanger with low quality refrigerant: the ideal solution should be saturated liquid; of course, this solution regards only evaporators. In this way, the refrigerant in the

inlet header is single-phase and there is not phase separation. Even in this case, in the open literature there are several papers and patents on this subject.

Hanson *et al.* (2001) proposed to install a fluid separator upstream the evaporator, in order to feed the evaporator with saturated liquid. The flash vapour is superheated by an internal heat exchanger, using the hot liquid at the condenser outlet, and then it is merged in the vapour at the evaporator outlet. The advantages are clear: besides the feeding of the evaporator, it is possible to reduce the superheat, thanks to the internal heat exchanger. In this way it is possible to avoid a large region of the evaporator fed by superheated vapour, with poor heat transfer characteristics. The main drawback is the need of two more components, the fluid separator and the internal heat exchanger, which represent an extra cost. Possible versions of this solution are the use of only the fluid separator, with a by-pass valve to draw out the flash vapour, or the use of only the internal heat exchanger. The former solution is shown in Figure 1.5.27: both the liquid and the flash vapour are sent to the evaporator, but in different zones, divided by a plate in the header. In this way the maldistribution is avoided, but a part of the evaporator is always dry, with low effectiveness; in addition, the system is less flexible. The latter solution is not described in the patent, being the simple use of an internal heat exchanger. Nevertheless, a well designed internal heat exchanger allows to feed the evaporator with very low quality refrigerant and to reduce the superheat. The result is close to that presented in the patent, but without the separator; this solution is investigated in paragraph 1.2.2. Another version of system with fluid separator was proposed by Elber and Hrnjak (2004): the main difference is that the flash vapour is merged into the vapour at the evaporator outlet before the internal heat exchanger. This solution is safer for the compressor and it allows a larger reduction of the superheat dedicated area; the refrigerant can even exit the evaporator with quality: this fact can be interesting for refrigerants strongly affected by dryout phenomenon, like CO_2. This solution, applied to a reversible machine, is shown in Figure 1.5.28.
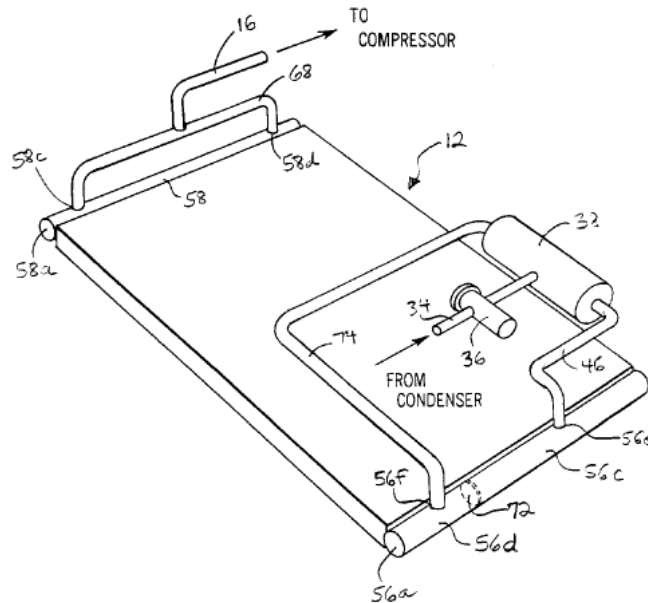
Figure 1.5.27: System with fluid separator and by-pass valve; (Hanson et al., 2001).
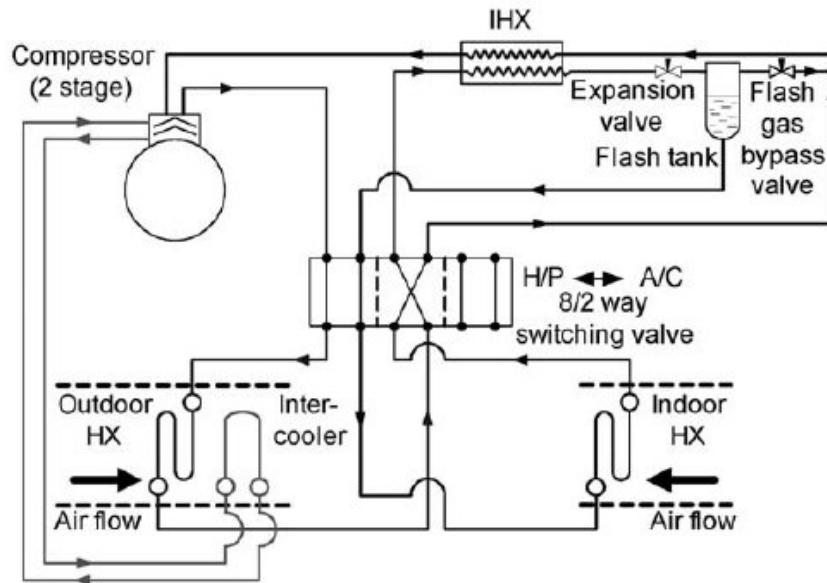
Figure 1.5.28: System with fluid separator and internal heat exchanger downstream the evaporator; (Elber and Hrnjak, 2004)

The third solution to increase the refrigerant distribution is to improve the local thermal transmittance in certain region of the heat exchanger external surface. The idea is to increase the heat transfer in the heat exchanger areas where a higher heat

flux is required (wet by liquid) to the detriment of dry regions. Taras *et al.* (2006) proposed two different solutions for evaporators; the first one is to increase the fin density in the tubes wet by liquid in order to increase the local heat transfer. The second one is to increase the air flow rate in those regions with higher heat transfer, using some baffles. These two solutions are shown in Figure 1.5.29(a) and (b) and in Figure 1.5.30.
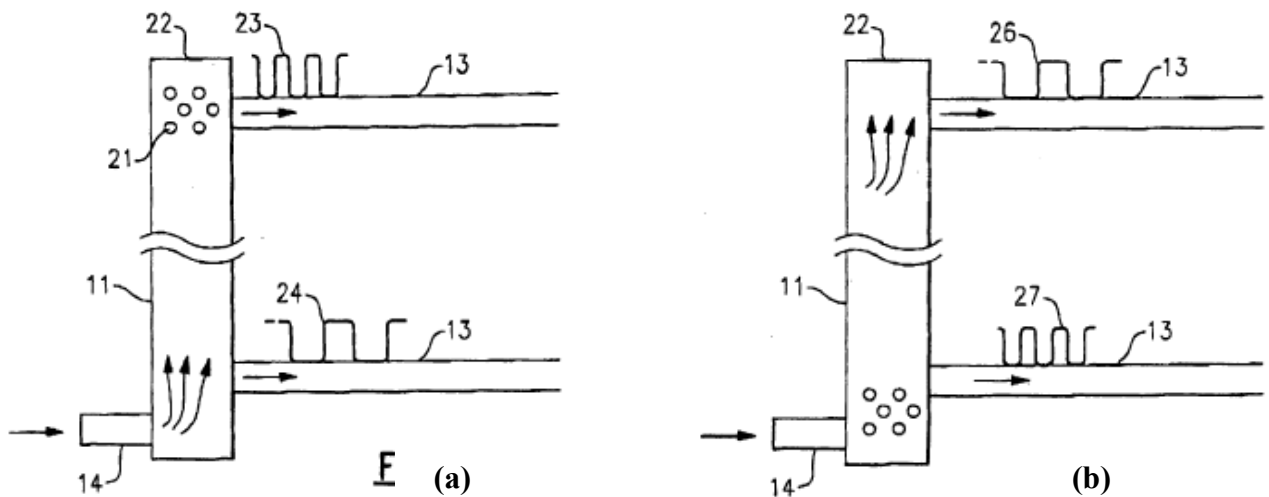
Figure 1.5.29: Evaporators with different fin density: solution for high fluid velocity (a) and low fluid velocity (b) in the header; (Taras et al., 2006).
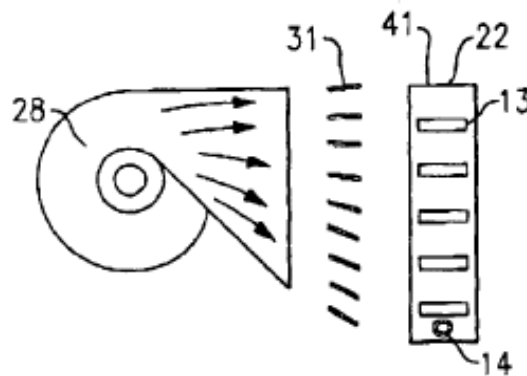
Figure 1.5.30: Evaporator with different local air flow rates against the surface; (Taras et al., 2006).

The main drawbacks of both these solutions are the poor flexibility and the fact that the maldistribution should be known before realizing these modifications. In some applications, with very stable conditions, this can be a minor problem, but if

the design is new or if the heat exchanger working conditions are variable, it is difficult to predict the flow distribution.

All the presented solutions regard a single-pass heat exchanger; actually, in a multipass heat exchanger, the maldistribution affects not only the first or the last passage, but it can occur also in the headers of the intermediate passages. The first and the third solutions (modifying the headers and concentrating the thermal transmittance) are suitable also for the intermediate passages, while the second one (feeding the heat exchanger with low quality refrigerant) can only improve the flow distribution in the first and in the last passage.

1.5.6 Technological constrains: thermal conduction (condensers or gas coolers)

The thermal conductivity through the fins of a microchannel heat exchanger can affect the effectiveness of the component and the efficiency of the whole cycle. This problem regards the gas cooling process, in carbon dioxide transcritical applications, and the condensation of mixture with a wide temperature glide, for example R407C. Park and Hrnjak (2007) experimentally studied this effect in a R744 serpentine gas cooler for air conditioning system. They proposed to solve this problem cutting the fins, in order to avoid thermal conduction, and recorded a 1.9÷3.9% increase of the thermal capacity. However, this solution is not technologically easy to realize nor cheap. If the gas cooler / condenser is a multipass heat exchanger, an easy solution is to choose an odd number of passages: the heat exchanger areas with the higher temperature difference are placed as far as possible. The gas cooler, with cut through the fins, is shown in Figure 1.5.31(a) and (b) and the results are plotted in the diagram of Figure 1.5.32. A condenser with an odd number of passages is shown in Figure 1.5.33.

(a)   (b)
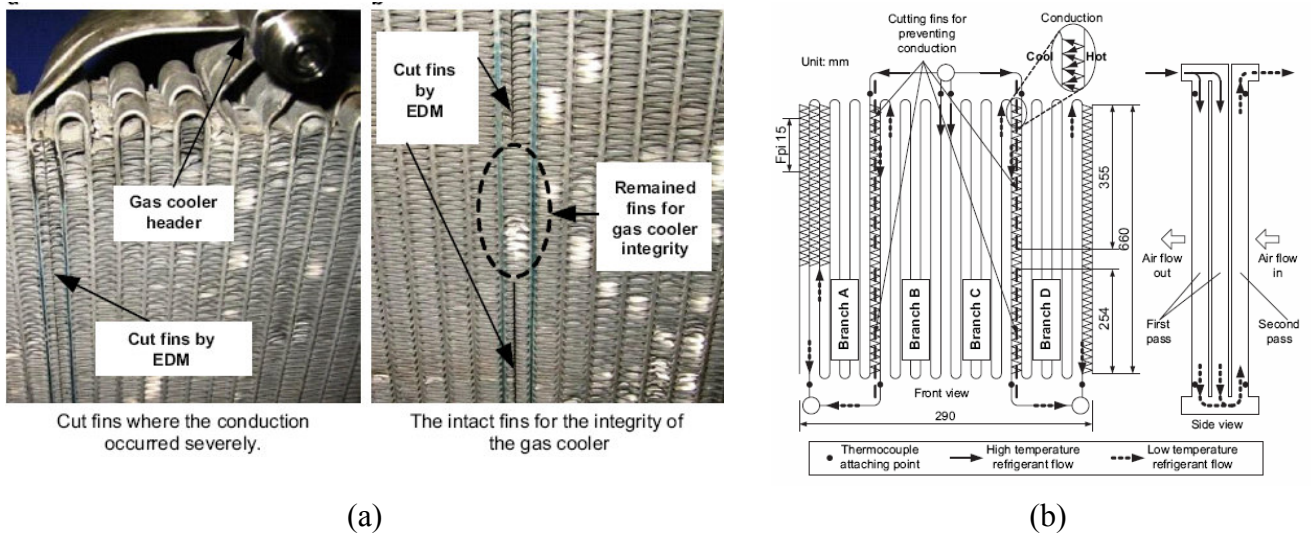
Figure 1.5.31: Photo (a) and scheme (b) of the gas cooler with cut through the fins; (Park and Hrnjak, 2007)
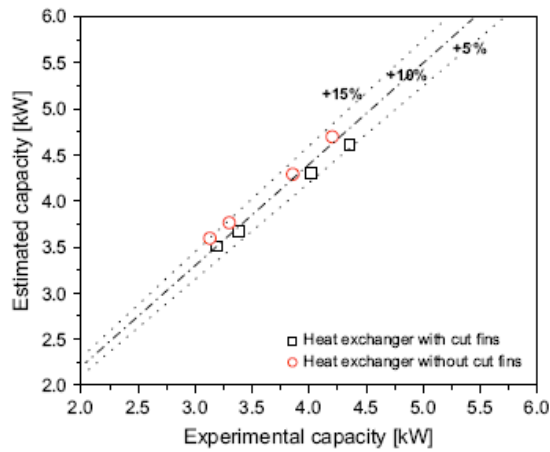
Figure 1.5.32: Comparison of measured vs. estimated capacity of the gas cooler with and without cut fins; (Park and Hrnjak, 2007)

146
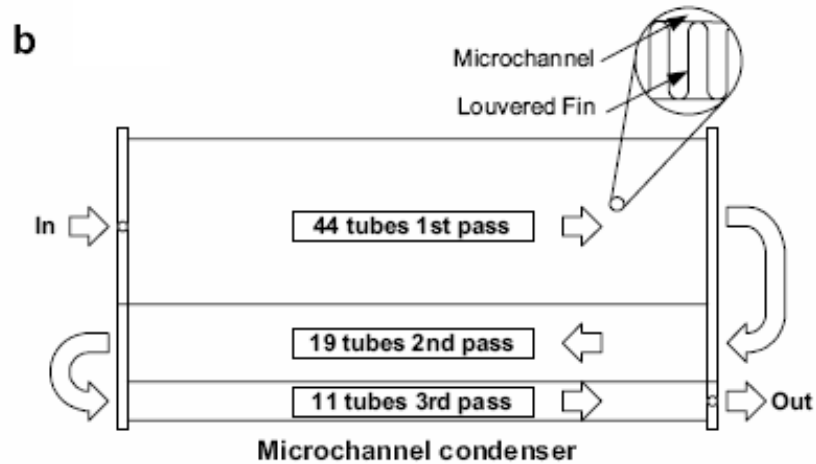
Figure 1.5.33: 3-passage R410A condenser; (Park and Hrnjak, 2008)

1.5.7 Technological constrains: moisture drainage and defrosting (evaporators)

The problems of the moisture drainage and the frosting management are the major constrains for a microchannel evaporator. The water formation on the cold surface of the evaporator implies an additional thermal resistance for the heat transfer, penalizing the cycle efficiency. The shape of the flat tube does not allow easy water drainage; if the temperature of the evaporator surface is below 0°C, the water freezes, blocking the air passage and the heat exchange. Some examples of evaporator covered by ice are reported in paragraph 1.5.7.2, Figures 1.5.38-1.5.40. At this point, the heat pump can not run any more and it is necessary to activate a defrosting system to free the heat exchanger surface. The melted water must be drained, otherwise the following frost cycle shall be very short and the defrosting energy increases. The management of frost/defrost cycles is an open problem for heat pump systems, being the energy optimization difficult to evaluate. In the literature several defrosting techniques are presented and described: the most common ones will be reported in the following.

1.5.7.1 Moisture drainage

The first step to realize a microchannel evaporator is to find an effective solution to drain away the condensate water. Being high the face velocity, this problem is less heavy in automotive applications; in addition, there are some control systems which do not allow the evaporation temperature to go below 0°C. For residential air conditioning, the face air velocity can not be too high, so the fans are not able to blow the water off. Kim *et al.* (2001) investigated the effect of the inclination of the evaporator on heat transfer coefficients and pressure drops. They studied 7 different inclinations, from θ =-60° to θ =60°, with and without a duct, placed upstream the evaporator, with the function of directing the air flow, as explained in Figure 1.5.34. They found that the air shear force significantly influences the sensible heat transfer, especially in case of large inclination angles, and the gravity plays an important role in water drainage.

Memory *et al.* (2006) presented a new model of microchannel evaporator, with a new fin design. The idea is to use the contact forces between water and aluminum, in order to help the air flow to push the water to the rear side of the heat exchanger. This kind of evaporator had been manufactured, for a period, by Modine, but at the moment it is no more produced. The schematic picture of the fin design is shown in Figure 1.5.35(a) and (b). The performance of this fin configuration was studied by Ping and Hrnjak (2009): the drainage of an evaporator in horizontal position, with this type of fins is significantly better than an evaporator with serpentine fins, both placed horizontally and vertically. As a consequence, the frosting time is longer, even if not as long as in a round tube evaporator. The performance of this kind of evaporator is the subject of Chapter 1.7.
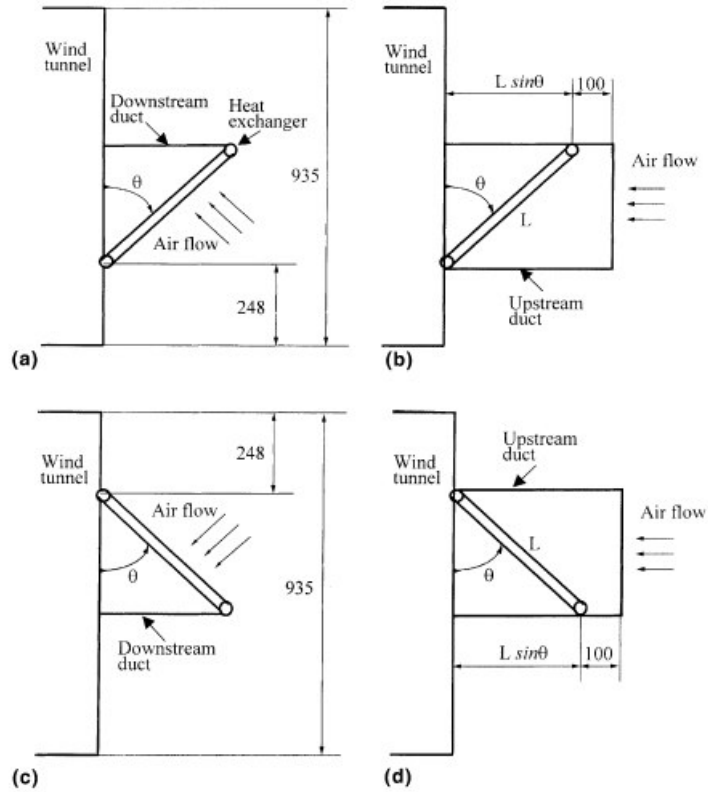
Figure 1.5.34: Schematic diagram of heat exchanger installation for forward inclination (θ >0°) and backward inclination (θ <0°): (a) θ > 0° without upstream duct; (b) θ > 0° with upstream duct; (c) θ < 0° without upstream duct; (d) θ < 0° with upstream duct; (Kim et al., 2001)
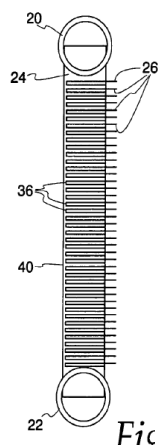
Figure 1.5.35(a): Schematic diagram of heat exchanger, top view; (Memory et al.,2006)
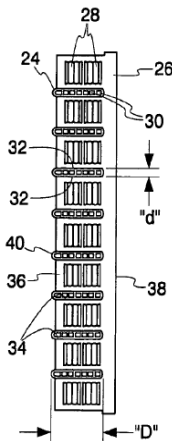
Figure 1.5.35(b): Schematic diagram of heat exchanger, side view; (Memory et al.,2006)

The importance of fin geometries under dehumidifying conditions was investigated by Kim and Bullard (2002): they studied 30 different heat exchanger samples. They found that the thermal hydraulic performance for a wet surface depends strongly on the fin configuration, especially the fin pitch and the louver angle (the louver pitch should also be important, but was not considered in the study). Large fin pitch (1.4mm) and large louver angle (27°) can increase the performance of the wet surface, especially at low Reynolds numbers. For small fin pitch (1.0 and 1.2 mm) and large louver angle (27°), sensible heat transfer and pressure drop are higher than for a dry surface for all operating conditions, suggesting that fin bridging decreases the cross sectional flow area. For small louver angle (<27°), the sensible heat transfer coefficients are smaller than that for dry surface, indicating the amount of condensate retained on the surface increases and it may significantly impair heat transfer.

Researches on the fin wettability were presented by Hong and Webb (2001), Min *et al.* (2001), Min and Webb (2002), Kim *et al.* (2002), Kim and Kang (2003) and ElSherbini and Jacobi (2006): they studied the effect of some treatment on the surface wettability and developed some simulation models, but they did not calculate the cycle efficiency penalization. An example of the effect of a wettability treatment is depicted in Figure 1.5.36.

(a)   (b)
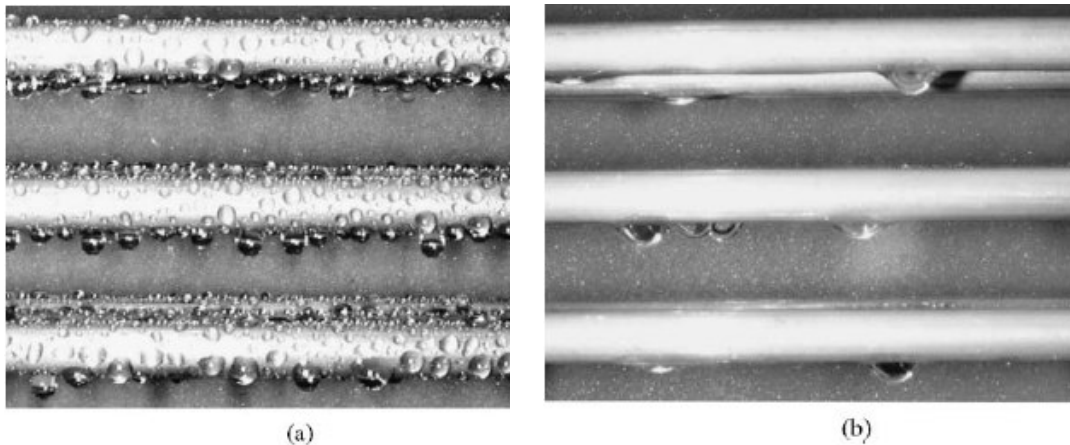
Figure 1.5.36: Comparison of liquid configurations flowing over (a) untreated tube surface and
(b) hydrophilic treated tube surface; (Kim and Kang, 2003)

1.5.7.2   Frost formation

The frost formation, on the evaporator surface, is affected not only by the water drainage capacity, but also by the refrigerant maldistribution. In fact, as pointed out in paragraph 1.5.5.1, the maldistribution implies different surface temperatures between different heat exchanger regions, and the frost tends to form in the coldest zone. Song *et al.* (2002) studied frost formation in the case of a R744 microchannel split system in heating mode under frosting conditions. They pointed out the refrigerant maldistribution through frost formation and recorded some parameters during the frosting. In Figure 1.5.37(a) and (b), the refrigerant temperatures at the evaporator inlet and outlet and the sensible capacity are plotted.

| (a) | (b) |
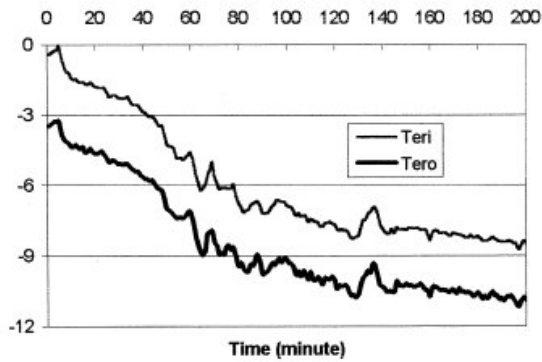
Figure 1.5.37(a): Refrigerant inlet and outlet temperature during frosting; (Song et al.,2002) | *Figure 1.5.37(b): Sensible capacity during frosting; (Song et al.,2002)*
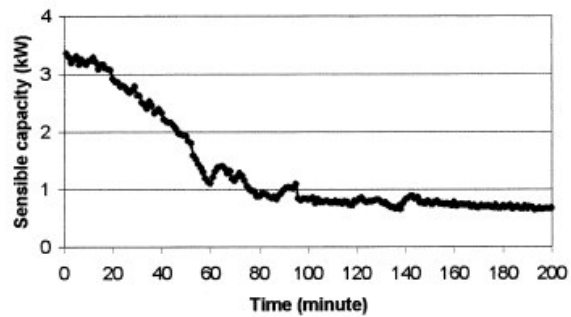
Shao *et al.* (2009) compared the performance of a round tube evaporator with a microchannel evaporator under frosting conditions. Both test results and simulation results show that the frosting period of the tested finned-tube heat pump system was much longer than that of the microchannel heat pump system. The microchannel evaporator, at the end of the frosting cycle, is shown in Figure 1.5.38.

Figure 1.5.38: The microchannel evaporator at the end of the frosting cycle; (Shao et al., 2009)

Xia *et al.* (2006) investigated the frost formation on four different microchannel evaporators and developed a predictive model. The calculated the variation of heat transfer coefficient, pressure drop, friction factor and Colburn factor, under frosting, defrosting and refrosting conditions. They found that the reduction in air-side flow rate and bridging of louver gaps by frost significantly reduce the air-side heat transfer coefficient as frost accumulates. The refrosting behavior becomes periodic after the third or fourth cycle; Figure 1.5.39 shows the frost formation is some consecutive cycles. Due to the fin geometry, the corner formed by two adjacent fins tends to hold droplets during a defrosting process. The droplets froze in subsequent refrosting cycles with significant effects on pressure drop and heat transfer. They pointed out that wettability has a direct effect on water retention, thus its impact on defrost and refrost should be profound. Jhee et al. (2002) investigated the effect of surface treatments during frosting/defrosting operations on a finned coil evaporator. They took into consideration a hydrophilic and a hydrophobic surface treatment; they found that frost with a higher density forms on a hydrophilic surface during frosting, and the water draining rate during defrosting is enhanced. On the other hand, the frost with a lower density forms on a hydrophobic surface and the draining water ratio in the frost melting period increases. Therefore, the hydrophilic treatment mainly influences the behavior of frosting while the hydrophobic treatment influences the behavior of defrosting. In view of the frosting, the surface treatment accelerates frost accumulation rather than

delaying it. As regards the defrosting performance, the defrosting efficiencies of surface-treated heat exchangers are enhanced by about 3.5% for the hydrophilic one and about 10.8% for the hydrophobic one. The weight of residual water which influences the performance of re-operation on the hydrophilic and hydrophobic evaporators is reduced by about 20% compared to that of the bare one. The effect of the surface during frosting/defrosting operations was investigated by Huang *et al.* (2009): they used an innovative anti-frosting paint in a finned coil evaporator; the results are shown in Figure 1.5.40. However, this method requires further research to strengthen its durability and cycling performance when used under practical conditions.
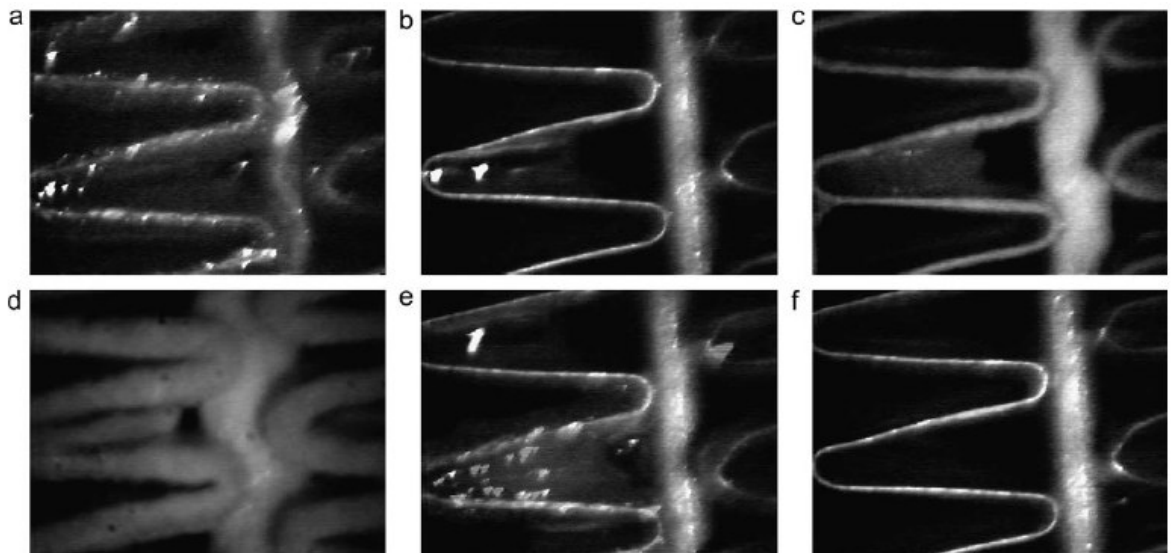
Figure 1.5.39: Images of fins between two successive defrosting cycles: (a) melting frost; (b) end of defrost; (c) refrost; (d) end of refrost; (e) re-melting; (f) end of second defrost; (Xia et al.,2006)
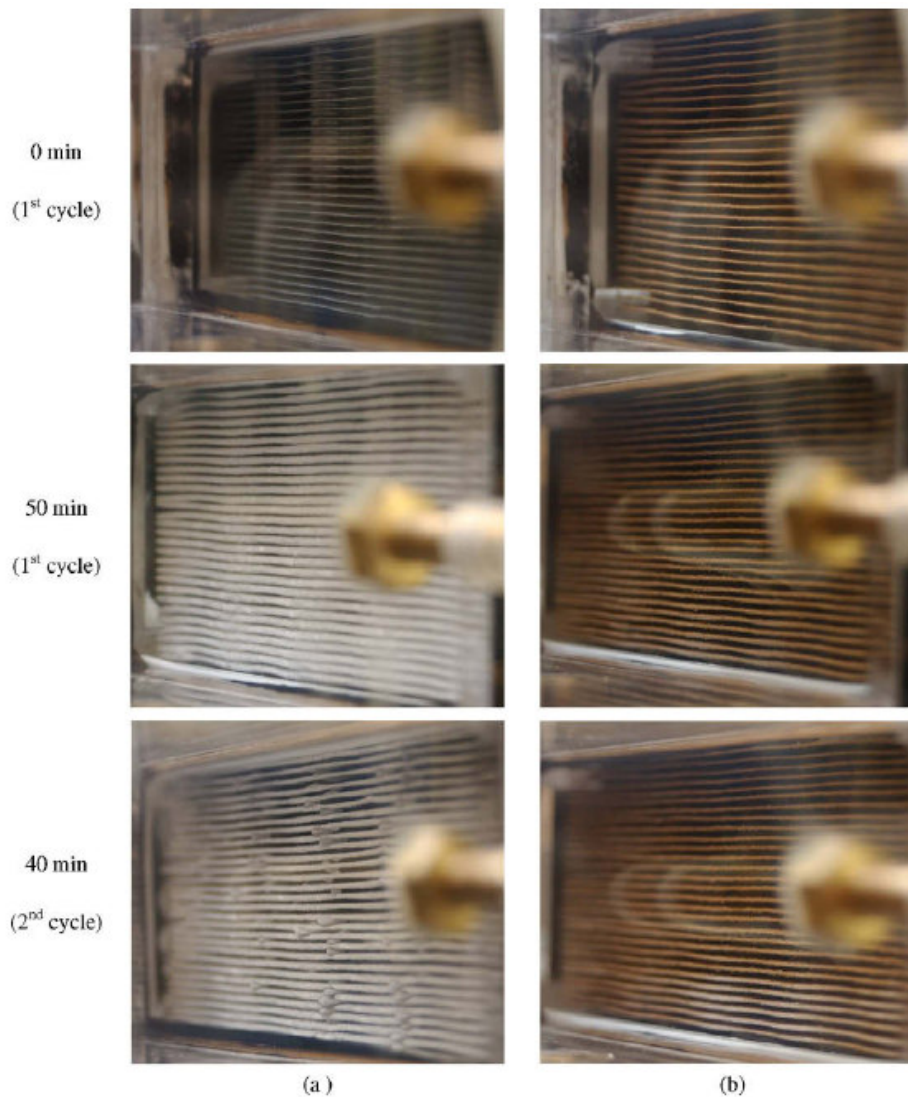
Figure 1.5.40: Comparison of frost deposition in an evaporator without (a) and with (b) the anti-frosting paint;(Huang et al., 2009)

Huang *et al.* (2007) studied the dynamic characteristics of a heat pump system with multi-circuit round tube evaporator controlled by a thermostatic expansion valve. The liquid refrigerant was not evaporated completely in some circuits which see the less airflow rate and a little liquid refrigerant flows out at the evaporator outlet. This implies that there is less superheat than the necessary MSS (minimum-stable-signal) of the thermostatic valve at the outlet of the evaporator and the valve had the intermittent hunting during the first two-thirds of the frosting period. In this period the valve can resume the stability by regulating the refrigerant flow rate into

the coils; in the last third of frosting period, the valve can no more regulate the fluid flow and the system is no under control.

Some authors proposed to control the frost formation by using electric fields. Joppolo and Molinaroli (2005) studied the ice crystal growth under the presence of an electric field; the frost formation changes considerably as a consequence of the strong interaction between the imposed field and the water dipolar molecule. They found that a non-uniform electric field is more effective than uniform electric field in reducing frost mass accumulation and a value of applied voltage that maximizes percentage mass reduction exists. They concluded that, with a low power consumption, the percentage mass reduction reached values up to 25 %. Similar researches were carried out by Tudor and Ohadi (2006): they studied the frost crystals growth pattern and mass accumulation on cold surfaces. Applying an electric field frequency spanned 370 Hz to 7.5 kHz, with a voltage of 14.5 kV, up to 46% frost reduction was obtained. Figure 1.5.41 is an image of the cold plate, with and without the use of this method. Figure 1.5.42 is a schematic picture of the different ice crystal growth, with and without the presence of an electric field (EHD method). In a previous paper, Tudor *et al.* (2005) proposed to use the electric field for defrosting; they used a of AC voltages in the range of 7–12 kV at a frequency of 700–5000 Hz. They found that defrosting an evaporator using this technique will minimize both the power load required and the defrosting time, thus substantially reducing the defrost power consumption. Actually, this method is no more quoted in the open literature.

(a)   (b)
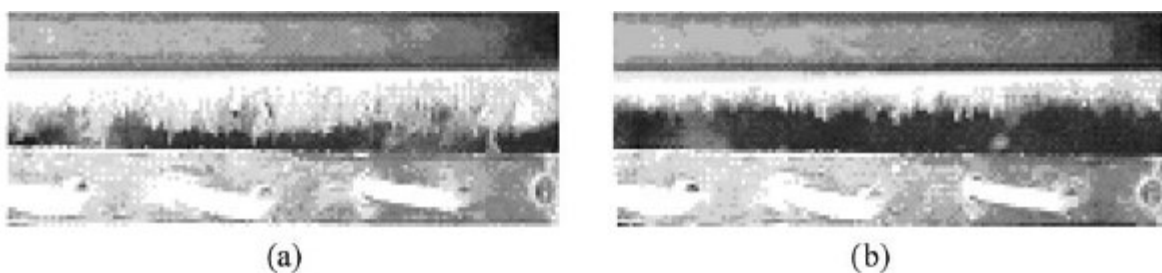
Figure 1.5.41: The cold plate, without (a) and with (b) the electric field;
(Tudor and Ohadi, 2006).
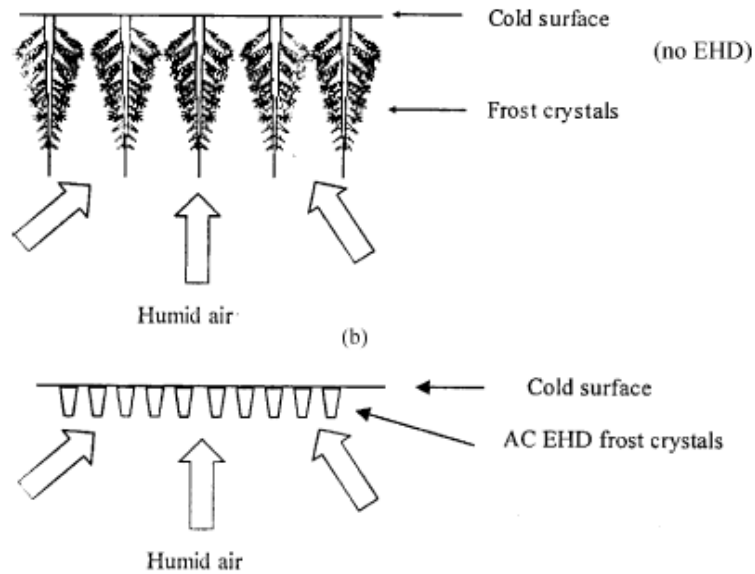
Figure 1.5.42: Different crystal growths, due to the presence of the electric field (EHD method); (Tudor and Ohadi, 2006).

1.5.7.3 Defrosting techniques

If the evaporator surface is covered by ice, the thermal flux fades due to the ice thermal resistance. The evaporation pressure decreases and the heat exchanger efficiency is more and more penalized. Thus, it is necessary to activate a process to remove the ice from the surface. The most common techniques to defrost an evaporator are:

- natural defrosting: if the evaporation temperature is close to 0°C, the defrosting can be done just turning off the system. This technique is very slow and can be done only if the amount of ice is small.

- defrosting through electrical heaters, utilizing the Joule effect. It is an easy technique, but the main drawbacks are the poor efficiency and the defrosting management. In fact, if the electrical heater is under-sized, it is not able to melt the whole ice amount and it accumulates on the surface cycle by cycle. On the contrary, if it is over-sized or if the cycles are too short, it can burn out.

- Reverse-cycle defrosting; it is one of the most common method. A reversing valve, or an 8/2 way switching valve, as shown in Figure 1.5.28 in the plant used by Elber and Hrnjak (2004), is needed. As pointed out by Huang *et al.*

156

(2009), many researchers studied the dynamic characteristics of this defrosting process, since the 1980s. This method presents several disadvantages. First, during defrosting, the indoor heat exchanger, which usually acts as condenser, serves as an evaporator, damaging the indoor comfort. Moreover, the indoor heat exchanger temperature is reduced to more or less -20°C; the cold blowing lasts for a while after resuming heating cycle because the compressor discharge gas heat is used to heat the surfaces of the indoor heat exchanger. In addition, the noise of the pressure equalization process during the reversing valve switching is considerable. Zhiyi *et al.* (2008) proposed a new solution to shorten the defrosting time through a refrigerant charge compensator. The compensator stores a certain amount of liquid, which is heated and dispelled to the circulated line at the beginning of defrosting process.

- Hot-gas bypassing defrosting; the hot-gas is pumped, through a by-pass valve, into the outdoor heat exchanger to melt the frost off the coil. This method is used for the multi-evaporators, where each evaporator is defrosted without interrupting the cooling of other evaporators. This method overcomes the disadvantages of the reverse-cycle defrosting, even if the defrosting time is higher, 2.89 times according to the comparison by Huang *et al.* (2009).

All these solutions imply a considerable energy consumption and penalize the system global efficiency, thus researcher interest on this topic is high. An open issue is to define the frequency and the duration of the frosting/defrosting cycles. In other words, the question is if it is more energy convenient to have many frosting/defrosting cycles, with low ice accumulation on the evaporator and thus low energy consumption for each defrosting process, or few frosting/defrosting cycles, but with more ice on the evaporator and higher energy consumption for each defrosting process. The answer is not easy, it implies long and expensive experimental tests and probably it is not univocal, but it depends on the type of evaporator and the running conditions.

1.5.8 Examples of systems using microchannel heat exchangers described in the literature

In the open literature a few experimental plants of heat pump using microchannel heat exchangers are described; in the following, some of them are presented.

Hoehne and Hrnjak (2004) developed a R290 chiller of 1-1.5 kW of refrigeration capacity. Thanks to the microchannel heat exchangers used, they were able to reduce the propane charge at 120g, below the limit of 150g fixed by the drafting of the international standard IEC 60335-2-24, Safety of household and similar electrical appliances, Part 2.24. The condenser is a two pass parallel flow heat exchanger and the evaporator is a two slab, multi-circuit serpentine microchannel evaporator, originally designed for mobile CO_2 applications (see Figure 1.5.43 and 1.5.44). According to the authors, with a better design of heat exchangers and compressor, a reduction of 50g/kW should be possible.

Figure 1.5.43: Two pass parallel flow condenser; Hoenhe and Hrnjak (2004).
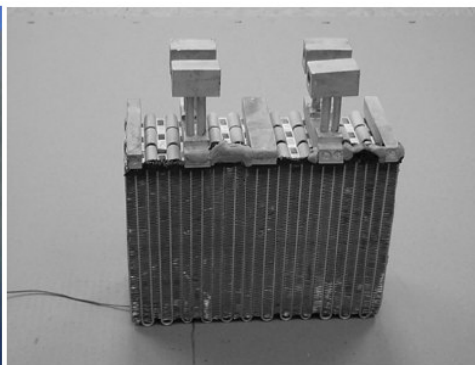
Figure 1.5.44: Two slab, multi-circuit serpentine microchannel evaporator; Hoenhe and Hrnjak (2004).

Hrnjak and Litch (2008) developed an ammonia chiller, with a plate heat exchanger as evaporator and two different configurations of condensers. They are a serpentine condenser and a parallel flow microchannel condenser (see Figure 1.5.45). The microchannel condenser allows reducing the charge to 20g/kW, lower than any current available air-cooled ammonia chiller on the market. The system is shown in Figure 1.5.46.

158

Chapter 1.5: Efficiency improvement related to heat exchanger type: the minichannel heat exchangers
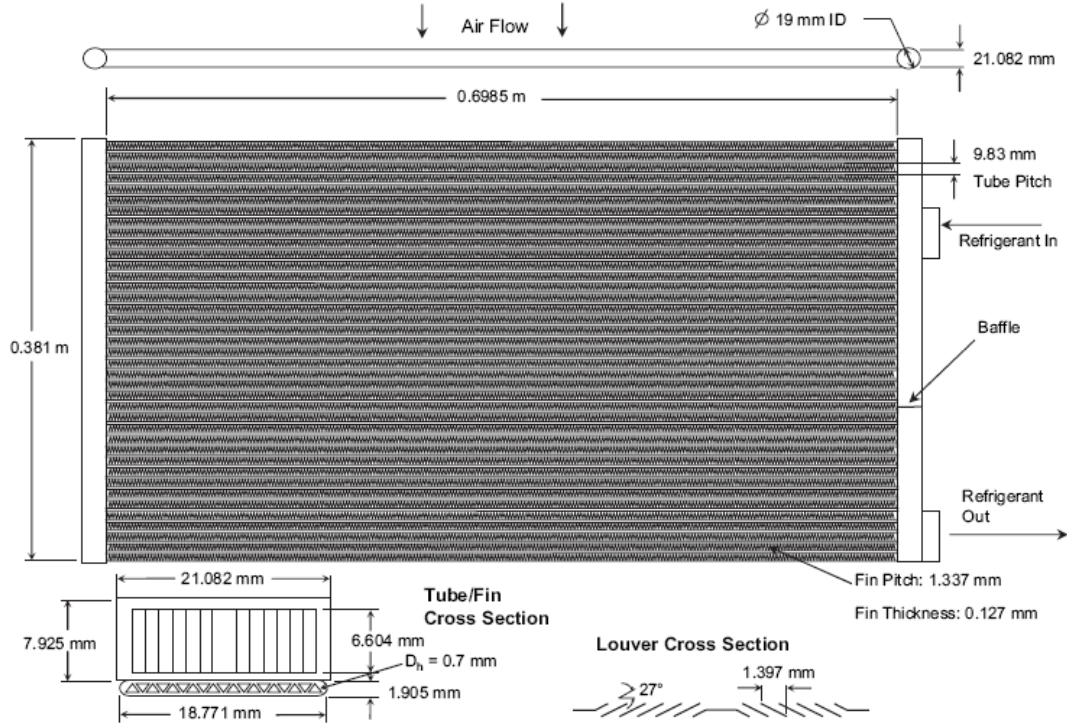
Figure 1.5.45: Microchannel parallel flow condenser; Litch and Hrnjak (2008).
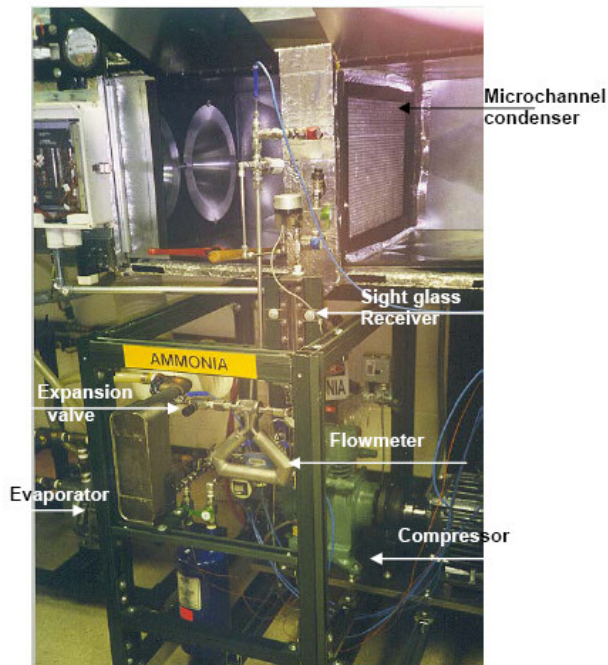
Figure 1.5.46: Ammonia chiller; Litch and Hrnjak (2008).

1.5.9 References

1. Akers W. W., Deans H. A., Crosser O. K., (1959), Condensing heat transfer within horizontal tubes, *Chem. Eng. Prog. Symp. Series*, 55:171-176.

2. Bajura R. A., Jones Jr. E. H., (1976), Flow distribution manifolds, *J. Fluid Engineering*, 98:654-666.

3. Balasubramanian P., Kandlikar S. G., (2004), Experimental study of flow patterns, pressure drop and flow instabilities in parallel rectangular minichannels, *Proc. of 2nd Int. Conf. on Microchannels and Minichannels*, ICMM2004-2371:475-481.

4. Cavallini A., Censi G ., Del Col D., Doretti L., Longo G. A., Rossetto L., (2002), Condensation of halogenated refrigerants inside smooth tubes, *HVAC&R Res.*, 8(4):429-451.

5. Cavallini A., Del Col D., Doretti L., Matkovic M., Rossetto L., Zilio C., (2005), Condensation heat transfer and pressare gradient inside multiport minichannels, *Heat Transfer Eng.*, 26(3):45-55.

6. Cavallini A., Del Col D., Doretti L., Matkovic M., Rossetto L., Zilio C., Censi G. (2006), Condensation in horizontal smooth tubes: a new heat transfer model for heat exchanger design, *Heat Transfer Eng.*, 27(8):31-38.

7. Cavallini A., Doretti L., Matkovic M., Rossetto L., (2006), Update on condensation heat transfer and pressure drop inside minichannels, *Heat Transfer Eng.*, 27(4):74-87.

8. Cheng L., Ribatski G., Wojtan L., Thome J. R., (2006), New flow boiling heat transfer model and flow pattern map for carbon dioxide evaporating inside horizontal tubes, *Int. J. Heat and Mass Transfer*, 49:4082-4094.

9. Chiarello M., Del Col D., (2007), Design rules for optimisation of heat exchangers to be used with natural working fluids, *Deliverable D12, COLL-CT-2004-500229* SHERHPA.

10. Chiba T., Toshihara T., (1999), Heat exchanger with a distribution device capable of uniformly distributing a medium to a plurality of exchanger tubes, *U.S. Patent No. 1999/5,901,785.*

11. Cho H., Cho K., Youn B., Kim Y. S., (2002), Flow maldistribution in micro-channel evaporator, *Int. Comp. Conf. Eng.*, R6-5:1-7.

12. Cicchitti A., Lombardi C., Silvestri M., Soldaini G., Zavattarelli R., (1960), Two-phase cooling experiments – pressure drop, heat transfer and burnout measurements, *Energia Nucl.*, 7:407-425.

13. Del Col D., Doretti L., Fantini F., Rossetto L., (2005), Predictive models for flow boiling in minichannels, *60° Congr. Naz. ATI*, ATI60.

14. Elber S., Hrnjak P., (2004), Flash gas bypass for improving the performance of transcritical R744 systems that use microchannel evaporators, *Int. J. Refrigeration*, 27:724-735.

15. ElSherbini A. I., Jacobi A. M., (2006), A model for condensate retention on plain-fin heat exchangers, *J. Heat Transfer*, 128:427-433.

16. Fantini F., (2005) Heat transfer in industrial applications, *Ph.D. thesis*.

17. Fornasieri E., (2007), Metodo e dispositivo per separare la fase liquida dal vapore per l'alimentazione di evaporatori ad espansione secca, *Brevetto 8208PTIT*.

18. Hanson O. W., Van Essen L. J., (2001), Evaporator with enhanced refrigerant distribution, *U.S. Patent No. 6,318,118*.

19. Haussmann R., (2001), Distributing/collecting tank for the at least dual flow evaporator of a motor vehicle air conditioning system, *U.S. Patent No. 6,199,401 B1*.

20. Hoehne M., Hrnjak P. S., (2004), Charge minimization in hydrocarbon systems, *Proc. 6th IIR G. Lorentzen Conf. on Natural Working Fluids*, 2c: 1-8.

21. Hong K., Webb R. L., (2000), Wetting coatings for dehumidifying heat exchangers, *HVAC&R Research*, 6(3):229-242.

22. Hrnjak P. S., (2004), Developing adiabatic two-phase flow in headers-distribution issue in parallel flow microchannel heat exchangers, *Heat Transfer Eng.*, 25(3):61-68.

23. Hrnjak P. S., Litch A. D., (2008), Microchannel heat exchangers for charge minimization in air cooled ammonia condensers and chillers, *Int. J. Refrigeration*, 31(4):6587-668.

24. Huang D., He Z. L., Yuan X. L., (2007), Dynamic characteristics of an air-to-water heat pump under frosting/defrosting conditions, *Applied Thermal Eng.*, 27:1996-2002.

25. Huang D., Li Q., Yuan X., (2009), Comparison between hot-gas bypass defrosting and reverse-cycle defrosting methods on an air-to-water heat pump, *Applied Energy*, 86:1697-1703.

26. Huang L., Liu Z., Liu Y., Gou Y., Wang J., (2009), Experimental study on frost release on fin-and-tube heat exchangers by use of a novel anti-frosting paint, *Exp. Thermal and Fluid Science*, 33:1049-1054.

27. Hwang Y., Jin D.-H., Radermacher R., (2007), Refrigerant distribution in microchannel evaporators, *IIR Int.Cong. Refrigeration*, ICR07, B1-670: 1-7.

28. Jhee S., Lee K.-S., Kim W.-S., (2002), Effect of surface treatments on the frosting/defrosting behavior of a fin-tube heat exchanger, *Int. J. Refrigeration*, 25:1047-1053.

29. Joppolo C. M., Molinaroli L., (2005), Frost formation control on a flat plate using electric fields: theoretical aspects and experimental results, *IIR Int. Conf.*, 073-TP-116.

30. Kandlikar S. G., Grande W. J., (2003), Evolution of microchannel flow passages – thermohydraulic performance and fabrication technology, *Heat Transfer Eng.*, 24:3-17.

31. Kandlikar S. G., Garimella S., Li D., Colin S., King M. R., (2005), Heat transfer and fluid flow in minichannels and microchannels, *Elsevier Ltd*.

32. Kim G., Lee H., Webb R. L. (2002) Plasma hydrophilic surface treatment for dehumidifying heat exchangers, *Exp. Thermal and Fluid Science*, 27:1-10.

33. Kim H.-Y., Kang B. H., (2003), Effects of hydrophilic surface treatment on evaporation heat transfer at the outside wall of horizontal tubes, *Applied Thermal Eng.*, 23:449-458.

34. Kim M. H., Youn B., Bullard C. W., (2001), Effect of inclination on the air-side performance of a brazed aluminium heat exchanger under dry and wet conditions, *Int. J. Heat and Mass Transfer*, 44:4613-4623.

35. Kew P.A., Cornwell K., (1997), Correlations for the prediction of boiling heat transfer in small-diameter channels, *Applied Thermal Eng.*, 17:705-715.

36. Koyama S., Kuwara K., Nakashita K., (2003), Condensation of refrigerant in a multi-port channel, *1st Int. Conf. on Microchannels and Minichannels*, 193-205.

37. Kulkarni T., Bullard C. W., Cho K., (2004), Header design tradeoffs in microchannel evaporators, *Applied Thermal Eng.*, 24:759-776.

38. Lee K. J., Lee S. Y., (2004), Distribution of two-phase annular flow at header-channel junctions, *Exp. Thermal and Fluid Science*, 28:217-222.

39. Macrì S., (2006), Efficiency improvements in split air conditioners: variable capacity and new heat exchangers technologies, *Carrier report*.

40. Memory S., Hughes G., Zhang W., Rogers C. J., Grohman C., Robinson E., Mielke R., Wattelet J. P., Gabbey L., Trapp R. J., (2006), Method of fabricating a heat exchanger, *U.S. Patent No. 7,032,313 B2*.

41. Min J., Webb R. L., (2002), Long-term wetting and corrosion characteristics of hot water treated aluminium and copper fin stocks, *Int. J. Refrigeration*, 25:1054-1061.

42. Min J., Webb R. L., Bemisderfer C. H., (2001), Long-term hydraulic performance of dehumidifying heat exchangers with and without hydrophilic coatings, *ASHRAE Transactions*, 107(1), p 268.

43. Mishima K., Hibiki T., (1996), Some characteristics of air-water two-phase flow in small diameter vertical tubes, *Int. J. Multiphase Flow*, 22:703-712.

44. Moser K. W., Webb R. L., Na B., (1998), A new equivalent Reynolds number model for condensation in smooth tubes, *J. Heat Transfer*, 120:410-417

45. Mukherjee A., Kandlikar S. G., (2005), Numerical study of the effect of inlet constriction on bubble growth during flow boiling in microchannels, *Proc. ICMM, 3rd Int. Conf. on Microchannels and Minichannels*, ICMM 75143:1-8.

46. Müller-Steinhagen H., Heck K., (1986), A simple friction pressure drop correlation for two-phase flow in pipes, *Chem. Eng. Process*, 20:297-308.

47. Nagasawa T., Torigoe E., Makihara M., (2002), Refrigerant evaporator with refrigerant distribution, *U.S. Patent No. 6,449,979 B1*.

48. Osthues J., Petz M., Zeitvogel B., (1998), Plate heat exchanger with a refrigerant distributor, *U.S. Patent No. 5,806,586*.

49. Pamitran A. S., Choi K. I., Oh J. T., Oh H. K., (2007), Forced convective boiling heat transfer of R-410A in horizontal minichannels, *Int. J. Refrigeration*, 30:155-165.

50. Park C. Y., Hrnjak P. S., (2007), Effect of heat conduction through the fins of a microchannel serpentine gas cooler of transcritical CO_2 system, *Int. J. Refrigeration*, 30:389-397.

51. Park C. Y., Hrnjak P. S., (2008), Experimental and numerical study on microchannel and round-tube condensers in a R410A residential air-conditioning system, *Int. J. Refrigeration*, 31(5): 822-831.

52. Pettersen J., (2004), Flow vaporization of CO_2 in microchannel tubes, *Exp. Thermal and Fluid Science*, 28:111-121.

53. Ribatski G., Wojtan L., Thome J. R., (2006), An analysis of experimental data and prediction methods for two-phase frictional pressure drop and flow boiling heat transfer in micro-scale channels, *Exp. Thermal and Fluid Science*, 31:1-19.

54. Shao L.-L., Yang L., Zhang C.-L., (2009), Comparison of heat pump performance using fin-and-tube and microchannel heat exchangers under frost conditions, *Applied Energy*, in press.

55. Song S., Bullard C. W., Hrnjak P. S., (2002), Frost deposition and refrigerant distribution in microchannel heat exchangers, *ASHRAE Trans.*, HI-02-13-2, 108(2): 1-10.

56. Subramanian V., Garimella S., (2005), Design of air-cooled R-410A microchannel condenser, *ASHRAE Trans.*, OR-05-1-1, 111(1): 1-16.

57. Taras M. F., Kirkwood A. C., Chopko R. A., (2006), Parallel flow evaporator non-uniform characteristics, *U.S. Patent No. 0102329 A1*.

58. Thome J. R., Ribatski G., (2005), State-of-the-art of two-phase flow and flow boiling heat transfer and pressure drop of CO2 in macro- and micro-channels, *Int. J. Refrigeration*, 28:1149-1168.

59. Thome J. R., (2006), State-of-the-art overview of boiling and two-phase flows in microchannels, *Heat Transfer Eng.*, 27(9):4-19.

60. Tompkins D. M., Yoo T., Hrnjak P., Newell T., Cho N., (2002), Flow distribution and pressure drop in micro-channel manifolds, *Int. Comp. Conf. Eng. at Purdue*, R6-4:1-8.

61. Tran T. N., Wambsganss M. W., France D. M., (1996), Small circular- and rectangular-channel boiling with two refrigerants, *Int. J. Multiphase Flow*, 22(3):485-498.

62. Tuckerman D. B., Pease R. F. W., (1981), High performance heat sink for VLSI, *IEEE Elect. Dev. Lett.*, EDL-2(5):126-129.

63. Tudor V., Ohadi M., 2006, The effect of stationary and sweeping frequency AC electric fields on frost crystal removal on a cold plate, *Int. J. Refrigeration*, 29:669-677.

64. Tudor V., Ohadi M., Salehi M. A., Lawler J. V., 2005, Advances in control of frost on evaporator coils with an applied electric field, *Int. J. Heat and Mass Transfer*, 48:4428-4434.

65. Vist S., Pettersen J., (2004), Two-phase flow distribution in compact heat exchanger manifolds, *Exp. Thermal and Fluid Science*, 28:209-215.

66. Wang C. C., Chiang D. C., Lu D. C., (1997), Visual observation of two-phase flow pattern of R-22, R-134a and R-407C in a 6.5 mm smooth tube, *Exp. Thermal and Fluid Science*, 15:395-405.

67. Wang W. W., Radcliff T. D., Christensen R. N., (2002), A condensation heat transfer correlation for millimetre-scale tubing with flow regime transaction, *Exp. Thermal and Fluid Science*, 26:473-485.

68. Webb R. L., Chung K., (2005), Two-phase flow distribution to tubes of parallel flow air-cooled heat exchangers, *Heat Transfer Eng.*, 26(4):3-18.

69. Wojtan L., Ursenbacher T., Thome J. R., (2005), Investigation of flow boiling in horizontal tubes: Part I – A new diabatic two-phase flow pattern map, *Int. J. Heat and Mass Transfer*, 48:2955-2969.

70. Xia Y., Zhong Y., Hrnjak P. S., Jacobi A. M., (2006), Frost, defrost and refrost and its impact on the air-side thermal-hydraulic performance of louvered-fin, flat-tube heat exchangers, *Int. J. Refrigeration*, 29:1066-1079.

71. Yan Y. Y., Lin T. F., (1999), Condensation heat transfer and pressure drop of refrigerant R134a in small pipe, *Int. J. Heat and Mass Transfer*, 42:697-708.

72. Yun R., Kim Y., Kim M. S., (2005), Flow boiling heat transfer of carbon dioxide in horizontal mini tubes, *Int. J. Heat and Fluid Flow*, 26:801-809.

73. Zhang P., Hrnjak P. S., (2009) Air-side performance evaluation of three types of heat exchangers in dry, wet and periodic frosting conditions, *Int. J. Refrigeration*, 32:911-921.

74. Zhang M., Webb R. L., (2001), Correlation of two-phase friction for refrigerants in small- diameter tubes, *Exp. Thermal and Fluid Science*, 25:131-139.

75. Zhang W., Hibiki T., Mishima K., (2004), Correlation for flow boiling heat transfer in mini-channels, *Int. J. Heat and Mass Transfer*, 47:5749-5763.

76. Zhiyi W., Xinmin W., Zhiming D., (2008), Defrost improvement by heat pump refrigerant charge compensating, *Applied Energy*, 85:1050-1059.

Chapter 1.6 MINICHANNEL CONDENSER: THE SIMULATION MODEL AND ITS VALIDATION THROUGH EXPERIMENTAL DATA

In this chapter the optimization of minichannel condensers is faced. A simulation program, developed in the Department of Fisica Tecnica, was modified and used to find the better trade-off between the number of passages and the number of tube per passage. The experimental data were provided by Rhoss S.p.A.; the support of Mr F. Ferrari and Mr E. Pasut is gratefully acknowledged.

1.6.1 Introduction

The energy optimization of a given geometry of minichannel condenser can be achieved just modifying the refrigerant path in the heat exchanger. In this way, the refrigerant velocity in each channel can be optimized, in order to achieve the highest cooling capacity. Configuration with two or four passages have been considered. To simulate the heat exchangers, a simulation code was used; this program was modified in order to take into considerations two important aspects, the air distribution and the refrigerant distribution. The code was modified using experimental data; air and refrigerant distribution were then related to geometrical factors which can affect this phenomena. The program was validated comparing the simulation results with experimental data of other tests. Thus the number of passages of some geometries was optimized and some guidelines for the manufacturing of minichannel condensers have been defined.

1.6.2 Description of the simulation model

To simulate the operation of refrigerating systems, a computer code in FORTRAN language was developed in the Department of Fisica Tecnica. It is

described in Casson *et al.* (2003) and Cecchinato *et al.* (2005). In this simulation model, the compressor is defined by correlations, based on experimental data, that provide performance values, in terms of mass flow rate and compression mechanical power, as functions of the operating conditions. Throttling valves are assumed as ideal: thermostatic expansion valves, used in traditional cycles, are able to keep a constant value of superheat at the outlet of the evaporator, whereas back-pressure valves, used in transcritical cycles, are able to keep a constant pressure value just upstream. Heat exchangers are defined by their geometrical parameters and are analytically simulated, as described in the next section. The input data for the simulation are the mass flow rate values of the external fluids (water and air) and their inlet properties. Finding the corresponding operating conditions of system means to solve different equations for subcritical and transcritical cycles (in the case of carbon dioxide).

1. *Subcritical cycle*: a non-linear two-equation, two-variable system in the suction pressure and discharge pressure variables is used.

$$
\begin{cases}
\dot{m}_{ev}\left(p_{cm,in}, p_{cm,out}\right) - \dot{m}_{cm}\left(p_{cm,in}, p_{cm,out}\right) = 0 \\[2em]
\dot{m}_{cm}\left(p_{cm,in}, p_{cm,out}\right) - \dot{m}_{cn}\left(p_{cm,in}, p_{cm,out}\right) = 0
\end{cases}
\tag{1}
$$

The system is solved by means of the Newton-Raphson method, where the partial derivatives are replaced by their approximation in term of incremental ratios (as the well known secant method). Two input parameters are a free choice of the user: vapour superheat at the evaporator outlet and subcooling of the liquid at the outlet of the condenser; the last is subjected to optimisation for the best energy efficiency.

2. *Transcritical cycle*: the previous system is reduced to a single non-linear equation with only one variable, the compressor suction pressure; as a matter of fact, in transcritical cycles, the back-pressure throttling valve keeps constant the gas cooler outlet pressure and consequently the compressor discharge pressure. Therefore the discharge pressure is not any longer an independent variable and the compressor plus the gas cooler are combined into a single unit, so as to form the equivalent of the condensing unit of a traditional system. The solving

procedure is the traditional secant method.

$$\dot{m}_{ev}\left(p_{cm,in}\right) - \dot{m}_{cm/gc}\left(p_{cm,in}\right) = 0 \ , \tag{2}$$

1.6.2.1 The simulation of heat exchangers

Two phase heat transfer is far from linearity and even more in the transcritical process occurring in the gas cooler, especially next to critical point, where the fluid properties are subjected to very large variations. Thus, to achieve good accuracy of calculation the heat exchangers are subdivided into a large number of volume elements, inside which the fluid properties are supposed uniform. In the present study finned tube heat exchangers are considered for evaporators and multi-tubular pipes-in-pipe counter-flow heat exchangers for condenser or gas coolers.

As far as the flow arrangement is concerned, the heat exchangers models are built according to the following rules:

- pipes-in-pipe exchangers are assumed conforming to perfect counter-flow;
- finned coil exchangers are subdivide into elementary volumes, three-dimensionally arranged so as to represent the real streams arrangement, resulting from cross-flow elements differently connected each other (Casson *et al.*, 2002). Basically, each volume is composed of a small stretch of tube and the related fins and includes information about the links with the adjacent elements for both the air side and the refrigerant side; to solve such a system, being known the inlet conditions of the fluids, an iterative calculation procedure is employed that assures a reliable and rather fast convergence to the solution. Counter-flow exchangers are much easier to be solved even if they also need an iterative procedure. A schematic diagram of the code is reported in Figure 1.6.1.

The evaluation of the refrigerants properties is carried out by an original subroutine, based on data interpolation: the related database was automatically generated using the subroutines of the NIST REFPROP 7.01 (2002) FORTRAN code. This approach, while in general retains the primitive accuracy of the code by NIST, greatly reduces the calculation time and, in some cases, even improves the accuracy by smoothing occasional discontinuities and by eliminating possible inconsistencies between constant pressure specific heat and enthalpy.

The air side heat transfer coefficient as a function of the air face velocity is provided by the manufacturer of the finned coil on experimental ground. The heat transfer coefficient in evaporation is calculated according to different correlations depending on the fluid: for R134a the Thome *et al.*(1998) model, which takes into account the effect of the flow patterns and of the dry-out, for CO_2 the dedicated model proposed by Pettersen *et al.* (2000), also accounting for the dry-out. Pressure drop is computed with Friedel (1979) correlation and for the pressure variations due to variation in momentum, void fraction is determined according to Rouhani and Axelsson (1970) model.

As far as pipes-in-pipe heat exchangers are concerned, for heat transfer coefficients during inside tube condensation, a recent model proposed by Cavallini *et al.* (2002) is employed, which predicts flow patterns, whereas for the heat transfer coefficient during single phase process (CO_2 or water), Gnielinski (1976) correlation is used. Pressure drops are calculated with the correlation by Friedel (1979) and the void fraction with the correlation by Rouhani and Axelsson (1970).
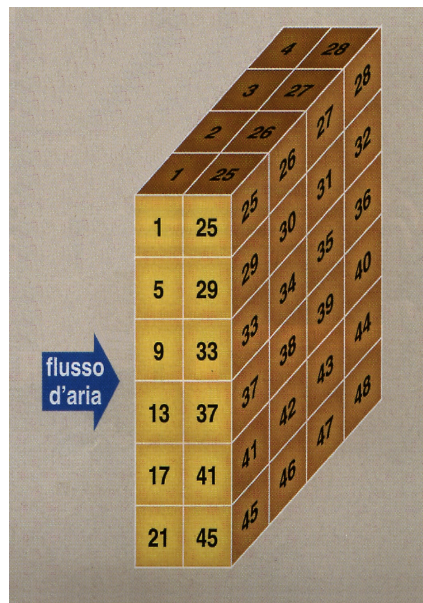
Figure 1.6.1: Schematic diagram of the simulation code

1.6.3 Modification of the simulation model

The simulation code has been modified starting from the results of the experimental test, carried out in the Rhoss R&D laboratory, on the following heat exchanger samples (Tables 1.6.1 and 1.6.2).

HX type	Test date	N. passages	N. tubes	Tube thickness	Chiller Model.
A	05/03/2008	2	80-19	16 mm	TCAEY 115
B	07/03/2008	2	52-42	25 mm	TCAEY 115
C	11/03/2008	4	60-17-9-8	25 mm	TCAEY 115
D	17/03/2008	2	57-42	16 mm	TCAEY 117

Table 1.6.1: Tested condenser samples

HX type	A - D	B – C
number of tube [-]	99	94
tube pitch [mm]	10.1	10.6
tube depth [mm]	16	25
tube length [mm]	1000	1000
tube thickness [mm]	2	3
hydraulic diameter [mm]	1.44	2.00
channels per tube [-]	7	10

Table 1.6.2: Geometrical features of the tested condenser samples

The testing conditions are resumed in Table 1.6.3.

Refrigerant	R410A	-
Air inlet temperature	35	°C
Air inlet relative humidity	50	%
Condensation temperature	50	°C
Evaporation temperature	4	°C
Subcooling	5	°C
Superheat	5	°C

Table 1.6.3: Testing conditions

In these experimental tests, a infra-red camera and an anemometer have been used, for the measurements of the surface temperature and the face air velocity, respectively.

The simulation code takes into account two hypothesizes which can not be accepted in this case:

- the face air velocity is considered homogenous on the condenser surface; actually, it varies, for example, from 1.44 to 2.56 m/s, as shown in Table 1.6.4. The face area was subdivided in 64 (8 x 8) regions, of the same area, and the face air velocity was measured through the anemometer.
- the refrigerant mass flow is the same for every tube; the infra-red camera images highlighted how the fluid distribution is not homogenous.

In the first case, the code is modified using the data of Table 1.6.4 and 1.6.5. The face air velocities depend on the tube thickness and the position of the fans, downstream the heat exchanger.

1.93	2.11	2.19	2.26	2.30	2.34	2.34	2.36
1.90	2.13	2.25	2.37	**2.45**	**2.52**	**2.47**	**2.49**
1.85	2.00	2.15	2.36	**2.44**	**2.51**	**2.48**	**2.48**
1.69	1.94	2.15	2.34	**2.46**	**2.47**	**2.45**	2.38
1.55	**1.74**	2.07	2.28	**2.44**	**2.55**	**2.52**	**2.44**
1.48	**1.78**	2.11	2.35	**2.51**	**2.56**	**2.55**	**2.50**
1.45	**1.70**	1.99	2.25	2.39	**2.44**	**2.46**	**2.46**
1.44	**1.65**	**1.80**	2.12	2.29	2.33	**2.41**	**2.43**

m/s	air velocity ≤ 1.80 m/s
m/s	air velocity ≥ 2.40 m/s

Air volumetric flow rate:
7965 m³/h

Table 1.6.4: Face air velocity of the minichannel condenser with tube thickness of 16 mm.

1.55	1.72	1.81	1.86	1.93	2.02	2.03	2.01
1.55	1.73	1.79	1.92	1.99	2.04	2.01	2.00
1.57	1.72	1.85	1.93	2.00	2.01	2.02	1.98
1.53	1.74	1.88	2.01	2.05	2.09	2.07	1.96
1.48	1.69	1.88	1.96	2.00	2.07	2.12	1.93
1.44	1.57	1.82	1.96	2.02	2.08	2.04	1.93
1.40	1.55	1.78	1.94	2.04	2.09	2.10	1.98
1.38	1.48	1.72	1.90	2.03	2.02	2.08	1.96

m/s	air velocity ≤ 1.80 m/s
m/s	air velocity ≥ 2.40 m/s

Air volumetric flow rate:

6739 m³/h

Table 1.6.5: Face air velocity of the minichannel condenser with tube thickness of 25 mm.

From the experimental data, it is possible to define the function of the face air velocity:

$$v_{AIR} = v_{AIR}(x, y, T, X_{f1}, Y_{f1}, X_{f2}, Y_{f2}, ..., X_{fN}, Y_{fN}) \tag{3}$$

where x and y are the two dimensions of the face area which define the position, T the tube thickness, X_{fi} and Y_{fi} the position of the *i*-th fan and N the number of fans. The equation was rearranged considering not the air velocities, but their variations from the average velocity: the new parameters are reported in Table 1.6.6 and 1.6.7 (the green cells represent the positions of the centers of the two fans) and Figure 1.6.2(a) and (b). The variables are rearranged considering the distances from the closest fan; equation (3) becomes:

$$\Delta v_{AIR} = \Delta v_{AIR}(\min(d_1, d_2, ..., d_N), T) \tag{4}$$

where Δv_{air} is the percentage face air velocity deviation from the average values, d_i the distance from the *i*-th fan center and N the number of fans; in this way, the face air velocity is expressed by a 1-variable equation, parametric with the tube thickness. The face air velocity of the *k*-th node of the simulation code will be

modified, multiplying the average value with the following variations. The found equations are in the following form and the coefficients are reported in Table 1.6.8.

$$\Delta v_{AIR} = A \cdot x^3 + B \cdot x^2 + C \cdot x + D \tag{5}$$

where x is the distance from the center of the closest fan.

-12.8	-4.6	-1.0	2.1	4.0	5.8	5.8	6.7
-14.1	-3.7	1.7	7.1	10.7	13.9	11.6	12.5
-16.4	-9.6	-2.8	6.7	10.3	13.4	12.1	12.1
-23.6	-12.3	-2.8	5.8	11.2	11.6	10.7	7.6
-29.9	-21.4	-6.4	3.1	10.3	15.3	13.9	10.3
-33.1	-19.5	-4.6	6.2	13.4	15.7	15.3	13.0
-34.5	-23.2	-10.1	1.7	8.0	10.3	11.2	11.2
-34.9	-25.4	-18.6	-4.2	3.5	5.3	8.9	9.8

Table 1.6.6: Face air velocity percentage variations of the minichannel condenser with tube thickness of 16 mm

-17.2	-8.1	-3.3	-0.6	3.1	7.9	8.4	7.4
-17.2	-7.6	-4.4	2.6	6.3	9.0	7.4	6.8
-16.1	-8.1	-1.2	3.1	6.8	7.4	7.9	5.8
-18.3	-7.1	0.4	7.4	9.5	11.6	10.6	4.7
-20.9	-9.7	0.4	4.7	6.8	10.6	13.2	3.1
-23.1	-16.1	-2.8	4.7	7.9	11.1	9.0	3.1
-25.2	-17.2	-4.9	3.6	9.0	11.6	12.2	5.8
-26.3	-20.9	-8.1	1.5	8.4	7.9	11.1	4.7

Table 1.6.7: Face air velocity percentage variations of the minichannel condenser with tube thickness of 25 mm

Percentage variation from the average velocity

Percentage variation from the average velocity

(a)

(b)
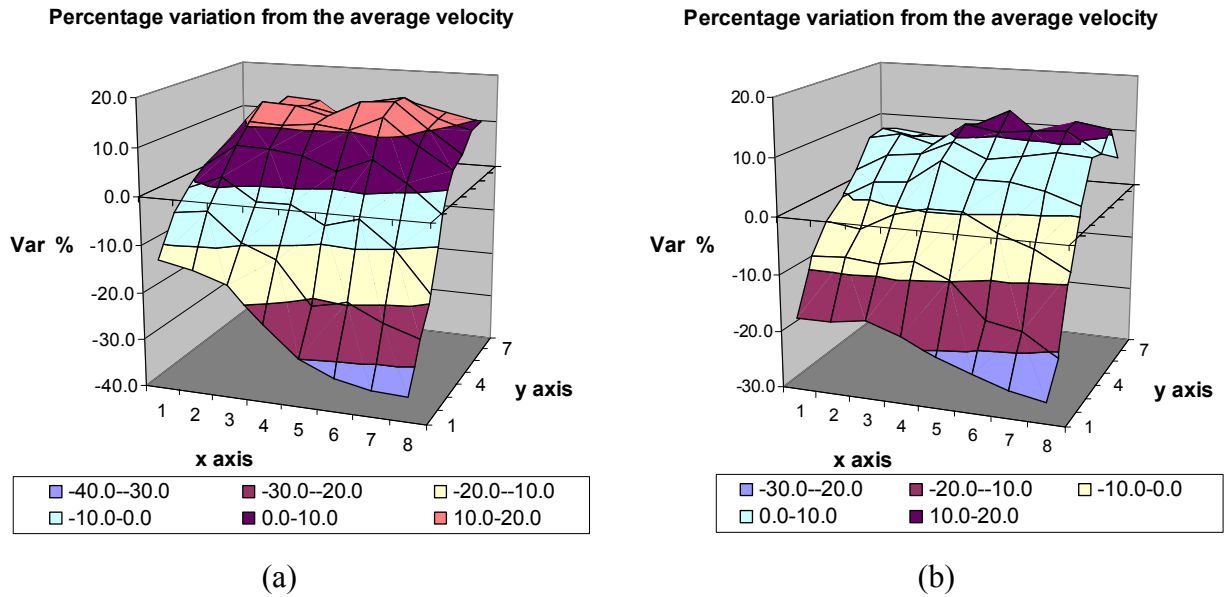
Figure 1.6.2: Face air velocity percentage variations of the minichannel condenser with tube thickness of 16 mm (a) and 25 mm (b)

Coefficients	Tube thickness 16 mm	Tube thickness 25 mm
A	0.0002	0.0001
B	-0.0279	-0.0214
C	0.3791	0.3868
D	10.0000	10.0000

Table 1.6.8: Coefficients of equation (5)

As regards the maldistribution of the refrigerant, the pictures of the infra-red camera have been used to evaluate the refrigerant mass flow feeding the tubes. The images point out that the most penalized passage is the first one; moreover, in this passage it is possible to characterized the desuperheat region and the onset of the two-phase zone. The face area is divided in 64 (8 x 8) regions, as shown in Figure 1.6.3 and the temperature of each zone is recorded. It is expressed as:

$$T_{SUR} = T_{SUR}(x, y) \tag{6}$$

where x and y are the two dimensions of the face area which define the position. Thus the external heat transfer coefficient is calculated, using the correlation of Chang and Wang (1997), and then the external heat transfer, through the following

equations:

$$\alpha_{\text{EXT GLOB}} = \alpha_{\text{EXT GLOB}}(x,y) \tag{7}$$

$$q_{\text{EXT}}(x,y) = \alpha_{\text{EXT GLOB}}(x,y) \cdot A_{\text{EXT}} \cdot \left[T_{\text{SUR}}(x,y) - T_{\text{AIR}} \right] \tag{8}$$

where $\alpha_{\text{EXT,GLOB}}$ is the external heat transfer coefficient, q_{EXT} the heat transfer, A_{EXT} the external area and T_{AIR} the external air temperature. The total heat transfer can be expressed through equation (9), but, in this case, only the heat transfer related to the desuperheat is considered; it is defined through equation (10), where $\overline{X}$ is the horizontal dimension where the two-phase region onset occurs and $\overline{Y}$ is the vertical dimension that represents the first passage.

$$q_{\text{EXT}} = \int_0^Y \int_0^X q_{\text{EXT}}(x,y)\,dxdy \tag{9}$$

$$q_{\text{DES}} = \dot{m} \cdot \Delta h_{\text{DES}} = \int_0^{\overline{Y}} \int_0^{\overline{X}} q_{\text{EXT}}(x,y)\,dxdy \tag{10}$$

Integrating along x, (10) becomes:

$$q_{\text{DES}}(y) = \int_0^{\overline{X}} q_{\text{EXT}}(x,y)\,dxdy = \dot{m}(y) \cdot \Delta h_{\text{DES}}(y) \tag{11}$$

where $\dot{m}$ is the mass flow rate and Δh_{DES} the enthalpy difference between the tube inlet and the onset of the two-phase region; it can be defined as:

$$\Delta h_{\text{DES}}(y) = h_{\text{inlet}}(y) - h_{\text{sat}} \tag{12}$$

where h_{inlet} is the enthalpy at the tube inlet and h_{sat} the saturated vapour enthalpy. Thus it is possible to make the mass flow rate of the *i*-th tube explicit, writing the equation (11) in a discrete form.

$$\dot{m}_i = \sum_{i=1}^{N} \frac{q_{DES,i}}{\Delta h_{DES,i}} \tag{13}$$

In this way, the distribution of the refrigerant in the first passage of the condenser can be defined.
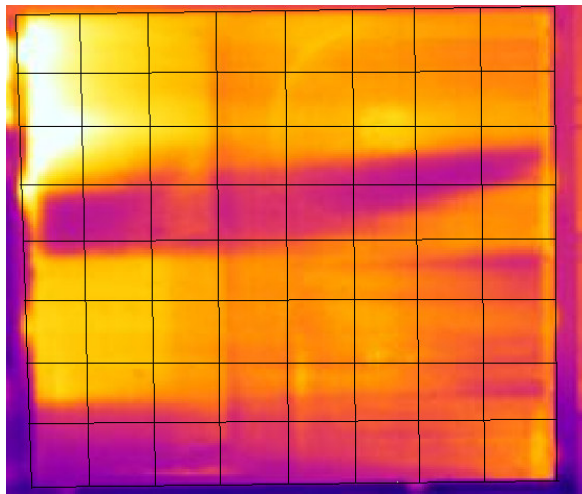
Figure 1.6.3: Example of infra-red picture: the face area is divided in 64 region and the temperature of each of them is recorded

The following step is to identify the main variables which affect the maldistribution in the condenser. This point is dealt with in Chapter 1.5. In this case, the following parameters have been considered:
- position of the inlet tube to the header
- inner diameter of the inlet tube of the header
- refrigerant mass flow rate
- number of tubes of the first passage
- inner diameter of the header
- roughness of the header material

The following non-dimensional parameters have been defined:

$$X_1 = \frac{Y_{inlet\ tube}}{Y_{I\ passage}} \tag{14}$$

$$X_2 = \frac{\varepsilon_{abs}}{\phi_{in\ header}} \qquad (15)$$

$$X_3 = \mathrm{Re}_{inlet\ tube} \qquad (16)$$

where:

$Y_{inlet\ tube}$:position of the inlet tube to the header [m];

$Y_{I\ passage}$:length of the header related to the first passage [m];

ε_{abs} :absolute roughness of the header [m];

$\phi_{in\ header}$: inner diameter of the header [m];

$\mathrm{Re}_{inlet\ tube}$:Reynolds number calculated for the inlet tube.

As for the face air velocity, the average mass flow rate in each tube is calculated; the percentage variation is calculated, according the experimental data, through two equation depending on these non-dimensional parameters. Two different correlations have been chosen to describe the variation, depending on if the considered tube is above or below the position of the inlet tube to the header. The two equations are:

$$\Delta \dot{m}_i = A \cdot X_1 + B \cdot X_2 + C \cdot X_3 + D \qquad (17)$$

if the i-th tube is above the position of the inlet tube to the header.

$$\Delta \dot{m}_i = A \cdot X_1 + B \cdot X_1^2 + C \cdot X_1^3 + D \cdot X_1^4 + E \cdot X_1^5 + F \cdot X_1^6 +$$
$$+ G \cdot X_2 + H \cdot X_3 + I \qquad (18)$$

if the i-th tube is below the position of the inlet tube to the header. The coefficients are reported in Table 1.6.9.

Coefficients	Tubes above the inlet tube	Tubes below the inlet tube
A	3.5098	-8.6945
B	29866.99	-0.3059
C	-0.000124	0.04494
D	90.00	-0.001435
E		1.81E-05
F		-7.95E-08
G		473911.6
H		-0.000639
I		90.00

Table 1.6.9: Coefficients of equation (18)

1.6.4 Comparison with experimental data

The results of the other experimental tests have been compared to the simulation data of the modified code. The testing facility will be described in paragraph 2.1.4. In Table 1.6.10 and in Figure 1.6.4 the comparisons between the experimental data (Q exp) and the simulation results (Q sim) of the condenser capacity are reported. It is worth noticing that the percentage errors are below 12% (only for one test above 8%). The post-processing of the code allows to investigate the simulated distribution of the refrigerant in the first passage of the condenser. The refrigerant mass flow rate of each tube is plotted in Figure 1.6.5 and 1.6.6, for two different tests: the effect of the position of the inlet tube to the header is clear (its position is shown by the black solid vertical line).

HX type	test	Q exp	Q sim	Differences	Errors
-	-	W	W	W	%
A	1	18230	18845	-615	-3.37
A	2	17780	16641	1139	6.40
A	3	16940	17281	-341	-2.02
B	4	18780	16677	2103	11.20
B	5	18090	18268	-178	-0.99
C	6	19080	17558	1522	7.98
C	7	19150	18461	689	3.60

Table 1.6.10: Experimental data and simulation results of different tests
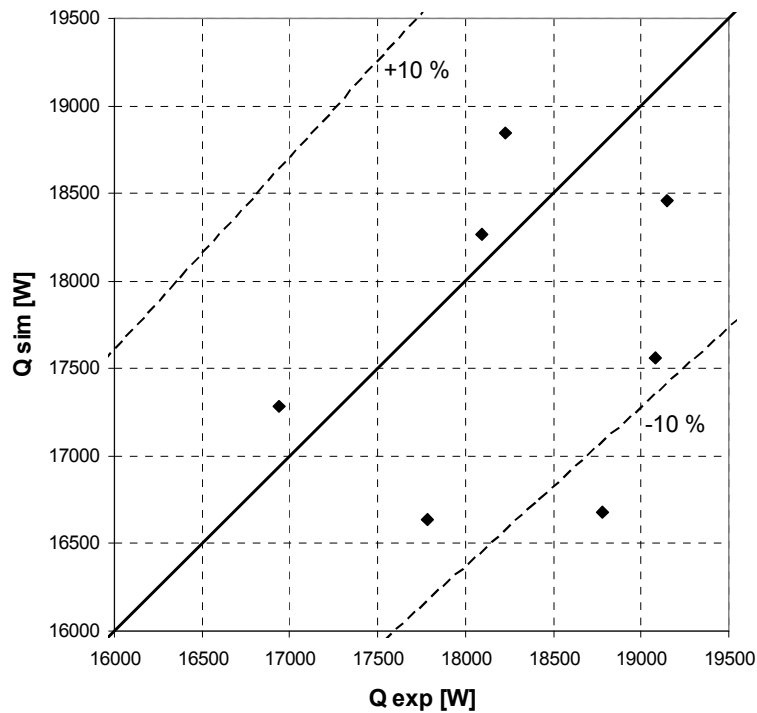
Figure 1.6.4: Experimental data vs. simulation results of different tests
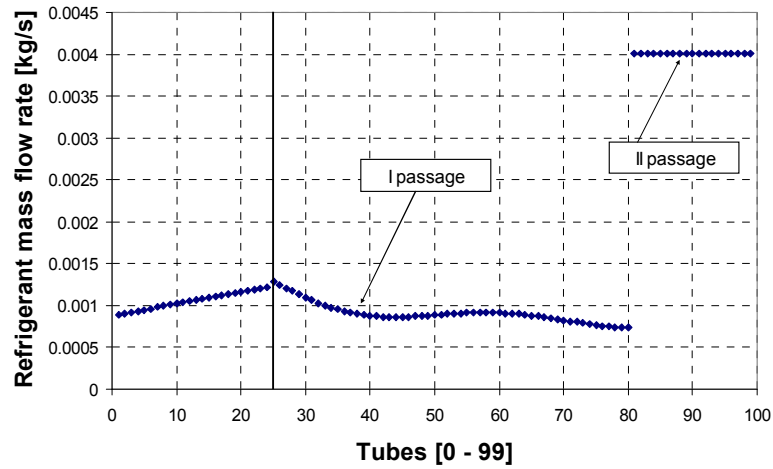
Figure 1.6.5: Refrigerant mass flow rate of each tube of the test n. 2, on condenser A
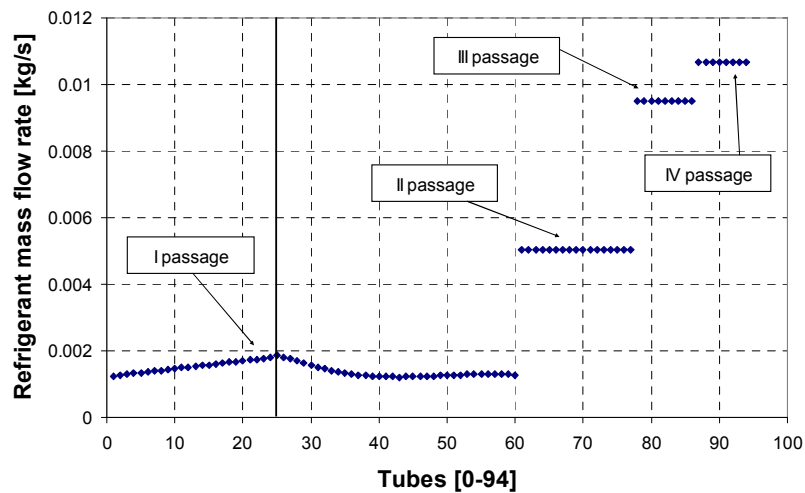
Figure 1.6.6: Refrigerant mass flow rate of each tube of the test n. 7, on condenser C

1.6.5   Optimization of the number of passages

The developed code was used to optimize the number of passages of some microchannel condensers. The chosen geometries are those commonly used by Rhoss; they are one reported in Table 1.6.2 and two more: they are all resumed in Table 1.6.11. The testing conditions are the same of those reported in Table 1.6.3;

the face air velocity is 1.87 m/s and the overall isentropic efficiency is assumed constant and equal to 0.7. The simulated number of passages are 2 and 4; in the case of 4 passages, the number of tube for each passage was calculated according to a linear law and to an exponential law.

chiller model	TCAEY 105-107	TCAEY 109-111	TCAEY 115
number of tube [-]	78	90	94
tube pitch [mm]	10.1	10.1	10.6
tube depth [mm]	16	16	25
tube length [mm]	627.5	627.5	1000
tube thickness [mm]	2	2	3
hydraulic diameter [mm]	1.44	1.44	2.00
channels per tube [-]	7	7	10

Table 1.6.11: Geometrical features of the optimized condenser samples

1.6.5.1 Condenser sample number 1 (TCAEY 105-107)

In the case of two passages, three configurations have been simulated:
-   same number of tube per passage (39-39)
-   existing configuration (66-12)
-   optimized number of tubes (41-37)

The simulation results are resumed in Table 1.6.12.

In Figures 1.6.7, 1.6.8 and 1.6.9, transmittance, pressure drop and heat transfer, of the first and the second passage, are plotted, respectively. The inside transmittance Ki is high for the passages with a low number of tubes, but the global transmittance is lower, being affected by the inside heat transfer area Ai. Thus the optimized configuration is the one that achieve the best agreement between transmittance and heat exchange area. The number of tubes of the second passage should not be too reduced, otherwise the heat transfer is too penalized.

	Passages	N tubes	Refrigerant average HTC	Heat transfer coefficient Ki	Transmittance Ai*Ki	Pressure drop	Heat transfer
			W/m²K	W/m²K	W/K	Pa	W
39-39	1	39	497	385	298	27	4120
	2	39	522	399	310	18	3227
41-37	1	41	550	416	339	33	4642
	2	37	603	445	327	25	3260
66-12	1	66	237	208	273	8	3999
	2	12	927	600	143	37	1197

Table 1.6.12: Simulation results for the condenser sample number 1, 2 passages
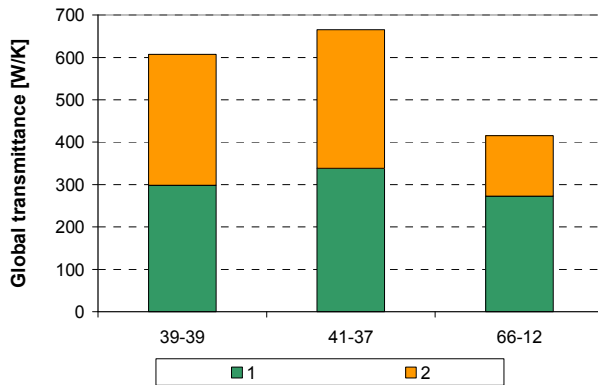
Figure 1.6.7: Global transmittance: simulation results for the condenser sample number 1, 2 passages
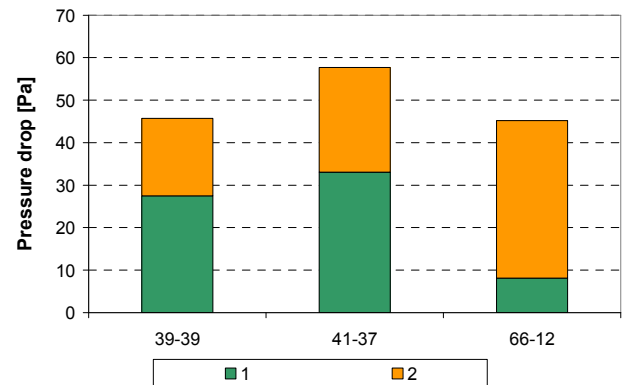
Figure 1.6.8: Pressure drop: simulation results for the condenser sample number 1, 2 passages

Figure 1.6.9: Heat transfer: simulation results for the condenser sample number 1, 2 passages

In the case of four passages, three types of configuration have been simulated:

- linear variation of the number of tubes (l1, l2, l3, l4)
- exponential variation of the number of tubes (e1, e2)
- same number of tubes (snt)

The results are resumed in Table 1.6.13 and plotted in Figures 1.6.10, 1.6.11 and 1.6.12. Even in this case, a too low number of tube in the last passage penalizes both the heat transfer and the pressure drop, as it can be notice for configurations l1 and l2. Using the same number of tube for each passage, a good performance can be achieved, as well as choosing the solutions e2, l3 and l4. It is worth underlining that the heat transfer for the 4-passage configurations is higher than for 2-passage configuration.

Figure 1.6.10: Global transmittance: simulation results for the condenser sample number 1, 4 passages

Figure 1.6.11: Pressure drop: simulation results for the condenser sample number 1, 4 passages

Figure 1.6.12: Heat transfer: simulation results for the condenser sample number 1, 4 passages

184

	Passages	N tubes	Refrigerant average HTC	Heat transfer coefficient Ki	Transmittance Ai*Ki	Pressure drop	Heat transfer
			W/m²K	W/m²K	W/K	Pa	W
e1	1	26	812	549	280	81	3792
	2	21	953	611	255	114	2223
	3	17	1129	679	232	103	1889
	4	14	1399	768	215	63	1535
e2	1	24	869	575	274	93	3657
	2	21	956	612	255	118	2225
	3	18	1082	661	237	98	1974
	4	15	1308	739	220	58	1622
l1	1	35	585	435	303	37	4131
	2	25	771	531	264	61	2449
	3	14	1226	713	198	79	1594
	4	4	4790	1255	100	336	456
l2	1	28	750	521	290	69	3887
	2	22	908	592	259	99	2290
	3	17	1116	674	228	93	1883
	4	11	1731	858	188	83	1245
l3	1	23	910	593	271	101	3597
	2	21	959	613	256	120	2227
	3	18	1084	662	237	100	1976
	4	16	1238	717	228	54	1710
l4	1	21	982	623	260	118	3447
	2	20	999	629	250	134	2149
	3	19	1040	645	244	97	2058
	4	18	1109	672	240	47	1876
snt	1	20	1032	642	255	128	3372
	2	20	999	629	250	136	2149
	3	19	1041	646	244	99	2058
	4	19	1058	652	246	44	1956

Table 1.6.13: Simulation results for the condenser sample number 1, 4 passages (previous page)

1.6.5.2   Condenser sample number 2 (TCAEY 109-111)

In the case of two passages, only two configurations have been simulated:
- same number of tube per passage (45-45): it resulted the optimized solution.
- existing configuration (51-39)

The simulation results are resumed in Table 1.6.14 and plotted in Figure 1.6.13, 1.6.14 and 1.6.15.

	Passages	N tubes	Refrigerant average HTC	Heat transfer coefficient Ki	Transmittance Ai*Ki	Pressure drop	Heat transfer
			W/m^{2}K	W/m^{2}K	W/K	Pa	W
51-39	1	51	421	347	352	20	5379
	2	39	487	391	303	13	3282
45-45	1	45	472	381	341	25	5182
	2	45	435	357	319	12	3560

Table 1.6.14: Simulation results for the condenser sample number 2, 2 passages.
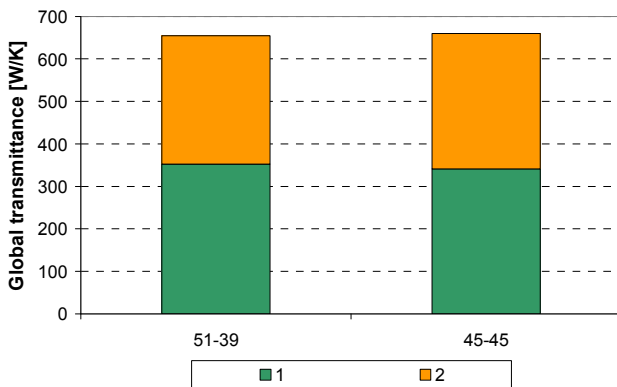
Figure 1.6.13: Global transmittance: simulation results for the condenser sample number 2, 2 passages
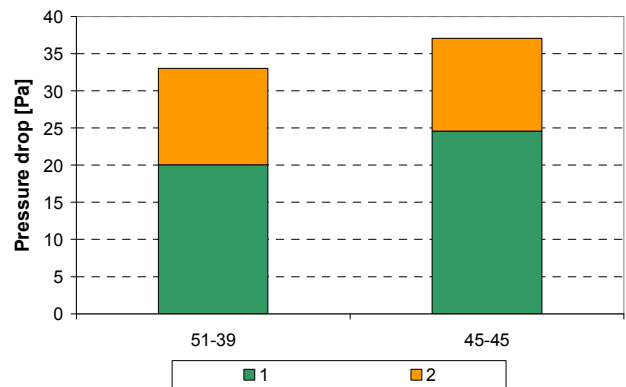
Figure 1.6.14: Pressure drop: simulation results for the condenser sample number 2, 2 passages
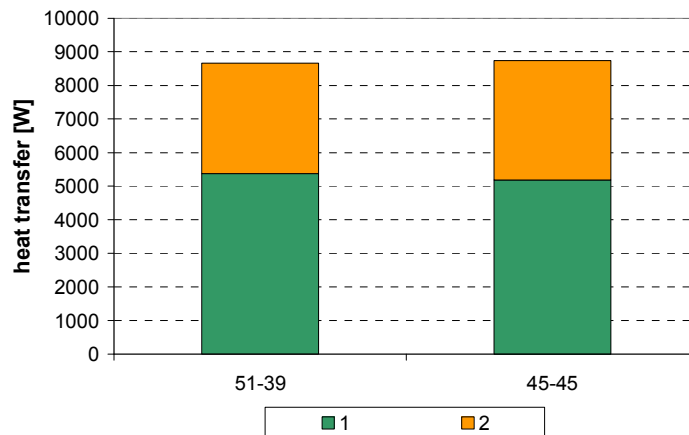
Figure 1.6.15: Heat transfer: simulation results for the condenser sample number 2, 2 passages

In this case the number of tube per passage of the used configuration is not strongly inhomogeneous like the previous sample. The differences between the two configurations are very small

In the case of four passages, four types of configuration have been simulated:

- used configuration (Tcaey)
- linear variation of the number of tubes (l1, l2, l3, l4)
- exponential variation of the number of tubes (e1, e2, e3)
- same number of tubes (snt)

The results are resumed in Table 1.6.15 and plotted in Figures 1.6.16, 1.6.17 and 1.6.18. The used configuration is acceptable, even if a solution with a larger number of tube in the last passage should be preferred. Configurations with few tubes in the last passage (e1 and l1) present high pressure drops; the best solutions are e3, l3 and l4, with around 20% of total tubes in the last passage.

	Passages	N tubes	Refrigerant average HTC	Heat transfer coefficient Ki	Transmittance Ai*Ki	Pressure drop	Heat transfer
			W/m²K	W/m²K	W/K	Pa	W
Tcaey	1	39	618	454	352	41	4753
	2	25	887	584	290	87	2558
	3	16	1268	728	231	108	1817
	4	10	2114	946	188	106	1140
e1	1	52	446	354	365	22	5060
	2	23	866	575	263	69	2331
	3	10	1685	849	169	142	1211
	4	5	3983	1197	119	250	568
e2	1	33	729	511	335	65	4471
	2	25	910	594	295	99	2580
	3	18	1183	699	250	106	2006
	4	14	1551	813	226	72	1541
e3	1	28	852	569	317	89	4187
	2	24	954	612	292	117	2517
	3	21	1110	673	281	100	2290
	4	18	1249	722	258	55	1801
l1	1	41	567	426	347	35	4717
	2	29	755	524	302	58	2793
	3	16	1215	710	226	74	1797
	4	4	5457	1302	104	423	439
l2	1	32	748	521	331	69	4411
	2	26	882	582	301	94	2655
	3	19	1133	682	257	96	2092
	4	13	1676	847	219	79	1445
l3	1	26	916	597	308	103	4059
	2	24	957	614	293	120	2519
	3	21	1065	656	274	98	2269
	4	19	1194	703	265	51	1992

l4	1	24	989	627	299	118	3917
	2	23	992	628	287	133	2442
	3	22	1028	642	281	95	2350
	4	21	1087	665	277	46	2155
snt	1	23	1004	633	289	122	3791
	2	23	729	511	234	66	2183
	3	22	881	582	254	72	2224
	4	22	1441	782	342	82	2410

Table 1.6.15: Simulation results for the condenser sample number 2, 4 passages
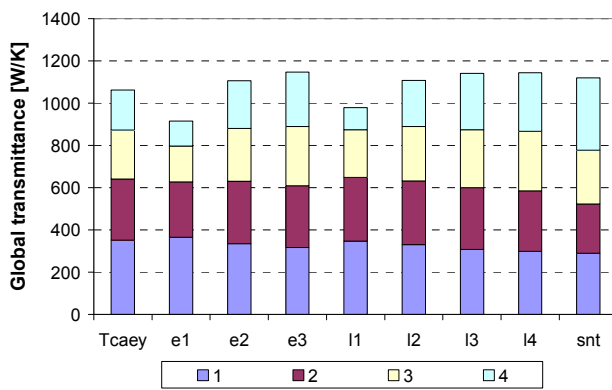
Figure 1.6.16: Global transmittance: simulation results

for the condenser sample number 2, 4 passages
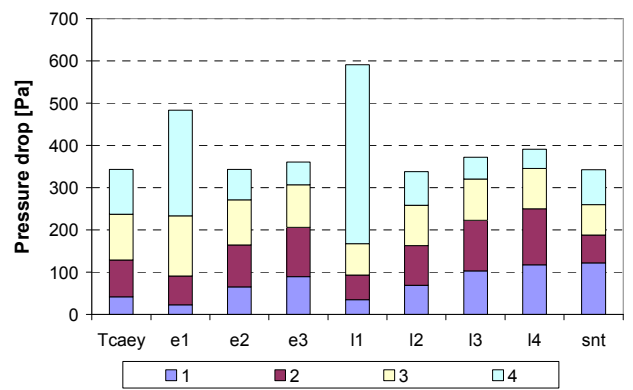
Figure 1.6.17: Pressure drop: simulation results for the
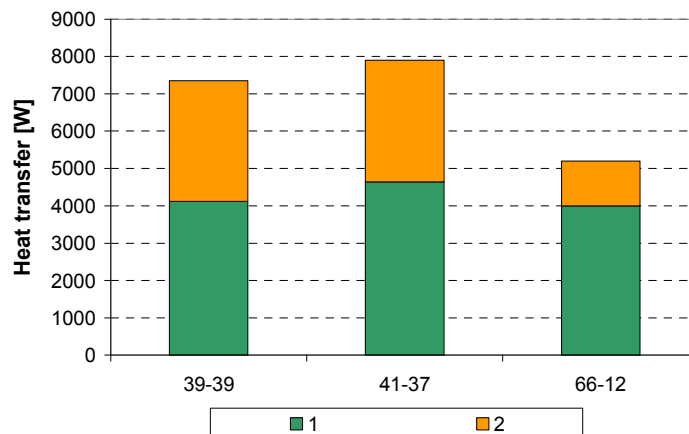
condenser sample number 2, 4 passages
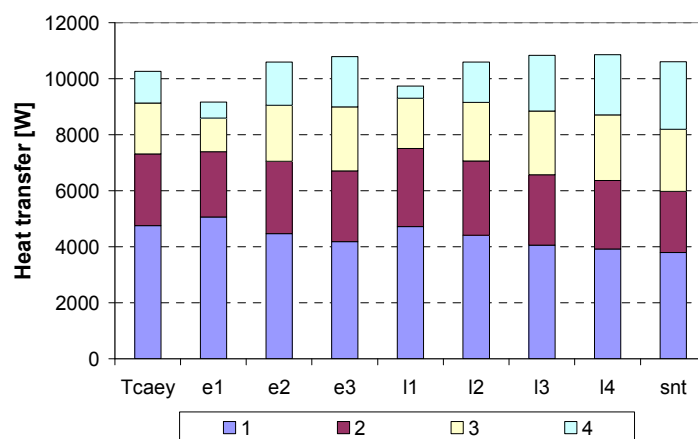
Figure 1.6.18: Heat transfer: simulation results for the condenser sample number 2, 4 passages

189

1.6.5.3 Condenser sample number 3 (TCAEY 115)

In this case, only the solution with 4 passages has taken into consideration; the investigated configurations are:

- linear variation of the number of tubes (l1, l2, l3, l4, l5, l6)
- exponential variation of the number of tubes (e1, e2, e3, e4, e5, e6)

The hypothesis that the number of tubes of the last passage were lower than 13 (15% of total tubes) is assumed. The aim is to simulate the fact that in the last passage only the liquid subcooling occurs. The most favorable configurations are l5, l6 and e6, with the higher number of tubes in the last passage. With a linear variation of the number of tubes, the performance of different solutions are quite similar, while with an exponential variation there are a sharp decreasing of heat transfer and increasing of pressure drop reducing the number of tube in the last passage. The results are resumed in Table 1.6.16 and plotted in Figures 1.6.19, 1.6.20 and 1.6.21.
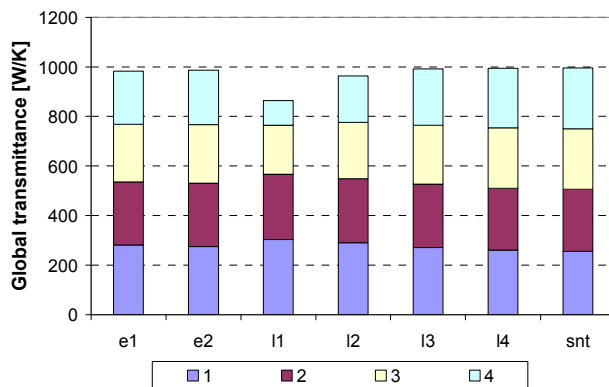

Figure 1.6.19: Global transmittance: simulation results for the condenser sample number 3, 4 passages
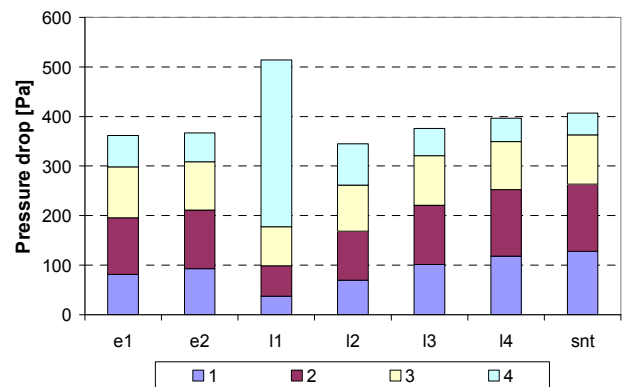

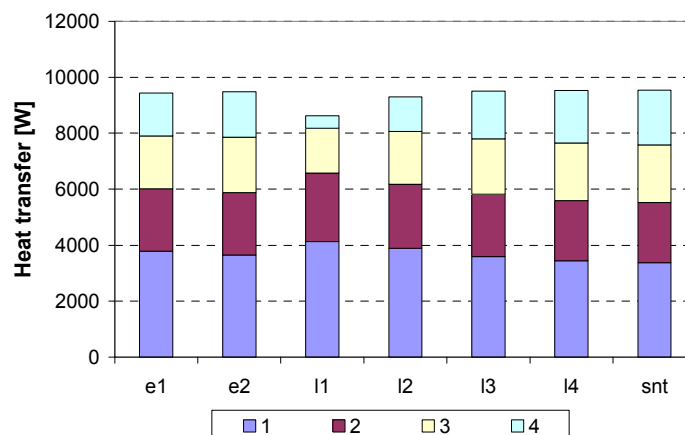Figure 1.6.20: Pressure drop: simulation results for the condenser sample number 3, 4 passages

190
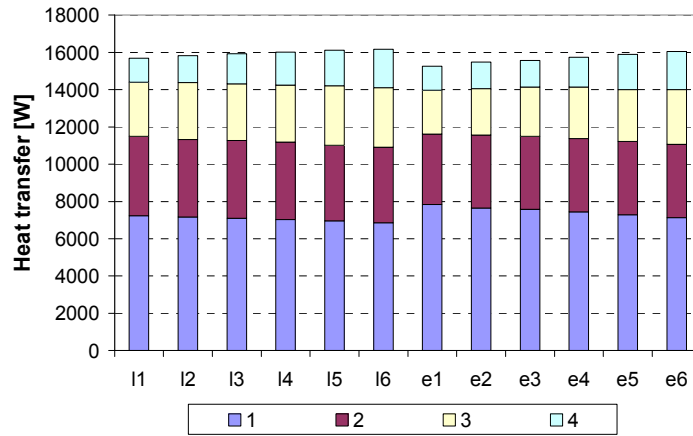
Figure 1.6.21: Heat transfer: simulation results for the condenser sample number 3, 4 passages

	Passages	N tubes	Refrigerant HTC	Ki	Ai*Ki	Pressure drop	Heat transfer
			W/m²K	W/m²K	W/K	Pa	W
I1	1	39	356	227	557	17	7229
	2	29	460	266	484	27	4264
	3	18	674	325	368	32	2912
	4	8	1498	443	223	51	1277
I2	1	38	366	232	553	18	7172
	2	28	477	271	477	30	4162
	3	19	650	320	382	32	3050
	4	9	1340	428	242	44	1439
I3	1	37	376	235	547	19	7100
	2	28	479	272	479	31	4168
	3	19	654	321	383	33	3053
	4	10	1211	414	260	39	1597
I4	1	36	386	239	541	20	7022
	2	28	481	273	480	31	4174
	3	19	656	321	383	34	3056
	4	11	1105	401	277	35	1751

I5	1	35	399	244	537	21	6952
	2	27	499	278	472	34	4066
	3	20	634	316	397	33	3192
	4	12	1019	389	293	32	1907
I6	1	34	409	248	529	21	6850
	2	27	500	278	472	35	4069
	3	20	635	316	397	35	3194
	4	13	948	378	309	29	2052
e1	1	47	299	203	598	13	7842
	2	25	507	281	441	31	3779
	3	14	807	353	311	45	2347
	4	8	1461	440	221	50	1281
e2	1	44	320	212	586	14	7643
	2	26	498	278	454	31	3911
	3	15	773	347	327	43	2495
	4	9	1302	424	240	43	1442
e3	1	43	327	215	582	15	7580
	2	26	500	279	455	31	3916
	3	16	737	339	341	40	2637
	4	9	1322	426	241	44	1443
e4	1	41	343	222	572	16	7442
	2	26	504	280	457	33	3926
	3	17	708	333	356	38	2779
	4	10	1198	413	259	39	1595
e5	1	39	360	229	561	17	7283
	2	26	508	281	459	34	3936
	3	17	714	334	357	41	2784
	4	12	1005	387	292	31	1900

e6	1	37	379	236	550	19	7130
	2	26	512	282	461	36	3945
	3	18	687	328	371	40	2925
	4	13	942	377	308	29	2050

Table 1.6.16: Simulation results for the condenser sample number 3, 4 passages

1.6.6 Conclusions

From the simulation results, it is possible to draw some conclusions and to define some guidelines for the design of an air-to-refrigerant minichannel condenser, in order to achieve the highest energy efficiency.

1. The heat transfer of a 4-passage configuration is higher than a 2-passage configuration, keeping the same geometry. The pressure drops increase of an order of magnitude, but they do not remarkably affect the heat exchange, being lower than 1 kPa.

2. For a 2-passage configuration, the number of tubes of the second passage should not be too low. An optimal splitting of the tubes is estimated to be 55-60% of total in the first passage and 40-45% of total in the second passage.

3. For a 4-passage configuration, an optimal splitting of the tubes should be defined according to a linear law. In this case, the efficiency of the condenser is acceptable even for configurations different from the optimal one, as pointed out for the condenser sample number 3. As an indication, the number of tubes in the last passage should be around 15% of the total. The number of tubes in the first passage should be around 35% of the total: if they are fewer than 30%, the pressure drops are too high; if they are more than 40%, the tubes are not properly fed, penalizing the heat transfer.

4. It is worth reminding that these conclusions are valid for R410A: changing the refrigerant, the behavior may be different, especially concerning the pressure drops. In addition, the heat exchanger geometries have not been modified, nor different positions of the inlet tube to the header have been taken into account.

5. The position of the inlet tube to the header should be around opposite the middle tube of the first passage, allowing a homogenous splitting of the refrigerant mass flow in the two directions.

1.6.7 References

1. Cavallini A., Censi G., Del Col D., Doretti L., Longo G. A., Rossetto L., (2002), In-tube condensation of refrigerants. *Ashrae Trans. #4507*, 108, Pt. 1.

2. Casson V, Cecchinato L., Corradi M., Fornasieri E., Girotto S., Minetto S., Zamboni L., Zilio C., (2003), Optimization of the throttling system in a CO_2 refrigerating machine, *Int. J. Refrigeration*, 26: 926-935.

3. Casson V, Cecchinato L., Del Col D., Fornasieri E., Zilio C., (2002), An innovative model for the simulation of finned coil evaporators, *12th Int. Heat Transfer Conf.*

4. Cecchinato L., Corradi M., Fornasieri E., Zamboni L., (2005), Carbon dioxide as refrigerant for tap water heat pumps: A comparison with the traditional solution, *Int. J. Refrigeration*, 28: 1250-1258.

5. Chang Y.-J., Wang C.-C., (1997), A generalized heat transfer correlation for louver fin geometry, *Int. J. Heat Mass Transfer*, 40(3):533-544.

6. Friedel L., (1979), Improved friction pressure drop for horizontal and vertical two-phase pipe flow. In: *Europ. Two-phase flow group meet*, Paper E2.

7. Gnielinski V., (1976), New equation for heat and mass transfer in turbulent pipe and channel flow. *Int. Chem. Eng.*, 16:359–68.

8. Lemmon E. W., McLinden M. O., Huber M. L., (2002), NIST Reference Fluid Thermodynamic and Transport Properties Refprop 7.0, *NIST Std. Database*.

9. Pettersen J., Rieberer R., Munkejord S.T., (2000), Heat transfer and pressure drop for flow of supercritical CO_2 in microchannel tubes. *SINTEF Report*, TR A5127.

10. Rouhani S. Z., Axelsson E., (1970), Calculation of volume void fraction in the subcooled and quality region, *Int. J. Heat Mass Transfer*, 13:383–393.
11. Thome J. R., Kattan N., Favrat D., (1998), Flow boiling in horizontal tubes. Part 3: development of a new heat transfer model based on flow pattern, *J Heat Transfer ASME*, 120:156-165.

Chapter 1.7 MINICHANNEL EVAPORATORS: CURSE OR BLESSING? STUDIED

SOLUTIONS

1.7.1   Introduction

In this chapter, the possibility of realizing a minichannel evaporator is studied; in the first part, the experimental tests on an innovative model of minichannel evaporator are reported. In the second part, some experimental tests on the water drainage capacity of different minichannel geometries are presented.

1.7.2   Part 1: experimental tests on an innovative model of minichannel evaporator

The performances of a minichannel evaporator (MCHX) are tested under different working conditions; they are compared to those of a traditional round tube heat exchanger (RTHX). These experimental tests were carried out during an experience, as visiting scholar, at the Air Conditioning and Refrigeration Center (ACRC) of the University of Illinois at Urbana-Champaign, in the same test facility described in Chapter 1.4. The testing conditions are those of a typical heat pump system. The parameters of interest include evaporation temperature, air-side pressure drop, effectiveness and heat transfer coefficient of the heat exchangers, cooling capacity and heat pump COP for air face velocity of 1.5 m/s. The same tests have been repeated in the same system equipped with an internal heat exchanger (IHX), to allow a better distribution of the refrigerant in the minichannel evaporator. In particular, the improvements of the system performance in frosting conditions due to the internal heat exchanger are highlighted.

1.7.2.1 Nomenclature

Being these experimental tests carried out during the experience at the ACRC, the name of the variables are the same of paragraph 1.4.2. Further variables are reported in the following.

Δp_air air- side pressure drop [Pa]

COP heat pump coefficient of performance [-]

U overall heat transfer coefficient [$Wm^{-2}K^{-1}$]

UA heat transfer coefficient [WK^{-1}]

1.7.2.2 The types of heat exchangers tested and the test facility

The testing facility is described in paragraph 1.4.3. The minichannel evaporator is described in the US. Patent 7,032,313 B2 (Memory *et al.*, 2006); as pointed out in paragraph 1.5.7, the major constrain in realizing a minichannel heat exchanger is the poor moisture drainage capacity of this geometry. This implies a detriment of the heat transfer properties and a reduction of the frosting time, under wet conditions and with temperatures below 0°C. Memory *et al.* (2006) developed this type of evaporator, which had been manufactured and sold by Modine with the name of PF^2, and presented at the 2006 AHR Expo, where it won the Cooling Innovation Award.

The peculiarity of this heat exchanger is that the fin depth is larger than the tube depth and the fins jut out the rear side of the evaporator, as depicted in Figure 1.7.1(a) and (b). The base concept is to take advantage of the contact forces between the water and the aluminum fins: the water is push to the rear side of the evaporator by the fans and it falls down by gravity. In this way it is possible to realize a minichannel evaporator with vertical headers and horizontal tubes.
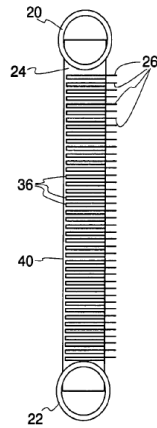
Figure 1.7.1(a): Schematic diagram of heat exchanger, top view; (Memory et al.,2006)
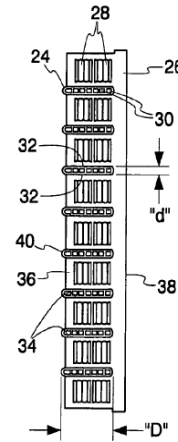
Figure 1.7.1(b): Schematic diagram of heat exchanger, side view; (Memory et al.,2006)
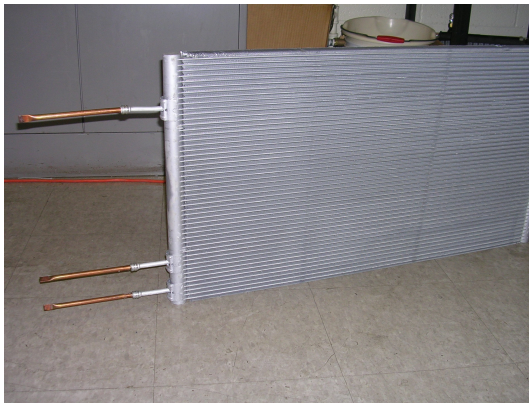
Figure 1.7.2: The minichannel evaporator (MCHX) tested

Passes (tubes)	4 (13,13,12,12)	-
Rows	1	-
MC tube major	27.00	mm
MC tube minor	1.90	mm
fin material	Al	-
fin type	louvered PF²	-
fin pitch	16	fpi
height	0.510	m
width	0.818	m
face area	0.417	m²
air-side HT area	17.802	m²

Table 1.7.1: Geometrical characteristics of minichannel evaporator (MCHX) tested

The two tested evaporator are shown in Figure 1.7.2 and 1.7.3 and their geometrical characteristics are resumed in Table 1.7.1 and 1.7.2. The round tube evaporator model is Daikin ODHX; the refrigerant path is shown in Figure 1.7.4. Both heat exchangers were initially designed as condensers. The face areas of the two evaporators are the same, but the air side heat transfer area of the round tube evaporator is larger, being the fin pitch smaller (20 fpi, that is a fin pitch of 1.27 mm). In addition, the round tube heat exchanger has two rows, while the minichannel heat exchanger has one single row.
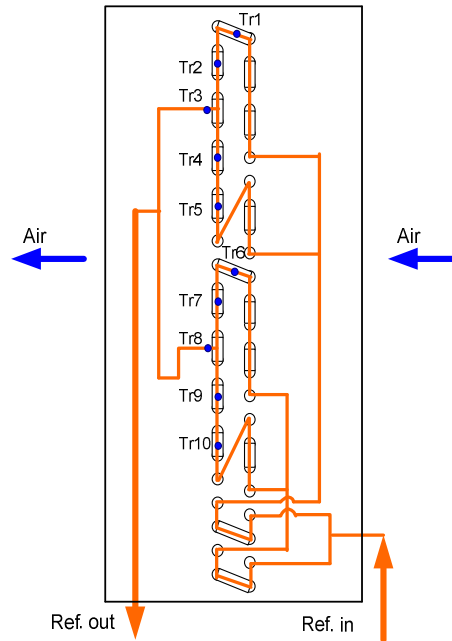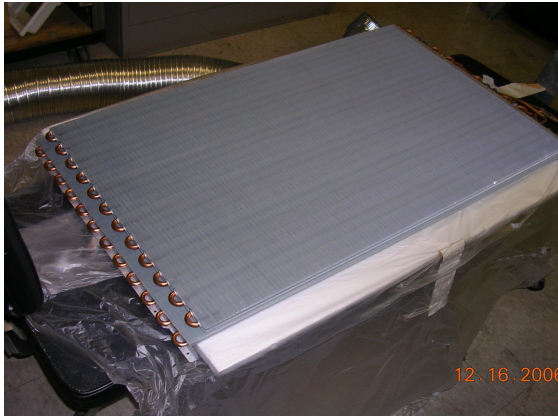
Figure 1.7.3: The round tube evaporator (RTHX) tested

Figure 1.7.4: The refrigerant path of the round tube evaporator (RTHX) tested

Tubes	48	-
Rows	2	-
tube OD	7.00	mm
tube ID	5.48	mm
fin material	Al	-
fin type	flat plate	-
fin pitch	20	fpi
height	0.504	m
width	0.829	m
face area	0.418	m²
air-side HT area	21.750	m²

Table 1.7.2: Geometrical characteristics of the round tube evaporator (RTHX) tested

The round tube condenser is Daikin IDHX; it is shown in Figure 1.7.5, the refrigerant path is depicted in Figure 1.7.6 and its geometrical characteristics are resumed in Table 1.7.3.

Figure 1.7.5: The round tube condenser
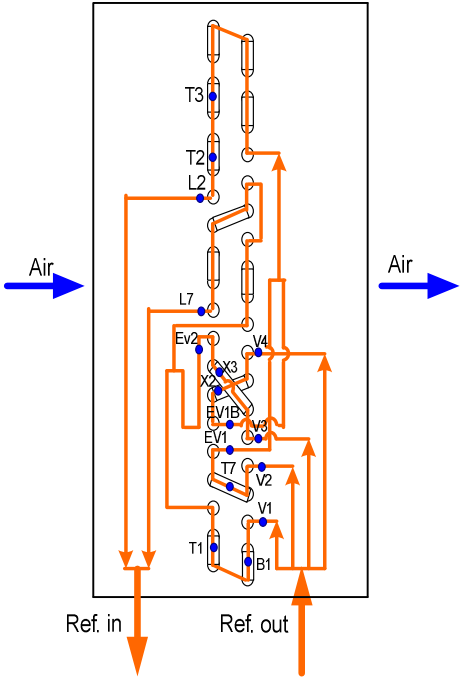
Figure 1.7.6: The refrigerant path of the round tube condenser

tube material	-	Cu
tube type	-	round tube
Tubes	-	40
Rows	-	2
tube OD	mm	6.35
tube ID	mm	4.83
Fin material	-	Al
fin type	-	louvered plate
fin pitch	fpi	21.17
height	m	0.360
width	m	0.610
core depth	mm	23.0
face area	m²	0.220
air-side HT area	m²	7.617
Ref. HT area	m²	0.370
core volume	cm³	5051
ref volume (w/o header)	cm³	446.3

Table 1.7.3: Geometrical characteristics of the round tube condenser

The internal heat exchanger, used in the second set of tests, is shown in Figure 1.7.7 and its geometrical characteristics are resumed in Table 1.7.4.

Figure 1.7.7: The internal heat exchanger (IHX).

Length	mm	381
Height	mm	25
Width	mm	6
Total exchange area	mm^2	9576

Table 1.7.4: Geometrical characteristics of the internal heat exchanger (IHX).

The compressor is a Daikin 2YC32GXD swing compressor; its image is in Figure 1.7.8.

Figure 1.7.8: Daikin swing compressor (www.daikinthai.com).

1.7.2.3   Testing conditions

In all the experimental tests, the conditions at the condenser were the usual ones of heating systems; the air temperature at the inlet was kept at 20°C and the refrigerant subcooling at the outlet was set at 5°C. At the evaporator, different testing conditions were considered:

- *design conditions*: the air temperature at the inlet was set at 6.5°C, the relative humidity at 75÷80% and the refrigerant superheat at 5°C.
- *low temperature*: the air temperature at the inlet was set at -6°C, the relative humidity at 60÷65% and the refrigerant superheat at 5°C.
- *high humidity*: the air temperature at the inlet was set at 2°C, the relative humidity at 85÷90% and the refrigerant superheat at 5°C.

The aim of the first test was to verify that the evaporator were actually able to dry the moisture formed on the heat exchange surface. The objective of the following tests was to investigate the behaviour of the evaporator under severe conditions, with low temperature and high humidity. In particular, the last condition is interesting for heat pump applications: the evaporator surface temperature is lower than 0°C and the presence of high humidity implies frost formation. The study of this phenomenon dynamics is a topical issue for heat pump applications.

The tests were carried out on both the heat exchangers described, round tube and minichannel. The same tests were repeated in the system, with the minichannel evaporator, with the internal heat exchanger. The use of an internal heat exchanger is not commonly recommended in R410A cycles (Domanski *et al.*, 1994); in this case, the objective is to investigate the effect of the regenerative heat exchanger on the distribution of the refrigerant in the minichannel evaporator, as suggested by Hanson *et al.* (2007). The internal heat exchanger allows both a better distribution in the first passage, being the refrigerant at the condenser outlet more subcooled and its quality at the evaporator inlet very low, and in the last passage, being smaller the superheated area. The increase of the heat pump COP is not the main topic, but the presence of the IHX causes a COP improvement due to the higher evaporation pressure.
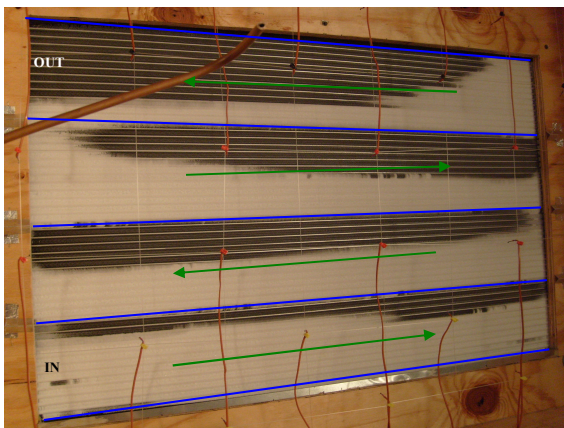
Figure 1.7.9: The minichannel evaporator at the end of a frosting cycle

Figure 1.7.10: The round tube evaporator at the end of a frosting cycle

The experimental tests have been conducted in the facility described in paragraph 1.4.3. The face air velocities of both the evaporator and the condenser were set at 1 m/s and kept constant during the test. For the tests in steady-state conditions, i.e. without frost formation, the data were recorded once the system was considered stable. On other hand, in the tests with high humidity and frosting conditions, the parameters of the system continuously changed while the frost had been growing. Thus, during the test, the system was continuously controlled, acting on the rotational speed of the compressor and on the throttling valve opening, and the data were recorded for the whole period of the test. The objective was to simulate the

actual running of heat pump systems, thus during the test the main tasks were:

- having a safe running of the compressor (superheat 5°C, subcooling at least 1°C);
- providing a constant thermal capacity.

The test ended when it is not possible to increase the compressor speed (max 70 Hz) or to close more the expansion valve. Examples of the minichannel evaporator and the round tube evaporator at the end of the frosting cycle are shown in Figure 1.7.9 and 1.7.10. In Figure 1.7.9, the regions with low heat transfer coefficients are highlighted: they are the parts not covered with ice, at the end of tests without the internal heat exchanger; the distribution of the four passages is also marked.

1.7.2.4   Results and discussion

Tests without the internal heat exchanger

For all the testing conditions, all the parameters of interest which describe the performance of the evaporator and of the whole system have been analyzed. The results of the first test (design conditions) are reported in Table 1.7.5.

In this case, the main objective was testing the drainage efficiency of the minichannel evaporator; during the test, the water in the surface is dragged away from the heat exchanger, there is no moisture accumulation and the conditions remain steady; the water formation during the test (20 minutes) is 5.1% lower than the round tube evaporator.

Comparing the minichannel heat exchanger to the round tube one, the evaporation temperature is positive and 0.41°C higher; the air-side pressure drop is 28.5% higher, the effectiveness and the heat transfer coefficient (UA) are 16.7% and 9.5% higher, respectively. The overall heat transfer coefficient (U) is 33.8% higher because the total heat transfer area is lower, while the capacity of the evaporator is the same. Considering the whole system, the heat pump COP is the same (0.7% lower).

Parameter	RTHX	MCHX
Tero_sat [°C]	-0.51	-0.10
Δp air [Pa]	20.5	26.3
UA [W/K]	567	620
U [W/m^{2}K]	26.0	34.8
Effectiveness [%]	54.0	63.0
Q evap [kW]	2.569	2.576
COP [-]	5.254	5.216
Water formation [g/20min]	350.1	332.3

Table 1.7.5: Experimental results of the tests in design conditions, without internal heat exchanger

The results of the test at low temperature are reported in Table 1.7.6; in this case the dew point temperature is lower than the surface temperature, so there is no condensation. The objective of this test is to investigate the behaviour of the evaporator at low temperature.

Considering the minichannel heat exchanger, the evaporation temperature is 1.5°C higher and the pressure drop is 24.0% higher. The effectiveness and the heat transfer coefficient are 27.2% and 14.4% higher respectively and the overall heat transfer coefficient is 39.8% higher. The cooling capacity and the heat pump COP are close, 4.6% and 3.6% higher.

Parameter	RTHX	MCHX
Tero_sat [°C]	-13.6	-12.1
Δp air [Pa]	15.8	19.6
UA [W/K]	332	380
U [W/m^{2}K]	15.3	21.3
Effectiveness [%]	39.0	49.6
Q evap [kW]	1.611	1.686
COP [-]	3.736	3.870

Table 1.7.6: Experimental results of the tests at low temperatures, without internal heat exchanger

The aim of the third test (high humidity) is to investigate the behaviour of the system in frosting conditions; in this case, the parameters are not steady, due to the frost formation, and the system needs to be controlled, as explained above.

The trends of some parameters of interest are plotted in Figures 1.7.11.

It is possible to notice that the air side pressure drop of the minichannel heat exchanger increases more sharply; the decreases of the effectiveness and the heat pump COP are due to the decrease of the evaporation pressure. At this point it is necessary to characterize a method to define the end of a frosting cycle, that is, in a real system, the moment when the heat pump stops running and the defrosting system starts to operate. This moment is considered when the evaporation pressure goes 1 bar below the value at the beginning of the test, with the evaporator surface free of ice. According to the test conditions, the frosting cycles can be considered of 2000 and 3600 seconds, respectively for the MCHX and RTHX evaporator.

Figure 1.7.11(a): Experimental results of the tests at high humidity, without internal heat exchanger: air-side pressure drop

Figure 1.7.11(b): Experimental results of the tests at high humidity, without internal heat exchanger: evaporator effectiveness
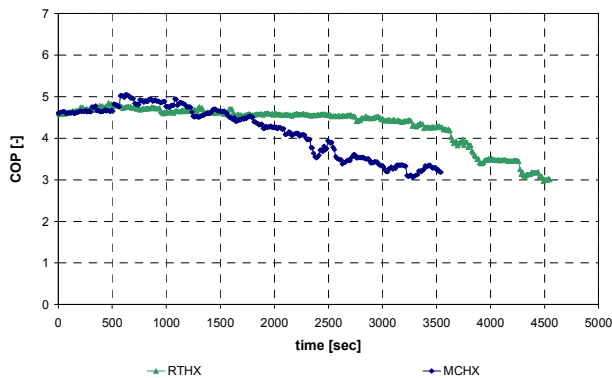
Figure 1.7.11.(c): Experimental results of the tests at high humidity, without internal heat exchanger: heat pump COP
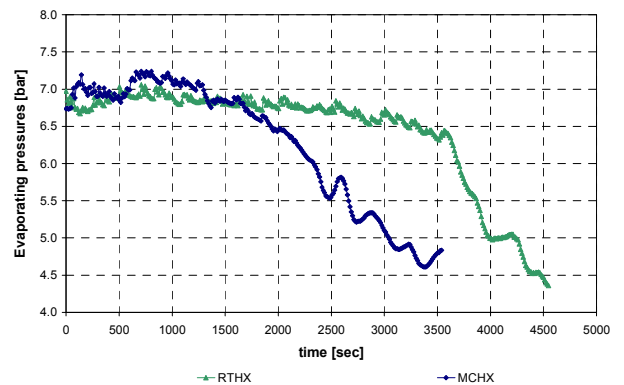
Figure 1.7.11(d): Experimental results of the tests at high humidity, without internal heat exchanger: evaporation pressure
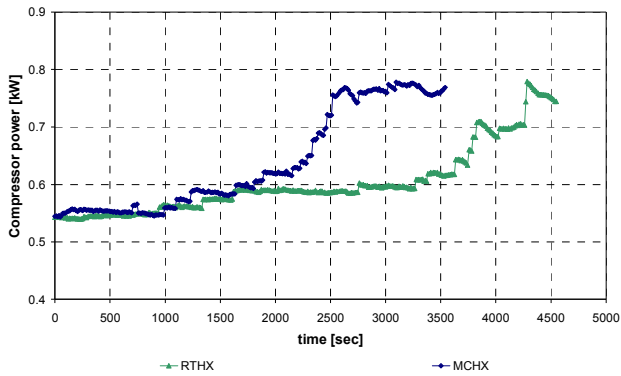
Figure 1.7.11(e): Experimental results of the tests at high humidity, without internal heat exchanger: compressor power consumption
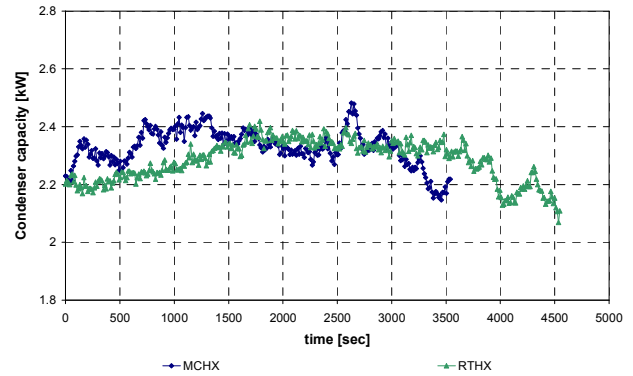
Figure 1.7.11(f): Experimental results of the tests at high humidity, without internal heat exchanger: condenser capacity

Tests with the internal heat exchanger

As pointed out in Chapter 1.5, the maldistribution can affect the frosting formation process; two suggested methods to improve the refrigerant distribution can be the use of a separator upstream the evaporator or the use of an internal heat exchanger.
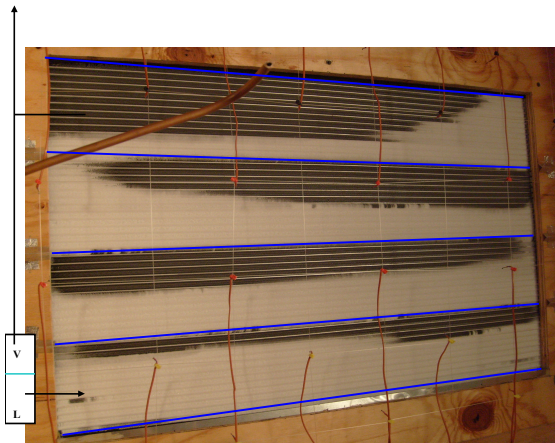
Figure 1.7.12(a): Solution with fluid separator
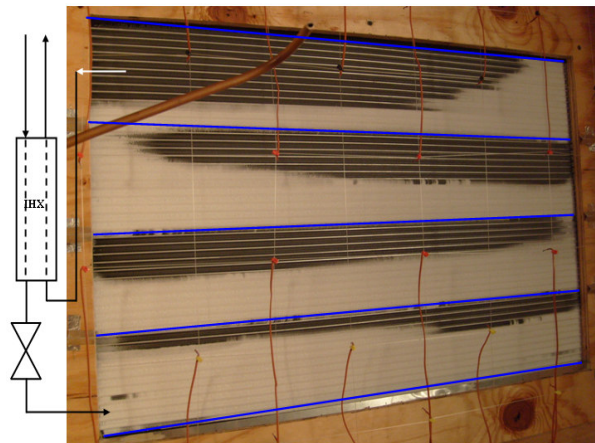
Figure 1.7.12(b): Solution with internal heat exchanger (IHX)

These solutions are schematically represented in Figure 1.7.12(a) and (b). The easier and more effective method was the use of an internal heat exchanger (IHX), shown in Figure 1.7.12(b).

The same tests described above were repeated with the internal heat exchanger

IHX in the system with the MCHX evaporator; the conditions at the condenser were the same of the previous tests. The refrigerant at the inlet header is close to saturated liquid; the superheat is set at 5°C at the outlet of the internal heat exchanger. In this way, the refrigerant at the evaporator outlet is two-phase and the superheated area of the evaporator, with low values of heat transfer coefficient, is reduced. The results of the test in the first condition (design conditions), of the system with MCHX evaporator and with or without internal heat exchanger, are resumed in Table 1.7.7. The system with internal heat exchanger allows a higher evaporation temperature (1.12°C higher); the air-side pressure drop is 16.5% higher than the system without IHX. The performances of the evaporator are higher: the effectiveness and the heat transfer coefficient are 19.1% and 50.0% higher, respectively.

Parameter	MCHX	MCHX with IHX
Tero_sat [°C]	-0.10	1.02
Δp air [Pa]	26.3	30.6
UA [W/K]	620	930
U [W/m^{2}K]	34.8	52.3
Effectiveness [%]	63.0	75.1
Q evap [kW]	2.576	2.710

Table 1.7.7 Experimental results of the tests in design conditions, with internal heat exchanger

The results of the tests at low temperature are shown in Table 1.7.8; these tests confirm the results of the previous table. Passing to the system with internal heat exchanger, the increase of the evaporation temperature of the system is 1.02°C. Even in this case, the increases of the effectiveness and of the heat transfer coefficient are remarkable: the effectiveness and the heat transfer coefficient are 20.4% and 68.2% higher, respectively.

Parameter	MCHX	MCHX with IHX
Tero_sat [°C]	-12.14	-11.12
Δp air [Pa]	19.6	27.7
UA [W/K]	380	639
U [W/m^{2}K]	21.3	35.9
Effectiveness [%]	49.6	59.7
Q evap [kW]	1.686	1.797

Table 1.7.8: Experimental results of the tests at low temperatures, with internal heat exchanger

The internal heat exchanger is more useful in frosting conditions: in this case the temperature of the evaporator heat transfer surface is higher and more homogeneous, thus the frost formation is delayed and uniform over the surface. It is worth to remind that the two evaporators, round tube and minichannel, were designed to act as condensers, so they are largely oversized; in addition, the superheat was set at 5°C, thus some regions of both heat exchangers are thermodynamically penalized, being the temperature difference between the air and the fluid very low
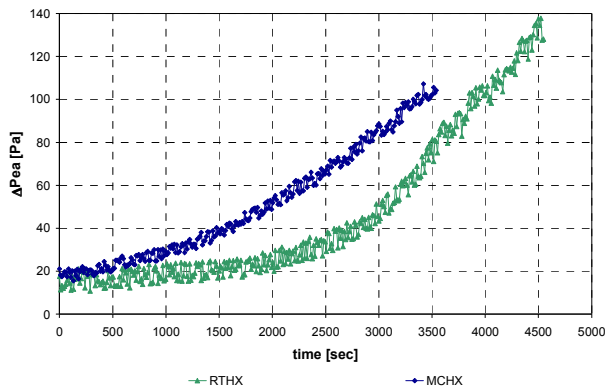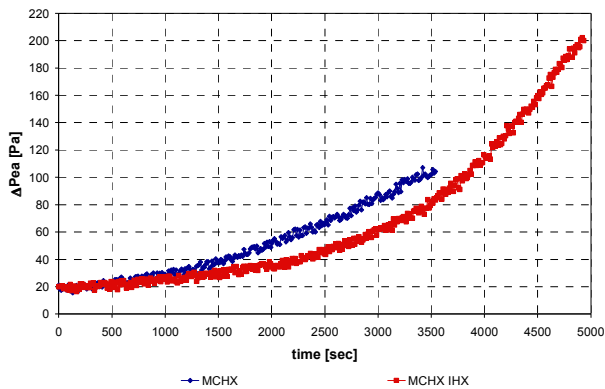

Figure 1.7.13(a): Experimental results of the tests at high humidity, with internal heat exchanger: air-side pressure drop
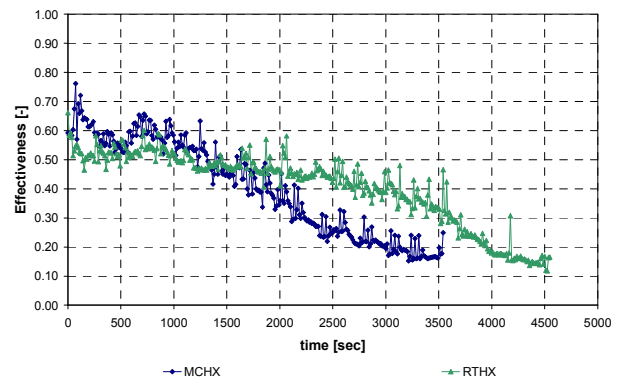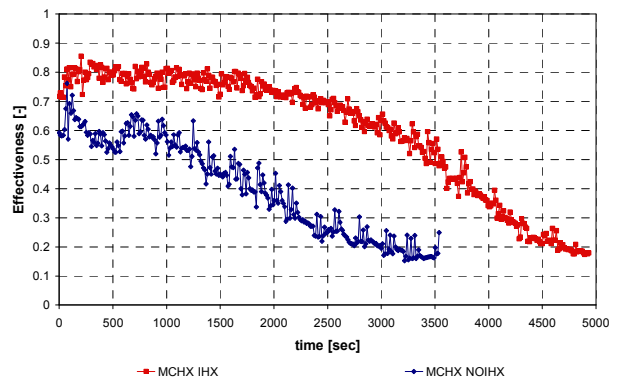

Figure 1.7.13(b): Experimental results of the tests at high humidity, with internal heat exchanger: evaporator effectiveness
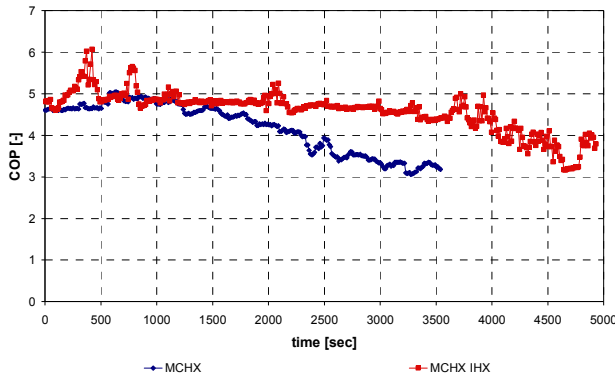
Figure 1.7.13(c): Experimental results of the tests at high humidity, with internal heat exchanger: heat pump COP
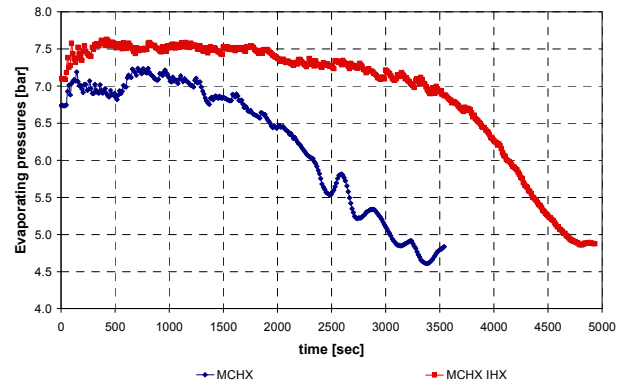
Figure 1.7.13(d): Experimental results of the tests at high humidity, with internal heat exchanger: evaporation pressure
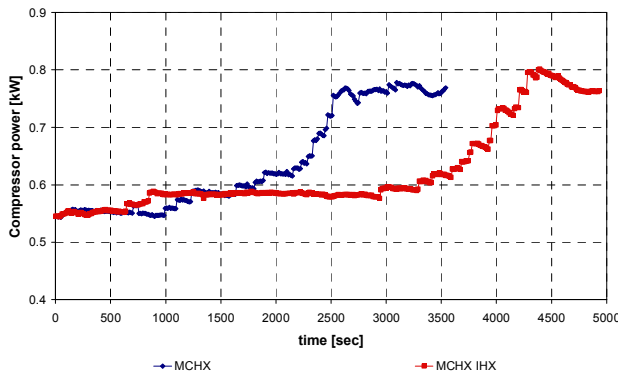
Figure 1.7.13(e): Experimental results of the tests at high humidity, with internal heat exchanger: compressor power consumption
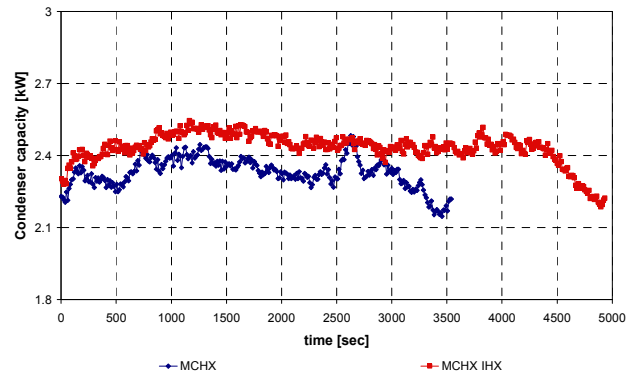
Figure 1.7.13(f): Experimental results of the tests at high humidity, with internal heat exchanger: condenser capacity

In Figures 1.7.13 the parameters of interests of the system with and without internal heat exchanger are plotted. The pressure drop of the system with internal heat exchanger increases less sharply than the same system without internal heat exchanger. The effectiveness and the evaporation pressure are higher, while the heat pump COP is almost the same. The trends of the different parameters highlight the better performance of the system in frosting conditions: the frosting time passes from 2000 to 3800 seconds.

In these tests, the evaporator surface at the beginning is completely dry and free of ice: this is an important limit of this analysis, because in real conditions the frost formation begins at the end of the defrosting cycle. If the water drainage of the heat exchanger is bad, the evaporator surface is actually wet and the frosting time is heavily reduced, increasing the energy consumption for defrosting. As pointed out

in Chapter 1.5, to have an effective advantage in the frosting/defrosting management, a good moisture drainage during the defrosting cycle is mandatory.

<u>Frosting formation during tests</u>

In Figures 1.7.14, 1.7.15 and 1.7.16, the frosting formation, during the tests at high humidity, for the different type of evaporator, is depicted. In Figure 1.7.14, the frosting cycle is almost completed for the MCHX evaporator, while the face area of the MCHX evaporator with IHX is still free of ice. In the RTHX, the ice is growing around the tube surface. After 2500 sec (Figure 1.7.15), the frosting cycle is completed for the MCHX evaporator; the maldistribution of the refrigerant is noticeable. The ice is growing on the surface of the MCHX evaporator with IHX and of the RTHX evaporator. The frosting process is almost completed even for the MCHX with IHX and for the RTHX after 3600 sec (Figure 1.7.16); the refrigerant distribution in the MCHX with IHX is better, especially in the first and in the last passage.

Figure 1.7.14(a): MCHX evaporator after1800 sec
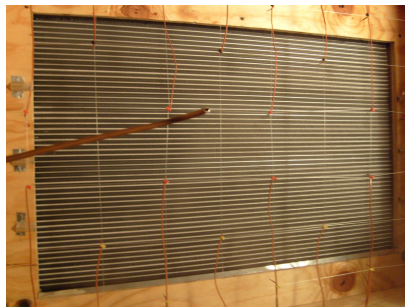
Figure 1.7.14(b): MCHX evaporator (with IHX) after1800 sec
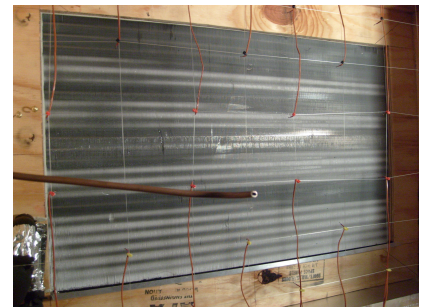
Figure 1.7.14(c): RTHX evaporator after1800 sec

Figure 1.7.15(a): MCHX evaporator after2500 sec

Figure 1.7.15(b): MCHX evaporator (with IHX) after2500 sec

Figure 1.7.15(c): RTHX evaporator after2500 sec

Figure 1.7.16(a): MCHX evaporator after3600 sec

Figure 1.7.16(b): MCHX evaporator (with IHX) after3600 sec
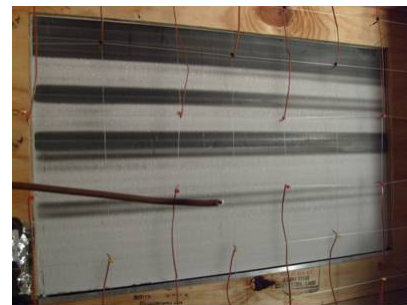
Figure 1.7.16(c): RTHX evaporator after3600 sec

1.7.2.5   Conclusions

In this study, two types of evaporators were compared: a conventional round tube heat exchanger (RTHX), and a minichannel heat exchanger with parallel flow (MCHX). In particular, the minichannel heat exchanger is a new designed model, with special fins which favor the water drainage from the evaporator surface. These two evaporators were tested in a heat pump system, under typical working conditions: under design conditions, with a positive evaporation temperature, at low temperature, with a low humidity and at high humidity, with a negative evaporation temperature.

Comparative analyses show the following.

Under design conditions, the cooling capacity and the heat pump COP of the two heat exchangers are close; the air-side pressure drop of the MCHX evaporator is 28.5% higher and the evaporation temperature is 0.41°C higher. The effectiveness and the heat transfer coefficient (UA) of the MCHX evaporator are 16.7% and 9.5% higher, respectively. MCHX total heat exchange surface is lower than that of the RTHX evaporator, so the overall heat transfer coefficient (U) is 33.8% higher. A good drainage of the water was observed in both the heat exchangers. The drainage capacity of the MCHX, even if it is lower than that of the RTHX, is good: the control parameters remain stable during the entire test.

The tests at low temperatures confirm this trend: the MCHX evaporation temperature and air-side pressure drop are 1.5°C and 24% higher, respectively. The effectiveness and the heat transfer coefficient are 27.2% and 14.4% higher respectively and the overall heat transfer coefficient is 39.8% higher. The cooling

capacity and the heat pump COP are close, 4.6% and 3.6% higher. The data of these tests confirm the ones of the tests under design conditions; the MCHX does not show any particular problems at low temperatures.

The objective of the tests at high humidity was to observe the frosting formation process on the two different evaporators; in this case the performance of the MCHX evaporators is lower. Because of the frosting formation, the conditions of the tests are not stable and the values of the parameters of interest change during the tests. It is important to understand the point when the frosting process can be considered completed and the defrosting operation must start. The objective is to avoid the system to run with low efficiencies, i.e. with low values of heat pump COP. As shown in Figure 1.7.11, for the system with the MCHX evaporator, the COP passes from 4.26 (at 2000 sec of run time) to 3.55 (at 2400 sec of run time), with a penalization of 16.7%. The behaviour of the system with the RTHX evaporator is the same, the COP passes from 4.19 (at 3600 sec of run time) to 3.40 (at 3900 sec of run time), with a penalization of 18.9%. These energy penalizations are related to a sharp decreasing of the evaporation pressures, as shown in Figure 1.7.11(d): for the MCHX evaporator, it passes from 0.646 MPa to 0.575 MPa in the considered period (2000 to 2400 sec of run time), for the RTHX evaporator, it passes from 0.640 MPa to 0.537 MPa in the considered period (3600 to 3900 sec of run time). Thus, the evaporation pressure can be considered a reliable control parameter for the management of the frosting-defrosting cycles. On other hand, it is clear that the frosting cycle of the MCHX evaporator (2000 sec) is far shorter than that of the RTHX (3600 sec), in the same running conditions; this aspect must be taken into account in an energy analysis of the two systems.

An internal heat exchanger (IHX) was installed in the system with the MCHX, to improve the distribution in the evaporator. The increases of the effectiveness and of the heat transfer coefficient are remarkable both under design conditions and at low temperatures, but the heat pump COPs of the systems remain almost the same. The most interesting results are those of the tests at high humidity: the completion of the frosting process is delayed, as shown in Figures 1.7.13. The heat pump COP passes from 4.37, at 3800 sec of run time, to 3.66 at 4250 sec of run time; in the same period, the evaporation pressure passes from 0.664 MPa to 0.577 MPa. Thus, the frosting cycle is longer than that of system without IHX, at the same running conditions. In this case, the amount of ice on the evaporator surface is larger and

214

the defrosting energy required shall be higher. The optimal management of frosting-defrosting cycle is an open issue and it should be the results of an energy analysis of various cycles in succession.

1.7.3 Part 2: experimental tests on different minichannel geometries

The importance of the water drainage on the performance of a minichannel evaporator has been dealt with in paragraph 1.5.7. In this part, some options are tested, in order to find the solution that can provide the best moisture drainage. Different geometries and a surface treatment have been considered. The heat exchanger samples were manufactured by Valmex SpA; the support of Mr. P. Faldelli, Mr. R. Brignoli and Mr. G. Betti is gratefully acknowledged

1.7.3.1 Studied geometries

The considered geometries are reported in Table 1.7.8. All those configurations have vertical tubes and horizontal headers: this position is the most favorable for the water drainage. The "A" sample is the traditional and the cheapest one: the depths of the tubes and of the fins are the same; its fin pitch and tube pitch are the largest ones, thus its external area is the smallest one. The fin depth of the "B" sample is larger than the tube depth: the aim is to investigate if this fact can increase the moisture drainage. This geometry was studied with two different fin pitch, 2.6 mm ("B") and 3 mm ("B mod"). As regards the C sample, its tube depth is larger than the fin depth: in this case, the external are of the tubes is the largest one. The chosen configurations are those which can provide the best results, not introducing technical solutions which can make more complex (and expensive) the manufacturing process. All of the finned coils have been manufactured in two versions, with and without a hydrophilic surface treatment, which can improve the water drainage. In addition, two different tube lengths have been chosen, 30 and 50 cm, to investigate its effect on the water drainage. In fact, with a higher tube length, the water path is longer and the drainage is more difficult.

216

	A	B	B mod	C
HX width [m]	1	1	1	1
N. tubes	80	99	99	99
Tube pitch [m]	0.0125	0.01	0.01	0.01
Tube depth [m]	0.021	0.016	0.016	0.021
Tube width [m]	0.002	0.002	0.002	0.002
Fin thickness [m]	0.0001	0.0001	0.0001	0.0001
Fin pitch [m]	0.004	0.0026	0.003	0.003
N. fin	250	384	333	333
Fin length [m]	0.0105	0.008	0.008	0.008
Fin depth [m]	0.021	0.018	0.018	0.018
Tube external area [m^2]	3.596	3.442	3.459	4.416
Fin external area [m^2]	4.410	5.474	4.747	4.747
External area [m^2]	8.006	8.917	8.206	9.163

Table 1.7.8: Tested heat exchanger geometries

The surface treatment is here schematically resumed:
- degreasing through an alkaline substance
- cleaning
- neutralization by nitric acid
- titanium chemical conversion
- cleaning and blowing
- hydrophilic surface treatment, through immersion in a bath composed by a polymer (nylon), Cr3 and an antibacterial product (optional)
- blowing
- heating at 120°÷160°C in furnace.

1.7.3.2 *Experimental tests*

These experimental tests are just comparative: the aim is to compare two solutions and to identify the one that can drain the larger quantity of water, under the same conditions. Thus it is important to keep the same conditions for both heat

exchangers, which are the same external area and the same water mass flow rate in the heat exchanger. The geometries have been modified as reported in Table 1.7.9: the number of tubes was changed in order to get the same external area. The external area is the one of a finned coil of face dimensions 300 x 300 mm; each external area was related to the maximum one, that is the one of the sample C. The tube length must be the same, thus the number of tube of each heat exchanger is increased.

	A	B	B mod	C
External area [m^2]	0.721	0.802	0.739	0.825
Ratio Ae/Ae max	0.874	0.973	0.896	-
Adjusted face area [m^2]	0.103	0.092	0.100	0.09
Adjusted external area [m^2]	0.825	0.825	0.825	0.825
HX width [m]	0.343	0.308	0.335	0.3
N. tubes	27	31	33	30

Table 1.7.9: Tested heat exchanger samples

The test facility is schematically depicted in Figure 1.7.18 and in the pictures of Figures 1.7.17. The two heat exchanger are placed inside a closed box of 93 x 93 x 61 cm, and fed with cold water (8°C) produced by a R404A chiller. The water mass flow rates are the same and they are regulated by two valves upstream both heat exchangers, in order to keep 1°÷1.5°C temperature difference between the water inlet and outlet. In the box, saturated vapor is sprayed inside: the hot vapor, coming into contact with the cold surfaces of the heat exchangers, condenses and the drained water is collected into two different small vessels, placed under both heat exchangers. The test duration can vary, according of the quantity of vapor produced by the vapor generator. At the end of the test, the two vessels are weighted and the quantities of water compared.

The most remarkable limit of this analysis is the absence of forced air flow against the heat exchangers, because of narrow dimensions of the testing box; in addition, the use of fans with electrical engines in a closed volume saturated with vapour was not safe. The study of the effect of air flow on the water drainage will be the subject of future researches in the Department of Fisica Tecnica.

(a)   *(b)*

(c)   *(d)*

Figure 1.7.17: The test facility; the two heat exchanger inside the box (a), the vapour inlet (b), the two valves (c) and the whole box (d)
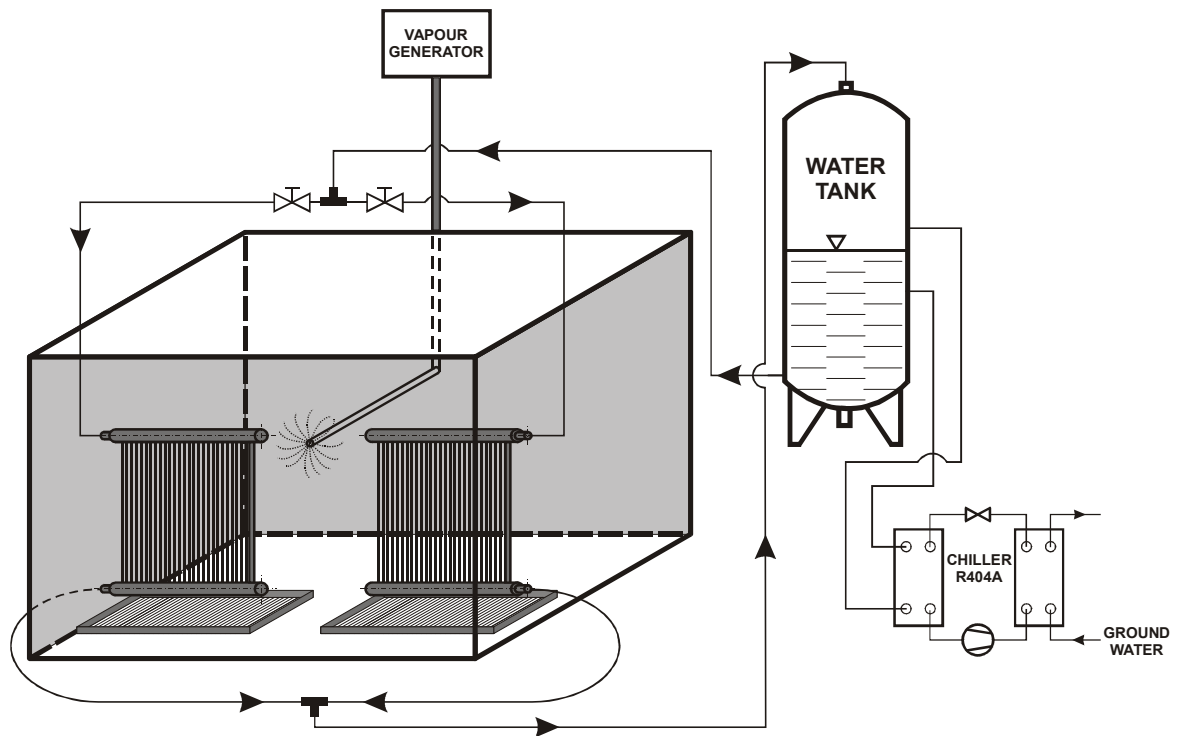
Figure 1.7.18: The test facility

1.7.3.3 Experimental results

The results of the comparison between the different options, without the surface treatment, are resumed in Tables 1.7.10. The configurations which drained the larger quantity of water are marked in yellow. The comparison between the options "A" and "B" was not carried out: actually, it should be the comparison between the best and the worst configuration. From these results, the best solution is "A", followed by "C", "B mod" and "B". Thus, the depth of the tube does not penalize the moisture drainage, while the fin pitch affects it, as proved by the comparison between "B" and "B mod". Without the surface treatment, the favored solution is that with the most space between the tubes and the fins, but which needs the largest face area to provide the same heat exchange. The experimental results are plotted in the following diagrams. The moisture drainages are reported in Table 1.7.11.

Type	A	B mod	A	C
Water quantity [g]	774	712	549	500
Difference [g]	62		49	
Difference [%]	8.01		8.93	
Time [m]	200		140	

Type	B	B mod	B	C
Water quantity [g]	322	361	499	566
Difference [g]	39		67	
Difference [%]	10.80		11.84	
Time [m]	100		160	

Type	B mod	C
Water quantity [g]	142	169
Difference [g]	27	
Difference [%]	15.98	
Time [m]	60	

Table 1.7.10: Test results for heat exchangers without surface treatment

Type	Total drainage [g/h]	Total drainage / external area [g/(m²h)]
A	230÷240	280
B	190÷200	230
B mod	200÷210	250
C	210÷220	260

Table 1.7.11: Water drainage for heat exchangers without surface treatment

In Tables 1.7.12, the comparisons of each configuration, with and without surface treatment, are reported. The treatment improves the water drainage, especially in the geometries with some solution to drain the moisture. For the "A" configuration, the improvement is negligible. Finally, the best solution without the surface treatment was compared to the most promising solution with the surface

treatment, in order to find a configuration with good drainage features but that does not need a too large face area. Thus, "A" and "C t" solutions have been compared: the difference is very low and it is possible to conclude that they drain the water in the same way. The water drainage (Table 1.7.13) is the same for "A" and "A t", while for the other configurations the drainages of the treated heat exchangers are higher.

Type	A	A t	B mod	B mod t
Water quantity [g]	270	281	359	405
Difference [g]	11		46	
Difference [%]	3.91		11.36	
Time [m]	80		110	

Type	C	C t	A	C t
Water quantity [g]	408	444	359	405
Difference [g]	36		46	
Difference [%]	8.11		11.36	
Time [m]	120		110	

Table 1.7.12: Test results for heat exchangers with surface treatment

Type	Total drainage [g/h]	Total drainage / external area [g/(m²h)]
A t	230	280
B mod t	210	250
C t	220	270

Table 1.7.13: Water drainage for heat exchangers without surface treatment

The last tests are those on the heat exchangers of 50 cm of tube length (Tables 1.7.14); the comparisons were made only between the two most promising configurations, "A" and "C". The advantage of the hydrophilic treatment is clear: the "C t" sample is able to drain more water than both "C" and "A", even if in the second case the difference is very low. Considering the drained water (Tables

1.7.15), it is worth notice that the specific quantity is not much lower than the quantity of the heat exchangers of 30 cm tube length (the percentage difference is lower than 10%).

Type	C	C t	A	C t
Water quantity [g]	312	365	630	659
Difference [g]	53		29	
Difference [%]	14.65		4.40	
Time [m]	60		110	

Table 1.7.14: Test results for heat exchangers of 50 cm tube length

Type	Total drainage [g/h]	Total drainage / external area [g/(m²h)]
A	340	250
C	320	230
C t	360	260

Table 1.7.15: Water drainage for heat exchangers without surface treatment

1.7.3.4 Conclusions

The objectives of these experimental tests were to investigate the water drainage attitude of different geometrical configurations of minichannel heat exchangers with vertical tubes and to identify one (or more) promising solution, in order to realize a minichannel evaporator. The importance of the moisture drainage in these evaporators is capital, as discussed in paragraph 1.5.7. In addition, the effects of a hydrophilic surface treatment and the tube length have been investigated. Some comparative test have been conducted in the laboratory of the Department of Fisica Tecnica; two heat exchangers, fed with cold water, were placed in a closed, vapour saturated volume, and the water drained, collected in two vessels, was weighted at the end of the test.

The following conclusions can be drawn:
- the configurations with fin depth larger than tube depth ("B" and "B mod") are not suitable for minichannel evaporators;

- the easiest and cheapest solution ("A") is able to drain the largest quantity of water, in the case of absence of surface treatment. On other hand, its external area is the smallest one: to reach the same heat capacity, a larger face area is needed;

- the solution with tube depth larger than fin depth ("C") is interesting, especially with a hydrophilic surface treatment: in this case, the performance is the same of the configuration "A";

- the hydrophilic surface treatment improves the quantity of drained water of around 10%, except for the configuration "A";

- higher fin pitch can favor the water drainage;

- the tube length affects the water drainage, but for a tube length of 50 cm its performance can be considered of the same order of the tube length of 30 cm, being lower of less than 10%.

The most remarkable limit of this analysis is the absence of forced air flow: it may favor the water drainage and it will be the subject of future researches in the Department of Fisica Tecnica.

1.7.4   References

1. Domanski P. A., Didion D. A., Doyle J. P., (1994), Evaluation of suction-line/liquid-line heat exchange in the refrigeration cycle, *Int. J. Refrigeration,* Vol. 17, No. 7, pp. 487-493.

2. Hanson O. W., Van Essen L. J., (2001), Evaporator with enhanced refrigerant distribution, *U.S. Patent No. 6,318,118 B2*.

3. Memory S., Hughes G., Zhang W., Rogers C. J., Grohman C., Robinson E., Mielke R., Wattelet J. P., Gabbey L., Trapp R. J., (2006), Method of fabricating a heat exchanger, *U.S. Patent No. 7,032,313 B2*.

PART 2   EFFICIENCY AT PART LOAD CONDITIONS

In this part, the subject of the energy efficiency is faced considering the system at part load conditions. This is a more recent and correct way to quantify the actual energy consumptions of a system.

In Chapter 2.1, a simplified method to evaluate the system performance at part load conditions is presented: The aim of this model is to provide an easy and reliable simulation tool, to overcome the problems of predicting the system energy consumption under different part load running conditions. In Chapter 2.2, different control modes of an air conditioning system are presented. In this case, the efficiency at rating conditions is the same: the objective is to achieve the higher seasonal energy efficiency. The different control algorithms are first simulating and then tested in industrial prototypes. In Chapter 2.3, a control algorithm for a radiant cooling system with fan coils, is presented. This control logic has been developed with the objective of reducing the energy consumption assuring the same level of comfort. The target is to maximize the sensible heat absorbed by the radiant system and the main limit is to prevent the water condensation on the panel surface.

Chapter 2.1   A SIMPLIFIED METHOD TO EVALUATE THE SEASONAL ENERGY
PERFORMANCE OF WATER CHILLERS

In this chapter the concept of seasonal energy efficiency is introduced. A mathematical model to evaluate the seasonal energy performance was developed, starting from the method proposed in Chapter 1.2; in that part, chillers EERs of different refrigerants, under different working conditions, are presented. Actually, air conditioning chillers usually do not operate at design conditions; performances at part load ratio were estimated and compared to experimental tests.

The present work is the subject of a paper ("A simplified method to evaluate the seasonal energy performance of water chillers", Cecchinato L., Chiarello M., Corradi M.) which, was submitted to and, at the moment, is being revised by the scientific committee of the *International Journal of Thermal Science*. The experimental data were provided by Rhoss S.p.A.; the support of Mr. M. Albieri, Mr. E. Pasut and Mr. P. Faldelli is gratefully acknowledged.

2.1.1   Introduction

In November 2008 the European Commission adopted a proposal for a new Energy Performance of Building Directive (EPBD). In order to certify the energy consumption of a building equipped with a vapour compression cycle refrigerating or heating unit, the seasonal efficiency must correctly be evaluated. In fact, many of the potential energy savings associated to building heating and cooling operations are related to the systems optimization under part load conditions, as pointed out by Adnot and Waide (2003) and Bettanini *et al.* (2003). Rating conditions, in fact, do not represent the usual operating conditions of the equipment over a season. To be really efficient, refrigeration units have to be designed not on the basis of nominal operating conditions but on a variety of part load conditions, which better reflect their real life behaviour associated to the variations of both the building load demand and the heat exchangers secondary fluid temperatures.

In the open literature there are several methods to evaluate the performance of a refrigerating or heating unit; EN ISO 13790 standard (2008) on the energy performance of buildings contains a calculation method of the monthly energy use under steady-state conditions hypothesis. In alternative the calculation of the building thermal load can be made using dynamic procedures (EN 15265, 2007). Whichever is the chosen method, the assessment of the primary energy consumption and of the average performance of the plant is a fundamental step for the correct evaluation of a building energy performance. Normally it is carried out in steady-state conditions on a time interval equal to the time step of the building load calculation method (one month for the EN ISO 13790 one and usually one hour for dynamic simulation methods) (UNI 11135, 2003). As far as vapour compression systems are concerned, this procedure consists of two steps. At first, basing on the actual temperature and mass flow rate values at the unit heat exchangers, the calculation of the cooling or heating capacity and of the system efficiency in terms of EER at full load working conditions has to be done. Second, the cooling or heating capacity regulation system effects on the refrigeration unit performance have to be evaluated. The part load ratio (PLR) can be defined as the ratio of the building thermal load and the machine full capacity. The part load influence is taken into account by multiplying the full load EER by a part load factor (PLF) calculated. The data necessary for the application of this procedure are often partly or completely lacking. The system full load performances as a function of temperature and mass flow rate values at the unit heat exchangers are sometimes present in manufacturer data sheets, but in most cases only nominal rating conditions are reported. As already pointed out by Bettanini *et al.* (2003), machine part load performances are never supplied. A PLR independent and constant value of the part load factor can be obtained if a manufacturer data sheet reports the ESEER index, namely the European Seasonal Energy Efficiency Ratio (ESEER), as defined by Eurovent (2005) and described in paragraph I1.2. PLF can be defined directly as the ratio of the ESEER and the machine EER at nominal rating conditions. European committee for standardization (CEN) TC113/WG7 is working to develop a similar European standard to rate seasonal performance indices of all HVAC equipments. In November 2009 a draft standard prEN 14825 was released and submitted to the CEN public enquiry.

Refrigeration systems simulation models are normally useless because of the

large amount of input data required for a full characterization. A simplified numerical method for the performance prediction of vapour compression heat pumps and chillers is used. This model was partly introduced in paragraph 1.2 to evaluate the EER of chiller and heat pump units under different external air temperature. In this chapter, that method is developed adding the correlations to evaluate the performance under part load conditions. It predicts the unit cooling or heating capacity and power absorption at part load conditions and at different heat exchangers secondary fluid inlet temperatures basing only on the nominal rating condition manufacturer declared results. The unit compressor performance data, together with thermal capacity control and simple refrigerant circuit information, are also needed. The proposed procedure is validated against experimental data of packaged air-cooled water chillers, operating on scroll compressors. Single compressor, double compressors and inverter driven units are tested.

2.1.2   Nomenclature

The used symbols are those presented in paragraph 1.2.2. In this section, the symbols related to the simulations at part load conditions are added.

C_c cycling degradation factor [-]

d heat exchanger hydraulic diameter [m]

fq compressor capacity partialization rate [-]

n circuits number [-]

n_f fans number [-]

PLF part load factor [-]

PLR part load ratio [-]

S cross sectional area [m^2]

w_P partialization power absorption correction factor [-]

w_Q partialization cooling capacity correction factor [-]

Greek letters

Δ difference

η_{el} electric efficiency [-]

Subscripts

el   electrical

load actual load condition

PL part load condition

2.1.3   Mathematical model

The mathematical model was introduced in paragraph 1.2.3. In this part it is developed introducing the equations for systems with cooling or heating capacity control and for performances under part load conditions.

2.1.3.1 Equations for systems with capacity control

In presence of systems with cooling or heating capacity control, such as multi-compressor scroll chillers, multi-step screw compressor machines or inverter driven units, equations (1) and (2) of paragraph 1.2.3 can be rewritten as a function of the number of active compressors, *N*, of the compressor capacity partialization rate, fq, the correction factors w_P and w_Q of the compressor performances as a function of the cooling capacity partialization step:

$$\hat{Q}_e = \sum_{k=1,N} \left(a_{1,k} + a_{2,k} \cdot T_e + a_{3,k} \cdot T_c + a_{4,k} \cdot T_e^2 + a_{5,k} \cdot T_e \cdot T_c + a_{6,k} \cdot T_c^2 + \ldots \right.$$
$$\left. \ldots + a_{7,k} \cdot T_e^3 + a_{8,k} \cdot T_e^2 \cdot T_c + a_{9,k} \cdot T_e \cdot T_c^2 + a_{10,k} \cdot T_c^3 \right) \cdot \frac{fq_k}{fq_{k,D}} \cdot w_{Q,k} \left(fq_k \right) \quad , \quad (1)$$

$$\hat{P}_k = \sum_{k=1,N} \left(b_{1,k} + b_{2,k} \cdot T_e + b_{3,k} \cdot T_c + b_{4,k} \cdot T_e^2 + b_{5,k} \cdot T_e \cdot T_c + b_{6,k} \cdot T_c^2 + \dots \right.$$

$$\left. \dots + b_{7,k} \cdot T_e^3 + b_{8,k} \cdot T_e^2 \cdot T_c + b_{9,k} \cdot T_e \cdot T_c^2 + b_{10,k} \cdot T_c^3 \right) \cdot \frac{fq_k}{fq_{k,D}} \cdot w_{P,k} \left(fq_k \right) \quad , \qquad (2)$$

If the number of refrigerant or secondary fluid circuits of the refrigeration unit does not correspond to the number of compressors, it is mandatory to correct equation (17) of paragraph 1.2.3. This expression expresses the heat exchangers design transmittance correction factor as a function of the actual unit working conditions. In general, the ratio between the number of active circuits, n, and their total number, n_D, depends on the machine architecture as a function of the number of active compressors, N; the new equation can be thus written as follow:

$$k = \left(\frac{A_{sf}}{A_{sf,D}} \right) \cdot \frac{1 + \left(\frac{\alpha_{sf}}{\alpha_r} \right)_D \cdot \left(\frac{A_{sf}}{A_r} \right)_D}{\left[\frac{\sum_{j=1,n_{sf}} \left(n_{sf,D} \cdot \frac{\dot{m}_j}{\dot{m}_D} \right)_{sf}^{m_{sf}}}{n_{sf}} \right]^{-1} + \left(\frac{\alpha_{sf}}{\alpha_r} \right)_D \cdot \left(\frac{A_{sf}}{A_r} \right)_D \cdot \left[\frac{\sum_{j=1,n_r} \left(n_{r,D} \cdot \frac{\dot{m}_j}{\dot{m}_D} \right)_r^{m_{sf}}}{n_r} \right]^{-1}} \quad , \qquad (3)$$

where $\dot{m}_j$ is the j-th refrigerant or secondary fluid circuit mass flow rate while the ratio between the secondary fluid heat transfer area in actual working and design conditions $\left(\frac{A_{sf}}{A_{sf,D}} \right)$ refers to the surface portion subject to heat transfer phenomena between refrigerant and secondary fluid. For example in an evaporator with two refrigerant circuits, each coupled to a compressor, and only one water circuit, this ratio is equal to 0.5 if one compressor is switched off. The auxiliaries design power absorption must also be corrected as a function of the secondary fluids active circuits:

$$P_{aux} = P_{aux,D} \left(\frac{n}{n_D} \right)_{sf} \qquad (4)$$

Usually air condensed units for civil and commercial refrigeration are equipped with condensation temperature control systems to assure safe working conditions for the compressor and the expansion valve. These systems regulate the condenser air volumetric flow rate in order to keep or the condensation temperature above a minimum value, $T_{c,min}$, or the pressure difference at the two ends of the throttling valve, above a minimum value, $\Delta p_{c,min}$. In this case, the system (16) of paragraph 1.2.3 must be replaced with the following constrained equations system:

$$\begin{cases} f_e\left(T_e, \dot{V}_{sf,c}\right) = UA_e - UA_{e,D} \cdot k_e = 0 \\ f_c\left(T_e, \dot{V}_{sf,c}\right) = UA_c - UA_{c,D} \cdot k_c = 0 \\ T_c = T_{c,min} \ \text{or} \ T_c = T\left(p_e + \Delta p_{min}\right) \end{cases} \tag{5}$$

Neglecting condenser air density and viscosity variations, fans power absorption depends on their speed control system as a function of the ratio between actual and design flow rate. For units with multiple fans in parallel and relay control, the power absorption can be expressed by:

$$P_{aux} = P_{aux,D}\left(\frac{\dot{V}_{sf}}{\dot{V}_{sf,D}}\right) = P_{aux,D}\left(\frac{n_{f,sf}}{n_{f,sf,D}}\right) \tag{6}$$

For fans with frequency regulation or with brushless motor, being the condenser averaged friction factor proportional to the q-th power of the Reynolds number and to the fan motor electrical efficiency, the following relation can be given:

$$P_{aux} = P_{aux,D} \cdot \left(\frac{\eta_{el,D}}{\eta_{el}}\right) \cdot \left(\frac{\dot{V}_{sf}}{\dot{V}_{sf,D}}\right)^{3+q} \tag{7}$$

2.1.3.2 Equations for part load condition running

The effect of the part load working of the refrigeration unit is calculated on the basis of its full load performance and strictly depends on its capacity control system. For single compressor units with simple relay control law, the part load

factor, PLF, can be calculated with the equations proposed in the European and Italian standards, PrEN 14825 (2009) and UNI 10963 (2001) respectively, as a function of the part load ratio, PLR:

$$PLF = \frac{PLR}{C_c \cdot PLR + \left(1 - C_c\right)} \tag{8}$$

where C_c is a degradation factor associated to the unit cycling operation losses. The part load factor is calculated as the ratio between the actual load condition, Q_{load}, and the unit full load cooling or heating capacity considering the operative secondary fluids temperature values. For a chiller or an heat pump system, the part load power absorption $P_{el,PL}$, cooling or heating capacity, $Q_{e,PL}$ and $Q_{c,PL}$, can be thus defined as a function of full load performance:

$$P_{k,PL} = PLF \cdot P_{el}, \ \ Q_{e,PL} = PLR \cdot Q_e \ \text{or} \ Q_{c,PL} = PLR \cdot Q_c \tag{9}$$

The system energy efficiency is subsequently obtained according to equations (10-11) of paragraph 1.2.3. In refrigeration units with multiple compressors or with compressors with different capacity steps, a step capacity control is usually adopted. In this case the full load capacity of each step is determined. It is now possible to determine the two steps which mostly approximate the actual load condition; the first one will have a lower capacity, the second one a higher one. The unit part load capacity, power absorption and efficiency are determined by linear interpolation between these two steps performances, as described in prEN 14825 (2009). If the smallest control step of the unit is higher than the required part load ratio, the performance data are obtained as detailed for single compressor units, considering this control step for calculating the unit full load parameters.

Finally for units with continuous capacity control by means of an inverter type compressor or by other means, the system (16) of paragraph 1.2.3 must be replaced with the following constrained equations system:

$$\begin{cases} f_e\left(T_e, fq\right) = UA_e - UA_{e,D} \cdot k_e = 0 \\ f_c\left(T_e, fq\right) = UA_c - UA_{c,D} \cdot k_c = 0 \\ Q_e = Q_{load} \ \text{or} \ Q_c = Q_{load} \\ fq \geq fq_{min} \end{cases} . \tag{10}$$

If the minimum continuous partialization rate, fq_{min}, determines a unit capacity higher than the actual load, the performance data are obtained as detailed for single compressor units, considering this minimum partialization rate for calculating the unit full load parameters.

2.1.4   The tested chillers and the test facility

Different packaged air-cooled water chillers, equipped with scroll compressors, are experimentally investigated. The chiller analyzed cooling capacity ranges from 25 to 50 kW.

Three systems were tested on the same test rig:

A1) single compressor unit;

A2) single compressor inverter driven unit, frequency operative range was 30-90 Hz;

A3) two compressors of the same size in tandem configuration;

The chillers main characteristics are summarized in Table 2.1.1. In every system, the evaporator superheat is controlled with a thermostatic expansion valve and no high pressure liquid receiver is present at the condenser outlet. The units condenser are ventilated with axial fans with fixed velocity which are switched on and off together with the compressor.

Chapter 2.1: A simplified method to evaluate the seasonal energy performance of water chillers

		Chiller		
		A1	**A2**	**A3**
Compressors				
Number		1	1	2
Manufacturer		Copeland	Danfoss	Copeland
Model		ZP154KCE -TFD	VSH088-G	1: ZP103KCE- TFD 2: ZP103KCE- TFD
Frequency range	[Hz]	50	30-90	50
Swept volume	[m^{3}h^{-1}]	24.7	12.8-37.8	1: 16.76 2: 16.76
Inverter		–	Danfoss CD302	–
Design info				
Refrigerant		R410A	R410A	R410A
Refrigerant circuits		1	1	1
Superheat	[K]	5	5	5
Water flow rate	[3600 kg s^{-1}]	4660	7395	6750
Fan power absorption	[W]	400	1050	1050

Table 2.1.1: Chillers data

The unit A1 cooling capacity is controlled by varying the compressor operation time on the base of the water tank outlet temperature. A simple relay control law is used, where the compressor is switched on and off when the controlled temperature reaches threshold values. During test water set point value was 7 °C while the temperature differential, namely the difference between the upper and lower threshold values, was set to 4 K.

The capacity of the unit A2 is controlled by varying compressor rotational speed by means of an inverter. The supply frequency is regulated by a feedback PID controller on the base of the water tank outlet temperature signal. If the compressor lower frequency value of 30 Hz is reached, the system is controlled with a relay law. During test water set point value was 7 °C whole temperature differential was set to 4 K during relay operations.

Unit A3 is a tandem unit with two compressors of the same size. This chiller is regulated with a relay water temperature control, being defined only two control states:

a) one compressor on and the other switched alternatively on and off,

b) only one compressor working intermittently.

The two compressors number of start-up is managed with a FIFO algorithm.

In Figure 2.1.1, the experimental test facility is schematically shown. The tested chiller is installed in a climatic room where air temperature can be controlled. The tested chiller is connected to a hydraulic section has a 45 liters water tank and a piping total volume of 36 liters. The pump constant water flow rate is 1.28 kg/s. The load section has an electrical heater, with a heating capacity in the range 0-80 kW and a 480 liters water tank. A brazed plate heat exchanger (BHE) is installed. Thermocouples and pressure transducers are placed as shown in Figure 2.1.1. Water temperatures are measured with Pt100 thermometers placed inside mixing chambers at the inlet and outlet of each heat exchanger. The refrigerant temperatures are measured with Pt100 thermometers placed on the pipe wall. A ±0.3 °C accuracy is estimated for all the temperature measurements. The refrigerant mass flow rate is measured by a Coriolis mass flow meter placed upstream of the throttling valve. The claimed accuracy is ±0.1% of reading. Water volumetric flow rates are measured by electromagnetic meters (accuracy ±0.2% of reading). The refrigerant pressures are recorded with strain-gauge transducers at compressor suction and discharge. The accuracy is ±10 kPa according to the calibration report from the manufacturer. Electrical absorbed power is recorded with an electronic transducer (with an accuracy ±0.5% of the reading value). All measurements signal are acquired with a 15 s sampling time.
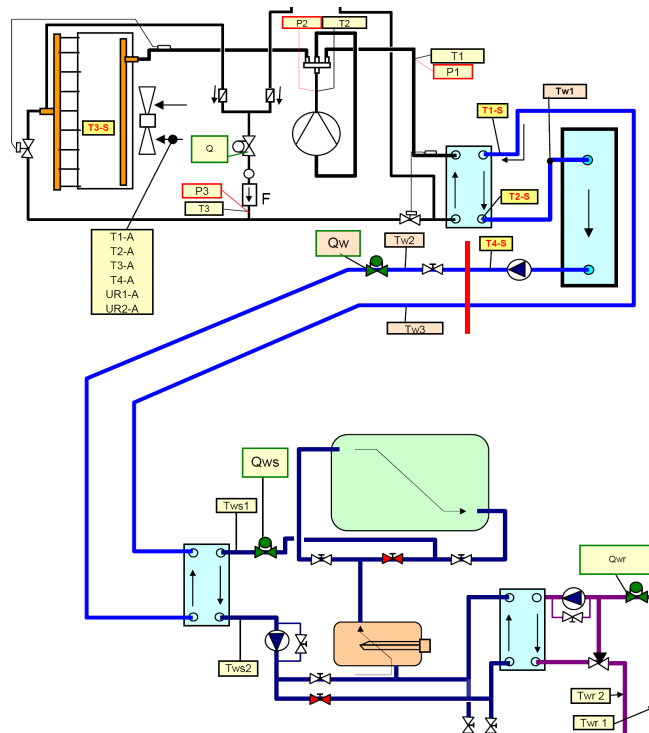
Figure 2.1.1: System test facility

2.1.5 Testing and simulation procedures

Tests have been carried out with the condenser positioned in a climatic room at constant air temperature. By controlling the heater thermal power, chillers have been tested in full load conditions and at part load conditions. Tests for determining seasonal energy efficiency ratios were further carried out following prEN 14825 (2008), Appendix A testing procedure. Climatic room air temperature was varied accordingly.

The mean systems efficiencies in terms of EER have been obtained by integrating the power absorption and the cooling capacity, computed from the instantaneous values of refrigerant mass-flow measured by a Coriolis effect mass flow meter, condenser outlet and evaporator outlet enthalpies, which are computed from pressure and temperature values on the basis of refrigerant properties as represented in the NIST Reference Fluid Thermodynamic and Transport Properties -

REFPROP, Version 7.0 (2002). The computed cooling capacity on the refrigerant side has been compared and validated with the computed capacity on the water side.

For relay controlled chiller working conditions, due to water temperature cycling during the test, the cooling capacity and the electrical power input were obtained from a time-integration of the energy balance on 4 duty cycles in thermal equilibrium conditions. The equilibrium was reached when the water tank outlet temperature average value of a duty cycle does not differ more than 0.2 K from the moving average value of the 4 previous cycles (see Figure 2.1.2). The chillers compression isentropic and volumetric efficiencies, η_{is} and η_v, are calculated with the following equations:

$$\eta_{is} = \frac{\dot{m} \cdot \left(h_{d,is} - h_s \right)}{P_{tot} - P_{fan}} \tag{11}$$

$$\eta_v = \frac{\dot{m}}{\dot{V} \cdot \rho_s} \tag{12}$$

where $\dot{m}$ is the refrigerant mass flow rate, h_s and $h_{d,is}$ are the compressor suction and isentropic discharge enthalpies, P_{tot} and P_{fan} are the total and fan supply power, $\dot{V}$ is the compressor swept volume and ρ_s the suction density.

238
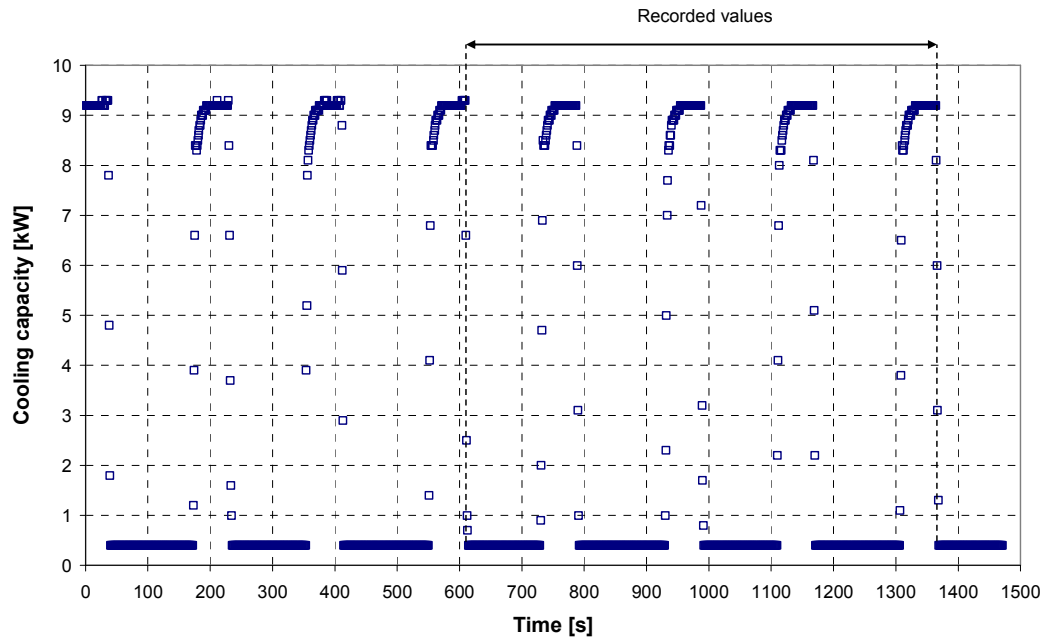
Figure 2.1.2: Example of experimental test recorded data (Chiller A1, external air temperature 20°C, water outlet temperature 7°C, PLR 25%).

The chillers were simulated with the mathematical model described in paragraph 1.2.3 and 2.1.3. The input data to the model are reported in Table 2.1.2. Compressors EN 12900 polynomial equations coefficients and the inverter driven compressor w_Q and w_P correction factors as a function of the supply frequency, were obtained from manufacturers catalogue data interpolation.

Refrigerant condensation and evaporation Reynolds m-th power coefficients were obtained with Cavallini and Zecchin (1971) and with the adapted Thonon correlation, proposed by Garcia-Cascales *et al.* (2007), in the hypothesis of dominant convective heat transfer, for the finned coil condenser and brazed plate evaporator respectively. Evaporator water Reynolds power coefficient was obtained from Muley and Manglik correlation (1999) while condenser air one was provided by the finned coil manufacturer.

		Chiller		
Design conditions		**A1**	**A2**	**A3**
Cooling capacity	[kW]	28.4	42.8	38.6
EER	[-]	2.30	2.36	2.39
Frequency	[kW]	50	90	1: 50, 2: 50
Condenser				
Saturation temperature	[°C]	52.8	51.6	49.7
Subcooling	[K]	0.0	4.5	0.0
A_{sf}/A_r	[-]	21.64	18.69	18.71
α_{sf}/α_r	[-]	$8.4 \cdot 10^{-3}$	$17.3 \cdot 10^{-3}$	$19.9 \cdot 10^{-3}$
Reynolds power coef., m_r	[-]	0.80	0.80	0.80
Reynolds power coef., m_{sf}	[-]	0.55	0.55	0.55
Secondary fluid		Air	Air	Air
Inlet temperature	[°C]	35	35	35
Temperature glide	[K]	12.4	10.7	10.4
Auxiliary power (fan)	[kW]	0.4	1.05	1.05
Evaporator				
Saturation temperature	[°C]	2.2	1.7	0.4
Superheat	[K]	5.0	5.5	5.0
A_{sf}/A_r	[-]	1	1	1
α_{sf}/α_r	[-]	1.013	1.000	0.987
Reynolds power coef., m_r	[-]	0.50	0.50	0.50
Reynolds power coef., m_{sf}	[-]	0.50	0.50	0.50
Secondary fluid		Water	Water	Water
Inlet temperature	[°C]	12.0	11.9	11.9
Temperature glide	[K]	5.2	5.1	4.9
Auxiliary power (pump)	[kW]	0.12	0.18	0.18

Table 2.1.2: Model input design conditions.

2.1.6 Experimental data and comparison with simulation results

A1-A3 chillers were tested on the experimental rig at full load and part load conditions. Condenser inlet air temperature, evaporator inlet water temperature and, for A2 unit, the compressor supply frequency were varied. Experimental test data and simulation results are listed in Tables 2.1.3 and 2.1.4.

Chiller A1

Experimental data		Part Load Factor PLF				
		100%	92%	91%	84%	78%
Air inlet temperature	[°C]	35.0	30.0	30.0	24.8	20.3
Water inlet temperature	[°C]	12.0	12.4	11.8	12.1	12.2
Evaporation temperature	[°C]	2.2	1.5	1.0	0.7	0.7
Condensation temperature	[°C]	52.8	48.2	47.9	43.2	39.2
Power absorption	[kW]	12.3	11.3	11.3	10.3	9.6
Cooling Capacity	[kW]	28.4	30.2	28.7	30.8	32.5
EER	[-]	2.30	2.66	2.73	2.77	3.40
Frequency	[Hz]	50.0	50.0	50.0	50.0	50.0

Model results		Part Load Factor PLF				
		100%	92%	91%	84%	77%
Air inlet temperature	[°C]	35.0	30.0	30.0	24.8	20.3
Water inlet temperature	[°C]	12.0	12.4	11.9	12.1	12.2
Evaporation temperature	[°C]	2.2	1.9	1.5	1.2	0.7
Condensation temperature	[°C]	52.8	48.9	48.6	44.6	40.7
Power absorption	[kW]	12.3	11.3	11.3	10.3	9.5
Cooling Capacity	[kW]	28.4	29.0	28.6	30.3	31.5
EER	[-]	2.30	2.56	2.54	2.94	3.32
Frequency	[Hz]	50.0	50.0	50.0	50.0	50.0

Table 2.1.3: A1 experimental data and simulation results at 12°C water inlet temperature for different working conditions

Chiller A2

Experimental data		Part Load Ratio PLR				
		100%	68%	42%	91%	44%
Air inlet temperature	[°C]	35.0	30.0	30.0	29.1	25.1
Water inlet temperature	[°C]	11.9	12.0	12.0	12.0	12.0
Evaporation temperature	[°C]	1.7	4.4	6.1	2.4	5.9
Condensation temperature	[°C]	51.6	40.8	37.7	43.3	35.3
Power absorption	[kW]	18.1	8.6	5.1	12.8	4.6
Cooling Capacity	[kW]	42.8	29.1	18.1	38.7	18.7
EER	[-]	2.36	3.36	3.56	3.02	4.09
Frequency	[Hz]	90.0	49.6	30.0	69.8	30.0

Model results		Part Load Ratio PLR				
		100%	67%	43%	88%	45%
Air inlet temperature	[°C]	35.0	30.0	30.0	29.1	25.1
Water inlet temperature	[°C]	11.9	12.0	12.0	12.0	12.0
Evaporation temperature	[°C]	1.7	4.0	5.7	2.5	5.5
Condensation temperature	[°C]	51.6	41.7	38.1	43.9	33.6
Power absorption	[kW]	18.1	8.8	4.9	12.6	4.6
Cooling Capacity	[kW]	42.8	28.7	18.3	37.8	19.1
EER	[-]	2.36	3.27	3.74	3.00	4.19
Frequency	[Hz]	90.0	49.6	30.0	69.8	30.0

Table 2.1.4: A2 experimental data and simulation results at 12°C water inlet temperature for different working conditions

Experimental tests were also conducted at fixed part load ratio, following the instruction of prEN 14825 (2009) in order to calculate the ESEER of the chiller. In this case, the system is controlled through the water temperature at the chiller outlet, set at 7°C. The results for the chiller A2 are reported in Table 2.1.5.

Chiller A2

Experimental data		Part Load Ratio PLR			
		100%	75%	50%	37%
Air inlet temperature	[°C]	35.1	30.3	25.1	20.0
Water inlet temperature	[°C]	11.9	10.7	9.5	8.8
Evaporation temperature	[°C]	1.7	2.4	2.2	2.9
Condensation temperature	[°C]	51.6	41.7	34.7	33.0
Power absorption	[kW]	18.1	10.0	6.0	4.3
Cooling Capacity	[kW]	42.8	32.3	21.4	15.8
EER	[-]	2.36	3.24	3.57	3.72
Frequency	[Hz]	90.0	59.0	39.3	30.0

Model results		Part Load Ratio PLR			
		100%	74%	53%	43%
Air inlet temperature	[°C]	35.1	30.3	25.1	20.0
Water inlet temperature	[°C]	11.9	10.7	9.5	8.8
Evaporation temperature	[°C]	1.7	2.2	2.4	2.4
Condensation temperature	[°C]	51.6	43.1	34.8	28.3
Power absorption	[kW]	18.1	10.6	6.1	4.2
Cooling Capacity	[kW]	42.8	31.7	22.8	18.2
EER	[-]	2.36	2.99	3.72	4.33
Frequency	[Hz]	90.0	59.0	39.3	30.0

Table 2.1.5: A2 experimental data and simulation results at 7°C water outlet temperature for different working conditions. Data for ESEER calculation.

Experimental tests were also carried out at the same external air temperature (35°C) and the same water temperature at the chiller inlet (12°C) or the same water temperature at the chiller outlet (7°C) but at different part load ratio. These tests were conducted on chiller A2 and A3; in the case of the tandem configuration, one or two compressors are active. Results are reported in Table 2.1.6, 2.1.7, 2.1.8 and 2.1.9.

Chiller A2

Experimental data		Part Load Ratio PLR						
		100%	94%	85%	76%	65%	53%	40%
Air inlet temperature	[°C]	35.1	35.0	34.9	34.8	34.9	34.9	34.9
Water inlet temperature	[°C]	12.0	12.0	12.0	12.0	12.1	12.0	12.0
Evaporation temperature	[°C]	1.7	2.4	3.2	4.0	5.0	5.6	6.3
Condensation temperature	[°C]	52.0	50.6	48.7	47.0	45.1	43.4	41.8
Power absorption	[kW]	18.9	16.5	13.9	11.7	9.4	7.5	5.7
Cooling Capacity	[kW]	42.8	40.0	36.5	32.6	28.0	22.8	17.2
EER	[-]	2.26	2.42	2.62	2.79	2.97	3.05	3.01
Frequency	[Hz]	90.0	79.9	69.9	60.1	49.7	40.0	30.0

Model results		Part Load Ratio PLR						
		100%	92%	84%	75%	64%	53%	40%
Air inlet temperature	[°C]	35.1	35.0	34.9	34.8	34.9	34.9	34.9
Water inlet temperature	[°C]	12.0	12.0	12.0	12.0	12.1	12.0	12.0
Evaporation temperature	[°C]	1.8	2.3	2.9	3.6	4.4	5.1	5.9
Condensation temperature	[°C]	51.6	50.2	48.9	47.5	46.1	44.6	42.7
Power absorption	[kW]	18.1	15.9	13.8	11.7	9.5	7.3	5.2
Cooling Capacity	[kW]	42.9	39.4	35.8	32.0	27.5	22.7	17.3
EER	[-]	2.37	2.48	2.60	2.74	2.90	3.09	3.32
Frequency	[Hz]	90.0	79.9	69.9	60.1	49.7	40.0	30.0

Table 2.1.6: A2 experimental data and simulation results at 35 °C air temperature and 12°C water inlet temperature for different part load ratios.

244

Chiller A2

Experimental data		Part Load Ratio PLR					
		100%	90%	79%	63%	49%	34%
Air inlet temperature	[°C]	35.0	35.0	35.0	35.0	35.0	35.0
Water inlet temperature	[°C]	11.5	11.1	10.7	9.9	9.3	8.5
Evaporation temperature	[°C]	2.0	2.3	2.7	2.2	2.9	3.3
Condensation temperature	[°C]	50.0	48.2	46.4	44.4	42.6	40.7
Power absorption	[kW]	15.5	13.2	11.1	9.1	7.4	5.8
Cooling Capacity	[kW]	39.1	35.2	30.9	24.7	19.3	13.3
EER	[-]	2.52	2.67	2.80	2.72	2.62	2.32
Frequency	[Hz]	80.0	70.0	60.0	50.0	40.0	30.0

Model results		Part Load Ratio PLR					
		100%	90%	79%	67%	54%	40%
Air inlet temperature	[°C]	35.0	35.0	35.0	35.0	35.0	35.0
Water inlet temperature	[°C]	11.5	11.1	10.7	9.9	9.3	8.5
Evaporation temperature	[°C]	1.9	2.2	2.4	2.5	2.7	2.7
Condensation temperature	[°C]	50.1	48.7	47.3	45.7	44.1	42.3
Power absorption	[kW]	15.8	13.7	11.6	9.4	7.2	5.1
Cooling Capacity	[kW]	39.0	35.0	30.7	25.9	20.9	15.5
EER	[-]	2.46	2.55	2.65	2.76	2.89	3.02
Frequency	[Hz]	80.0	70.0	60.0	50.0	40.0	30.0

Table 2.1.7: A2 experimental data and simulation results at 35 °C air temperature and 7°C water outlet temperature for different part load ratios.

Chiller A3

Experimental data		Part Load Ratio PLR					
		100%	100%	56%	53%	53%	52%
Air inlet temperature	[°C]	35.0	35.5	34.5	35.1	35.1	35.7
Water inlet temperature	[°C]	11.9	11.2	9.4	8.7	7.8	7.9
Evaporation temperature	[°C]	0.4	0.4	2.1	1.6	0.7	1.0
Condensation temperature	[°C]	49.7	50.1	43.0	43.1	43.3	43.4
Power absorption	[kW]	16.8	17.3	8.4	8.3	8.4	8.5
Cooling Capacity	[kW]	38.6	38.8	21.7	20.5	20.4	20.2
EER	[-]	2.39	2.33	2.81	2.68	2.63	2.57
Frequency	[Hz]	50.0	50.0	50.0	50.0	50.0	50.0
Active compressor	[n°]	2	2	1	1	1	1

Model results		Part Load Ratio PLR					
		100%	98%	57%	56%	54%	54%
Air inlet temperature	[°C]	35.0	35.5	34.5	35.1	35.1	35.7
Water inlet temperature	[°C]	11.9	11.2	9.4	8.7	7.8	7.9
Evaporation temperature	[°C]	0.4	0.0	1.4	0.8	0.0	0.1
Condensation temperature	[°C]	49.7	50.0	43.7	44.1	43.9	44.4
Power absorption	[kW]	16.8	16.9	8.0	8.1	8.0	8.1
Cooling Capacity	[kW]	38.6	37.8	22.0	21.4	20.9	20.8
EER	[-]	2.30	2.23	2.75	2.66	2.60	2.56
Frequency	[Hz]	50.0	50.0	50.0	50.0	50.0	50.0
Active compressor	[n°]	2	2	1	1	1	1

Table 2.1.8: A3 experimental data and simulation results at 35 °C air temperature and 7°C water outlet temperature for different part load ratios.

Chiller A3

Experimental data		Part Load Ratio PLR				
		100%	99%	62%	59%	58%
Air inlet temperature	[°C]	35.0	36.6	34.5	35.8	36.6
Water inlet temperature	[°C]	12.0	13.0	12.0	11.9	12.0
Evaporation temperature	[°C]	0.8	2.1	4.5	5.1	5.0
Condensation temperature	[°C]	49.8	52.1	43.3	43.1	44.0
Power absorption	[kW]	16.6	17.8	8.4	8.2	8.4
Cooling Capacity	[kW]	38.9	38.6	23.9	22.8	22.4
EER	[-]	2.437	2.251	3.090	3.044	2.904
Frequency	[Hz]	50.0	50.0	50.0	50.0	50.0
Active compressor	[n°]	2	2	1	1	1

Model results		Part Load Ratio PLR				
		100%	101%	61%	60%	60%
Air inlet temperature	[°C]	35.0	36.6	34.5	35.8	36.6
Water inlet temperature	[°C]	12.0	13.0	12.0	11.9	12.0
Evaporation temperature	[°C]	0.5	1.5	3.6	3.6	3.7
Condensation temperature	[°C]	49.7	51.4	44.2	45.3	46.0
Power absorption	[kW]	16.8	17.4	8.1	8.3	8.4
Cooling Capacity	[kW]	38.7	39.0	23.7	23.3	23.2
EER	[-]	2.30	2.24	2.93	2.82	2.77
Frequency	[Hz]	50.0	50.0	50.0	50.0	50.0
Active compressor	[n°]	2	2	1	1	1

Table 2.1.9: A3 experimental data and simulation results at 35 °C air temperature and 12°C water inlet temperature for different part load ratios.

In Figures 2.1.3 and 2.1.4 the comparison between predicted energy efficiency and cooling capacity as calculated by the proposed mathematical model and experimental data is shown. Despite three chillers were investigated under several conditions, any significant discontinuity in the results trends was not pointed out and all data were merged together on these two charts. It can be pointed out that approximately 86.8% and 92.1% of the predicted EER and cooling capacity values

respectively are consistent with the measured data within a relative deviation of ± 10%. If ± 5% deviation is considered, 65.8% and 86.8% of the predicted data are consistent. Table 2.1.10 reports average and standard deviations for the proposed model and the number of predicted values within ± 10% and ± 5% of experimental data.
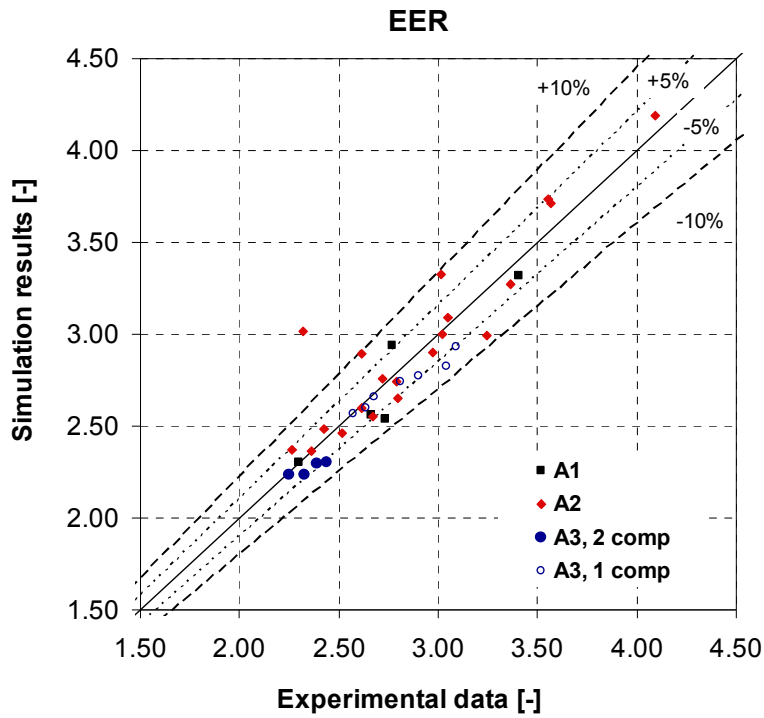
Figure 2.1.3: Comparison between model predicted energy efficiency and experimental results.

Cooling capacity
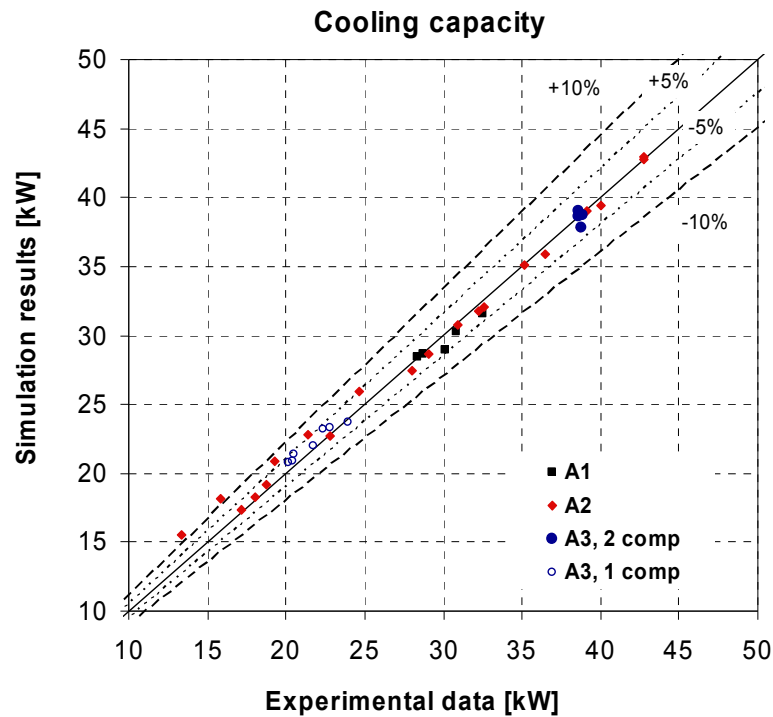
Figure 2.1.4: Comparison between model predicted cooling capacity and experimental results

		EER	Cooling capacity
Average deviation[a]	[%]	0.51	1.28
Standard deviation[b]	[%]	50.47	18.92
Points predicted within ± 10% of exp. data	[%]	86.8	92.1
Points predicted within ± 5% of exp. data	[%]	65.8	86.8

[a] $Ave.\,dev. = \frac{1}{n}\sum_{1}^{n}\left[\left(y_{pred} - y_{meas}\right)\times 100 / y_{meas}\right]$

[b] $Stan.\,dev. = \frac{1}{n}\sum_{1}^{n}\left[\left(y_{pred} - y_{meas}\right)\times 100 / y_{meas}\right]^{2} - Ave.\,dev.^{2}$

Table 2.1.10: Comparison between experimental measurements and model.

In Figures 2.1.5, 2.1.6 and 2.1.7, the comparison between the model estimated EER, evaporation and condensation temperature with the experimental ones is shown considering the influence of different operating parameters. In particular, in

Figure 2.1.5, the effect of the variation of the condenser inlet air temperature for the single scroll chiller A1 is accounted for, while water inlet temperature is kept constant at 12°C. In Figure 2.1.6, the sensitivity to the frequency on the estimation accuracy is pointed out for the inverter driven unit A2, while air temperature and water inlet temperature are maintained constant at 35 °C and 12 °C respectively. The model capability of predicting the tandem chiller A3 performance when evaporator water inlet temperature and the number of active compressors vary is plotted in Figure 2.1.7, keeping air temperature constant at 35 °C. The model larger deviations can be associated to A2 inverter driven chiller low supply frequency values and in particular to the underestimation of the compressor power absorption. This is strictly dependent from w_Q and w_P correction factors equations which were obtained from manufacturer catalogue data interpolation and resulted rather poor at low supply frequency.
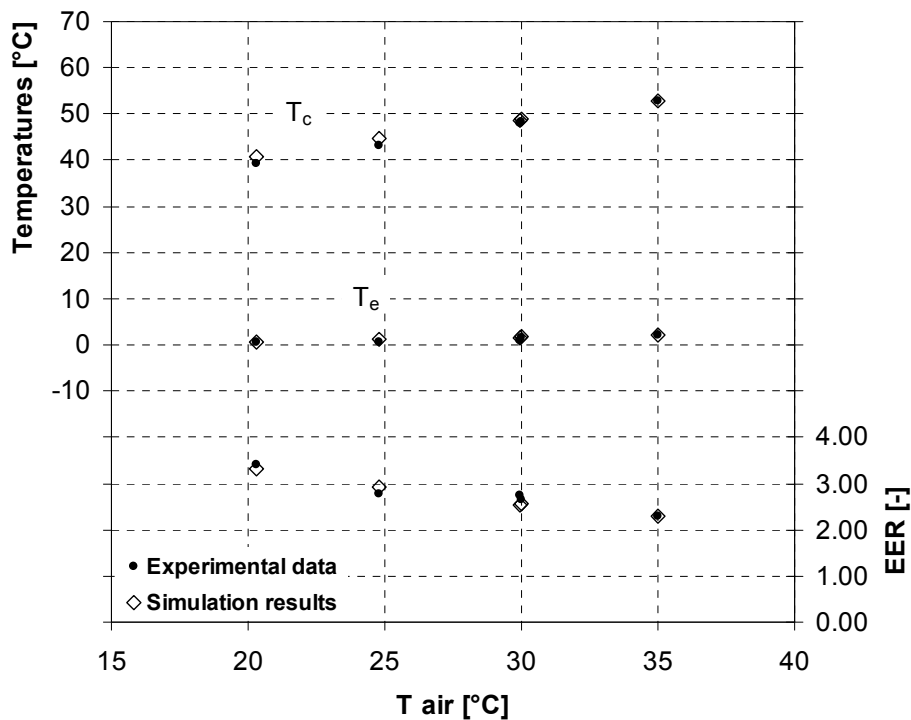

Figure 2.1.5: Experimental and simulated EER and saturation temperature values for A1 chiller at different air temperature and constant water inlet temperature (12°C).
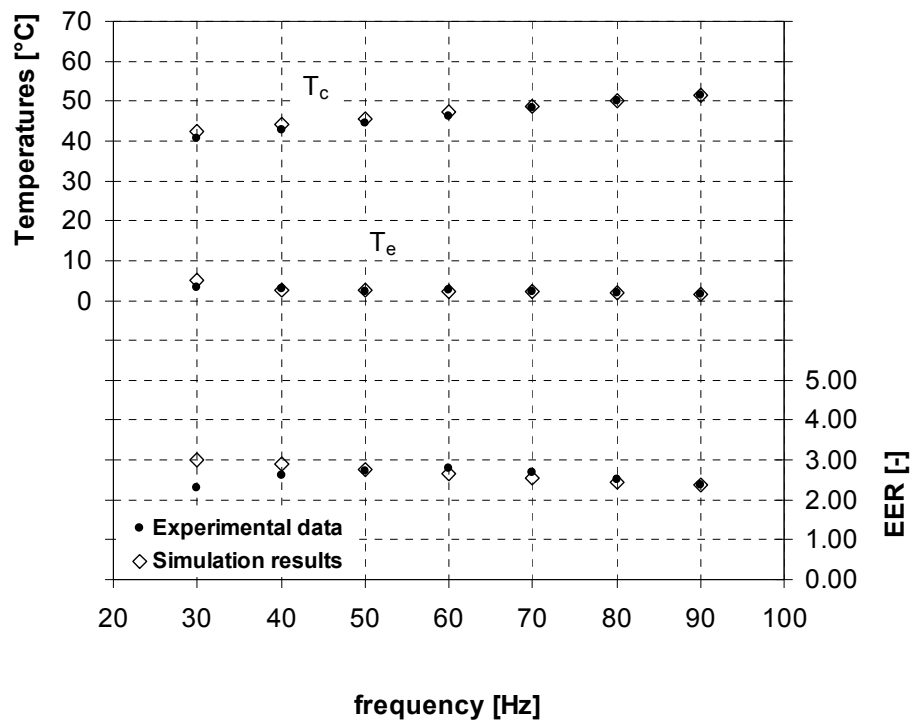
Figure 2.1.6: Experimental and simulated EER and saturation temperature values for A2 chiller at different compressor supply frequency values and constant water inlet temperature and air temperature (12°C).
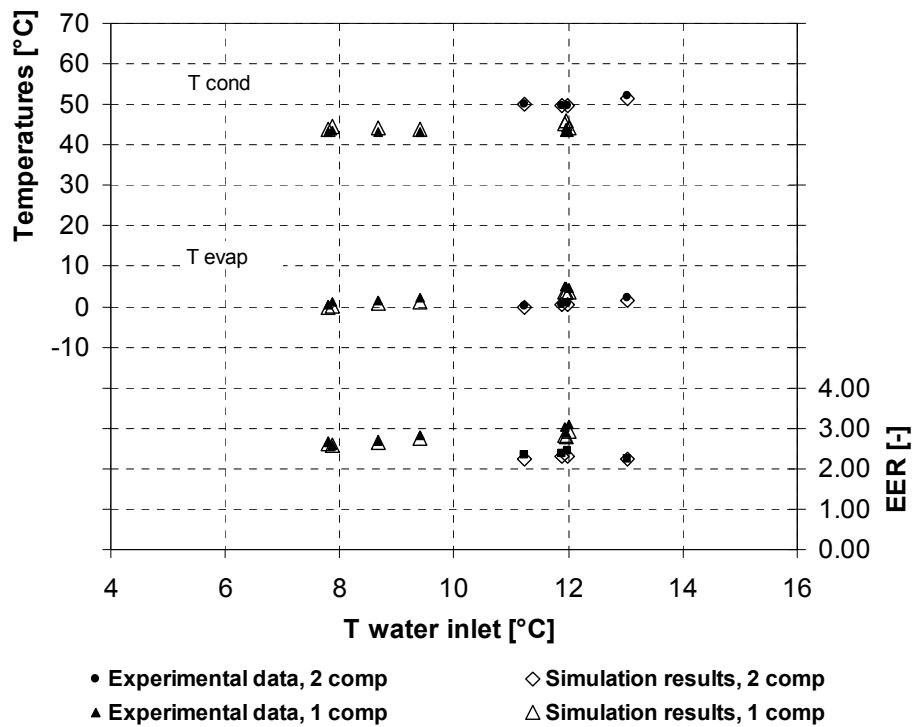
Figure 2.1.7: Experimental and simulated EER and saturation temperature values for A1 chiller at different water inlet temperature and constant air temperature. Data with two or only one active compressor are plotted.

In order to validate the proposed model under part load condition and to evaluate its capability of predicting yearly building energy consumptions, the experimental seasonal energy efficiency of the system was calculated. The seasonal efficiency has been evaluated for the load, air temperature and energy weighting coefficients with the SEERon (Seasonal Energy Efficiency Rating) calculation method for air to water units in a fan coil application as defined in the standard draft prEN 14825 (2009). In Table 2.1.11, both the experimental and simulated energy efficiency ratings EER for the four test conditions indicated in the calculation methodology and the seasonal energy efficiencies obtained for A1 and A2 units are reported. Model part load performance were obtained considering Table 2.1.1 A1 chiller data (columns 1 and 3 to 5) as full load conditions at the different air temperatures and a Cc degradation factor equal to 0.9 as suggested in the prEN 14825 standard. Experimental A1 chiller part load performances were measured with cycling tests. The model predicted SEERon values are in good agreement with experimental

results, the deviations are -3.2% and +5.1% for A1 and A2 chiller respectively.

	EER				SEER$_{on}$	Δ
Part Load Ratio [%]	25	50	75	100		
Ambient temperature [°C]	20	25	30	35		
Weighting coefficients [%]	30	40	26	4		
Experimental data						
A1	2.77	2.70	2.52	2.30	2.66	-
A2	3.72	3.57	3.24	2.36	3.48	-
Model results						
A1	2.62	2.52	2.64	2.30	2.57	-3.2%
A2	4.33	3.72	2.99	2.36	3.66	+5.1%

Table 2.1.11: Experimental seasonal efficiency ratio for A1 and A2 chillers.

2.1.7 Conclusions

In this Chapter a simplified numerical method for the performance prediction of vapour compression heat pumps and chillers is presented. The mathematical model estimates the unit cooling or heating capacity and power absorption at part load conditions and at different heat exchangers secondary fluids inlet temperatures basing only on the nominal rating conditions manufacturer declared results. The unit compressors performance data, together with thermal capacity control and simple refrigerant circuit information, are also needed. The proposed procedure was validated against experimental data of packaged air-cooled water chillers, operating on scroll compressors. Single compressor, double compressors and inverter driven units were tested. In chillers full load conditions approximately 86.8% and 92.1% of the predicted EER and cooling capacity values respectively are consistent with

the measured data within a relative deviation of ± 10%. If ± 5% deviation is considered, 65.8% and 86.8% of the predicted data are consistent. In order to validate the proposed model under part load condition, the chillers experimental seasonal energy efficiency ratios SEERon were calculated. Simulation results are in good agreement with experimental results, the deviations ranging from -3.2% to +5.1%. Thus, the proposed mathematical model showed a good accuracy in predicting both full load and part load chillers performance and appears to be a reliable tool to be implemented into dynamic building-plant energy simulation codes or into building energy certification tools.

2.1.8   References

1. Adnot J., Waide P., (2003), Energy Efficiency and Certification of Central Air Conditioners (EECCAC), *Final Report,* 3:39-68.
2. Bettanini E., Gastaldello A., Schibuola L., (2003), Simplified models to simulate part load performances of air conditioning equipments, *18th IBPSA Conf..* Proc. Building Simulation.
3. CEN EN 15265, (2007), Energy performance of buildings - Calculation of energy needs for space heating and cooling using dynamic methods - General criteria and validation procedures, European Committee for Standardization CEN.
4. CEN TC113/WG7, prEN 14825, (2009), Air conditioners, liquid chilling packages and heat pumps, with electrically driven compressors, for space heating and cooling – Testing and rating at part load conditions, European Committee for Standardization CEN.
5. EN ISO 13790, (2008), Energy performance of buildings - Calculation of energy use for space heating and cooling, International Organization for Standardization ISO.
6. Eurovent WG 6A, (2005), Eurovent certification program for liquid chilling packages, http://www.eurovent-certification.com.
7. Lemmon E. W., McLinden M. O., Huber M. L., (2002). "REFPROP 7.0", *NIST,* Standard Reference Database.

8. Muley A., Manglik R. M., (1999), Experimental study of turbulent flow heat transfer and pressure drop in a plate heat exchanger with chevron plates, *J. Heat Transfer*, 121(1):110-117.

9. UNI 10963, (2001), Condizionatori d'aria, refrigeratori d'acqua e pompe di calore. Determinazione delle prestazioni a Potenza ridotta, Ente Nazionale Italiano di Unificazione UNI (in Italian)

10. UNI 11135, (2003), Efficienza stagionale dei condizionatori, gruppi refrigeratori e pompe di calore- metodo di calcolo, Ente Nazionale Italiano di Unificazione UNI (in Italian).

11. UNI EN 12900, (2005), Refrigerant compressors. Rating conditions, tolerances and presentation of manufacturer's performance data, Ente Nazionale Italiano di Unificazione UNI.

Chapter 2.2   EFFICIENCY IMPROVEMENT BY USING DIFFERENT CONTROL MODES

In this chapter different control modes of a air conditioning chiller are studied. The objective is to achieve the highest seasonal energy efficiency, developing a control strategy that can improve the machine performance, not only under design conditions but also at part load ratios. Different solutions have been investigated, both on single compressor and on double compressor chiller units. These control strategies was developed by simulation environment based on Matlab/Simulink and compared to experimental tests.

The present work is the subject of two papers: Albieri M., Beghi A., Bodo C., Cecchinato L., 2009, Advanced control systems for single compressor chiller units, *International Journal of Refrigeration*, 32(5):1068-1076; Albieri M., Beghi A., Bodo C., Cecchinato L., Chiarello M., Fornasieri E., 2008, Refrigeratori d'acqua e pompe di calore con tecnologia per il basso consumo, *Mostra Convegno Expocomfort*, Milan, 11th −15th March 2008. The experimental data were provided by Rhoss S.p.A.; the support of Mr. M. Albieri and Mr. E. Pasut, for experimental tests, and of Mr. C. Bodo for theoretical modeling part, is gratefully acknowledged.

2.2.1   Introduction

As pointed out by the European Commission, a more prudent and rational use of energy resources and a reduction of the environmental impact of the energy use in buildings can be accomplished by increasing both the energy performance of new and existing buildings and the efficiency of cooling/heating systems. It is generally agreed that, in spite of the advancements made in computer technology and its impact on the development of new control methodologies for HVAC systems aiming at improving their energy efficiencies, the process of operating HVAC equipment in commercial and industrial buildings is still a low-efficient and high-energy consumption process (Yaqub and Zubair, 2001). Classical HVAC control techniques such as ON/OFF controllers (thermostats) and proportional-

integral-derivative (PID) controllers are still very popular, due to their low cost and ease of tuning and operation. Such simple control architectures can be easily tuned to operate the system at given, fixed design thermal loads. However, to achieve a satisfactory energy performance, more advanced strategies have to be employed. In fact, the actual thermal loads affecting the system vary in time and, therefore, the controller parameters have to be adjusted accordingly to prevent the production of thermal energy when there is no request from the user. Different authors demonstrated the applicability of advanced control methodologies to HVAC system management in order to improve its energy efficiency, mainly focusing on large capacity multi-chiller plants (Huguang and Cai, 2002; Shoureshi, 1993, Braun *et al.*, 1989a, Braun *et al.*, 1989b).

The improvement of the seasonal efficiency of HVAC systems can also be pursued through modifications of the traditional architectures of the plant. As pointed out by Venco (2003), the use of compressors of different size, connected to the same cooling circuit, can increase the system efficiency at part load ratios. An appropriate management of the ON/OFF cycles of the two uneven compressors can provide considerable energy savings of the unit.

In this chapter, a simulation environment based on Matlab/Simulink is presented; it is thus validated on a state-of-the-art experimental facility. The model was used to design an adaptive chiller controller that allows to substantially increase the energy performance of the system, as well as to achieve excellent regulation performances in process applications. As first step, the control of a low capacity HVAC system with single scroll chiller unit was developed, implemented on board and tested, comparing the performance to those of commercial units. The second step was applying the control to a multi-compressor chiller, comparing the seasonal energy efficiency of a chiller of two compressors of the same size and of different size. The SEERon indexes were calculated according to standard prEN 14825, as in explained in paragraph I1.2.

2.2.2   Nomenclature

A flow section [m^2]

cp specific heat at constant pressure [J kg^{-1}K^{-1}]

e   specific system energy [J kg^{-1}]

e$_c$ specific kinetic system energy [J kg^{-1}]

e$_p$ specific potential system energy [J kg^{-1}]

f   well-mixed volume fraction [-]

L   mechanical energy [J]

$\dot{m}$ mass flow rate [kg s^{-1}]

min   minimum function [-]

M   mass [kg]

Q   thermal energy [J]

RHS   right hand side

s   Laplace variable [-]

t   time variable [s]

t$_c$ water tank or piping time constant [s]

T   temperature [°C]

v   volumetric coordinate in the flow direction [m^3]

V   volume [m^3]

W   transfer function

x   linear coordinate in the flow direction [m]

ρ density [kg m^{-3}]

τ integration time [s]

Subscripts

f   water tank or piping well-mixed section outlet

H   hydraulic section

i   inlet

k   block index

259

L   load section

o   outlet

2.2.3   Mathematical model

In Figure 2.2.1 the block structure of the system is reported. Three basic blocks can be characterized:

1) the *energy production* section: a packaged air-cooled water chiller;
2) The *hydraulic* section: the chiller directly supplies a water tank connected to the user circuit with a constant flow rate pump. No primary/secondary system architecture is used.
3) The *load* section: the building thermal load and capacity is represented in the simulation scheme by an electrical heater and a water tank of suitable capacity. Such load model has been chosen to match the architecture of the experimental test facility on which the model has to be validated. The heat load is transferred to the hydraulic section by a plate heat exchanger (Plate HX in Figure 2.2.1).

The thermal behaviour of such a plant can be usefully analyzed by a lumped formulation of the conservation equations. The elements of the plant are simulated through blocks, and the heat transfer processes are considered as concentrated inside the blocks. Furthermore, the following hypotheses are introduced:

- The water thermal properties are considered constant;
- The water is considered incompressible;
- The three sections have constant water mass flow;
- There is no mass accumulation inside blocks;
- piping and water tanks are considered adiabatic.
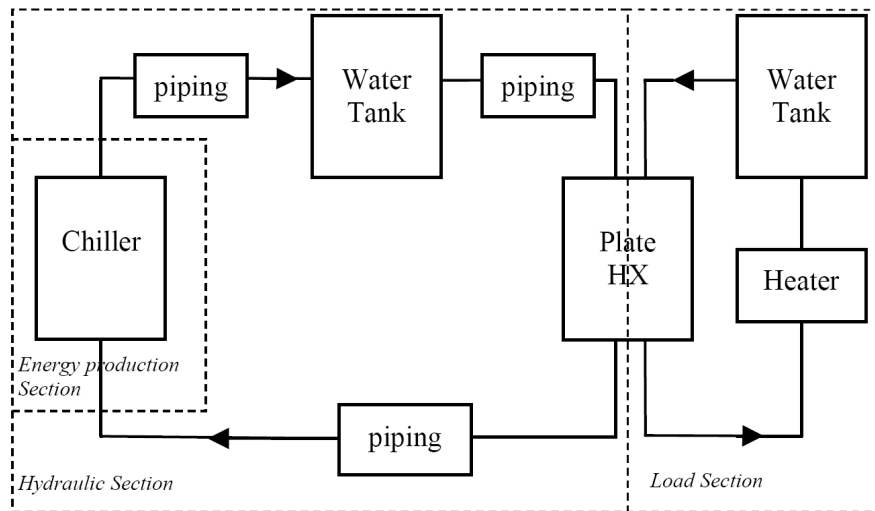
Figure 2.2.1: System test facility

The system dynamics are governed by the mass, momentum, and energy conservation laws. The mass and energy equations are implemented as block equations for each component of the plant, where each block is modelled as thermodynamic open system. The dynamic modelling was developed using Matlab/Simulink: the plant is schematically reported in Figure 2.2.2.
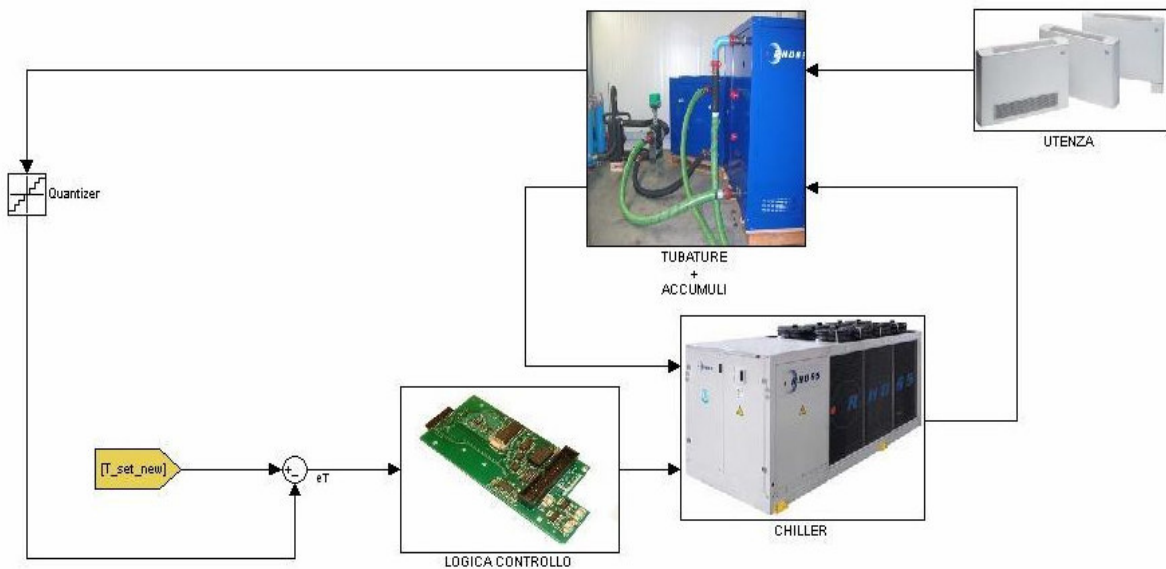

Figure 2.2.2: System test facility in Simulink

The dynamic behaviour of the plant is thus obtained solving the fluid flow problem and the energy balance. No solution of the momentum equation is needed because of the constant water mass flow assumption in the three sections. Thus the fluid flow problem consists only in the determination of the mass flow rate and the equations for the k-th block may be simply written as follows:

$$\dot{m}_{k,i} - \dot{m}_{k,o} = 0 \ , \tag{1}$$

where dependence on the time variable τ is omitted for notational convenience, when possible. The thermal problem consists in the determination of the temperature values at the outlet of the k-th block. The energy equation at time τ can be written as follows:

$$\dot{m}_{k,i} \cdot \left(c_p T_{k,i} + e_{p,k,i} + e_{c,k,i} \right) - \dot{m}_{k,o} \cdot \left(c_p T_{k,o} + e_{p,k,o} + e_{c,k,o} \right) + \frac{\partial}{\partial \tau} \int_0^{V_k} \rho e \, dv = \frac{dQ_k}{d\tau} - \frac{dL_k}{d\tau} \ . \tag{2}$$

Since the model has to be used for control design of systems with low capacity water storage tank, it is not possible to proceed under the well-mixed hypothesis for the water inside the system components as the model of Jian and Zaheeruddin (1998). In fact, the water contents and the dynamics of the water tanks strongly influence the behaviour of the chiller control system. Therefore, each water tank is modelled as two separate parts connected in series (see Figure 2.2.3).
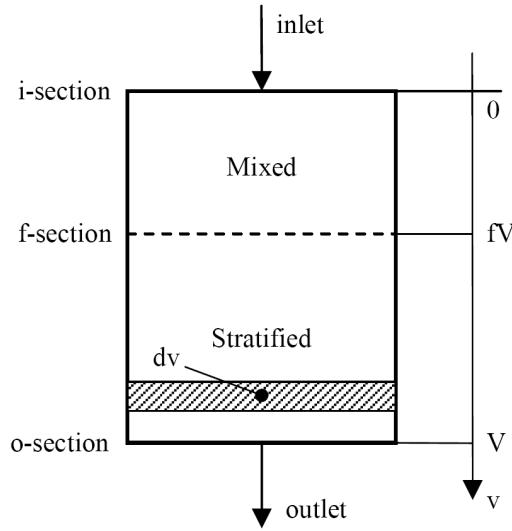
Figure 2.2.3: Water tank and piping scheme

In the first part a well-mixed condition is assumed, while in the second part a perfect stratification condition is considered. For the well-mixed section, with the above mentioned simplifying hypotheses and neglecting kinetic and potential energy variations, equation (2) at time τ becomes:

$$\dot{m}_{k,i} c_p T_{k,i} - \dot{m}_{k,o} c_p T_{k,f} + f_k \rho V_K c_p \frac{dT_{k,f}}{d\tau} = 0 \quad , \tag{3}$$

where f_k is the well-mixed section fraction of the tank total volume. This parameter is given as a function of a cylindrical tank geometric dimension and of the water velocity by means of FVM (Finite Volume Method) three-dimensional simulation.

For the stratified section of the water tank, the temperature in each infinitesimal volume *dv* depends only on the inlet time t of the associated infinitesimal water mass at the integration time τ, and equation (3) becomes:

$$\dot{m}_{k,i} c_p T_{k,f} (\tau) - \dot{m}_{k,o} c_p T_{k,o} (\tau) + \frac{\partial}{\partial \tau} \int_{f_k V}^{V_k} \rho c_p T_{k,i} (t) dv = 0 \quad . \tag{4}$$

Since no mixing occurs inside the stratified section of the water tank, the

volumetric coordinate v associated to the position of an infinitesimal water mass inside the tank can be expressed as a function of the time instant t when the water mass entered the stratified portion of the tank. The resulting expression for v with reference to the actual integration time τ:

$$v = f_k V_k + (\tau - t) \frac{(1 - f_k) V_k}{t_{c,k}} \quad , \tag{5}$$

where t_c is the tank section time constant defined as:

$$t_{c,k} = (1 - f_k) \frac{\rho V_k}{\dot{m}_{k,i}} \quad . \tag{6}$$

Differentiating (5) and substituting in (4), the following equation is obtained:

$$\dot{m}_{k,i} c_p T_{k,f}(\tau) - \dot{m}_{k,o} c_p T_{k,o}(\tau) + \frac{\partial}{\partial \tau} \int_\tau^{\tau - t_c} -\rho c_p \frac{(1 - f_k) V_k}{t_{c,k}} T_{k,f}(t) \, dt = 0 \quad , \tag{7}$$

and integrating (7), the final equation for the stratified section is determined:

$$\dot{m}_{k,o} c_p T_{k,o}(\tau) = \dot{m}_{k,i} c_p T_{k,f}(\tau - t_c) \quad . \tag{8}$$

Combining (8) and (3) at each time step, the water tank block energy equation is solved and the outlet temperature is determined. The two equations can also be merged using Laplace transforms, thus obtaining the following first-order transfer function for the tank:

$$W_k(s) = \frac{T_{k,o}(s)}{T_{k,i}(s)} = \frac{e^{-st_c}}{1 - s \dfrac{f_k \rho V_k}{\dot{m}_{k,i}}} \quad . \tag{9}$$

The same approach is used to model piping blocks, although the FVM analysis

indicated that water mixing is negligible for typical water velocity design conditions. The resulting simplified model for piping and tanks, derived under the above mentioned hypotheses, have been analyzed and validated by means of tests performed on the experimental facility, as described in paragraph 2.2.5.

For the particular system under consideration, chiller and heater water content can be neglected and the energy equation for these two blocks at time τ can be written as follows:

$$\dot{m}_{k,i} c_p T_{k,i} - \dot{m}_{k,o} c_p T_{k,o} = \frac{dQ_k}{d\tau} \quad , \tag{10}$$

where for the chiller, the RHS term, as well as the electrical absorbed power, is determined on the basis of data provided by the manufacturer as a function of water inlet temperature, mass flow, and external air temperature. Thus, the dynamic phenomena associated with heat and mass transfer, especially during start-ups, are neglected. For the heater, the RHS term is a boundary condition.

For the plate heat exchanger block, equation (10) is used for both the load and the hydraulic section. The RHS term in (10) is determined as a function of inlet temperatures defining a heat exchanger effectiveness ε and applying the ε-NTU method for heat exchangers:

$$\frac{dQ_k}{d\tau} = \varepsilon \cdot \min\left(\dot{m}_{k,i,H}, \dot{m}_{k,i,L}\right) \cdot c_p \left| T_{k,i,H} - T_{k,i,L} \right| \quad . \tag{11}$$

Once assigned the values of water mass flow rate, water temperature initial values and time dependent values of the heater power, the final system of non-linear equations obtained from equations (1) and (2) of each block and from equation (11) is integrated in the Matlab/Simulink simulation environment through an ode stiff solver.

2.2.4 Chiller control

Typically, a chiller without capacity control can be regulated in two different ways, namely by controlling the chiller evaporator water outlet or the chiller evaporator water inlet. In both cases, a relay control law is used, where the compressor is switched on and off when the controlled temperature reaches given threshold values. The difference between the upper and lower threshold values is called water temperature differential, and its value clearly affects the width of the oscillations of the supply water temperature as well as the number of start-ups of the compressor. A low value of the water temperature differential grants a higher control bandwidth and allows to obtain a more constant water temperature. On the other hand, there is an upper bound to the number of compressor start-ups per hour, which is fixed by the compressor manufacturer. As a consequence, there is an upper bound to the achievable control bandwidth. Also, the value of differential cannot be decreased arbitrarily, but there is a lower limit value which depends on the plant water content. While both control strategies maintain constant the user water supply temperature in full load conditions, outlet water temperature control provides better performance under part load conditions since it maintains the mean water supply temperature fairly constant during on/off operations. The performance of such control scheme can be further improved by implementing advanced strategies aimed at increasing the energy efficiency of the chiller and/or its accuracy in maintaining a given set point value of the supply temperature. Different Authors (Arguello-Serrano and Velez-Reyes, 1999, Braun *et al.*, 1989a) introduce the concept of thermal load estimation as the core for HVAC algorithm design, a load estimation scheme based on a Kalman filter (Anderson and Moore, 1979) has been developed. The knowledge of the (estimated) value of the load allows to adapt the controller parameters in order to achieve a desired objective, that can be a performance objective, or an energetic one. Also, some autotuning techniques are used, that allow to achieve satisfactory performance even if the plant, from the user side, is not completely known a priori. Here we mention only the main characteristics of the control algorithm but a full description will be found in Albieri *et al.* (2007b).

The main characteristics of the control algorithm are:

1) *Low energy consumption*: the objective is to combine comfort with low energy consumption. This is achieved by adjusting the set-point value and optimizing compressor efficiency on the basis of the actual load conditions. It is thus possible to achieve significant seasonal energy savings compared to water chillers and heat pumps of an equivalent power with traditional control logic (Braun *et al.*, 1989; Fornasieri, 2002).

2) *High precision*: it is possible to achieve as little oscillation as possible at part load conditions, both in terms of the average set-point water temperature delivered to the users and of standard deviation from the set-point temperature. Thanks to a special Virtual Tank function, the controller can work well also in systems with a low water content of down to 2 litres/kW cooling capacity, even without the presence of a water tank.

3) *Estimation of the system thermal inertia*: during the system first start-up the autotuning function can estimate the characteristics of the thermal inertia and system dynamics in order to identify the optimal value of the control parameters. This function is always active and makes it possible to adapt control parameters quickly to changes in the water circuit and thus in the system water contents.

4) *Optimization of the compressor management*: in the case of a chiller with two compressors of different size, the algorithm controls the start-ups of the two compressors according to the part load conditions, in order to achieve the highest energy efficiency. In this way there is a good agreement between the chiller load and capacity. The smaller compressor is used to provide a higher precision, maximizing the ON/OFF cycles. The bigger compressor is used to assure the needed capacity: in this case the number of start-ups is kept as low as possible, achieving a high energy efficiency even at part load ratio.

The studied controls are:

- *Outlet_FB*: water temperature controlled at the chiller outlet, fixed symmetric boundaries;

- *Inlet_FB*: water temperature controlled at the chiller inlet, fixed symmetric boundaries;

- *Outlet_MB*: water temperature controlled at the chiller outlet, moving symmetric boundaries;

- *Outlet_MAB*: water temperature controlled at the chiller outlet, moving boundaries with asymmetric positioning with reference of the fixed set-point temperature;
- *Outlet_MABFS*: water temperature controlled at the chiller outlet, moving boundaries with asymmetric positioning with reference of the set-point temperature, floating set-point;
- *Inlet_FB_E*: water temperature controlled at the chiller inlet, fixed symmetric boundaries, chiller with two compressor of the same size;
- *Outlet_MAB_E*: water temperature controlled at the chiller outlet, moving boundaries with asymmetric positioning with reference of the fixed set-point temperature, chiller with two compressor of the same size;
- *Outlet_MAB_UE*: water temperature controlled at the chiller outlet, moving boundaries with asymmetric positioning with reference of the fixed set-point temperature, chiller with two compressor of the different size;
- *Outlet_MABFS_UE*: water temperature controlled at the chiller outlet, moving boundaries with asymmetric positioning with reference of the set-point temperature, floating set-point, chiller with two compressor of the different size.

2.2.5 Simulation model validation

The test facility was already described in paragraph 2.1.4 and shown in Figure 2.1.1. It was used to validate the simulation model. The energy production section is equipped with a Rhoss TCAEY 130 packaged air-cooled water chiller with R410A refrigerant, cooling capacity of 29.1 kW and EER of 2.44 in the following operating conditions: condenser input air temperature 35°C; chilled water temperature 7°C; temperature differential at evaporator 5°C. The mono-compressor chiller is equipped with a single scroll compressor without capacity control (Copeland ZP154). The multi-compressor chiller is equipped with two scroll compressors without capacity control or of different size (Copeland ZP 90 and Copeland ZP 120, UNEVEN configuration) or of the same size (Copeland ZP 103 and Copeland ZP 103, EVEN configuration).

Tests have been carried out with the condenser positioned in a climatic room maintained at 35 °C air temperature. By controlling the heater thermal power, the chiller has been tested in full load conditions and at 25%, 50%, 75% part load conditions. The mean systems efficiencies in terms of EER have been obtained by integrating the power absorption and the cooling capacity, computed from the instantaneous values of refrigerant mass-flow, condenser outlet and evaporator outlet enthalpies, which are computed from pressure and temperature values on the basis of refrigerant properties as represented in the NIST Reference Fluid Thermodynamic and Transport Properties - REFPROP, Version 7.0 (2002). The computed cooling capacity on the refrigerant side has been compared and validated with the computed capacity on the water side.

A wide validation test campaign for the developed simulation environment has been carried out. Tests have been performed on the chiller with inlet water temperature control, for different values of the electrical heat load, condenser supply air temperature, water mass flow, set-point and differential. The system dynamics and energy performances obtained from experimental tests have been compared to those obtained in the virtual simulation environment. It is worth noticing that the chiller cooling capacity and absorbed power model are based on manufacture data which do not consider energy losses during compressor start-ups. As a consequence, the expected absorbed power is not exactly predicted, especially during the first period of the compressor working cycle.

2.2.6 An example of use of the validated algorithm: the study of the plant water quantity

The validated code is a powerful simulation tool to investigate the system behaviour, changing same parameters. In this case, a chiller of two compressors of the same size, water temperature controlled at the chiller outlet, fixed set-point and boundaries (Outlet_FB_E) is simulated. In this case the objective is to study the number of start-ups of the system related to the quantity of water in the circuit, at different part load ratio. The Figure 2.2.4 shows the case of the chiller with two compressors: the black and red dotted lines represents the maximum number of

start-ups in a hour, according to Bodo (2006). The number of ON/OFF cycles strongly depends on the quantity of water and it decreases increasing the inertia of the system. There is just one local minimum, at 50% of part load ratio.
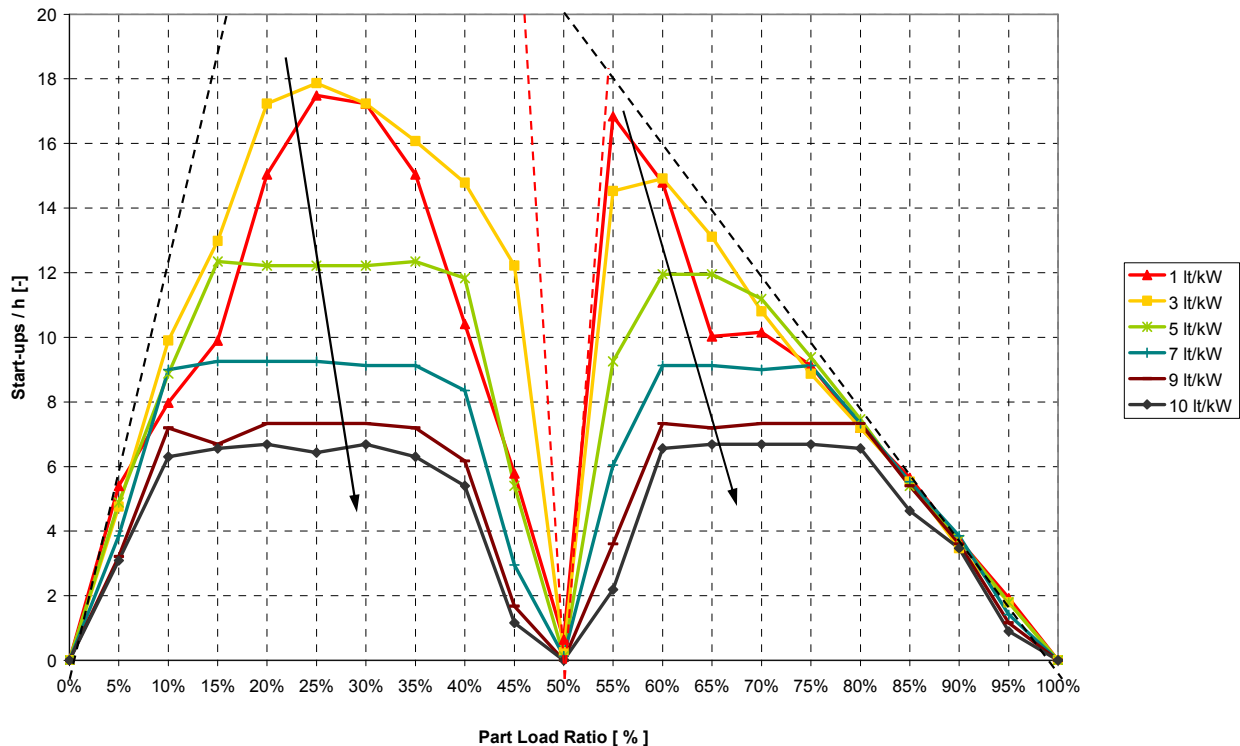

Figure 2.2.4: Number of start-ups for different water quantities in the circuit, for a 2-compressor chiller

The same simulation was carried out in a chiller of four compressors of the different size (two ZP 120 and two ZP 90), water temperature controlled at the chiller outlet, fixed set-point and boundaries (Outlet_FB_UE). The results are shown in Figure 2.2.5. The behaviour of the chiller, related to the quantity of water, is the same of the previous case. It is worth noticing that there are three local minimums, at 30%, 60% and 85% of part load ratio. Being the size of the two bigger compressor the 30% of the whole required load, the circuit inertia implies a delay of the higher minimum, that should be at 80% of part load ratio.
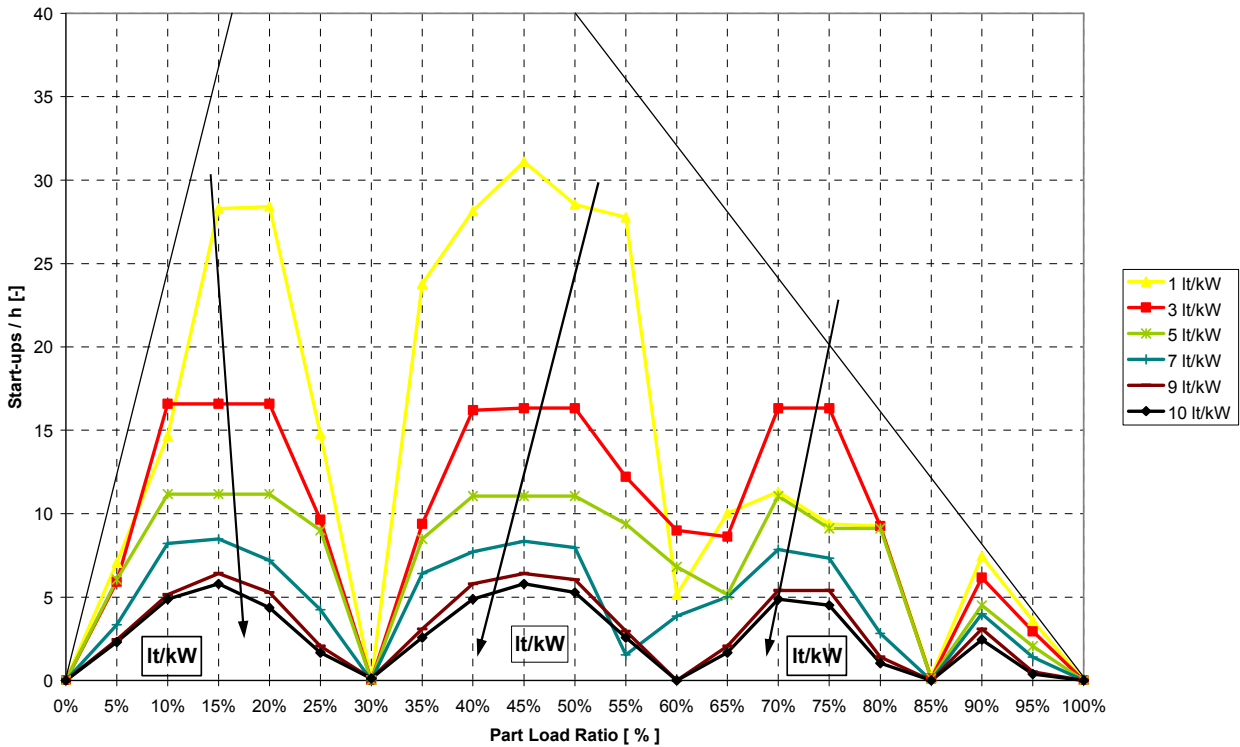
Figure 2.2.5: Number of start-ups for different water quantities in the circuit, for a 4-compressor chiller

2.2.7 Development and performances of the adaptive algorithm

2.2.7.1 Virtual development and prototyping

The fully validated simulation environment of the chiller plant system has been extensively used to design the adaptive algorithm. In fact, the simulation environment is able to reproduce all the system transient and steady state behaviours which are crucial to assess the performance of the control system. In the following, the performances of the control algorithm are illustrated by reporting the time behaviour of some key quantities, as well as an indication of its energy performance given in terms of energy efficiency rating (EER). Two different types of chiller have been investigated, mono-compressor and multi-compressor; the modelled controls are those reported in paragraph 2.2.4.

2.2.7.2 Mono-compressor chiller (simulation results)

The adaptive controller minimizes the water outlet temperature oscillation by appropriately changing the water differential, and thus the upper and lower boundary temperature, as a function of the part load ratio.
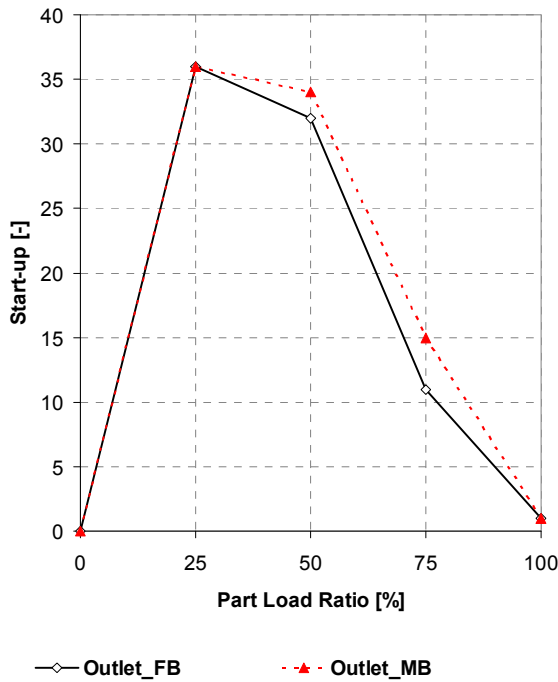

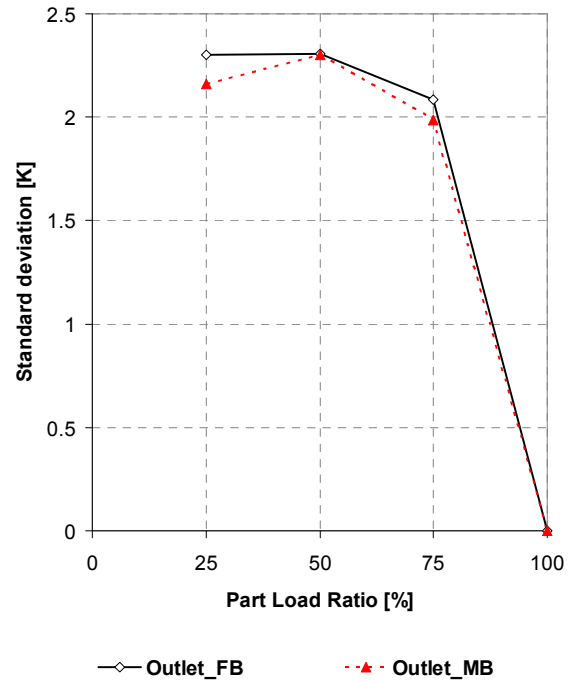*Figure 2.2.6: Number of start-ups for different controllers during four hour cycling operation*

Figure 2.2.7: Chiller water outlet standard deviation from set-point temperature for different controllers

In Figures 2.2.6 and 2.2.7, the number of start-ups and the standard deviation from the outlet water set-point (7°C) is plotted for a standard outlet water temperature control (Outlet_FB) with 4.8 °C differential and for the adaptive control which uses a moving boundary logic (Outlet_MB). Comparing the results, it can be pointed out that the developed control allows a greater precision, reducing standard deviation and increasing the number of start-up in particular for values of the part load ratio between 25% and 75%. The standard deviation of the traditional control is very close to the adaptive control one at 50% part load ratio because the standard control water temperature differential is optimized for this load condition.

An improved version of the control allows an asymmetrical positioning of the two

boundaries with reference to the set-point temperature (Outlet_MAB). In Figure 2.2.8, the difference between the average outlet water temperature during an on-off cycle and the set point temperature of the previous system is compared to this improved control. The moving asymmetrical boundary algorithm appears to be extremely accurate up to 50% part load ratio, below this value the controller antifreeze function reduces its performance.

The adaptive controller improves the system energy efficiency by adjusting the outlet water set-point value on the basis of the actual load conditions. If the part load ratio decreases, the control rises the set-point thus increasing the efficiency rating of the chiller. In Figures 2.2.9 and 2.2.10, the floating set-point control algorithm (Outlet_MABFS) is compared with both an outlet and inlet water temperature control in terms of average outlet water temperature and EER. It is worth noting that for part load ratios lower than 75%, the EER improvement with respect to the outlet water temperature control varies from 7.3% to 3.0%
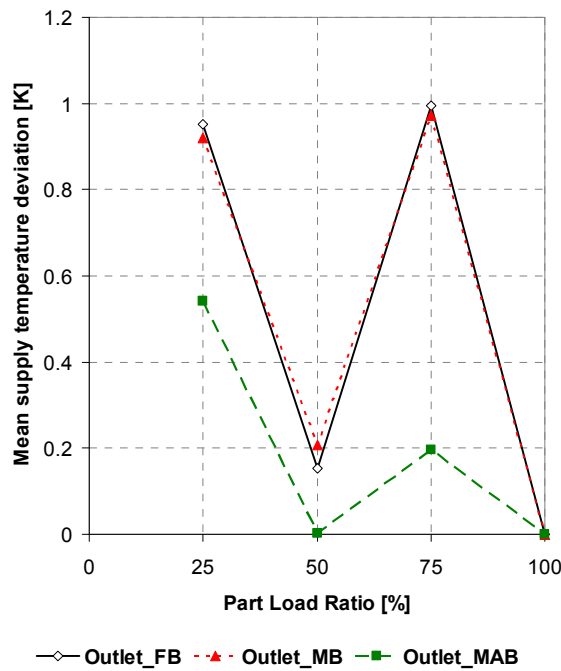
Figure 2.2.8: Difference between average (on+off period) chiller water outlet temperature and set-point temperature for different controllers
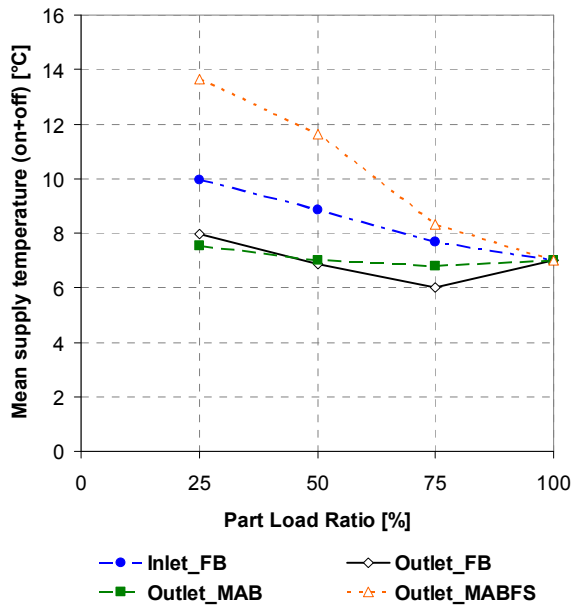
Figure 2.2.9: Average (on+off period) chiller water outlet temperature for different controllers
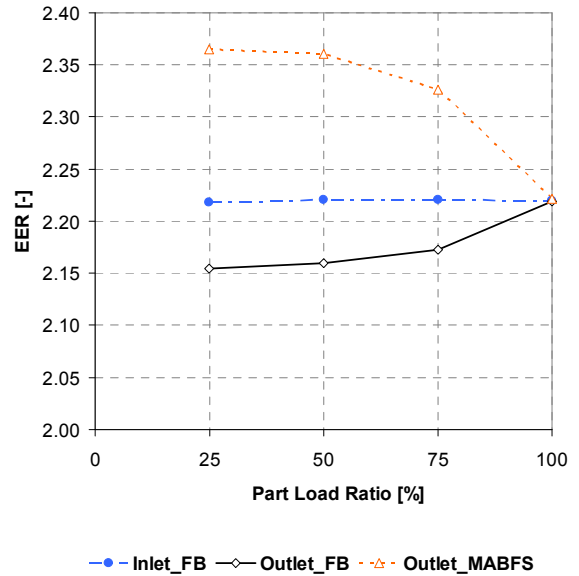
Figure 2.2.10: Chiller Energy Efficiency Rating for different controllers

2.2.7.3 Multi-compressor chiller (simulation results)

The same adaptive controller was implemented in the multi-compressor chiller. The optimal management of the compressors of different size allows to operate with cooling capacities close to the actual system load, thus with less fluctuations of the controlled parameter.

Figure 2.2.11: Start-ups of the UNEVEN chiller during 4 hour of ON/OFF running
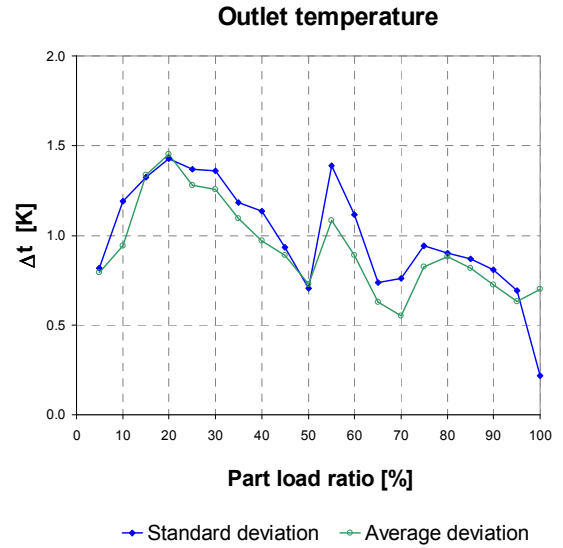
Figure 2.2.12: Standard deviation and average deviation of the outlet water temperature to the set-point value.

In Figure 2.2.11, the number of start-ups of the system with two compressors of different size (UNEVEN system) are reported; besides them, the maximum number of start-up of each compressor, in 4 hour time, is highlighted. The controller is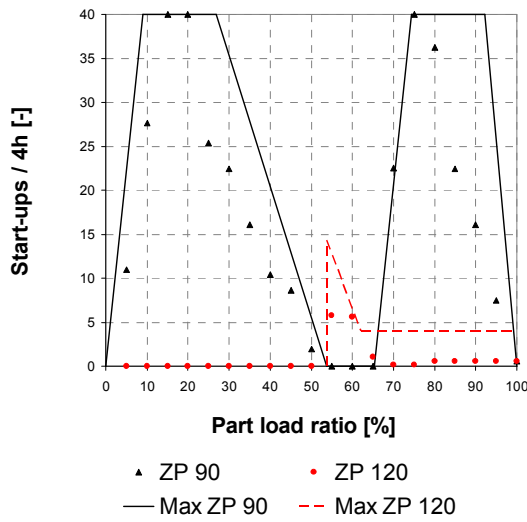 an adaptive control which uses a moving boundary logic with an asymmetrical positioning of the two boundaries with reference to the set-point temperature (Outlet_MAB_UE). The smaller compressor (Copeland ZP 90) makes a larger number of ON/OFF cycles, providing a high precision. On other hand, the bigger compressor (Copeland ZP 120) tends to operate in continuous running, assuring the required cooling capacity and minimizing the power consumption.

In Figure 2.2.12 the standard deviation and the average deviation are reported. Both values are always below 1.5°C, showing the efficiency of the control algorithm. It is worth noticing that both curves presents three local minimums: the controller allows to minimize the error of the controlled parameter whenever one of the two compressors (or both of them) runs at full load.
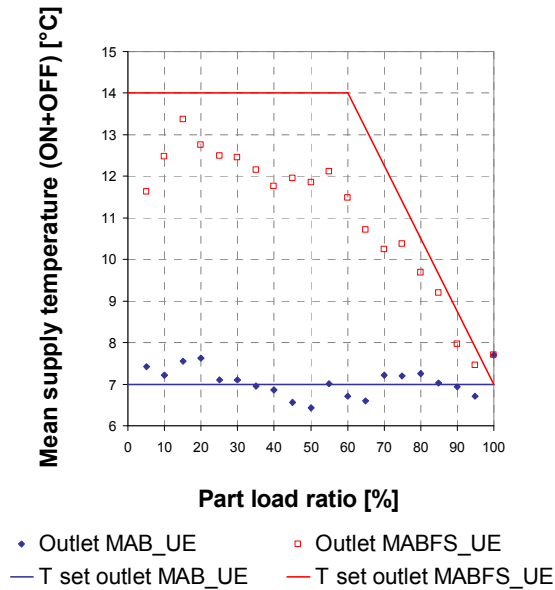
Figure 2.2.13: Mean supply temperature during ON/OFF running, for two different controllers
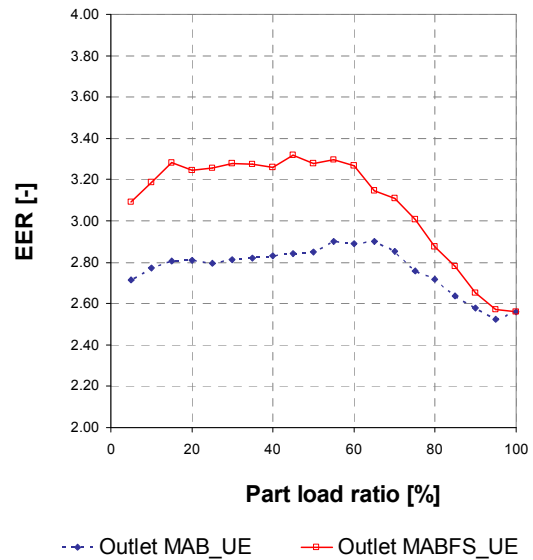
Figure 2.2.14: EER during ON/OFF running, for two different controllers.

In Figures 2.2.13 and 2.2.14, the floating set-point control algorithm (Outlet_MABFS_UE) is compared with an outlet water temperature control with fixed set-point ((Outlet_MAB_UE, 7°C) in terms of average outlet water temperature and EER. In Figure 2.2.13, the mean supply temperatures, during the whole ON/OFF cycle, are plotted, with the results of the simulations, against the part load ratio. In Figure 2.2.14 the EERs of the two controllers are plotted against the part load ratio; the efficiency of the system with floating set-point is around 15% higher than the system with fixed set point at part load ratios lower than 60%. At high part load ratios, the two temperatures get close each other, approaching the value of 7°C; in this case the values of EER decrease sharply, tending to the values of the system at fixed set-point.

2.2.8 Experimental tests; the seasonal energy efficiency rating

Finally, the developed algorithm has been then implemented on board of a commercial chiller units, and its performance has been evaluated on the

experimental testing facility. The parameters are evaluated during the whole (on+off) running period.

2.2.8.1 Mono-compressor chiller (experimental data)

In Figures 2.2.15 and 2.2.16, the experimental and virtual results of the floating set-point control algorithm (Outlet_MABFS), of the standard outlet water temperature control (Outlet_FB) and of the inlet water temperature control (Inlet_FB) are compared in terms of average (on+off period) chiller water outlet temperature and EER. It is worth noticing that for the floating set-point algorithm while the simulated average supply temperature is in good agreement with the experimental data, the experimental average EER is 2.3% higher than the virtual one (see Figure 2.2.15). This was ascribed to the chiller absorbed power model obtained from manufacturer data that are not very accurate at high evaporation temperature.
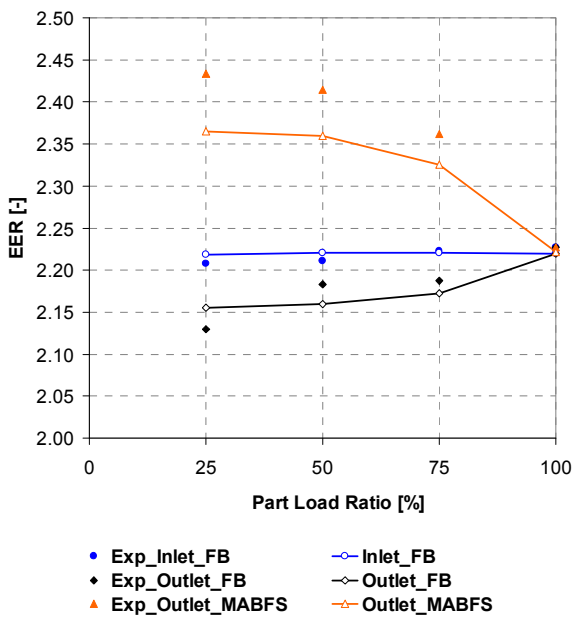

Figure 2.2.15: Experimental and simulated EER values, for three different control algorithms
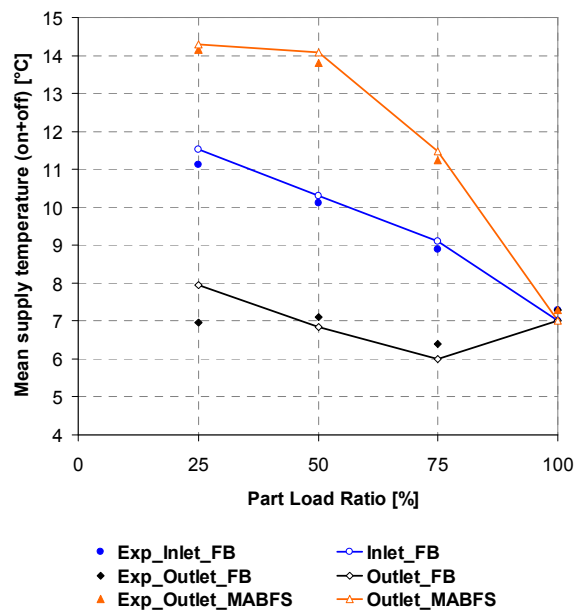

Figure 2.2.16: Experimental and simulated mean supply temperature during ON/OFF running, for three different control algorithms.

In order to have a rough evaluation of the seasonal energy saving of a building in which a chiller equipped with the adaptive controller is installed, the experimental seasonal energy efficiency of the system was calculated. The seasonal efficiency has been evaluated for the load, air temperature and energy weighting coefficients used in the calculation of the ESEER (European Seasonal Energy Efficiency Rating) in prEN 14825 (2009).

	EER				Seasonal Efficiency	Δ [%]
Part Load Ratio [%]	25	50	75	100		
Ambient temperature [°C]	20	25	30	35		
Weighting coefficients [%]	23	41	33	3		
Inlet_FB	3.06	2.88	2.57	2.23	**2.80**	2.8
Outlet_FB	2.94	2.79	2.54	2.23	**2.72**	-
Outlet_MABFS	3.28	3.09	2.69	2.23	**2.97**	9.1

Table 2.2.1: Experimental seasonal energy rating for three different control algorithms

In Table 2.2.1 the energy efficiency ratings EER for the four test conditions indicated in the calculation methodology and the seasonal energy efficiencies obtained for the inlet control, the moving asymmetrical boundary algorithm and the floating set-point control are reported. The floating set-point control algorithm seasonal energy rating improvement with respect to the adaptive outlet water temperature control and to the standard inlet control is 9.1% and 6.2% respectively.

2.2.8.2   *Multi-compressor chiller (experimental data)*

In Figures 2.2.17 and 2.2.18, the experimental and virtual results of the floating set-point control algorithm (Outlet_MABFS_UE) and of fixed set-point (Outlet_MAB_UE, 7°C) are compared in terms of average (on+off period) chiller water outlet temperature and EER.
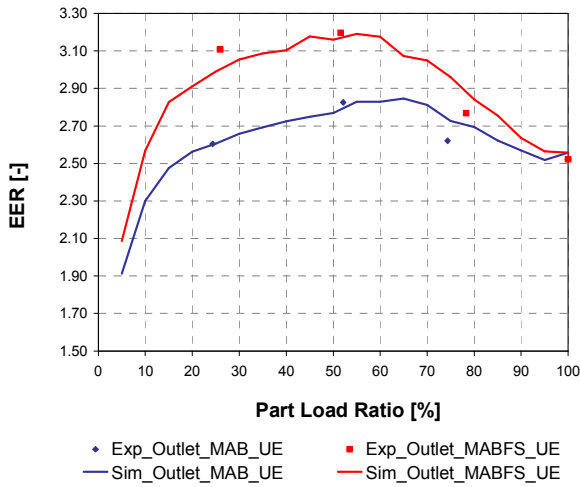
Figure 2.2.17: Experimental and simulated EER values, for two different control algorithms of the multi-compressor chiller
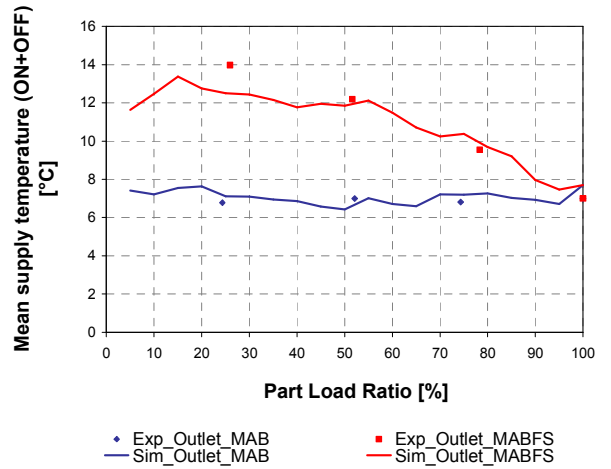
Figure 2.2.18: Experimental and simulated mean supply temperature during ON/OFF running, for two different control algorithms of the multi-compressor chiller.

It is worth noticing that the experimental data are in good agreement with the simulation results. At low part load ratio, the unit efficiency is strongly penalized, in both cases. This penalization is due to the fan power consumption, that considerably affects the averaged power consumption. As regards the outlet temperature, the system is able to keep its value at the set-point, in both cases, even at low part load ratios.

To verify the efficiency of the adopted technological solutions, an experimental test campaign has been conducted on chillers of the same size, but operating according to different control logics. Experimental test have been carried out on chillers with compressors of the same size in tandem configuration, with control of the inlet water temperature, at fixed set-point (Inlet_FB_E, 12°C) and of the outlet water temperature, moving boundaries with asymmetric positioning with reference of the fixed set-point temperature (Outlet_MAB_E, 7°C). The same tests have been carried out on chillers equipped with compressors of different size, with control of the outlet water temperature, moving boundaries with asymmetric positioning with reference of the fixed set-point temperature (Outlet_MAB_UE, 7°C) and floating set point (Outlet_MABFS_UE). The energy efficiency of the different solutions are compared in Figure 2.2.19. The energy improvement related to the use of compressors of different size is remarkable: the EER increasing of the

Outlet_MAB_UE, in comparison with Outlet_MAB_E, is 4.8% at part load ratio of 50% and 5.7% at part load ratio of 75%. Comparing the controllers Outlet_MAB_UE and Outlet_MABFS_UE, it is possible to highlight the energy advantage of the use of a floating set-point. The EER improvement is 11.6% for part load ratio of 50% and 5.3% for part load ratio of 75%. Finally, the system with two compressors of different size and floating set-point of the water outlet temperature is more efficient than the traditional control based on the inlet temperature; however, it is not able to assure the same level of precision of the water supply temperature of the solution Outlet_MABFS_UE.

Figure 2.2.19: Experimental EER values, for different control algorithms of the multi-compressor chiller

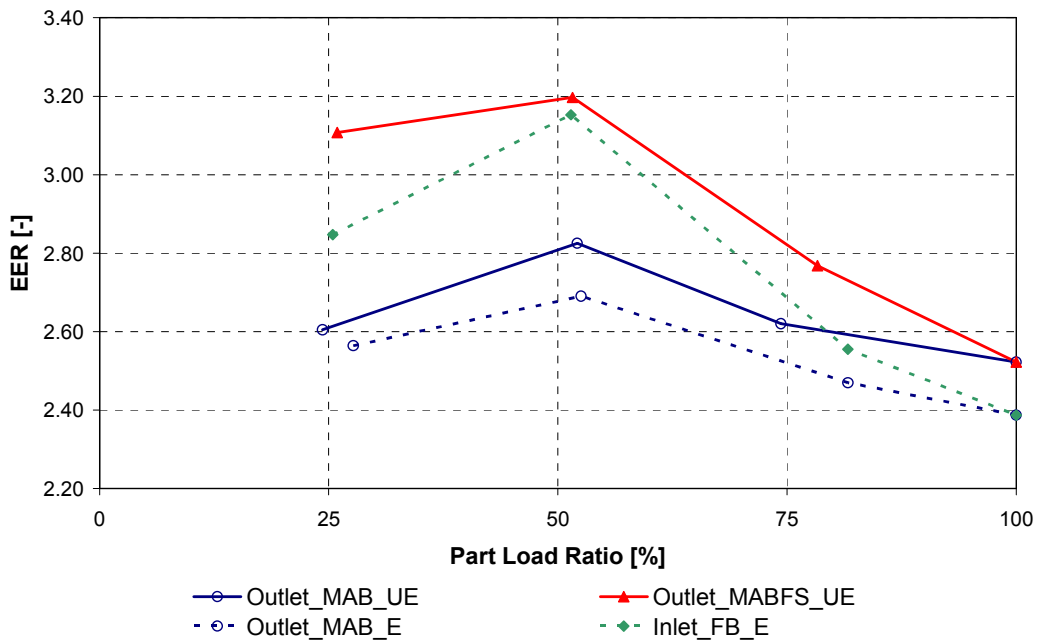|	EER				Seasonal Efficiency	Δ [%]
Part Load Ratio [%]	25	50	75	100		
Ambient temperature [°C]	20	25	30	35		
Weighting coefficients [%]	23	41	33	3		
Outlet_MAB_UE	3.48	3.60	3.06	2.52	**3.37**	-
Outlet_MABFS_UE	4.28	4.07	3.44	2.52	**3.86**	14.7

Table 2.2.2: Experimental seasonal energy rating for two different control algorithms of the multi-compressor chiller

To provide an overall evaluation of the seasonal energy saving, the ESEER (European Seasonal Energy Efficiency Ratio) was calculated, according to prEN 14825 (2009), extending its application to the case with floating set point (EECCAC, 2003). In Table 2.2.2, the energy efficiency ratings EER for the four test conditions indicated in the calculation methodology and the seasonal energy efficiencies obtained for the controllers with fixed set-point and with floating set-point are reported. The Outlet_MABFS_UE control seasonal energy rating improvement with respect to the Outlet_MAB_UE control is 14.7%.

2.2.9   Conclusions

In this Chapter, the issue of determining and improving the energy efficiency of a chiller under all running conditions is faced. The evaluation of the efficiency follows the directions of the European Community, considering the ESEER index as reference. A simulation environment for the design of advanced chiller control systems was developed. The novelty of the adopted approach with respect to existing ones is that all of the dynamic behaviours that are relevant for controller design have been taken into account (see, e.g., the modelling of water tanks), while neglecting or simplifying other dynamic phenomena that contribute only marginally to the assessment of the overall controller-plant performance.

The model has been satisfactorily validated in a state-of-the-art experimental

facility, by performing an extensive validation campaign. The environment has been used to design a novel control algorithm for single scroll compressor, packaged air-cooled water chillers, which allows to increase both control accuracy and energy performance. It is worth noticing that the availability of a fully validated virtual environment allows to obtain an assessment of the system performance by means of virtual tests that would be very difficult and time consuming, to be performed on experimental test facilities or commercial plants. This is fully in agreement with the experience in other control engineering applications, such as the automotive field, where the use of virtual prototyping tools is nowadays a common practice.

A control algorithm, for chiller and heat pump systems, has been developed; it assures a high precision of the water supply temperature and, at the same time, it maximizes the energy efficiency at part load ratio. The controller can be implemented both in mono-compressor systems and in multi-compressor systems, even with compressors of different size. Through the simulation results and the campaign of experimental tests, it has been found that the efficiency and the precision are considerably higher than those of traditional controllers for HVAC systems.

2.2.10 References

1. AA.VV. (2003), Energy Efficiency and Certification of Central Air Conditioners (EECCAC), *Ed. Armines*, 3:52-59.
2. Albieri M., Beghi A., Bodo C., Cecchinato L., (2007a), Nuovo algoritmo per l'efficienza energetica, *CDA*, 9: 52-58 (in Italian).
3. Albieri M, Beghi A, Bodo C, Cecchinato L., (2007b), Adaptive Chiller Control for Advanced HVAC Applications. Under submission to *IEEE Trans on Automation Sc and Eng*.
4. Anderson B.D.O., Moore J.B., (1979), Optimal Filtering, *Prentice Hall*.
5. Arguello-Serrano B., Velez-Reyes M. (1999), Nonlinear Control of a Heating, Ventilating, and Air Conditioning System with Thermal Load Estimation, *IEEE Trans. Contr. Sys. Tech.*, 7(1): 56-63.

6. Bodo C., (2006), Algoritmo di supervisione e controllo per macchine frigorifere, *Degree Thesis* (in Italian).

7. Braun J.E., Klein S.A., Mitchell J.W. Beckman W.A. (1989a), Methodologies for optimal control to chilled water systems without storage, *ASHRAE Transactions*, 95(1): 652-662.

8. Braun J.E., Klein S.A., Mitchell J.W. Beckman W.A. (1989b), Applications of Optimal Control to Chilled Water Systems without Storage, *ASHRAE Transactions*, 95(1): 663-675.

9. CEN TC113/WG7, prEN 14825, (2009), Air conditioners, liquid chilling packages and heat pumps, with electrically driven compressors, for space heating and cooling – Testing and rating at part load conditions, European Committee for Standardization CEN.

10. Fornasieri E. (2002), Refrigeratori d'acqua con compressore volumetrico: come promuovere l'efficienza energetica, *43rd Convegno Internazionale AICARR*, 3: 17-46 (in Italian).

11. Huguang Z., Cai L., (2002) Decentralized nonlinear adaptive control of an HVAC system. *IEEE Trans Sys Man Cyb Part C: Appl and Rev*; 32(4): 493–498.

12. Jian W.L., Zaheeruddin M., (1998), Sub-Optimal on-off switching control strategies for chilled water cooling systems with storage. *App. Therm. Engineering*; 18(6): 369–386.

13. Lemmon E.W., McLinden M.O., Huber M.L. (2002), NIST Reference Fluid Thermodynamic and Transport Properties, *Refprop 7.0*, NIST Std. Database.

14. Shoureshi R. (1993), Intelligent control systems: Are they real?, *J. Dynamic Syst., Measur. Contr.*, 115: 15-19.

15. Venco S. (2003), L'importanza ai fini del risparmio energetico del funzionamento a carico parziale dei sistemi idronici centralizzati, *Incontri tecnici AICARR* (in Italian).

16. Yaqub M., Zubair S. M., (2001), Capacity control for refrigeration and air conditioning systems: A comparative study, *Int. J. Energy Res. Tech.*, 123: 9-99.

Chapter 2.3 DEVELOPMENT OF A CONTROL ALGORITHM FOR RADIANT COOLING SYSTEMS WITH FAN COILS

In this chapter a control algorithm for a radiant cooling system with fan coils is presented. This controller was developed using a simulation code Simulink/Matlab and it will be implemented in industrial systems of Rhoss SpA. The objective is to find a control logic that allows minimizing the seasonal energy consumption, assuring an acceptable level of comfort. This work will be the subject of future papers. The support of Mr. L. Cecchinato and Mr. M. Rampazzo, for the theoretical modeling part, is gratefully acknowledged.

2.3.1 Introduction

The increasing effort toward the reduction of the energy consumption associated to buildings heating and cooling processes and the growing attention to indoor environmental quality in dwellings and offices are increasing the use of radiant systems for heating and cooling. On other hand, the lack in experience and well-established design methods is perceived by thermal plant engineers. Moreover, lower energy consumptions and better comfort levels can be provided mainly by the correct regulation of the radiant system. The control of radiant systems is fundamental in cooling mode, when these systems operate coupled with fan-coils, air handling units or dehumidifiers. In addition, the thermal inertia of a radiant system can suggest the use of a supervisor algorithm, able to predict the temperature fluctuations and to set the thermal load of the system.

2.3.2 Nomenclature

α   convection heat transfer coefficient [W/(m^2 K)]

c_v specific heat at constant volume [J/(kg K)]

dA   infinitesimal area [m^2]

G   mass flow [kg/s]

h   enthalpy [J/kg]

k   thermal conductivity [W/(m K)]

PMV Predicted Mean Vote [-]

PPD Percentage People Dissatisfied [-]

Q   thermal load [J]

$\hat{Q}$ forecast thermal load [J]

ρ   density [kg/m^3]

S_h heating/cooling energy generated in the room [W]

T   temperature [°C]

t   time duration [s]

τ   time [s]

V   air volume [m^3]

w(I,j) weighting factors (of EWMA method matrix)

$$\frac{k_w}{\rho_w \cdot c_{v,w}}$$ thermal diffusivity [m^2/s]

Subscripts:

a   air

a_e   external air

c   chiller

dew   dew point

fc   fan coil

i   input

j   j-th air node

max   maximum

min   minimum

o   output

ON   ON cycle

rc   radiant cooling

set   set point value

sv   supervisor

w   wall

3wv   3-way valve

2.3.3   The simulation environment

The simulation environment is a Simulink/Matlab code, called IBPT (International Building Physics Toolbox), developed by the Danmarks Tekniske Universitet (Nielsen *et al.*, 2002; Weitzmann, 2003) and by the Chalmers University of Technology (Rode *et al.*, 2003; Kalagasidis, 2003a; Kalagasidis 2003b).

In state-of-the-art simulation tools for building energy calculation, the calculation domain is subdivided into a wall domain, Ω_w, which identifies all building masonry parts, and an air domain, Ω_a, which identifies all volumes containing air. A lumped parameter approach is commonly adopted for the air domain, subdividing it into a number of nodes corresponding to the building rooms or groups of rooms. The physical model, defined over the whole computation domain, is expressed by the following equations, where the index *j* refers to the generic *j*-th lumped air volume:

$$P_j \in \Omega_a , \quad V_i \cdot \frac{\partial \left(\rho_{a,j} \cdot c_{v,a,j} \cdot T_{a,j} \right)}{\partial \tau} = \int \alpha_w \left[T_w - T_{a,j} \right] dA_{w,j} + \\ + G_j \left[h_{j,i} - h_{i,o} \right] + S_{h,j} \cdot V_j \tag{1}$$

$$P \in \Omega_w , \quad \frac{\partial \left(\rho_w \cdot c_{v,w} \cdot T_w \right)}{\partial \tau} = \nabla \left(k_w \nabla T_w \right) + S_h , \tag{2}$$

where S_h is volumetric heat generation or extraction rate.

For resolution of the previous equations, a proper set of boundary conditions is needed. Usually for equations (1), Dirichlet-type conditions at the air inlet enthalpy are adopted. On the other hand for equation (2), a Neumann-type condition is imposed on the portion of the wall surface which is in contact with the external environment. The phenomenological coefficients which characterize heat transfer (α_w) are evaluated according to common correlations reported in open literature. The described physical model is characterized by strong coupling among equations, mainly due to equation (2), which depends on the temperature profile inside the masonry structures.

In order to create a numerical code for simulating the physical model, a discretization technique is considered for the masonry structures domain. According to the finite difference method (FDM), structures are discretized with a suitable mesh. Numerical convenience suggests to introduce a uniform temperature distribution hypothesis on the *yz* plane, thus reducing the problem to a mono-dimensional one. As far as the modelling of embedded radiant surface heating/cooling systems is concerned, a bi-dimensional *xz* mesh to discretize equation (2) is considered, adopting Dirichlet-type conditions at the water inlet temperature. A multi-scale integration is introduced to reduce computational time.

2.3.4   The control algorithm

In this Thesis, different control methods of radiant cooling system are investigated, and a simulation program to analyze of the thermal environment is developed. Also by simulations on the control methods of the radiant floor and

ceiling cooling system, the control performance and applicability of each control method were analyzed with regard to floor surface condensation and comfort (Lim *et al.*, 2006).

The control methods can be systematically classified according to control parameters. In a control system, the control parameters are divided into input variables, controlled variables, and manipulated variables. The input variables such as room air temperature, operative temperature, outdoor air temperature, floor surface temperature, and room air humidity could be measured by temperature and humidity sensors. Because air temperature is the most commonly controlled condition in radiant floor heating and cooling system, room air temperature or operative temperature are determined as the controlled variable. The manipulated variable, which causes the necessary changes in controlled variables, could be the water flow rate or water temperature because controlled variables can be regulated by adjusting these variables. Various control methods for heating based on the water flow rate or the water temperature have been presented in literatures.

Two common types of control methods are used to manipulate water flow rate:

1. on/off bang-bang control, so called on/off control, which can supply water by fully opening or shutting down the valve;

2. variable flow control, which can adjust the flow rate of supply water continuously.

A variable flow control system can be used for minimizing pump energy while maintaining design conditions, but this system is more complicated and difficult for controlling flow rate precisely in the range of low-flow rates.

To manipulate supply water temperature, two types of control methods are generally used:

1. the outdoor reset control, which is an open loop approach where the temperature of the water sent to the slab is proportional to the outdoor temperature. Common intuition holds that for any existing heating system, there is a hot water temperature that corresponds linearly to a given outside air temperature. But this open loop control responds ineffectively to disturbances in indoor temperature.

2. the outdoor reset with indoor temperature feedback control, which controls supply water temperature by sensing both the outdoor temperature and indoor temperature. In radiant floor cooling, internal load elements, such as

lighting and people, can badly affect increases in the indoor temperature, therefore, the supply water temperature should be not only a function of the outdoor temperature but also that of the indoor temperature. Indoor temperature feedback may be provided by an indoor temperature sensor that allows the outdoor reset control to automatically shift its reset line downward to compensate for internal heat gain or upward to compensate for internal heat loss. The reset line maintains the same slope as that of the outdoor reset control, and shift value is calculated by using the information about the change rate of the indoor air temperature with PID logic.

In European countries, supply water temperature control is generally applied by operating a 3-way valve, and control system can vary according to the zones inside the buildings by operating a thermostatic valve.

In this Thesis, in order to conduct a comparative analysis on control methods for radiant cooling system, computer simulations on the water temperature control such as traditional control methods and a new control method based on PMV control were performed. In the new control algorithm, the manipulated variable is the water temperature and the controlled variable is the Predictive Mean Vote (Fanger, 1970). This conventional index gives the mean thermal sensation vote on a standard scale of thermal feeling for a large group of persons in a given indoor climate. It is a function of two human variables and four environmental variables, i.e. clothing insulation worn by the occupants, human activity, air temperature, air relative humidity, air velocity and mean radiant temperature, respectively.

2.3.4.1 The supervisor

It is assumed that the thermal load, at the time step k, is proportional to the difference between a function Ω of actual PMV and the supply water temperature and to the duration of 3-way valve ON cycle by a coefficient ξ:

$$Q(k) = \xi \cdot \left(\Omega\left(PMV(k)\right) - T_{rc,i}(k)\right) \cdot t_{3wv,ON}(k), \tag{3}$$

where Ω gives an equivalent temperature from PMV and is obtained by polynomial regression from experimental data set.

It is worth noticing that, in relation to the thermal load, the right water

temperature (from the energy saving and comfort point of view) should maximize the duration of 3-way valve ON cycle (i.e. 100% of time).

For this purpose, if the thermal load is supposed constant, an equivalent water temperature can be calculate, for a desired PMV set point and maximum duration of 3-way valve ON cycle, as:

$$T_{sv}(k) = \Omega(PMV_{set}) - (\Omega(PMV(k)) - T_{rc,i}(k)) \cdot \frac{t_{3wv,ON}(k)}{t_{3wv,ON,max}},$$
(4)

In this way a supervisory strategy can be design.

Given a series of thermal load data, and a fixed subset size, the thermal load forecast is obtained by resorting to an exponentially weighted moving average (EWMA) that applies weighting factors which decrease exponentially. The weighting for each older data point decreases exponentially, giving much more importance to recent observations while still not discarding older observations entirely.

Specifically, the thermal load data set is organized by a matrix (rows of days and columns of supervision time steps) and the fixed subset size results an [(n-days)×(m-time)] steps matrix. A weighting exponentially matrix is associated to the fixed subset. The thermal load forecast relative to d day and m time-step results:

$$\hat{Q}(d,m) = \frac{\sum_{i,j} w(i,j) \cdot Q(i,j)}{\sum_{i,j} w(i,j)},$$
(5)

In Figure (2.3.1) the EWMA control scheme is depicted.

Therefore, the water temperature set point, relative to m step, can be calculated as

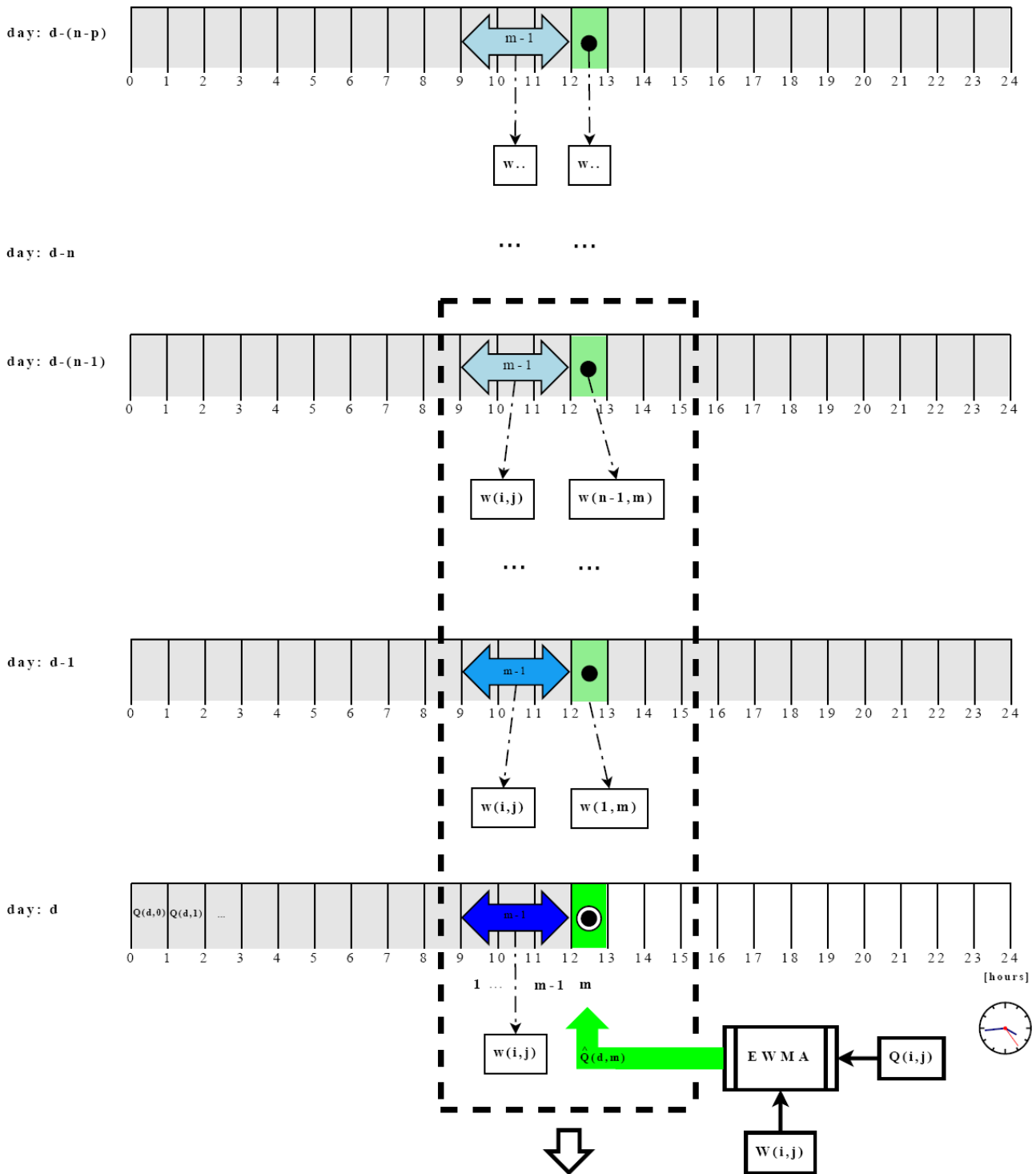$$T_{sv}(d,m) = \Omega(PMV_{set}) - \frac{1}{\xi} \cdot \frac{\hat{Q}(d,m)}{t_{3wv,ON,max}},$$
(6)

Figure 2.3.1: Thermal load forecasting by exponentially weighted moving average

The supervisor steps are stated as follows:

- Step 1. Read in system information including thermal load data archive
- *Step* 2. Calculate the thermal load forecast relative to next time step by equation (5).
- *Step* 3. Calculate the water temperature set point by equation (6).
- *Step* 4. Output results.

2.3.4.2 The temperature and humidity control

The cooling system is depicted in Figure 2.3.2: actually, both floor and ceiling are active surfaces, but in Figure 2.3.2 only the ceiling radiant system is represent, for simplicity. The water mass flow rate, at the chiller outlet, is sent partly to the fan coils, partly to the radiant cooling system. The supply water temperature is controlled through a 3-way valve, mixing the water from the chiller with the water at the panel outlet.
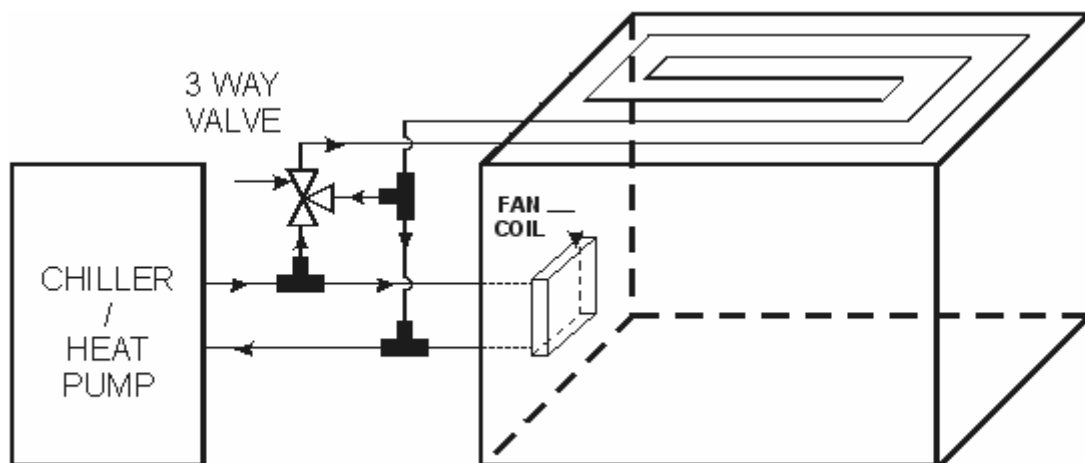
Figure 2.3.2: The cooling system

In a cooling system there are two variables which must be controlled to provide the needed level of comfort: temperature and humidity. In the case of a radiant cooling system, the humidity control represents a constrain: in fact, being the surface condensation forbidden, the surface temperature of the panel must be higher than the air dew point temperature. In this case, the humidity control is performed through fan coils; in this way, they completely absorb the latent heat, but also a part of the sensible heat. Thus, at this point it is possible to fix two basic points of this

control:

- the limit: the panel supply temperature must be higher than the air dew point temperature
- the objective: to maximize the fraction of sensible heat absorbed by the radiant cooling system

The controller will act on three different sections of the circuit:

- chiller: management of the outlet water temperature;
- fan coils: management of ON/OFF cycles, in order to assure comfort and dew control
- radiant system: management of ON/OFF cycles and supply water temperature.

In the following, the control logic will be explained, in comparison with traditional control methods of cooling systems on the market.

Cooling radiant system

In the traditional control methods, the supply temperature is fixed (for example at 15°C) or calculated according to a climate curve. Then this temperature is corrected considering the dew point temperature:

$$T_{rc,i} = \max(T(T_{a\_e}), T_{dew} + dT_{min}),$$ (7)

where dT_{min} is a minimum temperature difference between the supply temperature and the dew point temperature (for example, it can be fixed at 1 K).

The proposed control logic has the objective to take advantage of the EWMA supervisor, keeping the supply temperature as close as possible to that estimated by the algorithm. Equation (7) becomes:

$$T_{rc,i} = \max(T_{sv}, T_{dew}),$$ (8)

Chiller

In common chiller, the water temperature at the chiller outlet is constant and fixed at 7°C. In this way, the chiller is forced to produce water at very low temperature, even if the part load is low; this implies a high number of ON/OFF cycle of the

294

compressor, penalizing the energy efficiency. The developed control algorithm defines the water temperature at the chiller outlet in this way:

$$T_{c,o} = \min(T_{rc,i}, T_{dew} - dT_{dew,c}),$$
(9)

where $dT_{dew,c}$ is the minimum temperature difference between the dew point and the water temperature at the chiller outlet. In this way, the control of the surface condensation on radiant panels is not performed through equation (7), but through the combination of equations (8) and (9).

Fan coils

In traditional system, the ON/OFF control of fan coils is set according two bands: air temperature band (for example, between 27° and 28°C) and relative humidity band (for example, between 55% and 65%). The limit of this control is that these two parameters are not independent: if the temperature decreases, the relative humidity can increase, leading to heavy out-of-bands, as shown in the Mollier diagram of Figure 2.3.3.

To overcome this constrain, a new parameter was chosen, which takes into account the effect of both variables. This parameter is the Predicted Mean Vote (Fanger, 1970), as defined in CEN ISO 7730 (1994), at the following conditions:

CLO=0.5 clo;
MET=1.2 met;
VEL=0.1 m/s;
WME=0 met.

In addition, fan coils have the task to control the humidity, to avoid surface condensation on the panels: another band, for the dew point temperature, was set as following

$$T_{dew\_max} = T_{rc,i} - dT_{dew,min},$$
(10)

$$T_{dew\_min} = T_{rc,i} - dT_{dew,max},$$
(11)

where $dT_{dew,min}$ and $dT_{dew,max}$ fix the thresholds of the dew point temperature

band; in this way, fan coils keep the dew point temperature lower than the panel surface temperature.
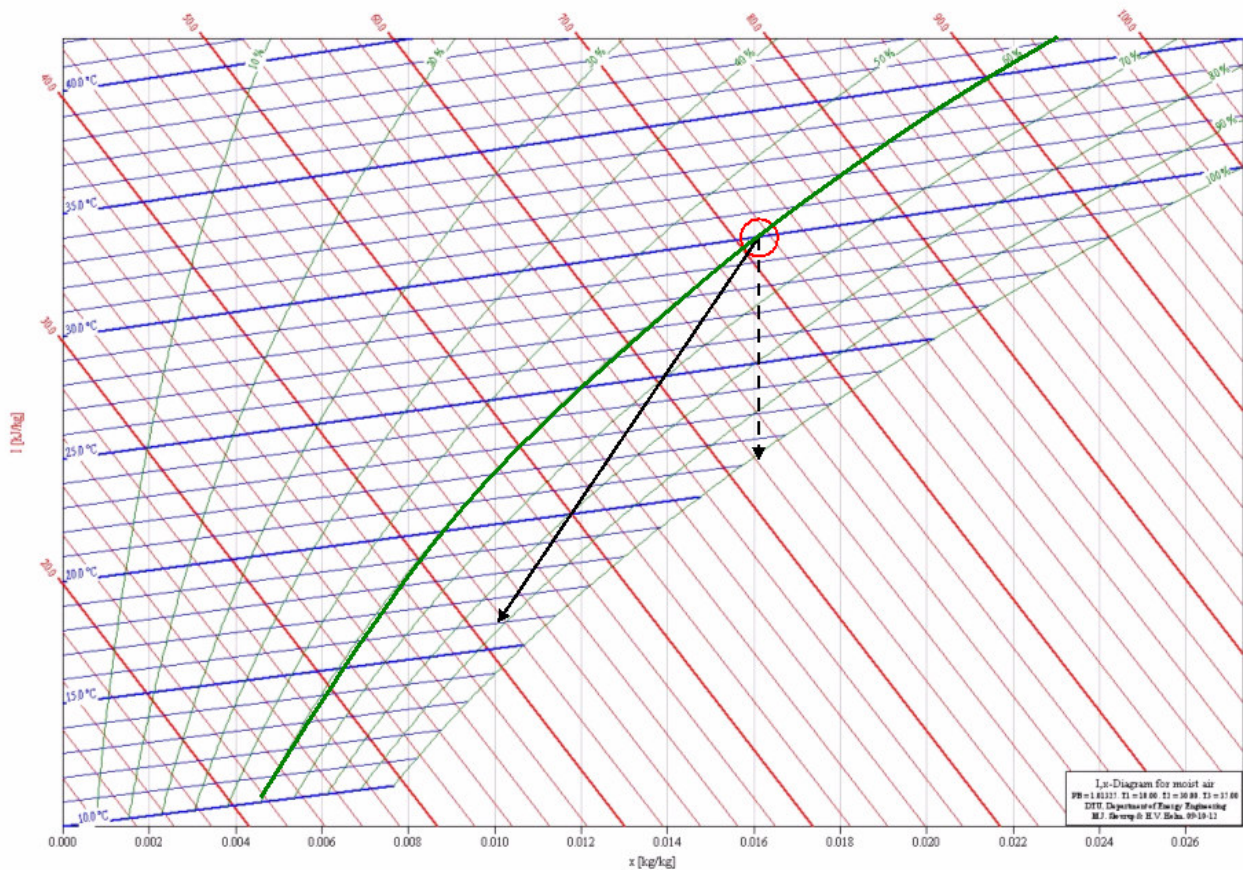
Figure 2.3.3: Cooling and dehumidification in Mollier diagram.

2.3.5   Simulation results

2.3.5.1   Simulated room

An office with a total volume of 48.6 m^3, placed in Venice (North East Italy) has been simulated. Its linear dimensions are 4 m (north and south sides), 4.5 m (east and west sides) and 2.7 m height. In the west side there is a window 2.7 m wide and 1 m high (see Figure 2.3.4); the glass of the window is double-glaze, filled with Argon, as described in Table 2.3.1. The exterior walls of the north and west sides

(wall (1)) are made of 5 cm bricks, 6 cm air space and 16 cm hollow bricks, covered by plaster in both sides, as resumed in Table 2.3.2. The exterior walls of the south and east sides (wall (2)) are made of 16 cm bricks, 6 cm glass wool insulation and 16 cm hollow bricks, covered by plaster in both sides, as resumed in Table 2.3.3.
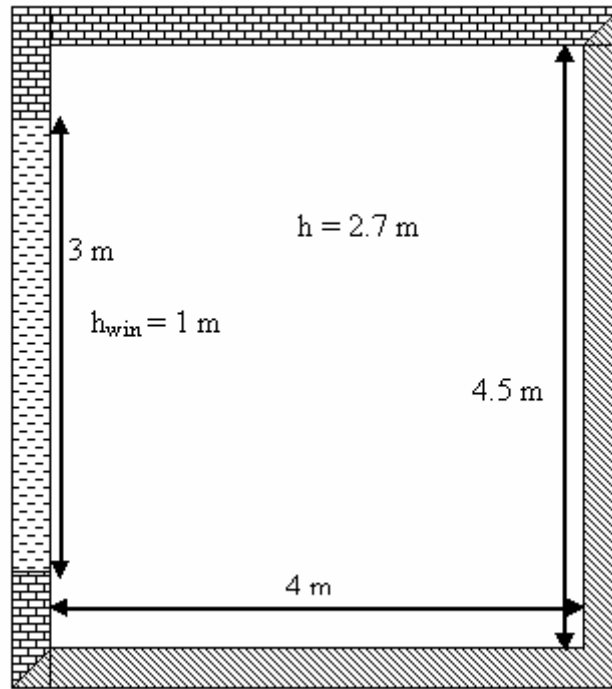
Figure 2.3.4: The simulated room

Name	D [mm]	TSol [-]	RSolFront [-]	RSolBack [-]	TVis [-]	RVisFront [-]	RVisBack [-]	TIR [-]	EmissFront [-]	EmissBack [-]
Front Glass	0.004	0.821	0.074	0.074	0.896	0.081	0.081	0.0	0.84	0.84
Argon	0.016	-	-	-	-	-	-	-	-	-
Rear Glass	0.004	0.471	0.077	0.119	0.612	0.077	0.107	0.0	0.84	0.163

Table 2.3.1: The glass composition

Name	Thickness [m]	Thermal conductivity [W/mK]	Density [kg/m^3]	Specific heat capacity [J/kgK]	Surface Emissivity [-]
plaster	0.02	0.5	2000	910	0.9
brick	0.05	1.2	2000	910	-
air	0.06	0.375	1	1000	-
air-brick	0.16	0.5	1100	840	-
plaster	0.02	0.5	2000	910	0.9

Table 2.3.2: The wall (1) composition

Name	Thickness [mm]	Thermal conductivity [W/mK]	Density [kg/m^3]	Specific heat capacity [J/kgK]	Surface Emissivity [-]
plaster	0.02	0.5	2000	910	0.9
hollow brick	0.16	0.5	1100	840	-
glass wool	0.04	0.033	72	800	-
hollow brick	0.16	0.5	1100	840	-
plaster	0.02	0.5	2000	910	0.9

Table 2.3.3: The wall (2) composition

The radiant system consists of tubes embedded in a 7 cm concrete slab, placed on a 5.5 cm insulating panel. It is reported in Table 2.3.4. The tube pitch is 9 cm and the tube inside diameter is 6 mm; the tubes are laid out in a spiral pattern and the radiant area consists of two circuits, with a total water mass flow rate of 300 kg/h. Every fan coil has a nominal capacity of 815 W, with an air volumetric flow rate 339 m^3/h.

Name	Thickness [m]	Thermal conductivity [W/mK]	Density [kg/m^3]	Specific heat capacity [J/kgK]	Surface Emissivity [-]
Wood pavement	0.020	0.200	770	2200	0.9
Adhesive layer	0.003	0.200	1100	850	-
Concrete	0.070	1.200	2100	880	-
Ashlar polystyrene layer	0.030 + 0.025	0.033	30	800	-
Reinfoced concrete	0.160	1.100	2200	870	-
Plaster	0.001	0.700	1200	880	0.9

Table 2.3.4: The panel composition

2.3.5.2 Simulation conditions and results

The simulations were set during summer time (June, July and August).

An external air infiltration of 24.3 m^3/h (0.5 Vol/h) was simulated. As regards the internal gains, the presence of 3 people, with a personal computer each, and a laser printer, was considered. The simulated activity is that of a common office: the business time is 8 a.m. to 5 p.m., with an hour of lunch break (12 a.m. to 1 p.m.) and weekend closing.

The following conditions have been investigated:
- three different dT$_{dew,c}$: 4°, 5° and 7°C;
- two different fan coil size: 2 and 3 times the nominal size;
- three different T$_{dew}$ bands: for 1°÷3°, 2°÷4° and 3°÷5°C, where the first number is dT$_{dew,min}$ and the second one dT$_{dew,max}$, respectively.

The radiant cooling band was set at 25÷27°C and the fan coil PMV band was set at 0.3÷0.8 (temperature 27÷28°C; relative humidity 55÷65%).

They are all compared to a traditional control, with T$_{c,o}$=7°C and T$_{rc,i}$=15°C, with fan coil twice the nominal size; the temperature difference to the dew point temperature (dT$_{min}$ of equation (7)) is set 1 K.

The results are reported in Table 2.3.5(a), (b) and (c); some parameters of interest

are plotted in Figure 2.3.5, 2.3.6, 2.3.7 and 2.3.8.

Considering the average EER of the chiller, the controller provides the best results for $dT_{dew,c}$ =4°C, while for $dT_{dew,c}$ =7°C the energy efficiency is lower than that of the traditional control. The higher performance is explained by the higher water temperature at the chiller outlet: for $dT_{dew,c}$ =4°C it is above 13.5°C, while for the traditional control it is set, constant, at 7°C. As regard the PMV, the most comfortable solutions are those with a larger size of fan coil (three times the nominal size). It is worth noticing that all the different settings of the developed controller present a higher level of comfort in comparison with a traditional controller. This aspect can be noticed considering the percentage of total time when the conditions are above the fixed thresholds (time over in Tables 2.3.5): in the case of a traditional control it is 39%, while in the worst case with the developed algorithm this percentage is 29.8%. On other hand, it is worth observing the minimum temperature difference between the panel supply water temperature and the dew point temperature: it is always higher than 1 K. If one wants to increase this temperature difference, shifting the T_{dew} band from 1°÷3°C to 2°÷4°C, the minimum temperature difference become higher than 2 K, while further shift to 3°÷5°C produces not remarkable effects.

		dT$_{dew,c}$ 4°C fc x 2	dT$_{dew,c}$ 5°C fc x 2	dT$_{dew,c}$ 7°C fc x 2
	dT$_{dew,c}$ [°C]	4	5	7
	T$_{c,o}$ [°C]	14.32	12.74	9.90
	T$_{rc,i}$ [°C]	19.22	18.76	18.45
	EER [-]	3.832	3.760	3.644
	Q$_{cooling}$ [kJ]	2576891	2653001	2712181
	Q$_{electrical}$ [kJ]	672427	705644	744389
	Q$_{fc}$ [kJ]	903212	941660	995028
	run time fc [%]	61.3	57.1	50.0
	run time rc [%]	81.0	80.1	79.0
	run time c[%]	97.0	97.2	97.2
average	PMV [-]	0.371	0.325	0.288
	PPD [%]	9.8	8.7	8.0
minimum	PMV [-]	-0.784	-0.787	-0.731
	PPD [%]	0.0	0.0	0.0
maximum	PMV [-]	1.322	1.188	1.187
	PPD [%]	41.4	34.7	34.6
	time over [%]	29.0	23.7	19.1
	d$_{Tdew}$ minimum [°C]	1.5	1.7	1.6

		dT$_{dew,c}$ 4°C fc x 3	dT$_{dew,c}$ 5°C fc x 3	dT$_{dew,c}$ 7°C fc x 3
	dT$_{dew,c}$ [°C]	4	5	7
	T$_{c,o}$ [°C]	13.52	12.06	9.74
	T$_{rc,i}$ [°C]	18.95	18.64	18.57
	EER [-]	3.766	3.709	3.656
	Q$_{cooling}$ [kJ]	2675545	2700672	2691272
	Q$_{electrical}$ [kJ]	710485	728185	736159
	Q$_{fc}$ [kJ]	1091314	1089473	1028284
	run time fc [%]	49.6	44.2	35.2
	run time rc [%]	78.7	78.1	78.8
	run time c[%]	97.3	97.2	97.3
average	PMV [-]	0.282	0.272	0.293
	PPD [%]	7.8	7.6	7.9
minimum	PMV [-]	-0.733	-0.724	-0.766
	PPD [%]	0.0	0.0	0.0
maximum	PMV [-]	1.104	1.055	1.050
	PPD [%]	30.7	28.5	28.3
	time over [%]	18.1	15.4	18.9
	d$_{Tdew}$ minimum [°C]	1.6	1.2	1.2

		$dT_{dew,c}$ 5°C (2°-4°C) fc x 2	$dT_{dew,c}$ 5°C (3°-5°C) fc x 2	$T_{c,o}$=7°C $T_{rc,i}$=15°C
	$dT_{dew,c}$ [°C]	5	5	0
	$T_{c,o}$ [°C]	12.61	12.46	7.01
	$T_{rc,i}$ [°C]	19.37	19.46	18.44
	EER [-]	3.738	3.722	3.670
	$Q_{cooling}$ [kJ]	2595156	2593260	2597209
	$Q_{electrical}$ [kJ]	694313	696659	707632
	Q_{fc} [kJ]	1011935	1060681	801009
	run time fc [%]	60.3	62.9	32.3
	run time rc [%]	78.5	77.8	69.4
	run time c[%]	97.4	97.3	96.7
average	PMV [-]	0.358	0.352	0.393
	PPD [%]	9.3	9.2	9.5
minimum	PMV [-]	-0.729	-0.732	-0.830
	PPD [%]	0.0	0.0	0.0
maximum	PMV [-]	1.286	1.336	1.122
	PPD [%]	39.6	42.1	31.5
	time over [%]	29.8	29.0	39.0
	d_{Tdew} minimum [°C]	2.4	2.4	1.9

Table 2.3.4(a), (b) and (c): Simulation results
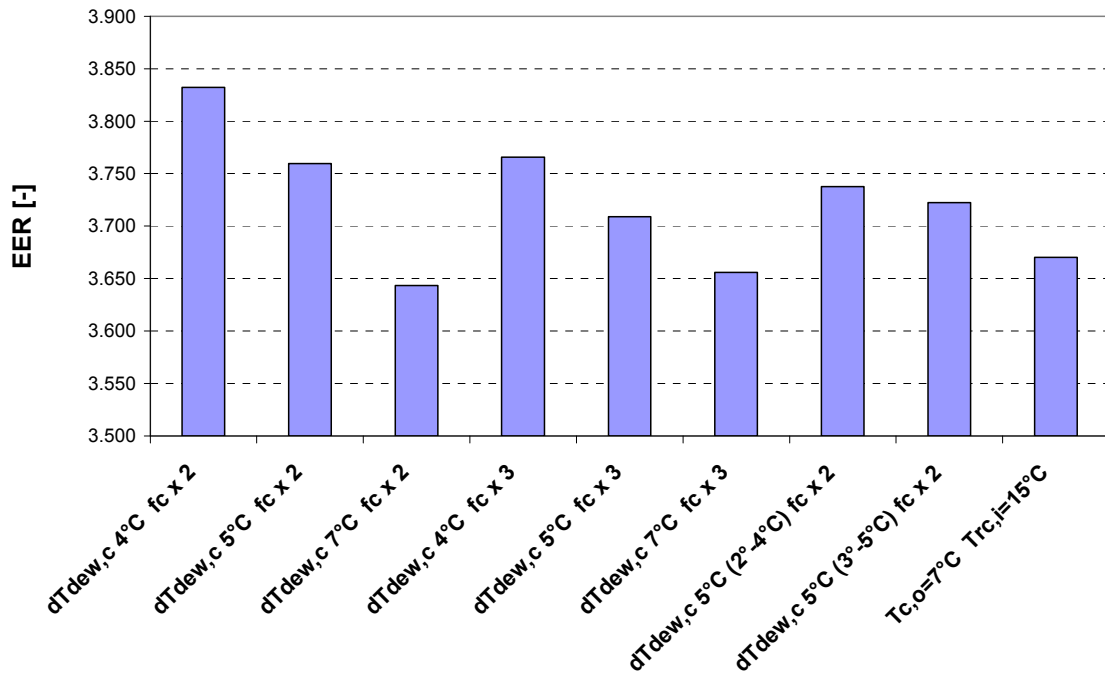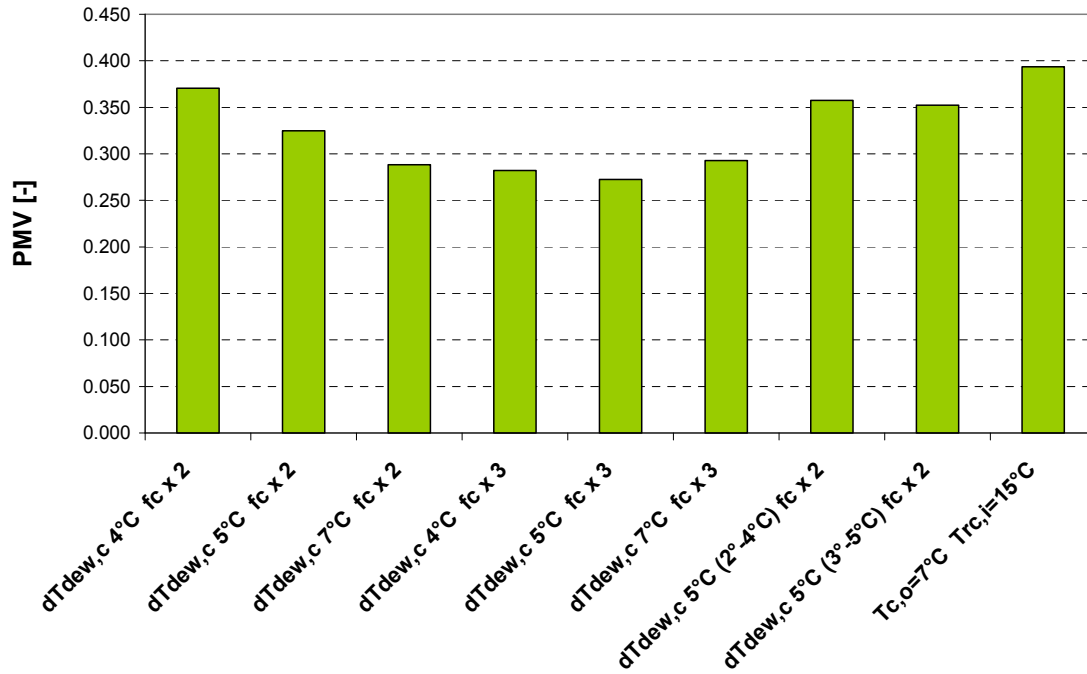
Table 2.3.5: Simulation results (EER)

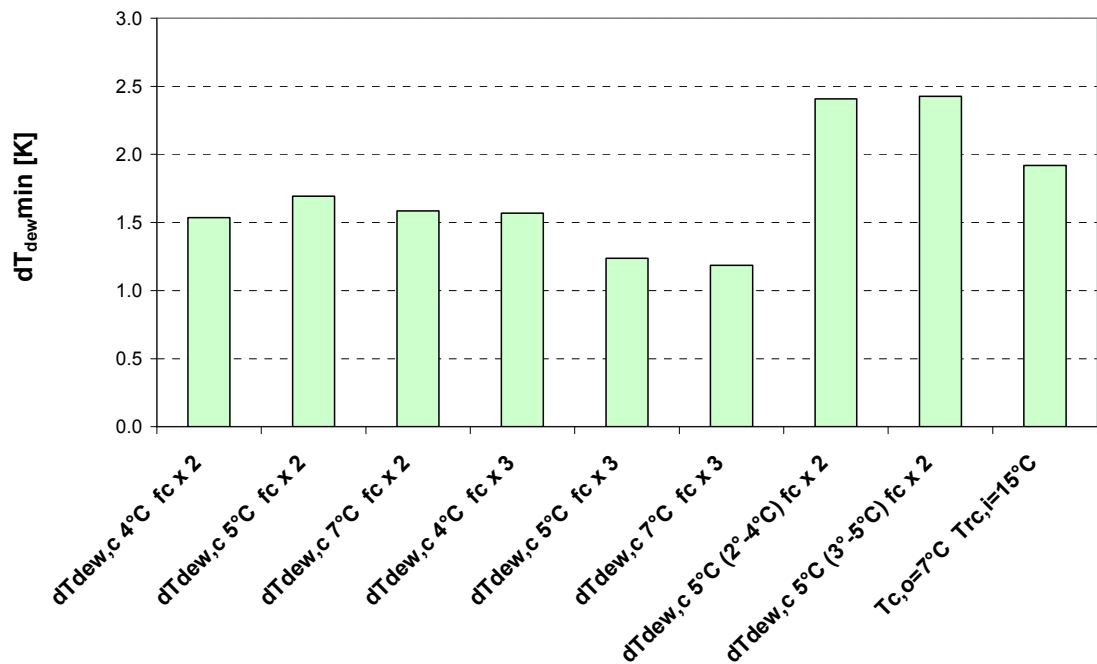*Table 2.3.6: Simulation results (PMV)*

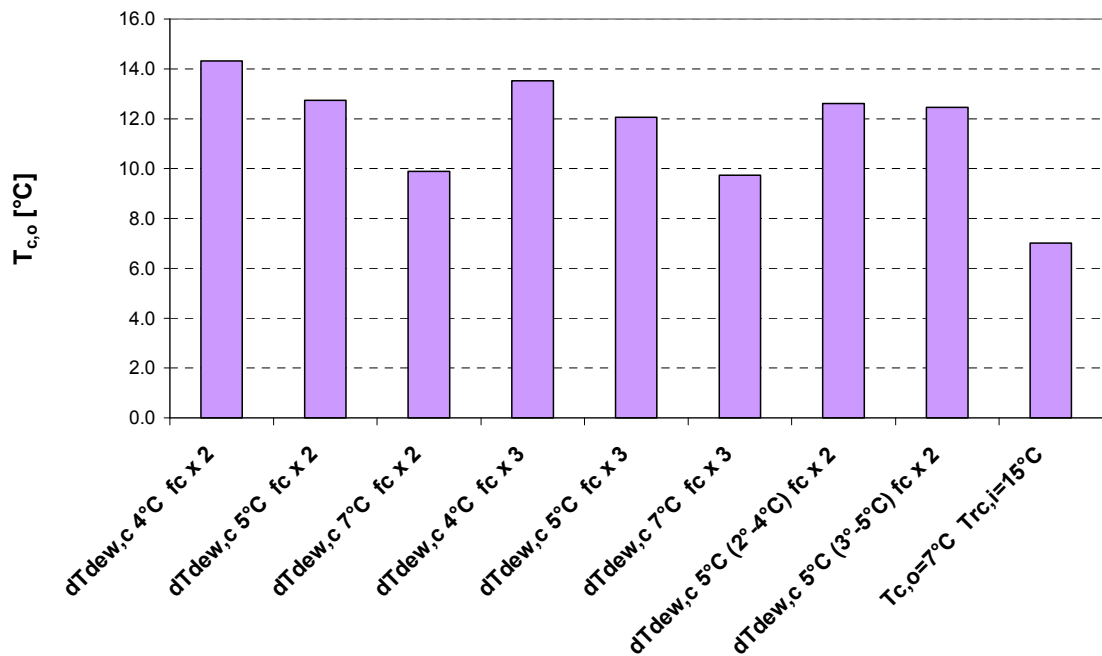*Table 2.3.7: Simulation results (dT$_{dew}$min)*

Table 2.3.8: Simulation results (T$_{c,o}$)

2.3.6   Conclusions

A new control algorithm for radiant cooling system with fan coil has been developed and simulated. This control logic takes advantage of a supervisor (EWMA) that is able to estimate the water supply set point temperature and to predict the temperature variations. The objective of the controller is to maximize the fraction of sensible heat absorbed by the radiant cooling system, while fan coils supply the total latent heat. On other hand, the main constrain is the surface temperature of the panel: it must be higher than the dew point temperature, to avoid surface condensation.

Different settings of the developed control logic have been simulated. The higher energy efficiency has been achieved setting the $dT_{dew,c}$ at 4°C, while the higher level of comfort was reached using over sized fan coils (three times the nominal size). Thus the most interesting settings seem to be:

- $dT_{dew,c}$ = 4°C, fc x 3. In this case the EER is 2.6% higher and the PMV is 0.11 lower than those of a traditional control. The minimum temperature difference between the radiant cooling water inlet and the dew point, during the simulation time, is 1.6 K and the percentage of time when the comfort conditions are above the fixed thresholds is 18.1%.

- $dT_{dew,c}$ = 5°C, fc x 3. In this case the EER is 1.0% higher and the PMV is 0.12 lower than those of a traditional control. The minimum temperature difference between the radiant cooling water inlet and the dew point, during the simulation time, is 1.2 K and the percentage of time when the comfort conditions are above the fixed thresholds is 15.4%. This solution assures a higher level of comfort.

- $dT_{dew,c}$ = 4°C, fc x 2. In this case the EER is 4.4% higher and the PMV is 0.02 lower than those of a traditional control. The minimum temperature difference between the radiant cooling water inlet and the dew point, during the simulation time, is 1.5 K and the percentage of time when the comfort conditions are above the fixed thresholds is 29.0%. This solution assures higher energy efficiency, keeping the same level of comfort.

Thus the controller is able to assure both a higher energy efficiency and a higher level of comfort. Further improvements of this control logic will regard multi-room environments or systems with air handling units instead of fan coils.

2.3.7   References

1. CEN ISO 7730, (1994), Moderate thermal environments---determination of the PMV and PPD indices and specification of the conditions for thermal comfort, *International Organization for Standardization*.
2. Fanger P. O., (1970), Thermal comfort, *Danish Technical Press*.
3. Kalagasidis A. S., (2003a), H-Tools. International Building Physics Toolbox. Block documentation, *Dept. of Building Physics, CHT*, Report R-02:3.
4. Kalagasidis A. S., (2003b), HAM-Tools. International Building Physics Toolbox. Block documentation, *Dept. of Building Physics, CHT*, Report R-02:6.
5. Lim J. H., Jo J. H., Kim Y. Y., Yeo M. S., Kim K. W., (2006), Application of the control methods for radiant floor cooling system in residential buildings, *Building and Environment*, 41(1):60-73.
6. Nielsen T. R., Peuhkuri R., Weitzmann P., Gudum C., (2002), Modeling building physics in Simulink – Working draft, *BYG-DTU*, Sagsrapport BYG-DTU SR-02-03.
7. Rode C., Gudum C., Weitzmann P., Peuhkuri R., Nielsen T. R., Kalagasidis A. S., Hagentoft C. E., (2003), International Building Physics Toolbox. General report, *Dept. of Building Physics, CHT*, Report R-02:4.
8. Weitzmann P., (2003), A floor heating module using an S-function approach for the International Building Physics Toolbox, *BYG-DTU*, Sagsrapport BYG-DTU.

Conclusions

In the present work, the theme of the energy efficiency of air conditioning and heating systems was faced, analyzing different methods to improve the plant performances. The high number of components, cycle configurations and control parameters makes this task uneasy and, often, without an univocal solution. As a conclusion, it is important to make some consideration concerning the effects of the studied solutions.

The first aspect that has been dealt with in this thesis is the importance of the refrigerant: an appropriate choice of operative fluid(s) is one of the basic steps in system design. Recent regulations in environmental matters limit the number of allowable refrigerants and a new perception of the problem pushes researchers and companies to the use of natural fluids. This choice presents some drawbacks: the fluid may have good properties, but it is toxic (like ammonia) or flammable (like hydrocarbons), or it may be safe, but it has a low efficiency (like carbon dioxide). Thus, at the moment, the alternative is between the study of different solutions to increase the energy efficiency of fluids like carbon dioxide or the realization of safer plants which allow the use of dangerous fluids.

In the first case, different plant configurations were studied in the present work (Chapters 1.2 and 1.3). Even if carbon dioxide, at the moment, presents too low energy efficiency for air conditioning applications, its use in refrigeration systems is becoming more and more common. In additions, cycle configurations with staged throttling can provide remarkable improvements of plant performances

In the second case, the objective is to design systems with low quantity of refrigerant: an incidental fluid leakage should not cause heavy damages. The study of more and more efficient heat exchangers, with reduced sizes and inside volumes, but high heat transfer area, is pushed by this necessity (Chapters 1.4 to 1.7). The current interest of researchers and companies is addressed to minichannel heat exchangers: their low cost and high efficiency justify the attention. They are widely used in automotive applications, but some problems for HVAC&R systems are not yet completely overcome. The two heaviest questions are the maldistribution of the refrigerant and the water drainage. The fluid maldistribution affects both condensers and evaporators and it strongly penalized the heat exchanger

effectiveness: a wide part of the heat exchanger can be not fed by refrigerant and it results "not activated". As regards water drainage, this drawback precludes the use of minichannel heat exchangers as evaporators; by now, proposed solutions do not provide any satisfactory results.

The concept of energy efficiency of an air conditioning, heating or refrigerating system has been revised in recent years. The evaluation of a plant efficiency based only on the design conditions can lead to wrong considerations, especially if the system runs at part load conditions for a large fraction of life time. Thus the definition of seasonal efficiency was introduced. The problem is to record and to collect the required data for the seasonal efficiency index (ESEER): manufacturers usually give performance data at rating conditions, being tests at part load conditions too expensive. Thus an easy and reliable tool for the calculation of seasonal efficiency, as that presented in Chapter 2.1, is needed.

This new sensitivity of the question is leading to the development of innovative system control methods, in order to increase the energy efficiency at part load ratio. In the present work, two possible ways to optimize a system have been presented. The first control mode regards the energy efficiency of a single or tandem compressor chiller unit. The algorithm manages the start-ups of the compressor, assuring high water temperature control and low energy consumptions under all running conditions. The second controller regards a radiant cooling system combined with fan coils: the control algorithm minimizes the sensible heat exchange of fan coils, manages the humidity and prevents water condensations on the panels, assuring comfort and low energy consumptions.

The analysis of the seasonal energy consumption reveals that the importance of an efficient controller is remarkable. New solutions to optimize a system running under part load conditions are gaining more and more interest: an example can be the use of free-cooling solutions in air conditioning system, that minimizes the energy consumption when the climate conditions do not require the full load running of the unit.

Ringraziamenti

Alla conclusione di questa esperienza voglio ringraziare tutti coloro che mi hanno aiutato e supportato in questi tre anni di lavoro.

In primo luogo la mia famiglia, papà Sergio e mamma Carla, che non mi hanno mai fatto mancare il loro appoggio, specie nei momenti di stanchezza.

Quindi tutti i miei "compagni di viaggio": i prof. Ezio Fornasieri e Claudio Zilio, che ringrazio soprattutto per il loro sostegno morale e psicologico, oltre che per quanto ho potuto imparare lavorando con loro.

Luca Cecchinato, che in questo 2010 sarà impegnato in battaglie decisive (matrimonio e concorso da ricercatore, in bocca al lupo!), la neo-mamma Silvia Minetto, compagna di trasferte a Salerno e Copenaghen, e il neo-papà Marco Corradi, in grado di risollevarmi il morale ogni giorno con le sue uscite.

Giovanni Schiochet, con il quale, dopo quasi dieci anni, "abbiamo finito di fare un'ombra sola!" (Bud Spencer a Terence Hill in "Due superpiedi quasi piatti", tanto per fare anch'io una citazione colta): in bocca al lupo per la tua esperienza americana!

I compagni di ufficio, il "rosso" (in tutti i sensi) Wilmer Pasut e la luminosa Valeria De Giuli, che ha avuto il merito di sopportarci per tre anni senza lamentarsi, se non per il freddo. Gli altri dottorandi, in particolare Beppe Emmi, con il quale ho condiviso l'esperienza della "piccionaia"; l'acustica Martina Pontarollo e il tenore PierGiorgio Cesaratto. Ferdinando Mancini, ottimo ricercatore ma pessimo allievo di dialetto veneto, al quale sarebbero serviti altri due-tre anni di "pendolarismo" in treno con me per poter finalmente parlare da veneto doc. Simone Mancin, che ha il grande merito (o privilegio) di dividere l'ufficio col duca-conte (er Corradi).

Inoltre voglio ricordare due fuoriusciti, come me, del Dipartimento, Cristian Rinaldi, ex compagno di appartamento e futuro padre, e Francesca Fantini, anima delle feste e di rimpatriate varie.

E' stato un piacere condividere con voi questi tre anni, non so dove e se potrò trovare un posto di lavoro con un'atmosfera come quella del DFT.

Manuel Chiarello